Author:
Morales Garcia, Nuria M

Title:
The feeding ecology of Mesozoic mammals

A biomechanical approach

The feeding ecology of Mesozoic mammals

A biomechanical approach

By

NURIA MELISA MORALES GARCIA

School of Earth Sciences
UNIVERSITY OF BRISTOL

A dissertation submitted to the University of Bristol in accordance with the requirements of the degree of DOCTOR OF PHILOSOPHY in the Faculty of Science.

NOVEMBER 2020

Word count: 35,425

Abstract

Over 150 million years of mammalian evolution occurred in the Mesozoic. Mammalian diet knowledge helps us understand the ecological structure of terrestrial communities and prevailing environmental conditions. Jaws are commonly preserved in the fossil record and inform on diet. In this thesis, I set out to investigate the relationship between jaw functional performance and diet in small mammals, using a combination of biomechanics, geometric morphometrics and phylogenetic comparative methods. Firstly, I used a combined approach of 2D form and function. I analysed the jaw shape of small extant mammals of known diets and the mechanical advantage of their adductor muscles. The combination of these data revealed differences in form and function between herbivores, carnivores, and insectivores. I found a very good correspondence between previously proposed diets of Mesozoic mammals and the results of this analysis. Secondly, I wanted to use a 3D approach to the study of jaw functional performance using Finite Element Analysis (FEA), commonly used in palaeontology to study feeding behaviour. FEA largely uses tomography-based models, which are expensive and time-consuming. Therefore, I decided to validate the use of simplified 3D models (called extruded models) built from photographs using two early mammal jaws as a case study. I found extruded models to be a viable alternative for large scale FEA studies. Thirdly, I used extruded FE models to study jaw functional performance in modern small mammals. I found differences in stress distribution between insectivores, hypercarnivores, mesocarnivores, and herbivores: most Mesozoic mammals resembled insectivores, and a few hypercarnivores. Put together, modern small mammals of different diets can be distinguished using jaw shape, mechanical advantage values, and stress distribution patterns. We can use this information to infer diet in Mesozoic mammals. Jaw functional performance corroborates the hypothesis that most Mesozoic mammals were insectivores, and a few taxa were carnivores.

Dedication and acknowledgements

First and foremost I would like to thank my wonderful supervisory team: Emily Rayfield, Christine Janis and Pam Gill. I feel incredibly lucky to have been supported and guided these past four years by an incredible team of kind, accomplished and extraordinary women in science. Thank you for dedicating so much of your time (and patience) to ensure I become a better scientist.

I would like to thank the amazing Palaeobiology Research Group of the University of Bristol. I began my journey in Bristol five years ago and in that time I have become a much better palaeontologist, but also a better person. I have met so many lovely people during my time in the UK, that I'm now proud to call my friends. I cannot choose favourites, so in alphabetical order, thank you for making my time in the department great: Antonio, Catherine, Celine, Delphine, Emma, Gareth, Guillermo, Liz, Marta, Rhys, Steve, Suresh, and Susana.

I would not be where I am if if wasn't for my wonderful family, so this thesis is dedicated to you. I love you, mum and dad, I know it has not been easy having two daughters who live on the other side of the world, but I really value that you gave us the liberty to pursue our dreams. Lore, my wonderful sister, you've made sure to take care of me all these years we've been living far from home. I really treasure how close we've become in recent years, I love you.

Chris, undoubtedly, the best part about moving to the UK was meeting you and having the chance to start building a life with you. We were with each other throughout both our PhD journeys and I wouldn't have had it any other way. You were there through all the ups and downs of these past few years, giving me all your love and support. Thank you for looking out for me and loving me unconditionally. I'm very much looking forward to the next chapter of our lives together.

This thesis was performed with support from CONACYT (Consejo Nacional de Ciencia y Tecnología), México (PhD scholarship, #689870)

AUTHOR'S DECLARATION

I declare that the work in this dissertation was carried out in accordance with the requirements of the University's Regulations and Code of Practice for Research Degree Programmes and that it has not been submitted for any other academic award. Except where indicated by specific reference in the text, the work is the candidate's own work. Work done in collaboration with, or with the assistance of, others, is indicated as such. Any views expressed in the dissertation are those of the author.

SIGNED: ..... DATE: .....

TABLE OF CONTENTS

List of Tables

List of Figures

GLOSSARY

adductor muscles Muscle that pulls a structure towards the midline of the body. In the case of the jaw, includes **temporalis**, **masseter** and pterygoid muscle groups. 12, 15, 22, 23, 28, 44, 83, 93

allotherian Mesozoic mammalian orders with molars with longitudinally arranged pairs of cusps. Term used to refer to the orders Haramiyida and Multituberculata. Not a monophyletic group. 11, 24, 44, 93

biomechanics Study of function and movement in biological structures using the principles of mechanics. 16, 22, 47, 67

cladotherian Stem-based taxon comprising all the taxa that are more closely related to therian mammals than to *Spalacotherium* ([12]). 14

Crown Mammalia see **crown mammals**. xv, xxiv, 3

crown mammals The group which contains the common ancestor of all living mammals (i.e., monotremes, placentals and marsupials) and all its descendants. xxiii, xxiv, 4–6, 8, 65

docodontan Elongated molars with two rows of tall cusps, which are connected by transverse crests. Characteristic of the Order Docodonta. 4, 30–32, 72, 86, 90

ecomorphological Relates to the interplay between morphology and ecology of an organism. 14, 21, 23

eupantotherian Paraphyletic group encompassing peramurids, amphitheriids and dryolestoids. xxiii, 6, 11

eupantotherians see **eupantotherian**. 10

Eutheria The group which contains the common ancestor of extant placentals and all its descendants. xv, xxiii, xxiv, 3, 6

eutherian see **Eutheria**. 8, 41

eutherians see **Eutheria**. xxv, 8, 10, 33, 35, 41, 44

faunivorous Animal who eats other animals, either vertebrates or invertebrates. 4, 11, 22, 30, 41, 43, 44, 65, 66, 90

geometric morphometrics Technique used to quantify and compare shape by using landmark and semilandmark coordinates which are then analysed using statistical tools. 16, 19, 21, 22, 27, 29, 66, 71, 72, 89, 92

Gondwana Ancient supercontinent which incorporated the modern-day southern landmasses (i.e., South America, Africa, India, Oceania and Antarctica). 6

Laurasia Ancient supercontinent which incorporated the modern-day northern landmasses (i.e., North America and Eurasia). 6, 8, 10

Mammalia The group containing the common ancestor *Sinoconodon* and crown Mammalia, and all its descendants. xv, xxiv, 3

mammaliaform stem-mammal see **mammaliaform stem-mammals**. 4

mammaliaform stem-mammals Paraphyletic group. **Mammalia**, minus **crown mammals**. These are the earliest mammals, all their representatives are extinct. xv, xxiv, 3, 4, 6, 8, 10, 12, 14, 16

masseter Muscle of mastication, which arises from the zygomatic bone in the skull and attaches towards the ventral area of the ascending ramus of the mandible. Found only in mammals. xi, xvi, xviii, xxiii, 12, 15, 21, 27, 34–41, 43, 44, 52, 69, 84, 90, 95

Metatheria The group which contains the common ancestor of extant marsupials and all its descendants. xv, xxiv, 3, 6

metatherian see **Metatheria**. 8

metatherians see **Metatheria**. xxv, 8, 10, 33, 35, 41, 44, 84, 87

morphospace A mathematical representation of a series of morphological traits, as visualised in a scatter plot. xvii, 24, 27, 30, 32, 33, 35, 72, 73

non-mammaliaform cynodonts Paraphyletic group containing the clade Cynodontia minus the **Mammalia**. All their representatives are extinct. 4

non-therian crown mammals Paraphyletic group. **Crown Mammalia**, minus therians. Includes the extant monotremes and several extinct orders. xv, xviii, 3, 10, 25, 32, 35, 43, 67, 68, 76

phylogenetic comparative methods Array of statistical techniques used to test various hypothesis related to evolution, diversification, and extinction on the basis of the proposed relationships of the organisms studied. 16, 19, 89

temporalis Muscle of mastication, which arises from the temporal fossa of the skull and inserts into the coronoid process of the jaw. xi, xvi, xviii, xxiii, 12, 15, 21, 27, 34–38, 40, 41, 43, 44, 52, 69, 84, 90, 93, 95

therian-crown mammals The group which contains the common ancestor of **eutherians** and **metatherians** and its descendants. xv, xviii, 3, 6, 25, 67, 68, 76

trechnotherian The group including *Zhangheotherium*, therian mammals, their most common ancestor, and all their descendants [12]. 8

tribosphenic Molars in which the protocone of the upper dentition opposes a talonid basin on the lower dentition. 6, 11

triconodont Tooth in which the three main cusps are aligned anteroposteriorly, characteristic of the order Eutriconodonta. Triconodont-like teeth present in mammaliaform stem-mammals like *Sinoconodon* and Morganucodonta. 4, 5

Yinotheria Group containing the orders Shuotheridia, Henosferida, Ausktribosphenida, and Monotremata. xv, 3, 6

Acronyms

ANOVA Analysis of variance. xi, 28, 30

CT Computed tomography. xi, xii, xvii, 46, 47, 49, 50, 54–57, 62, 63, 91, 92

FDA Flexible Discriminant Analysis. 28

FE Finite Element. xi, xii, xvii, 15, 19, 20, 45–52, 54–63, 65, 67–69, 77, 85

FEA Finite Element Analysis. xi, 14–16, 18–20, 45, 46, 48, 50, 52, 62, 65, 67, 69, 83, 85, 86, 91, 92, 94

FEM Finite Element Method. 14, 15

m1 First lower molar. xviii, 27, 28, 34, 38, 69, 71, 75, 76, 79, 82, 84, 85, 93

MA Mechanical advantage. 33, 35, 38, 97

MAM Mechanical advantage of the masseter. xi, xvi, xviii, 28, 34–38, 41, 43, 44, 90, 95

MAT Mechanical advantage of the temporalis. xi, xvi, xviii, 28, 34–38, 41, 43, 44, 90, 95

PCA Principal components analysis. 27, 72, 78

PERMANOVA Permutational multivariate analysis of variance. xi, 28, 34

PGLS Phylogenetic Generalised Least Squares. xvi, 28, 37, 39, 40

CHAPTER 1

INTRODUCTION

Two-thirds of the evolutionary history of mammals took place during the Mesozoic (251.9-66 Mya) [96, 98]. However, most research done into mammalian palaeobiology has been focused on Cenozoic taxa. The Cenozoic (66-0 Mya), also known as the "Age of Mammals", is often portrayed as the era in which mammals, finally free of the constraint of dinosaurs, diversified and became the dominant vertebrate group on the planet. On the other hand, Mesozoic mammals were often depicted as rat-like, generalised insectivores living under the shadow of dinosaurs. Recent discoveries, and research carried out in the past three decades, are gradually changing this story. In this thesis, I hope to contribute to our understanding of Mesozoic mammals, from both an ecological and functional standpoint. In this introduction, I present an overview of our current knowledge about Mesozoic mammals, including their taxonomic and ecological diversity, their geographic distribution, and evolutionary history. Later, I describe the biomechanical tools used in this thesis to analyse the dietary behaviour of these mammals, define my thesis aims, and finish by briefly describing the research chapters presented in this thesis. The taxonomic terminology used in this thesis is described in the Glossary. Unless specified otherwise, the term 'mammal' will be used to refer to both mammaliaform stem-mammals and crown mammals.

1.1 An overview of Mesozoic mammals

Mammals are a clade of vertebrates characterised by a series of distinct hard anatomical features, including a craniomandibular joint formed by the dentary and squamosal, a promontorium in the petrosal, and well-separated jugular and condylar foramina [98] (Figure 1.1). Fossil evidence of mammals dates back to the Late Triassic, with some of the oldest examples including *Gondwanadon tapani* from the Carnian of India [45] and *Adelobasileus cromptoni* from the

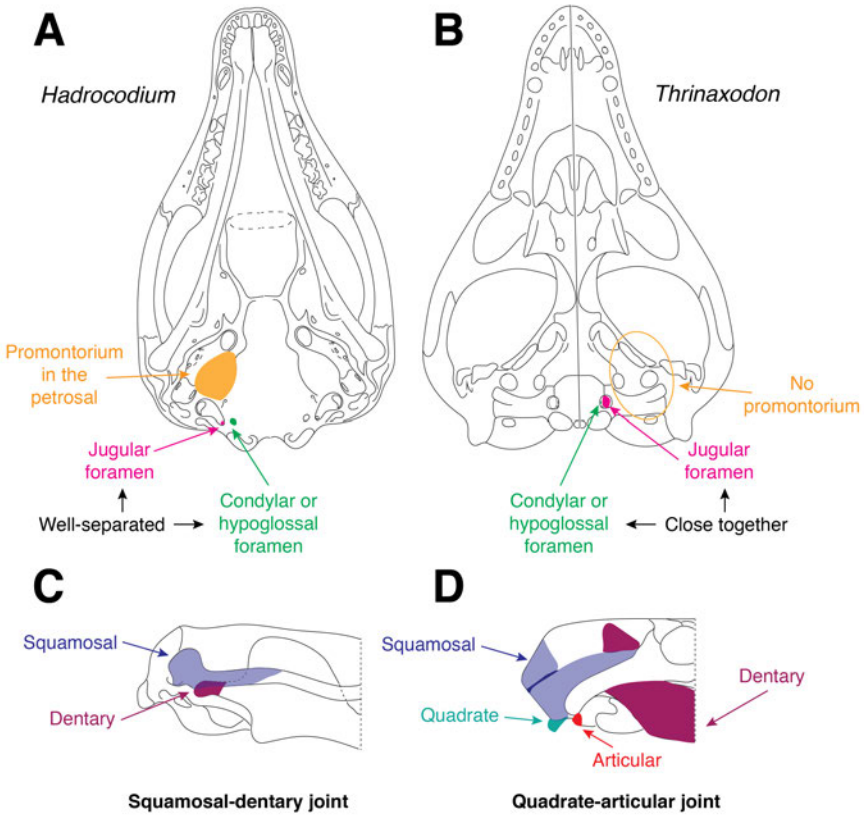

Figure 1.1: **Comparison of the skull and jaw of a mammal (*Hadrocodium*, on the left) and the skull of a non-mammaliaform cynodont (*Thrinaxodon*, on the right)**. A) Articulated skull and jaw of *Hadrocodium* in ventral view, B) Skull of *Thrinaxodon* in ventral view, C) Articulated skull and jaw of *Hadrocodium* in lateral view, D) Articulated skull and jaw of *Thrinaxodon* in lateral view. Modified from [98] and [116]

Norian of the United States [112].

Mesozoic mammals were taxonomically and ecologically diverse. During this era, there were approximately 20 orders of mammals (compared to 31 extant orders), which had an almost worldwide distribution [98, 156]. Although generally small, Mesozoic mammals had a wide range of sizes, ranging from shrew-size (e.g., *Microdocodon*: 5-9 g; [247]) to badger-size (e.g., *Repenomamus giganticus*: 12-14 kg; [88]). Exceptionally preserved fossils show a diversity of lifestyles, including swimming (*Castorocauda*, [94]), gliding (*Volaticotherium*, *Maiopatagium*, *Xianshou*, and *Vilevolodon*, [122, 144, 145]), fossorial (*Fruitafossor* and *Docofossor*, [123, 124]), and arboreal (*Arboroharamiya* and *Agilodocodon*, [146, 246]) forms. Mandibular and dental morphology also show a diversity of dietary types: carnivory (including piscivory), herbivory, insectivory and omnivory [30] (Figure 1.2). Here, I present an overview of the diversity of mammals throughout the Mesozoic (Figure 1.2), including their geographic distribution and most relevant morphological characteristics.

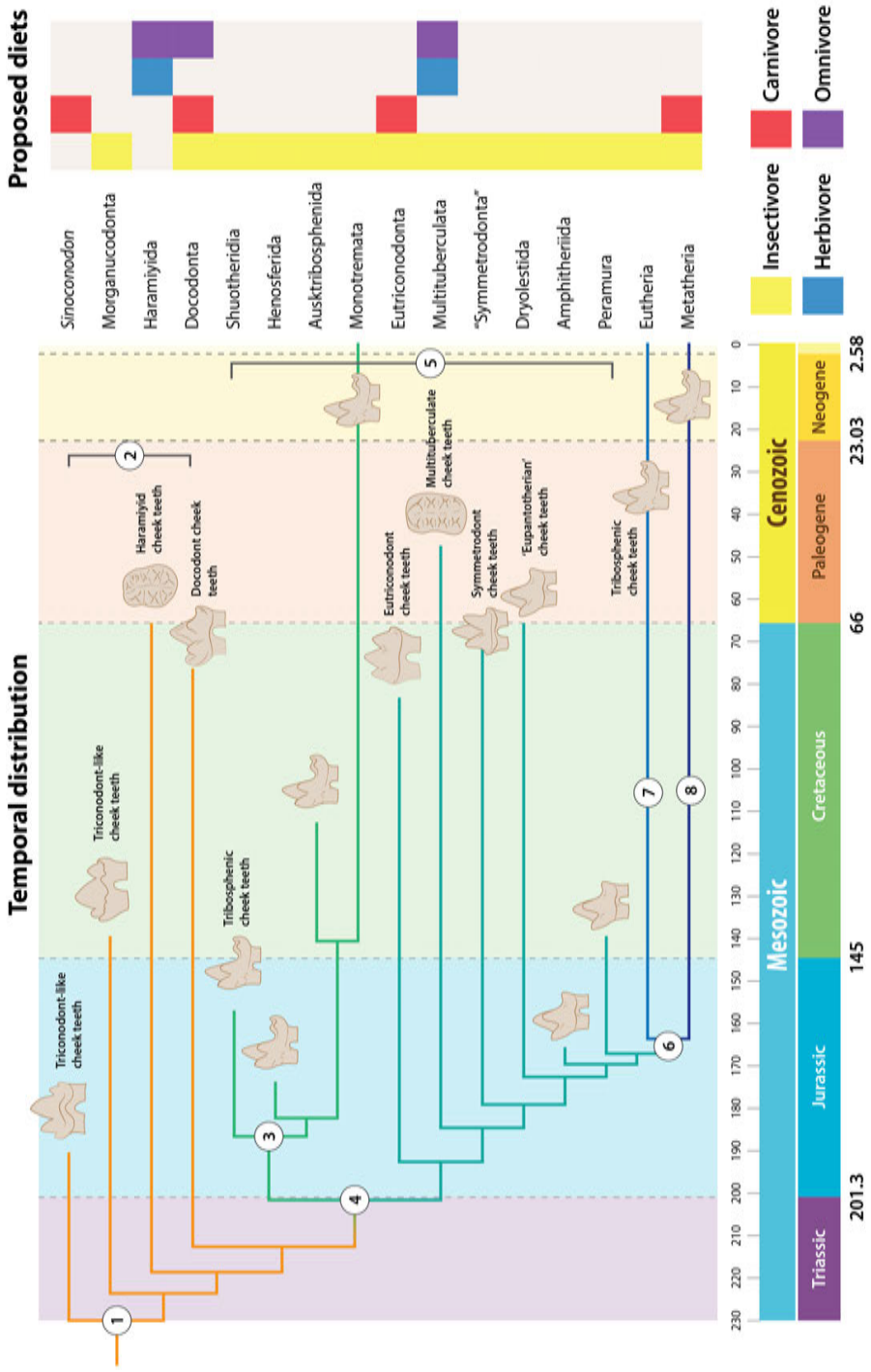

Figure 1.2: **Time-scaled Mesozoic mammal phylogeny at order level**. Includes dental type and suggested diet for the different clades [98]. 1) **Mammalia**, 2) **mammaliaform stem-mammals**, 3) **Yinotheria**, 4) **Crown Mammalia**, 5) **non-therian crown mammals**, 6) **therian-crown mammals**, 7) **Eutheria**, 8) **Metatheria**. Phylogeny based on [38].

1.2 Mammals throughout the Mesozoic

1.2.1 Late Triassic (Figure 1.3)

Mammals first originated during the Late Triassic. During this time, the **mammaliaform stem-mammal** orders Morganucodonta and Haramiyida, as well as the genera *Sinoconodon* and *Kuehneotherium*, inhabited Europe [98]. The morganucodontid *Gondwanadon tapani* was also present in India during the Late Triassic [45]. Morganucodontids were all small mammals (shrew to mouse size: 20-80 g) characterised by the presence of **triconodont**-like teeth and a double articulation of the jaw with the skull (dentary-squamosal and quadrate-articular). Like other **mammaliaform stem-mammals**, they have a trough on the medial side of the jaw which accommodates the postdentary bones, which eventually become the middle ear bones in **crown mammals** [98].

Haramiyids are mammaliaform stem-mammals characterised by molariforms with complex occlusal patterns, with two longitudinal rows of multiple cusps [98]; their dental morphology is indicative of an omnivorous or herbivorous diet [117]. Triassic haramiyids are mostly known from isolated teeth, except for *Haramiyavia* for which dentaries and scattered postcranial remains have been found [117]. There is debate on whether *Haramiyavia* shows the presence of a postdentary trough in the mandible, but later Jurassic haramiyids, like *Arboroharamiya*, lack this structure. The lack of a postdentary trough indicates the development of middle ear ossicles [143].

Sinoconodon, whose common ancestry with extant mammals defines Mammalia, dates back to the Rhaetian of France [76]. Like morganucodontids, it also has **triconodont**-like teeth which, in *Sinoconodon*, has been associated with a carnivorous or insectivorous diet. Unlike morganucodontids, *Sinoconodon* is placed in a more basal position due to its pattern of tooth replacement: anterior teeth replaced multiple times, like **non-mammaliaform cynodonts**, and postcanines replaced anteroposteriorly like mammals [98, 121].

The oldest records of *Kuehneotherium* come from the Rhaetian of Saint-Nicolas-de-Port, France, and consist mainly of isolated teeth [49]. More recently a second genus of kuehneotherid has been described from the same locality [49]. *Kuehneotherium* was originally considered a symmetrodontan, given its reversed triangle molar pattern [98]; however, more recent studies (e.g., [120]) recognise *Kuehneotherium* as a mammaliaform stem-mammal.

1.2.2 Early Jurassic (Figure 1.4)

By the Early Jurassic, a new order of **mammaliaform stem-mammals** joined the morganucodontids and haramiyids: the Docodonta. The oldest record of docodonts comes from India (*Gondtherium dattai* [1]) [174]. Docodonts were a very ecologically diverse group, characterised by the presence of **docodontan** molars adapted for an omnivorous or **faunivorous** diet; however,

[1] *Gondtherium*, *Dyskritodon*, and *Indobaatar* were found in the Upper Member of the Kota Formation which might be either Toarcian (Early Jurassic) or Aarlenian (Middle Jurassic) [95]

Figure 1.3: **Late Triassic distribution of mammals.** Countries with known fossils of Triassic mammals highlighted in orange. Map made with MapChart [149].

docodonts did not diversify taxonomically or ecologically until the Middle Jurassic.

The Early Jurassic also saw the appearance of the **crown mammals**; particularly, the Eutriconodonta and Multituberculata. The eutriconodontans were a very diverse order of mammals named after their distinctive **triconodont** molar pattern: three main cusps aligned anteroposteriorly. They are also characterised by the lack of both an angular process of the mandible and a postdentary trough. The taxa belonging to this order are considered to have been mostly faunivorous, and had a large diversity of body sizes, including some of the largest among Mesozoic mammals [98]. During the Early Jurassic, they were restricted to India (*Dyskritodon indicus*[1]), but later gained a more widespread distribution across Laurasia [173].

Another group of highly successful mammals appeared during the Early Jurassic: the multituberculates. At this time, multituberculates were only found in India (*Indobaatar zofiae*[1]: [164]), but would go on to become the single longest lived clade of mammals, as they did not go extinct until the Late Eocene (38-33.9 Ma). Multituberculates are **crown mammals** characterised by their intricate multicusped molar pattern and the complex morphology of their jaws, somewhat reminiscent of extant rodents; likewise, their skulls were wide and compressed dorsoventrally. Based on dental complexity studies, multituberculates probably had very diverse feeding preferences ranging from animal-dominated omnivory to herbivory [239]. Multituberculates were an exceptionally diverse group of mammals which attained an almost worldwide distribution, with the exception of Antarctica.

The best well-known fossil material of *Kuehneotherium* comes from the Early Jurassic of Wales, which was extensively described by Gill [74], and includes isolated teeth and dentary

fragments. The feeding ecology of *Kuehneotherium* has also been studied: Gill et al. [75] found evidence of niche partitioning between **mammaliaform stem-mammals**, *Morganucodon* and *Kuehneotherium*, in an Early Jurassic fauna.

1.2.3 Middle Jurassic (Figure 1.4)

All three orders of **mammaliaform stem-mammals** persisted into the Middle Jurassic. Docodonts had their heyday during the Middle Jurassic, spreading across Asia and reaching the United Kingdom. Docodonts were ecologically diverse during this time: putatively piscivorous swimming forms, like *Castorocauda*, and arboreal forms, like *Agilodocodon*, were found in China [94, 142, 146].

New orders of **crown mammals** evolved, including the **Yinotheria** (orders Shuotheridia and Henosferida), as well as the Dryolestida, Amphitheriida and Peramura [98]. Members of the subclass Yinotheria are grouped together by the presence of the postdentary trough and a 'clear morphological break' between the last and second to last premolar [98]. This subclass is comprised of the order Shuotheridia and the clade Australosphenida: a **Gondwanan** radiation of mammals that includes the extant monotremes. Shuotheridians are a Middle to Late Jurassic order of mammals found only in **Laurasia** (China, Russia and the United Kingdom) which have pseudo-tribosphenic molars [119]. On the other hand, australosphenidans are only found on southern continents and are characterised by the presence of **tribosphenic** cheek teeth (lost in extant monotremes), which were acquired independently to the tribosphenic molars of therians [115]. Among australosphenidans, the order Henosferida is restricted to the Middle Jurassic of Argentina (*Henosferus* and *Asfaltomylos*) and Madagascar (*Ambondro*) [98, 115].

Three more clades of **crown mammals** first appeared during the Middle Jurassic: the orders Dryolestida, Amphitheriida and Peramura. The oldest fossil evidence of these clades has been found in Morocco (Dryolestida and Amphitheriida, [83]), Ethiopia (possible Peramuran occurence, [35]), and the United Kingdom (Amphitheriida and possibly Peramura and Dryolestida, [210]). Both Dryolestida and Peramura persisted well into the Cretaceous, whereas Amphitheriida is restricted to the Middle Jurassic. These groups are sometimes grouped together on the basis of their '**eupantotherian**' cheek teeth and the presence of an angular process in the dentary [98].

1.2.4 Late Jurassic (Figure 1.4)

The Late Jurassic saw the appearance of the **therian-crown mammals** and, more specifically, eutherian mammals. The oldest eutherian mammal fossil is *Juramaia sinensis*, which lived 160 million years ago during the Middle-Late Jurassic in China [125]. Therian mammals comprise **Eutheria** (the group which includes modern placentals) and **Metatheria** (the group which includes modern marsupials); they are characterised by the presence of **tribosphenic** teeth (acquired independently to those of australosphenidans) and viviparity, among many other skeletal characteristics. Eutherians and metatherians differ in several respects, including the

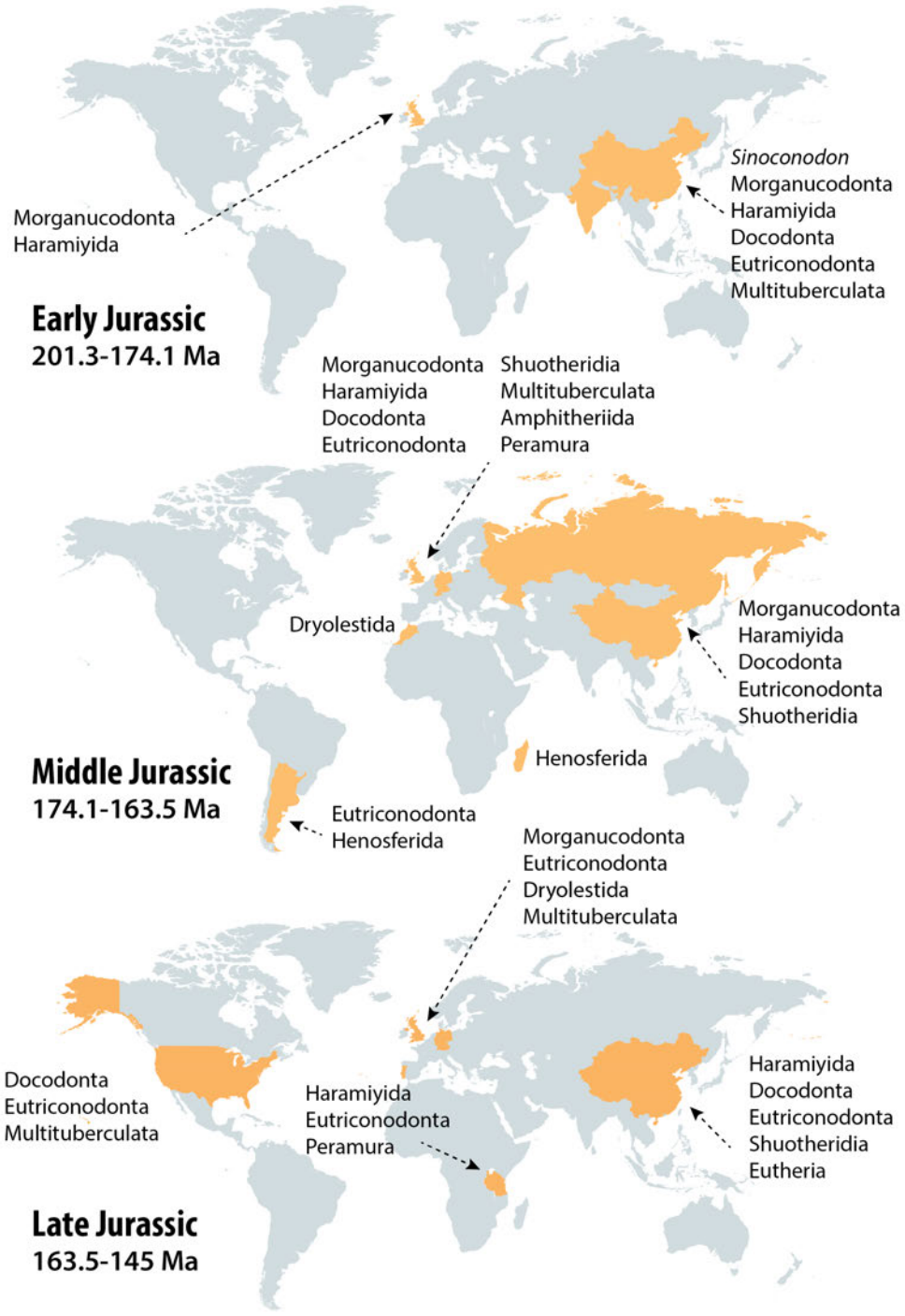

Figure 1.4: **Jurassic distribution of mammals.** Top: Early Jurassic, middle: Middle Jurassic, bottom: Late Jurassic. Countries with known fossils of Jurassic mammals highlighted in orange. Map made with MapChart [149].

lack of epipubic bones in most eutherians, the presence of an inflected angle of the mandible in metatherians, and the extremely altricial newborns in marsupials [98]. During the Late Jurassic, eutherians were only found in China, but would expand their distribution across **Laurasia** during the Cretaceous [98, 125, 142].

1.2.5 Early Cretaceous (Figure 1.5)

In terms of ordinal diversity, the Early Cretaceous was the most successful period of Mesozoic mammal evolution. All orders of **mammaliaform stem-mammals** still persisted in this period (morganucodontans are represented by *Purbeckodon*, known from isolated teeth only: [25, 50]). Eutriconodontans had diversified and spread to most of Asia, Europe, Africa and the United States [98]. The largest Mesozoic mammal ever found, *Repenomamus*, lived during the Early Cretaceous in China [88]. *Repenomamus* is also the only Mesozoic mammal with direct evidence for carnivory: preserved stomach contents showed this mammal ate a juvenile dinosaur, *Psittacosaurus* [88]. Multituberculates had also spread across Asia, Europe, Northern Africa, North America and Australia [98, 188]; likewise, **eutherians** were now found in North America [34].

Two new families of **crown mammals**, Spalacotheriidae and Zhangheotheriidae, first appeared in the fossil record of the Early Cretaceous. Earlier studies had grouped them together (with other taxa, such as the mammaliaform stem-mammal *Kuehneotherium*) in the clade "symmetrodonta", based on their reversed-triangular teeth pattern [98, 211]. Both families are also characterised by small body sizes, and very slender jaws with no angular process [98]. Later studies, revealed that symmetrodontans are either paraphyletic or polyphyletic, and that the families Spalacotheriidae and Zhangheotheriidae are stem **trechnotherians** [10, 12, 98, 120]. Early Cretaceous spalacotheriidans and zhangheotheriidans have been found in Western Europe, Eastern Asia and North America; the family Zhangheotheriidae is restricted to the Early Cretaceous [12, 98].

Both monotremes [6, 187] and **metatherians** [17, 47] appeared during the early Cretaceous. The earliest monotreme found to this date is *Teinolophos trusleri* (known from several partial mandibles and an isolated premolar) and, unlike modern monotremes (e.g., the platypus and echidna), *Teinolophos* was a toothed monotreme [186]. The order Ausktribosphenida (included in the clade Australosphenida with monotremes) also dates back to the Early Cretaceous but, unlike monotremes, fossil material of ausktribosphenidans has only been found in this period. There are only two genera of ausktribosphenidans, both restricted to Australia: *Bishops* and *Ausktribosphenos* [187].

Even though most modern **metatherians** (i.e., marsupials) live in Australia, this group might have originated in China [17]. The oldest metatherian known was thought to have been *Sinodelphys slazayi* [118]; however, its identity as a **metatherian** is now being debated and it is now thought to have been a **eutherian** mammal [17]. If that is the case, the oldest metatherian fossils known are from the late Early Cretaceous of North America (order Deltatheroida) [17, 47].

Given that the earliest eutherian known are at least 50 million years older, there is a large gap in knowledge regarding Late Jurassic/Early Cretaceous metatherian fossils [17, 125].

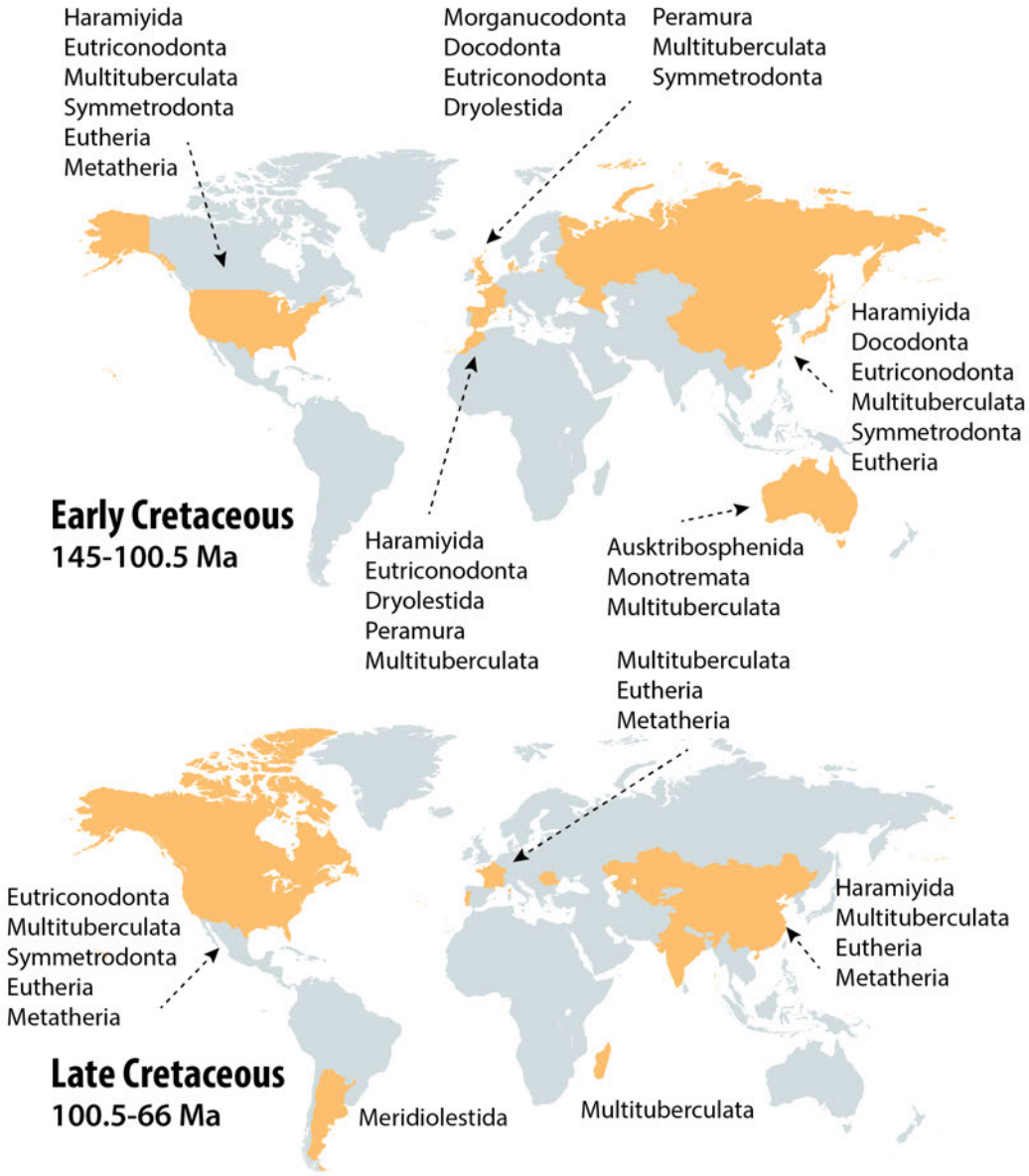

Figure 1.5: **Cretaceous distribution of mammals.** Top: Early Cretaceous, bottom: Late Cretaceous. Countries with known fossils of Cretaceous mammals highlighted in orange. Map made with MapChart [149].

1.2.6 Late Cretaceous (Figure 1.5)

By the Late Cretaceous, haramiyids were the only remaining order of **mammaliaform stem-mammals** [4]. Among **non-therian crown mammals**, eutriconodontans and spalacotheriidans were restricted in distribution to North America [72, 98]. Dryolestids went extinct by the end of the Early Cretaceous, but the clade Meridiolestida (suggested by some authors to belong to the clade Dryolestoidea, [32]) was found in South America (as opposed to the Laurasian distribution of dryolestids) [32, 98]. More recently, the hypothesis that meridiolestidans belong to the clade Dryolestoidea has been disputed, and meridiolestidans are now thought to be more closely related to spalacotheriidans [12]. Multituberculates were widespread across **Laurasia**, but a couple of records indicate their presence in Madagascar [98, 104]. To this date, there are no records of Late Cretaceous monotremes [168], but were likely still found in Australia. As far as we know, most monotremes (with the exception of *Monotrematum* from the Early Paleocene of Argentina [165]) remained in Australasia for all their evolutionary history. By the Late Cretaceous, the australosphenidans (except for the monotremes) and the '**eupantotherians**' were extinct [98, 168]. Eutherians and **metatherians** were now widespread across North America, Asia and Western Europe [98]. Out of all the mammalian clades that lived during the Mesozoic, **eutherians**, **metatherians**, monotremes, multituberculates, and meridiolestidans survived the K/Pg extinction event [32, 98, 159]. Multituberculates survived until the Late Eocene, although their taxonomic diversity during the Cenozoic was lower than in the Mesozoic [229, 239]. The fossil record of meridiolestidans spans from the Late Cretaceous to the Early Miocene [32, 159].

Mesozoic mammals were widespread geographically and were taxonomically diverse (over 300 genera spread across around 25 lineages) [98, 113]. Many orders, such as the multituberculates, haramiyidans, eutriconodontans and docodontans were longer lived (>70 million years) than most extant mammal orders. Compared to extant mammals, Mesozoic taxa were small, but they still had a wide range of body sizes: going from approximately 5 grams all the way up to 14 kilograms [88, 98, 247]. Exceptionally preserved fossils of these mammals are prime evidence that they were more ecologically diverse than once thought [113]; however, the vast majority of the fossil record of Mesozoic mammals are isolated teeth and jaws. Fortunately for us, teeth and jaws are the main sources of evidence regarding the diets of mammals. Understanding their diets contributes to our knowledge of the ecological structure of Mesozoic mammalian communities, which can, in turn, aid our understanding of the prevailing vegetation and climatic conditions in these palaeocommunities [30]. So, how can we infer the diets of Mesozoic mammals?

1.3 Feeding ecology in Mesozoic mammals

Direct evidence regarding the diet of Mesozoic mammals is restricted to the preserved stomach contents of the eutriconodontan *Repenomamus robustus*, which contained the remains of a juvenile dinosaur [88]. Indirect evidence for the diet of the earliest mammals is much more abundant,

and comes from teeth and jaws.

There are two main ways the diets of Mesozoic mammals have been inferred by using their teeth: by looking at their overall morphology and by using advanced analytical techniques which look at the wear and complexity of the occlusal surface (e.g., microwear and orientation patch count, [26, 60, 232]). By looking at the overall morphology of the teeth of Mesozoic mammals, most orders are considered insectivores, including most clades with **tribosphenic**, symmetrodont and **eupantotherian** cheek teeth. A few orders, like the Docodonta and Eutriconodonta are considered to have been more **faunivorous** (Figure 1.2). The feeding ecology of orders with pairs of longitudinally-arranged series of cusps, like the haramiyidans and multituberculates [98], has long been debated and ranges from herbivory to faunivory and omnivory [239].

Microwear analysis and dental complexity allow us to more accurately determine the diets of individual taxa, and independently corroborate observations made on overall morphology alone. Dental microwear analysis is used to correlate a microscopic pattern of pits and scratches in the surface of a tooth with the physical properties of the food items consumed by the individual [26]. This technique has been widely used to infer the physical properties of the food ingested during the last meals of an animal [147]. Dental microwear has been used to infer the diet of a large number of mammals, including ungulates, carnivorans, rodents, kangaroos, among others [26]. Among Mesozoic mammals, it has been used in a few taxa, including *Morganucodon watsoni*, *Kuehneotherium praecursoris* [75], and *Didelphodon vorax* [238]. In both of these studies, extant taxa of known diets were used as a comparative basis to infer the diets of Mesozoic mammals: bats in the case of *Morganucodon* and *Kuehneotherium* [177], and various small- to medium-sized marsupials and placentals in the case of *Didelphodon* [238].

Orientation patch count (OPC) is a measure of dental complexity, which has been shown to correlate well with feeding ecology in extant rodents, carnivorans and bats [60, 203]. This technique has been used to infer the diet of Late Jurassic to late Eocene multituberculates. Late Jurassic to Early Cretaceous taxa were shown to be carnivorous or animal-dominated omnivores and, towards the latest Cretaceous, multituberculates were mainly herbivores or plant-dominated omnivores [239]. Although OPC is a powerful tool for inferring diets in extinct mammals, it requires the teeth to be preserved three-dimensionally and many Mesozoic mammal teeth are preserved two-dimensionally in flattened slabs [30].

Another source of evidence regarding the dietary performance of mammals is the lower jaw. Jaw shape has been used to infer diet in Mesozoic mammals by Grossnickle and Polly [80]. This study found that non-**allotherian** mammals (i.e., Mesozoic mammals not belonging to the orders Haramiyida or Multituberculata) and Late Jurassic-Early Cretaceous multituberculates have similar jaw shape to extant **faunivorous** taxa, while Late Cretaceous multituberculates are more akin to extant herbivores.

Biomechanical analyses have also been used to study the feeding ecology of mammals. Of special relevance is the study by Gill et al., [75], who used a suite of biomechanical techniques

to study niche partitioning between the Early Jurassic **mammaliaform stem-mammals** *Morganucodon* and *Kuehneotherium*. Their study used three biomechanical techniques: mechanical advantage, finite element analysis and second moment of area. Below I describe in detail the first two analyses, as they form the basis for this thesis.

1.4 Mechanical advantage

A lever is a system consisting of beam-like object rotating around a fixed point, with the purpose of transmitting energy from one point of the beam to another (Figure 1.6). There are three main parts of a lever: the fulcrum (i.e., fixed point), the effort (or input force) acting upon the system and the load (or resistance) placed upon the system [138]. There are three types of lever, defined by the position of the fulcrum, effort and load relative to each other. First-class levers have the fulcrum placed between the effort and the load (e.g., seesaw and scissors), second-class levers have the load placed between the fulcrum and the effort (e.g., wheelbarrow and nutcracker), and in third-class levers the effort is located between the fulcrum and the load (e.g., tweezers and hammer) [14]. Jaws function as a lever system: a beam-like bone rotates around a fixed point (the jaw condyle), to transmit energy input by the jaw-closing muscles (i.e., **adductor muscles**) at the back of the jaw, to the bite point towards the front of the jaw. With the exception of some rodents, the mammalian jaw is generally regarded to work as a third-class lever [40].

Levers transmit a force input into the system (e.g., jaw adductor muscle input force) to provide a greater output force (e.g., bite force) to displace a load (e.g., food); this is known as leverage. The ratio of these two forces is known as mechanical advantage. Another way to describe the leverage of a system is by calculating the velocity ratio of a lever, which is calculated by dividing the length of the in-lever (i.e., distance moved by the effort) by the length of the out-lever (i.e., distance moved by the load). In the case of the mammalian jaw, it corresponds to the moment arm of the adductor musculature (i.e., **temporalis**, **masseter** and pterygoid) divided by the distance from the jaw condyle to the biting point [75, 87] (Figure 1.7). In an ideal system with no energy losses, mechanical advantage and velocity ratio are equivalent. Therefore, the former is often known as actual mechanical advantage and the latter is known as ideal mechanical advantage [14]. Leverage represents a trade-off between force production and speed: higher mechanical advantage values denote a system with a higher force output and lower values indicate a system optimised for speed. Changing the length of the in- and out-levers (and therefore the position of the effort and load relative to the fulcrum) will alter the leverage of a system for increased speed or force output [14].

Animals can optimise their speed or force output for feeding by using different strategies: the length of the jaw, the relative position of the condyle, the length of the coronoid process and the presence of an angular process, among others, are all different means to modify the mechanical advantage of the jaw. Skulls and jaws optimised for either speed or force production relate to the

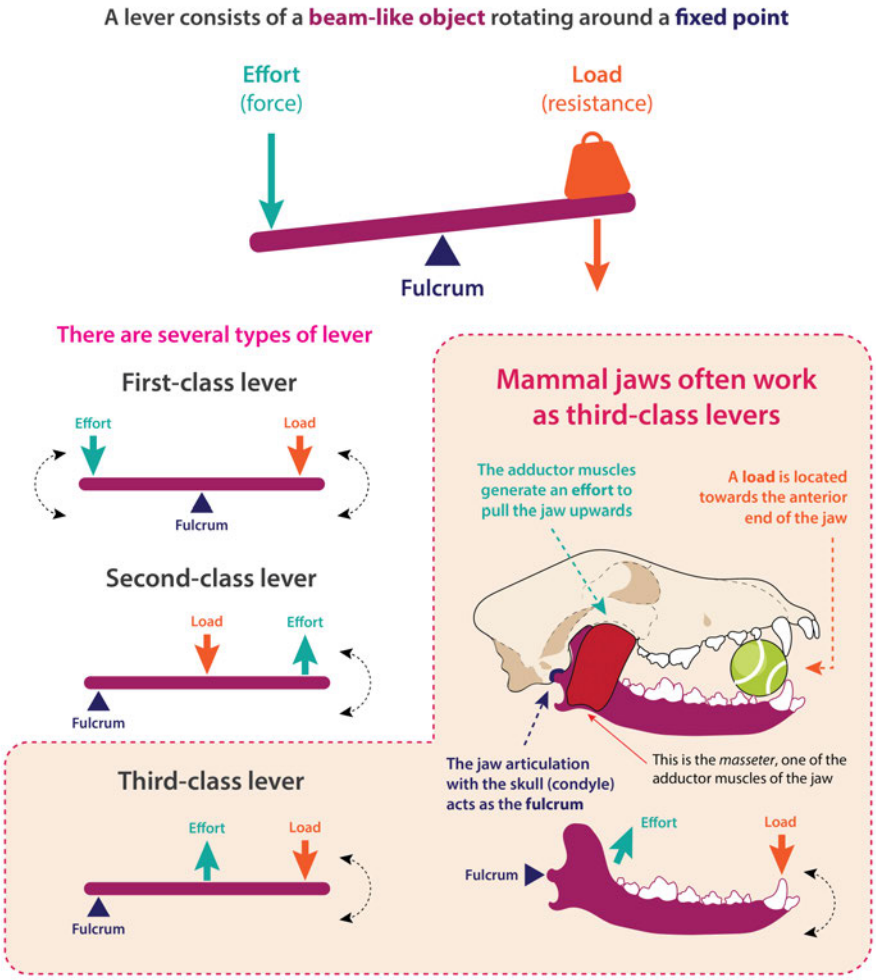

Figure 1.6: **Types of lever.** This diagram describes the three different types of lever and explains how the mammalian jaw works as a third-class lever using a dog biting on a tennis ball as an example.

dietary behaviour of the animals. For example, extant parrots (Order Psittaciformes) optimise their short beaks for force production (i.e., high mechanical advantage) for cracking/ripping tough seeds, while sand-pipers, snipes and phalaropes (Order Scolopacidae) optimise their long beaks for faster bites (i.e., low mechanical advantage) and for probing in sediment for small prey [154]. Within different lizard families, herbivorous species have higher mechanical advantage values than carnivorous species [217] and among natricine snakes, piscivore species have lower mechanical advantage (and faster gapes) than frog-eating snakes [85].

Mechanical advantage studies have also been performed in mammals, both modern and extinct. Among extant mammals the relationship between diet and mechanical advantage has been studied in primates [101, 231], squirrels [27, 102], bats [57, 202], otters [223], and bears

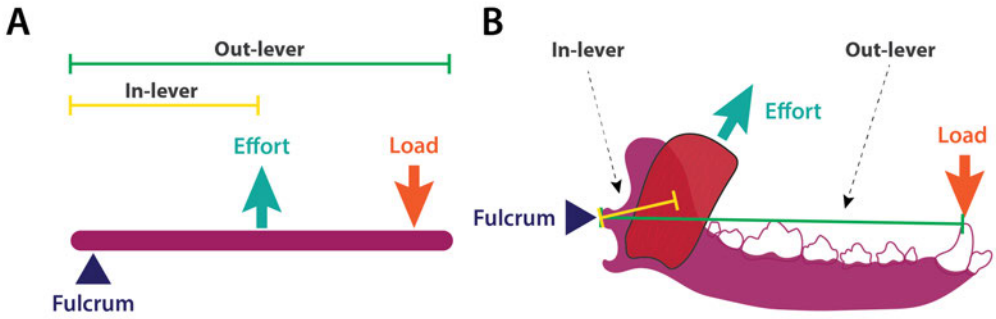

Figure 1.7: **Graphical representation of mechanical advantage**, shown in A) a traditional third-class lever, and B) the mammalian jaw.

[199], among others. By establishing a relationship between mechanical advantage and feeding in certain extant clades, the dietary behaviour of closely related extinct taxa can be assessed using this functional parameter. Such studies include the analysis of the killing behaviour of sabertooths [59], the feeding behaviour of dire wolves [5], the dietary evolution of giant armadillos [48], and the feeding habits of early Miocene South American ungulates [28]. Mechanical advantage data has also been used in functional studies of Mesozoic mammal jaws. Among these, Gill et al. [75] used comparative mechanical advantage data to study the feeding behaviour of **mammaliaform stem-mammals** *Morganucodon* and *Kuehneotherium*, Grossnickle [78] analysed the yaw and pitch in the jaws of **cladotherian** mammals, and Benevento et al. [16] studied the **ecomorphological** disparity of mammals along the Mesozoic/Cenozoic transition.

1.5 Finite Element Analysis

Another way of analysing how a system (in this case the mammalian jaw) responds to its environment, is to use an engineering-based technique called Finite Element Analysis (**FEA**) [183]. This computational technique is commonly used in the design of aircraft, buildings, cars, among other things, to understand how these structures would interact with their surroundings. For example, if a large number of lorries were to cross a bridge at the same time: how much stress and deformation would the structure be subjected to? Would the bridge remain intact under the weight or would it collapse? The intricacy of structures such as these makes it difficult to readily evaluate how they would perform when subjected to a complex loading scenario. By using the Finite Element Method (**FEM**), we can break down these complex structures into a discrete number of units, whose response to loading can be more easily assessed using mathematical equations [52, 100].

FEA is a computational method which involves several stages (Figure 1.8, also see Appendix E for a more detailed explanation of the process). First, we need a digital representation of the

structure of interest, which can be 2D or 3D. Biological **FE** models in 2D are generally built from photographs and 3D models are typically built from tomographic data. These models can be built in a variety of software: 2D models are built in computer-aided design (CAD) software (e.g., Autodesk Inventor) or 3D computer graphic software (e.g., Blender [Blender Foundation], Autodesk Maya [Alias System Corporation]), while 3D models are built in tomographic visualisation and analysis software (e.g., Avizo [Thermo-Fisher Scientific], Mimics [Materialise NV], 3D Slicer [The Slicer Community], Dragonfly [ORS], among others). Once the model has been built, it is then imported into computer-aided engineering and finite element analysis software (e.g., HyperMesh [Altair Engineering] and/or Abaqus [Simulia]).

The second stage involves breaking down the structure into a series of smaller interconnected units: this is called meshing. A mesh consists of a series of elements of known shape and size and the points in which elements are connected to each other are known as nodes. Mesh convergence tests are needed to determine the ideal number of elements present in a mesh (i.e., mesh density) [23]; this entails running a series of analyses where everything remains equal except for the number of elements. The ideal number of elements will be achieved when the results of the analysis remain relatively similar despite increasing the number of elements.

During the third stage, the material properties of the structure of interest are assigned to the model. In the case of bone, the elastic material properties Young's modulus and Poisson's ratio are specified. Young's modulus is the relationship between stress and strain of the material; it is a measure of stiffness. Poisson's ratio describes the transverse strain (perpendicular to the direction of loading) of a material relative to its axial strain (in the direction of loading): it is the ratio of relative contraction to relative expansion of a material. For example, when a rubber band is stretched it contracts perpendicular to loading and expands in the direction of loading; this relative expansion and contraction is known as Poisson's effect and is numerically expressed as Poisson's ratio. The Poisson's ratio of cortical bone ranges between 0.15 and 0.45, but it is typically set to 0.3 [198].

The fourth stage consists of indicating the points along the structure where movement will be impaired, these are known as boundary conditions. For example, the movement of a jaw will be restricted to particular degrees of freedom at the articulation with the skull and at the bite point. The fifth stage involves assigning virtual loads to the model. It is important to note that 'loading' in **FEA** and the load on a lever (in the mechanical advantage section) refer to different things; loading in the construction of **FE** models is actually equivalent to the 'effort' in a lever system. By assigning loads to an **FE** model, we virtually replicate the pull of the **adductor muscles** of the mandible (i.e., **temporalis**, **masseter** and pterygoid): we need to specify both the direction and the force (in Newtons) these muscles are pulling with. Taking into account the geometry and material properties of the structure, the last stage of the **FEM** is to analyse how the model responds to the loads and boundary conditions applied upon it. Generally, data on stress, strain and deformation are used to assess the performance of the structure. There are

two ways of visualising these parameters: graphically using 'heatmaps' (see Figure 1.8, step 6) that indicate where the highest or lowest areas of stress or strain are located in the structure, or numerically (the FE software being used can generate a spreadsheet with individual stress, strain and deformation values by element or node).

This numerical output can be further analysed using different approaches. Descriptive statistics, including measurements of central tendency (e.g., mean, median), are generally presented to summarise the overall stress and strain experienced by the structures. Such measurements, however, are not informative unless the mesh used is homogeneous in size; Marce-Nogue et al., [130] proposed the alternative 'mesh-weighted arithmetic mean' which accounts for the element size heterogeneity of the mesh. More recently, Marce-Nogue et al., [131] introduced the 'intervals method', which presents a new way of analysing **FEA** output data. This method sorts the elements in the mesh based on their stress values and assigns them to particular intervals of known volume, allowing the **FEA** output to be analysed in a multivariate comparative framework. This output can then be analysed using other methods such as linear discriminant analysis. This method has been successfully used to discriminate between different feeding ecologies among armadillos [131] and to elucidate the mode of life of the primate, *Paralouatta* [178].

The use of **FEA** in **biomechanics** has been widely validated [21], using both in vivo (e.g., [44, 136, 148, 171]) and ex vivo (e.g., [22]) data from modern animals. The precision which models should be built with has also been thoroughly tested, including the choice of material properties, mesh generation and density, boundary conditions, and loading, among others (e.g., [23, 105, 132, 161, 193, 218, 227]).

Finite Element Analysis has mainly been used to evaluate the mechanical performance of the skull and jaw of a broad number of extinct and modern species; to a lesser extent, the mechanical performance of limb elements has also been assessed (Table 2). In particular, **FEA** has been performed on Mesozoic mammal cranial material, but these studies are scarce. Firstly, Gill et al., [75] analysed the biomechanical performance of the jaws of **mammaliaform stem-mammals** *Morganucodon* and *Kuehneotherium* with the aim of elucidating their dietary behaviour. A second study using **FEA**, explored how the miniaturisation of the mammalian jaw influenced the evolution of the middle ear [110]. Finally, Adams and colleagues (2019) studied the skull and jaw performance of the multituberculate *Kryptobaatar* as a means of testing the competitive exclusion hypothesis for the extinction of multituberculates [2].

1.6 Thesis aims, objectives, and chapter breakdown

1.6.1 Thesis aims

The main aim of this thesis is to infer diet in Mesozoic mammals by analysing their jaw shape and functional performance, using a combination of biomechanical techniques, **geometric morphometrics** and **phylogenetic comparative methods**. To do so, small extant mammals of

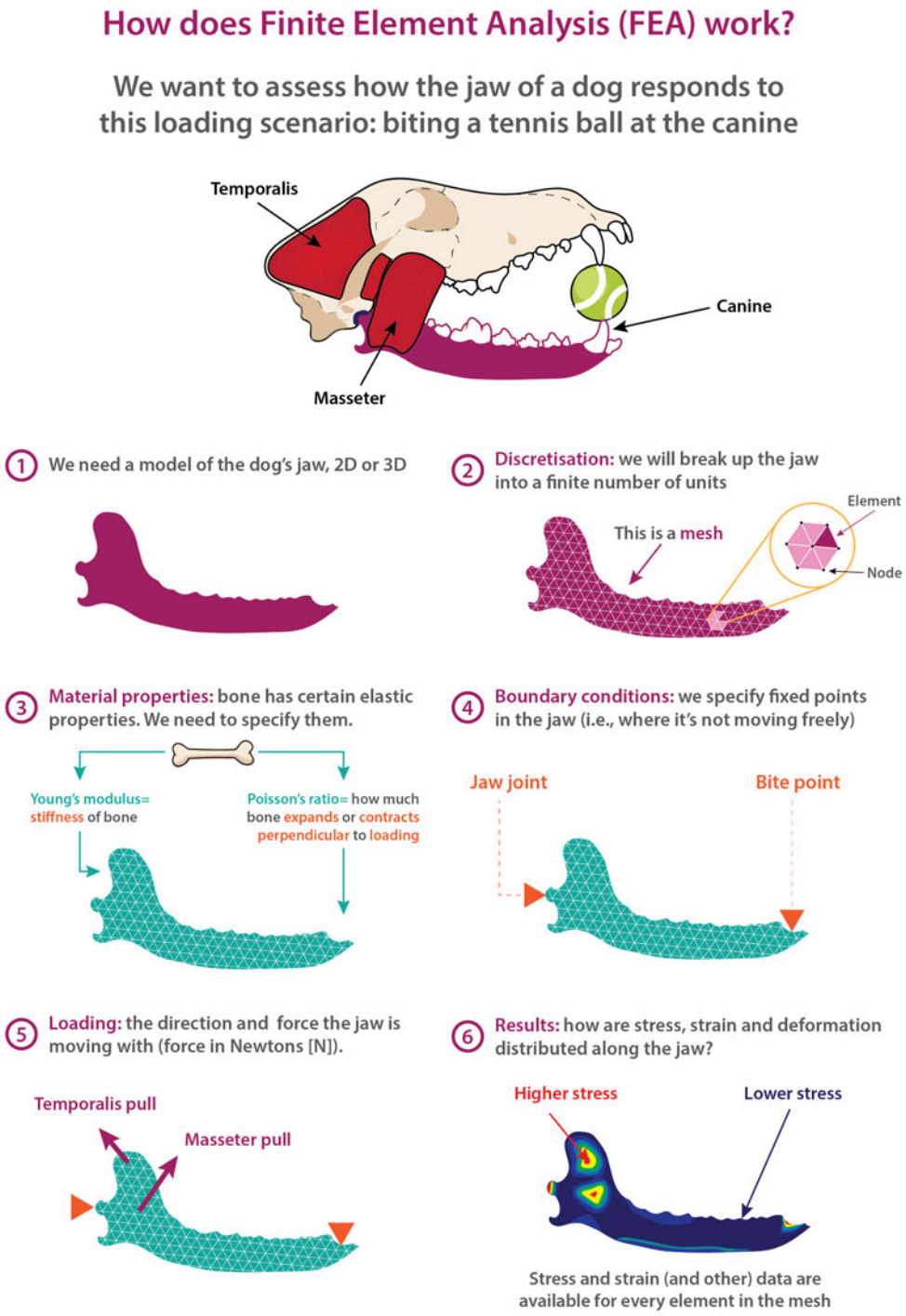

Figure 1.8: **Generalised summary of the stages of Finite Element Analysis**, using the jaw of a dog biting at the canine as an example.

Study material	Description of the study	Reference
	Extant taxa	
Skull	Mechanical performance of the skull of crocodilians	[169]
	Mastication mechanics of catarrhine primates	[192]
	Functional evolution of the feeding system of rodents	[41]
	Feeding behaviour of marmosets and tamarins	[55]
	Feeding behaviour of bats	[56]
	Feeding behaviour of bears	[212]
Jaw	Bite force capabilities of the great white shark	[242]
	Digestive physiology of ungulates	[67]
	Dietary behaviour of armadillos	[209]
	Dietary behaviour of primates	[134]
	Dietary behaviour of ungulates	[248]
	Extinct taxa	
Skull	Feeding ecology and biting capabilities of Miocene piranhas	[82]
	Dietary behaviour of capitosaurs	[71]
	Mode of life and feeding strategies of temnospondyls	[70]
	Cranial mechanics of theropods	[180–182, 184]
	Bite force and cranial biomechanics of the largest fossil rodent	[42]
	Dietary behaviour of *Australopithecus*	[219]
	Feeding behaviour of the thylacine	[241]
	Feeding behaviour of the marsupial lion	[240]
	Feeding behaviour of giant bear *Agriotherium africanum*	[158]
Jaw	Dietary behaviour of *Acanthostega* and other tetrapodomorph jaws	[155]
	Dietary behaviour of an Upper Jurassic pliosaur	[68]
	Dietary behaviour of the giant hyena-like carnivore *Dinocrocuta*	[225]
	Mechanical performance of ceratopsid dinosaur jaws	[127]
Limb elements	Hindlimb posture and locomotion in extinct tetrapods	[18]
	Hindlimb posture and locomotion in extinct theropods	[19]
	Analysis of the prey dispatching capabilities of dromaeosaurid claws	[128]
	Functional study of the tyrannosaurid arctometatarsus	[214]
Fossil trackways	Analysis of the formation of fossilised trackways	[62, 62, 135]
	Mesozoic mammals	
Skull & jaw	Skull and jaw performance of the multituberculate *Kryptobaatar*	[2]
Jaw	Dietary behaviour of *Morganucodon* and *Kuehneotherium*	[75]
	On the miniaturisation of the mammalian jaw & the evolution of the middle ear	[110]

Table 1.1: **Select examples of FEA studies in vertebrates.** Includes studies on extinct and extant taxa (highlighting those on Mesozoic mammals) focusing on either the skull, jaw, limb elements or fossilised trackways.

known diets are used as a comparative basis. This thesis aims to study diet in Mesozoic mammals because two-thirds of the evolutionary history of mammals took place during this era; therefore, understanding the ecology of these extinct mammal lineages is key to our knowledge of Mesozoic palaecommunities and underpins our knowledge of the later Cenozoic burst in mammalian diversity.

1.6.2 Thesis objectives

- **Chapter 2:**

  - To establish a relationship between jaw shape and diet in small extant mammals, using 2D **geometric morphometrics**
  - To explore the relationship between mechanical advantage and diet among extant mammals
  - To use our knowledge of how jaw shape and mechanical advantage relate to diet in extant mammals to infer the diets of Mesozoic mammals, using Principal Components Analysis and **phylogenetic comparative methods**, such as phylogenetic generalised least squares regressions

- **Chapter 3:**
  - To validate the use of the novel extruded **FE** models (i.e., simplified 3D models built from photographs) for their use in Finite Element Analysis

- **Chapter 4:**
  - To explore the relationship between jaw functional performance and diet in extant mammals using Finite Element Analysis
  - To analyse **FEA** stress output data in a comparative multivariate framework using the recently developed Intervals Method
  - To infer diet in Mesozoic mammals by comparing their jaw stress distribution with those of extant mammals of known diets.

- **Chapter 5:**
  - To discuss the findings of the previous research chapters, in terms of the contribution of this thesis to our knowledge of Mesozoic mammals and in terms of the use of biomechanical techniques for the study of mammal diets.

1.6.3 Chapter breakdown

Chapter 2 explores the relationship between jaw shape, mechanical advantage and diet in small extant mammals, with the purpose of using these data to infer diet in Mesozoic mammals. Establishing proxies for diet is our paramount importance, since ecological traits such as diet are essential for better understanding Mesozoic community dynamics. Here, jaw shape analysis is performed with 2D **geometric morphometrics**, using a combination of fixed landmarks and sliding semi-landmarks. This study is based on the paper by Grossnickle and Polly [80] and expanded to include a functional metric (i.e., mechanical advantage). The relationship between jaw shape and diet is tested in a phylogenetic context using Procrustes ANOVAs. Finally, using these two metrics, a phylogenetic flexible discriminant analysis is performed to infer probable diets in Mesozoic mammals. The results indicate that the combination of jaw shape and

mechanical advantage data is a powerful predictor of diet among small mammals and thus we can use these proxies for confidently inferring diet in Mesozoic mammals. The findings of this study corroborate the hypothesis that most Mesozoic taxa were insectivorous, but some clades (e.g., eutriconodontans) had a carnivorous diet. This chapter has been submitted for publication in *Nature Communications Biology* (Morales-García et al., 2020).

Chapter 3 presents a validation study on the use of simplified 3D jaw models for **FEA**, henceforth called "extruded **FE** models". Traditionally, 3D **FE** models are built using tomography data, which can be expensive and sometimes inaccessible. Here I devise the novel extruded **FE** models, which are relatively easy and quick to produce, and are built using only photographs in freely available software. The utility of these models was then validated using Early Jurassic mammals *Morganucodon* and *Kuehneotherium* by comparing their resulting stress and strain with those of Gill et al., [75]. I find that extruded **FE** models can closely replicate stress patterns, as well as absolute stress and strain values (in comparison to those obtained from tomography-based models), and their ease of building proves ideal for performing large scale studies. This validation study is published as **Morales-García, N. M.**, Burgess, T. D., Hill, J. J., Gill, P. G., & Rayfield, E. J. (2019). The use of extruded finite-element models as a novel alternative to tomography-based models: a case study using early mammal jaws. *Journal of the Royal Society Interface*, 16(161), 20190674.[150]

Chapter 4 presents a large-scale study on the biomechanical jaw performance of extant small mammals and Mesozoic mammals. Having validated the use of extruded **FE** models in Chapter 3, this chapter uses these models to perform **FEA**. First, I explore the relationship between stress distribution in the jaws of extant mammals and their dietary preferences, using the Intervals Method of Marcé-Nogué et al., [131]. I found that stress distribution patterns in the jaws of small mammals can distinguish between insectivores, mesocarnivores, hypercarnivores and herbivores. Having established this relationship, I compare the resulting stress distribution in the jaws of Mesozoic mammals to those of modern mammals, with the purpose of inferring the diets of the extinct taxa: most Mesozoic mammals have stress distribution patterns similar to modern insectivores and a few taxa are similar to modern placental hypercarnivores. As in Chapter 2, this study seeks to establish new proxies for diet among small mammals, in order to enrich our knowledge of Mesozoic community dynamics. Additionally, this chapter aims to identify functional traits unique to different dietary groups which can be used to not only study Mesozoic mammals, but other clades of small mammals. This study was performed in collaboration with former MSc student Kit Lam (Wilfred) Tang and has been submitted to *PLoS Biology* as **Morales-García, N. M.**, Tang, K.L., Gill, P.G., Janis, C.M., and Rayfield, E.J.

Chapter 5 presents a summary of all the key findings of the previous chapters, and explores future perspectives.

CHAPTER 2

JAW SHAPE AND MECHANICAL ADVANTAGE ARE INDICATIVE OF DIET IN MESOZOIC MAMMALS

This chapter has been accepted in *Nature Communications Biology* as: **Morales-Garcia, N.M.**, Gill, P.G., Janis, C.M., and Rayfield, E.J. 2021. Jaw shape and mechanical advantage is indicative of diet in Mesozoic mammals.

Nuria Melisa Morales co-designed the study, collected the data, ran the analyses, and wrote the manuscript. Pam Gill, Christine Janis and Emily Rayfield contributed to the design of the study, supervised the project and commented on the manuscript.

2.1 Abstract

Jaw morphology is closely linked to both diet and biomechanical performance, and jaws are one of the most common Mesozoic mammal fossil elements. Knowledge of the dietary and functional diversity of early mammals informs on the ecological structure of palaeocommunities throughout the longest era of mammalian evolution: the Mesozoic. Here, we analyse the relationship between form and function in the jaws of 70 extant and 45 extinct mammals spanning the Late Triassic-Late Cretaceous, using **geometric morphometrics** and mechanical advantage of the **masseter** and **temporalis**. In extant mammals, jaw shape discriminates well between dietary groups. Mechanical advantage values on their own are not very informative of dietary ecology. The combination of both metrics provides a clear separation between insectivores, carnivores and herbivores. This relationship is informative of diet among Mesozoic mammals. We provide an explanation for this difference in jaw shape and function, which sets the basis for future **ecomorphological** studies.

2.2 Introduction

Our understanding of Mesozoic mammals has drastically improved in the past three decades. Once thought to have been conservative in locomotory modes and dietary preferences, Mesozoic mammals are now considered to have been more ecologically diverse [30, 96, 98]. In a similar fashion, it was thought that they were restricted to small sizes (< 5 kg), but some taxa, like *Repenomamus giganticus* (approx. 12-14 kg) indicate greater body size diversity among Mesozoic mammals [88, 96, 98]. Fossils of complete skeletons reveal a diversity of locomotor lifestyles, including swimming, gliding, fossorial, and arboreal forms; craniodental morphology also indicates a diversity of diets (see [81, 113] and references therein). The majority of the evolutionary history of mammals (127 million years [65%]) took place during the Mesozoic [98], and so the study of Mesozoic mammal evolution also underpins our understanding of their later radiation. Although the most abundant remains of Mesozoic mammals are their teeth, lower jaws are also relatively common. Study of jaw shape and jaw **biomechanics** can increase our understanding of their dietary and functional evolution, and has the potential to contribute to our knowledge of the ecological structure of Mesozoic mammalian communities, in turn aiding our understanding of the prevailing vegetation and climatic conditions [30].

Ecomorphological analyses, which study potentially predictive relationships between organismal morphology and ecology (see ref. [63] for review), are one approach to the study of the dietary preferences of Mesozoic mammals. Such analyses have widely been used in mammals; in particular, the correlation of jaw morphology with dietary preferences. For example, the position of the condyle with respect to the tooth row [43]; the dimensions of the jaw (e.g., the length of the diastema and the coronoid process, and the depth of jaw ramus) [93]; and the predominance of one or other of the **adductor muscles** [233] have all been used to inform on diet. With respect to Mesozoic mammals: morphometry-driven approaches include landmark-based **geometric morphometrics** studies on jaw shape (e.g., [80]), and functionally-informed studies include analyses of jaw ratios (e.g., [16]), jaw mechanics and tooth wear [75]. For example, Grossnickle and Polly [80] compared the jaw shapes of extant and Mesozoic mammals and found a clear separation between Mesozoic herbivores (multituberculates) and those with other diets. Gill et al. [75] employed a suite of biomechanical techniques to show diverging dietary preferences in an Early Jurassic faunal assemblage, between stem mammals *Morganucodon* and *Kuehneotherium*. More recently, Grossnickle [79] analyzed a comprehensive set of functional metrics in the jaws of extant therian mammals and identified a set of characteristics distinguishing herbivorous from **faunivorous** taxa across different clades, including the size of the angular process and the length of the posterior portion of the jaw.

Here we use a combination of morphometric- and functionally-driven approaches to study the relationship between mechanical advantage (used as a proxy for adductor muscle performance) and jaw shape in Mesozoic mammals and small extant mammals. Mechanical advantage is the ratio of the length of the in-lever (i.e., lever arm of the muscle) divided by the length of the

out-lever (i.e., distance from the jaw condyle to the biting point) (see Fig. 2.3b) [75, 87], and so is a measure of the performance of the **adductor muscles** (i.e., how much force is produced at the bite point as a result of force being input by the muscles). A high mechanical advantage indicates a jaw optimized for bite force, while a low mechanical advantage indicates a jaw optimized for closure at speed. This metric has been used to study adductor muscle performance in Cenozoic mammals (including extant taxa) such as carnivorans (e.g., [5]), rodents (e.g., [27]), and bats (e.g., [201]), among others. Comparative mechanical advantage of the jaw (or a similar biomechanical metric) has been used as a proxy for prey choice and feeding ecology in stem mammals [75], to study the yaw and pitch of the jaws of Mesozoic therian mammals and relatives [78], and to analyze **ecomorphological** disparity during the Mesozoic/Cenozoic transition [16].

The aim of our study is to determine whether there is a large-scale functional relationship between shape and function in the jaws of small mammals that could be used as an **ecomorphological** proxy to elucidate the dietary preferences and behavior of Mesozoic taxa. While the jaw shapes of many multituberculates indicate a herbivorous or omnivorous diet [80], there is no clear consensus on the diets of many Mesozoic taxa typically considered as "generalized

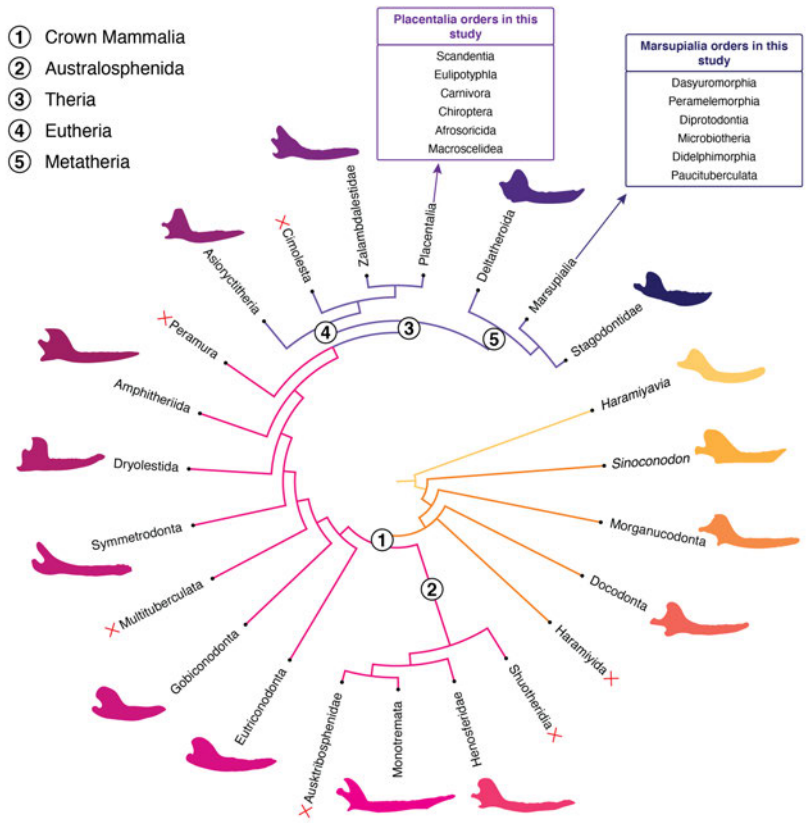

Figure 2.1: **Summary of the phylogeny used in this study**. Overall topology from refs. [38, 91]. Other references in Methods section. Red crosses indicate clades not included in the study.

insectivores". Here we include only such generalized taxa (Fig. 2.1) and exclude multituberculates and haramiyidans. We use extant taxa of small mammals of known diets to explore the relationship between jaw shape and mechanical advantage, and to evaluate suitable proxies for diet in Mesozoic mammals. A list of taxa used in this study is presented in Table 2.1.

2.3 Materials and Methods

2.3.1 Materials

For a diagram of the methods used in this paper, refer to Figure 2.2. We used photographs of the jaws of 70 small extant mammals and 45 extinct Mesozoic mammalian taxa spanning the Late Triassic to the Late Cretaceous. The full list of taxa can be seen in Table 2.1. The extant taxa chosen for this study (29 marsupials in six orders, 41 placentals in six orders) are based on those used in Grossnickle and Polly [80]; new taxa were added for greater taxonomic and dietary diversity. Following ref. [31], most extant mammals in our sample weigh under 5 kg as most Mesozoic mammals were under this body mass threshold. Five extant species over 5 kg were included in the sample (i.e., *Sarcophilus harrisii*, *Lynx rufus*, *Lontra canadensis*, *Taxidea taxus* and *Procyon lotor*) to reflect the upper body size limit of larger Mesozoic mammals such as *Repenomamus* (12 to 14 kg, [88]).

For this study, we chose to exclude the Mesozoic haramiyids and multituberculates, and only to focus on non-**allotherian** Mesozoic taxa. Grossnickle and Polly [80] had previously determined that the jaw shape of multituberculates is different from other non-allotherian Mesozoic mammals. We attempted to include allotherians of different diets in the sample, but they all plotted in their own area of **morphospace**, far away from other non-**allotherian** Mesozoic mammals. They were also dissimilar to any extant mammals in our sample (Fig. A.5). Compared to non-allotherian Mesozoic mammals and extant mammals of different diets, multituberculates and haramiyids had higher mechanical advantage values, which skewed posterior analyses and prevented us from seeing clear differences between dietary groups among extant mammals (Fig. A.9). Allotherians have a very derived jaw morphology, dissimilar to other Mesozoic mammals and extant small mammals, they also had palinal jaw movements, unlike any other extant or extinct mammal [103], which could lead to a unique biomechanical biting performance. Therefore, we decided to exclude allotherians from this sample, with the exception of *Haramiyavia*, which is probably not closely related to later Jurassic euharamiyids, following ref. [99].

Photographs of extant mammal jaws were obtained from the online databases: Animal Diversity Web (ADW) of the University of Michigan [153] (https://animaldiversity.org), the Natural History Museum (NHM) online database (https://data.nhm.ac.uk) and the Field Museum online database (https://collections-zoology.fieldmuseum.org). For a detailed list of the extant mammal specimens used in this study refer to Table 2.1 and S2 Data. All photographs were reviewed by NMMG to ensure the jaws were all captured in the same orientation; some photographs were

rotated in order to have the horizontal ramus of the jaw parallel to the x axis.

The extinct taxa considered in this study include ten stem mammals, 19 **non-therian crown mammals**, and 16 **therian-crown mammals**. Photographs were primarily obtained from the literature (for a full list of the literature used to source these photographs refer to Supplementary Data 1). Additionally, photographs were taken from specimens held at the Institute of Paleobiology, Polish Academy of Sciences (Warsaw, Poland), at the Oxford University Museum of Natural History (Oxford, United Kingdom), at the Natural History Museum (London, United Kingdom), and at the Steinmann Institut, Universität Bonn (Bonn, Germany). Photographs were taken by NMMG.

Dietary information for extant taxa was obtained from the Animal Diversity Web [153]. Proposed dietary preferences for Mesozoic mammals were obtained from the literature. The full list of taxa, their dietary preferences, and the detailed sources of this information can be seen in Tables A.1, A.2 and A.3 in Appendix A and in S2 Data. While no Mesozoic mammals specialized for herbivory (i.e., some multituberculates and haramiyidans) were included in our sample, we decided to include some extant herbivores whose jaw morphology is not as derived as that of rodents for comparative purposes.

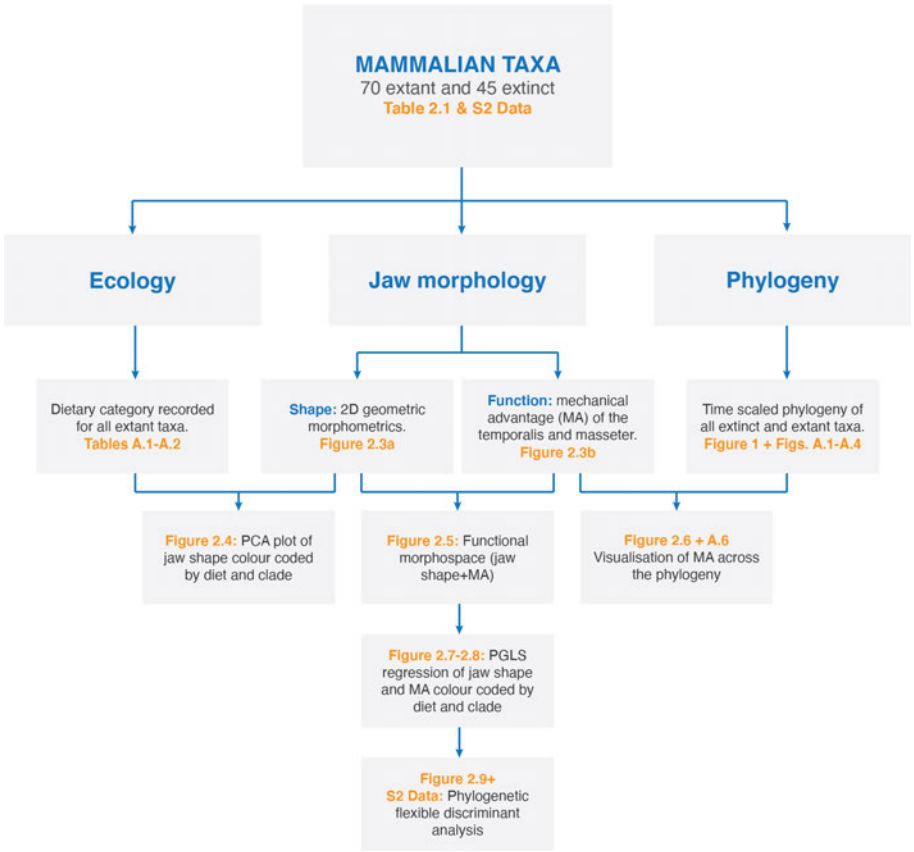

Figure 2.2: **Summary of the methods, figures and tables presented in this paper.**

Extinct mammals		Extant mammals			
Stem mammals		Marsupialia		Placentalia	
1	*Haramiyavia*	***Diprotodontia***		***Scandentia***	
2	*Sinoconodon*	46	*Bettongia penicillata*	75	*Tupaia splendidula*
3	*Morganucodon*	47	*Potorous tridactylus*	76	*Tupaia dorsalis*
4	*Dinnetherium*	48	*Thylogale billardierii*	77	*Tupaia glis*
5	*Castorocauda*	49	*Dendrolagus goodfellowi*	***Carnivora***	
6	*Haldanodon*	50	*Dorcopsulus vanheurni*	78	*Nandinia binotata*
7	*Docofossor*	51	*Petaurus breviceps*	79	*Leopardus wiedii*
8	*Docodon*	52	*Pseudocheirus peregrinus*	80	*Lynx rufus*
9	*Agilodocodon*	53	*Acrobates pygmaeus*	81	*Felis margarita*
10	*Microdocodon*	54	*Phalanger orientalis*	82	*Prionodon pardicolor*
Non-therian crown mammals		55	*Trichosurus vulpecula*	83	*Genetta genetta*
11	*Fruitafossor*	***Dasyuromorphia***		84	*Paradoxurus hermaphroditus*
12	*Henosferus*	56	*Dasyurus hallucatus*	85	*Fossa fossana*
13	*Teinolophos*	57	*Dasyurus geoffroii*	86	*Galidia elegans*
14	*Phascolotherium*	58	*Sarcophilus harrisi*	87	*Crossarchus oscurus*
15	*Yanoconodon*	59	*Parantechinus apicalis*	88	*Herpestes javanicus*
16	*Triconodon*	60	*Phascogale tapoatafa*	89	*Lycalopex griseus*
17	*Trioracodon*	61	*Antechinus swainsonii*	90	*Vulpes corsac*
18	*Volaticotherium*	62	*Antechinus flavipes*	91	*Mephitis macroura*
19	*Argentoconodon*	63	*Sminthopsis crassicaudata*	92	*Conepatus humboldtii*
20	*Gobiconodon*	64	*Planigale ingrami*	93	*Nasua narica*
21	*Repenomamus*	65	*Myrmecobius fasciatus*	94	*Bassaricyon gabbii*
22	*Spalacotherium*	***Peramelemorphia***		95	*Procyon lotor*
23	*Origolestes*	66	*Perameles gunnii*	96	*Taxidea taxus*
24	*Zhangheotherium*	***Microbiotheria***		97	*Eira barbara*
25	*Maotherium*	67	*Dromiciops gliroides*	98	*Lontra canadensis*
26	*Crusafontia*	***Didelphimorphia***		99	*Mustela nivalis*
27	*Amblotherium*	68	*Philander andersoni*	***Chiroptera***	
28	*Amphitherium*	69	*Chironectes minimus*	100	*Pteropus vampyrus*
29	*Vincelestes*	70	*Metachirus nudicaudatus*	101	*Noctilio leporinus*
Therian crown-mammals		71	*Marmosa robinsoni*	102	*Artibeus jamaiciensis*
30	*Deltatheridium*	72	*Monodelphis americana*	103	*Chrotopterus auritus*
31	*Didelphodon*	73	*Caluromys derbianus*	104	*Myotis lucifugus*
32	*Eodelphis*	***Paucituberculata***		105	*Plecotus auritus*
33	*Alphadon*	74	*Rhyncholestes raphanurus*	***Eulipotyphla***	
34	*Sinodelphys*			106	*Blarina brevicauda*
35	*Juramaia*			107	*Atelerix albiventris*
36	*Eomaia*			108	*Parascalops breweri*
37	*Maelestes*			109	*Solenodon paradoxus*
38	*Asioryctes*			***Afrosoricida***	
39	*Sasayamamylos*			110	*Microgale cowani*
40	*Kennalestes*			111	*Microgale brevicaudata*
41	*Daulestes*			112	*Tenrec ecaudatus*
42	*Uchkudukudon*			113	*Potamogale velox*
43	*Kulbeckia*			***Macroscelidea***	
44	*Barunlestes*			114	*Elephantulus rufescens*
45	*Zalambdalestes*			115	*Elephantulus brachyrhynchus*

Table 2.1: **Complete list of all the taxa used in this study.** Taxa numbers used in Figures 2.4, 2.7, and 2.8

2.3.2 Methods

2.3.2.1 Phylogenetic Information

We built a phylogeny in Mesquite incorporating all the taxa used in this study (see the Figs. A.1, A.2, A.3, and A.4. The overall topology of the phylogeny of the Mesozoic taxa was from refs. [38, 91]; additional sources were used to refine the position of *Haramiyavia* [99], and the phylogenetic relationships within Morganucodonta [146] Docodonta [247], Australosphenida [197], Eutriconodonta [73, 113], Symmetrodonta [129], Dryolestidae [11], Metatheria [237], and Eutheria [7, 8, 17, 106]. Similarly, the overall topologies of the Placentalia and Marsupialia phylogenies were obtained from refs. [215] and [137], respectively. Supporting literature was needed to account for all taxa included within Scandentia [190], Carnivora [157], Chiroptera [3], Eulipotyphla [216], and Afrosoricida [208].

The phylogeny was time-scaled using the 'equal' method of Brusatte et al., [24] using the package 'paleotree' 3.3.0 [13] in RStudio 1.2.1335 (RStudio team). Appearance dates for extinct taxa were obtained from the Paleobiology Database (http://fossilworks.org) and ref. [197]. Divergence dates to constrain the nodes were obtained from a diversity of phylogenies of Mesozoic taxa [38, 91, 99], Marsupialia [137], Scandentia [190], Carnivora [157], Chiroptera [3], Eulipotyphla [216], Afrosoricida [172] and Macroscelidea [213].

2.3.2.2 Geometric Morphometrics

We performed a 2D **geometric morphometrics** study using fixed landmarks and sliding semi-landmarks in the jaws of small extant and extinct Mesozoic mammals. We used the same fixed landmarks as Grossnickle and Polly [80], with the exception of landmark 7 (i.e., posteroventral-most point of the angular process). We removed this from our analysis because many taxa in our study did not have an angular process. Additionally, we incorporated 58 sliding semi landmarks as seen in Figure 2.3. All jaws were landmarked using TPS software by Rohlf [191]: tpsUtil was used in the construction of a file containing all images to landmark, tpsDig was used to digitize landmarks and semi-landmarks, and tpsRELW was used for Procrustes alignment and relative warp analysis. The resulting XY coordinates for the extant data were submitted to a Principal Components Analysis (**PCA**) in RStudio, using the package 'geomorph' [1]; convex hulls were drawn to indicate the **morphospace** occupation of the different dietary categories. The Mesozoic mammal jaw shape data was then projected onto the extant mammal morphospace by multiplying their XY coordinates by the PC variable loadings of the extant taxa (i.e., PC rotation scores).

2.3.2.3 Mechanical Advantage

We measured the moment arms of resistance at the **m1** and at the anterior end of the jaw, as well as the lever arms of the **temporalis** and **masseter** muscles in ImageJ following Figure 2.3

(modified from ref. [5]); these measurements roughly estimate the lever arms of both superficial and deep heads of the adductor muscles of the jaw. The lever arm of the medial pterygoid muscle, although not considered here, is probably very similar to that of the masseter. The approach taken here represents an oversimplification of muscle architecture and does not take into consideration any features of skull morphology that might change the lever arms of the adductor muscles. We calculated the mechanical advantage of the **adductor muscles** as follows: lever arm of the muscle divided by the moment arm of resistance at the bite point (**m1** or jaw tip). A limitation of this technique lies on its 2D approach: using this method, we can only calculate the lever arms for pitch rotation, while any three-dimensional movement of the jaw (i.e., jaw or roll) cannot be quantified). Additionally, these measurements assume that the position of the pitch axis of rotation is at the jaw joint in all taxa.

2.3.2.4 Data visualisation

Jaw shape and mechanical advantage were plotted together in a morphofunctional landscape in MATLAB R2019a 9.6.0 (The MathWorks, Inc., Natick, Massachusetts) following a protocol from Dr. J. A. Bright and previously used in Navalón et al., [154]. Mechanical advantage values were plotted on a phylogeny of the taxa of interest using the package 'phytools' version 0.6.99 [185] in RStudio.

2.3.2.5 Statistical and phylogenetic comparative methods

Statistical analyses follow Navalón et al., [154] who quantitatively tested the relationship between beak shape, mechanical advantage and feeding ecology in modern birds. In order to test for significant differences in jaw shape between dietary groups, Procrustes **ANOVAs** were run in R using the package geomorph 3.1.2 [1]. Phylogenetic Generalized Least Squares (**PGLS**) regressions were run in R using the package geomorph 3.1.2 [1] to test the relationship between jaw shape and mechanical advantage in a phylogenetic context. One way **PERMANOVAs** were run in PAST 3.24 [84] to test for significant differences between dietary groups on the basis of their mechanical advantage values.

A phylogenetic flexible discriminant analysis (phylo **FDA**) was performed following ref. [152]. We performed this analysis to determine the posterior probability of the Mesozoic taxa of belonging to one of our established dietary categories (i.e., herbivore, carnivore or insectivore), while considering their phylogenetic relationships. Extant omnivores were not included in this study because of their large dietary variability. The analysis was performed in R Studio 1.2.1335 using the packages ape 5.3 [163], class 7.3-15 [189], geiger 2.0.62 [166], lattice 0.20-38 [204], mda 0.4-10 [86], nnet 7.3-12 [189], using the source data (phylo.fda.v0.2.R) of ref. [152]. This analysis was performed by using the scores obtained from the **PGLS** regressions, for both muscles (**MAM** and **MAT**) and biting points (**m1** and jaw tip).

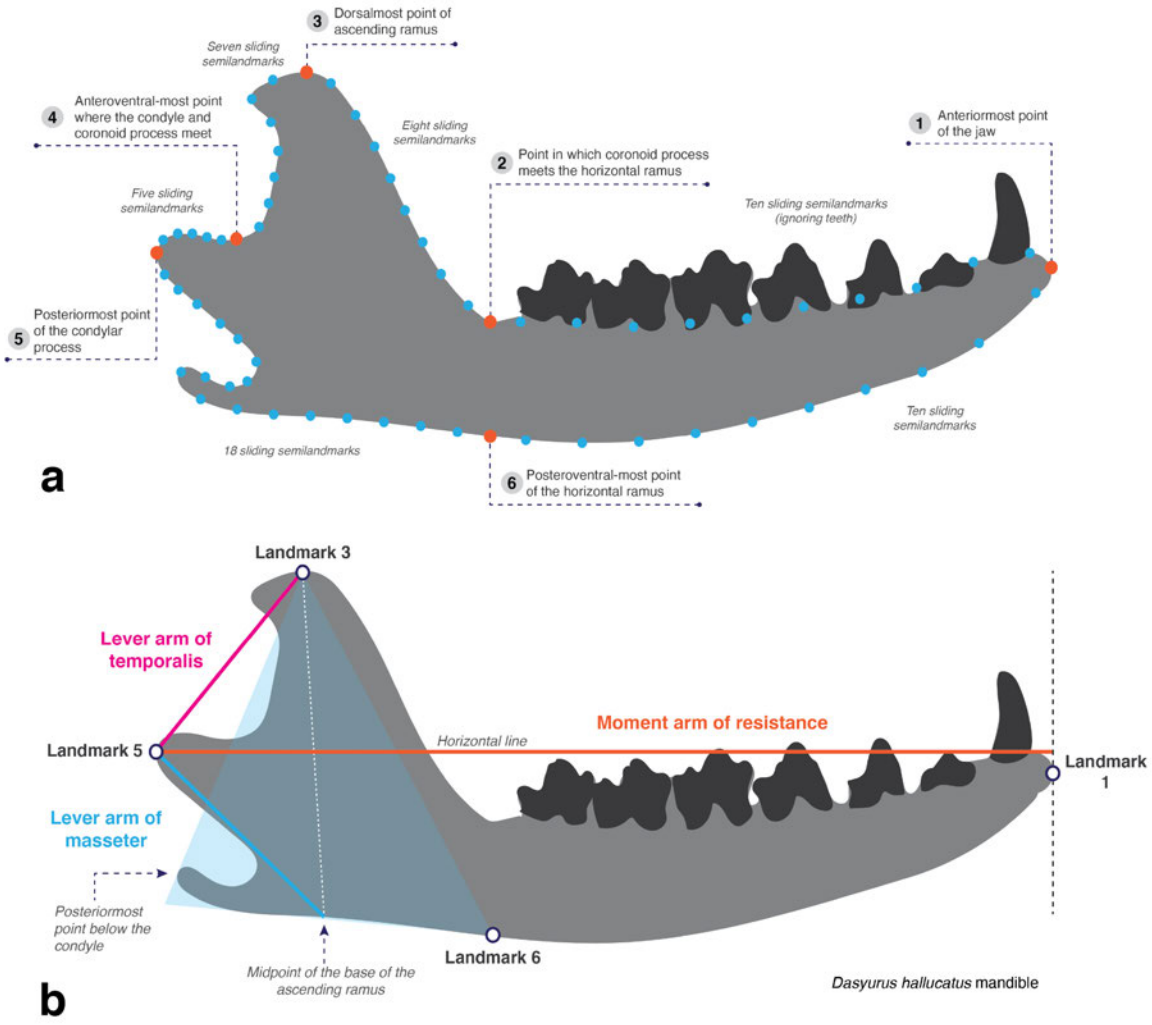

Figure 2.3: **Data acquired from the jaws of Mesozoic and extant small mammals.** A) Jaw landmarking regime used in this study. Modified from [80]. In orange: 6 fixed landmarks; in blue: 58 sliding semi landmarks. B) Lever and moment arm measurements taken in this study. Modified from [5].

2.4 Results

2.4.1 Jaw shape variation and diet in small mammals

Using 2D **geometric morphometrics** (Fig. 2.3a), we found that jaw shape is a good proxy for diet among small extant mammals. In Figure 2.4, taxa with negative PC1 scores have shorter jaws, and taxa with positive PC1 scores have longer jaws; taxa with positive PC2 scores have taller ascending rami and taxa with negative PC2 scores have shorter ascending rami. Among extant mammals, most dietary categories (excluding omnivores) can be distinguished along PC1

(Fig. 2.4a): herbivores plot at the negative end of PC1, insectivores towards the positive end, and carnivores in between. These categories are also statistically different from each other (Table 2.2), showing that jaw shape can distinguish between most major dietary types. However, our data cannot distinguish between carnivores and omnivores.

Data on the jaw shape of Mesozoic mammals were projected onto the extant taxa **morphospace** (Fig. 2.4b). In order to determine whether jaw shape could be used as a dietary proxy in Mesozoic mammals, we obtained previous independent determinations of likely diets, which variously employed dental morphology, tooth wear facets and body size (e.g., [20, 30, 39, 75, 80, 94, 98, 124, 167, 194, 195, 207, 235]). We saw a very good correspondence between previous proposed diets for Mesozoic mammals and their position on the **morphospace**.

2.4.1.1 Stem mammals

Most stem mammals plot within the **morphospace** of extant insectivores and have positive PC1 scores. One exception is *Sinoconodon* (taxon #2, Fig. 2.4), which plots in the morphospace of extant carnivores; *Sinoconodon* is considered a carnivore based on dental morphology [113]. *Haramiyavia* (#1) is thought to have been a plant-dominated omnivore [117] based on dental morphology, but here it plots within the morphospace of extant insectivores. Both morganucodontans in this study, *Morganucodon* (#3) and *Dinnetherium* (#4), have similar PC1 scores to extant insectivores, echoing the findings of Gill et al. [75].

Molar morphology indicates omnivorous or **faunivorous** diets for docodontans; here they mostly plot within the **morphospace** of extant insectivores, with the exception of *Haldanodon* (#6) and *Docofossor* (#7). *Agilodocodon* (#9) was previously considered a plant-dominated omnivore, with exudativorous dental features which indicated a diet mainly composed of plant sap [146]; more recently, Wible and Burrows [234] contradicted this hypothesis and suggested that the teeth of *Agilodocodon* most closely resemble those of extant insectivores. Here, *Agilodocodon* plots firmly within the morphospace of extant insectivores, close to the insectivorous dusky antechinus (*Antechinus swainsonii*, #61) and the elephant shrews (*Elephantulus rufescens* [#114] and *E. brachyrhynchus* [#115]), which are insect-dominated omnivores.

According to Ji et al., [94] the swimming **docodontan**, *Castorocauda* (#5), has dental features

		Carnivore vs		Herbivore vs		Insectivore vs
Statistic	**Herbivore**	**Insectivore**	**Omnivore**	**Insectivore**	**Omnivore**	**Omnivore**
R^2	0.15795	0.1455	0.03417	0.25987	0.06404	0.06499
F	4.1266	4.5973	1.6628	6.6712	2.6686	3.0582
Z	3.0431	3.0556	1.2966	3.4824	2.1976	2.4708
P	**0.003**	**0.001**	0.098	**0.001**	**0.017**	**0.005**

Table 2.2: **Summary of the Procrustes ANOVA (Type II, Conditional SS) performed for jaw shape data as a function of dietary group.** Significant p values (<0.05) in **bold** letters.

indicative of feeding on aquatic invertebrates and small vertebrates, like fish. *Castorocauda* is often depicted as being carnivorous and, particularly, piscivorous [30, 94, 146]. The jaw shape of *Castorocauda* is similar to that of modern day insectivores, supporting the notion of this **docodon-**

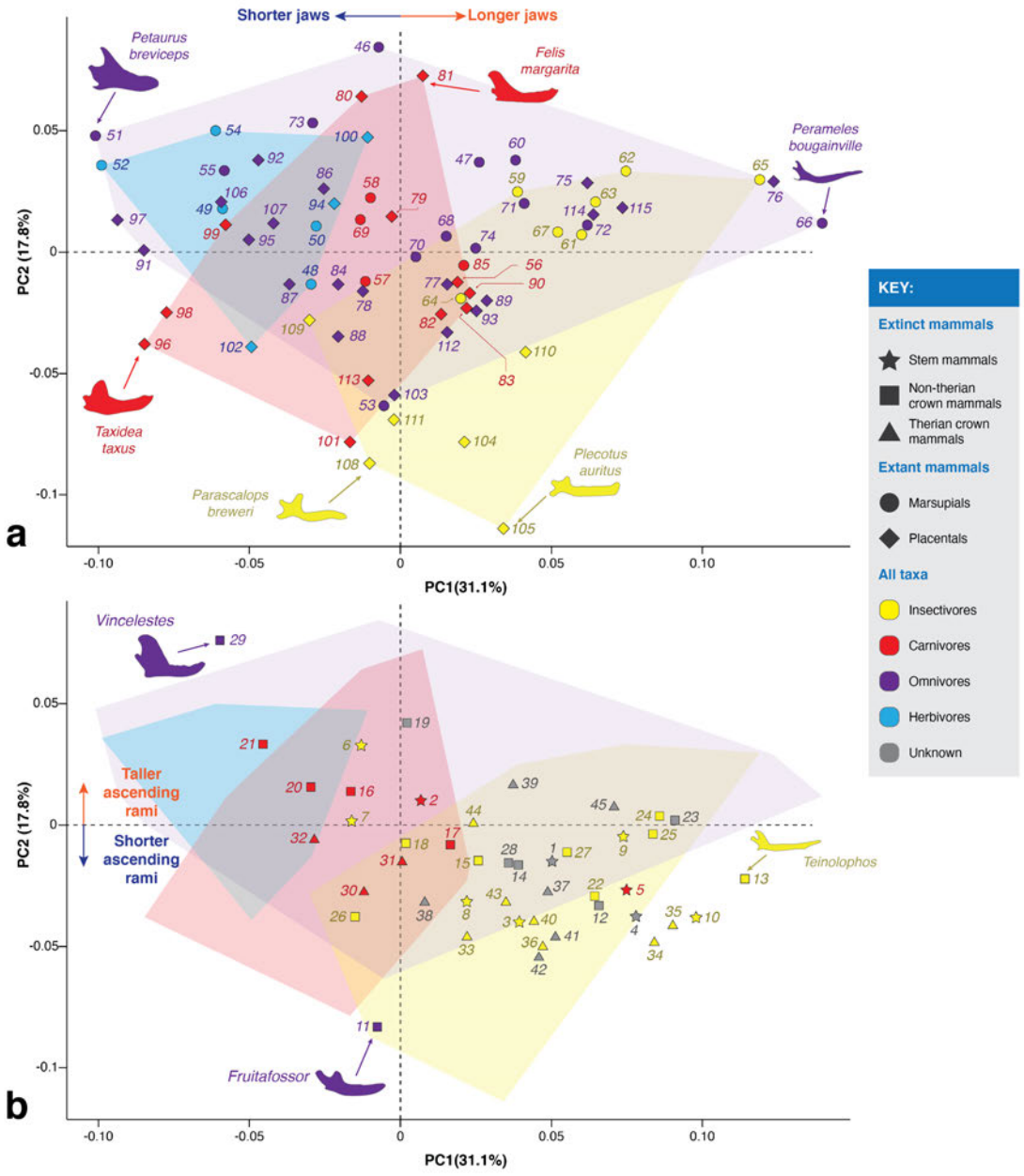

Figure 2.4: **Scatter plots of the Principal Component Analysis (PCA) results (PC1 vs PC2).** a) Extant taxa, b) Extinct taxa. Convex hulls shown for extant insectivores (yellow), carnivores (red), omnivores (purple) and herbivores (blue). Icon colours indicate known dietary categories of extant mammals and suggested dietary categories for Mesozoic mammals (obtained from the literature). See Table 2.1 for taxon names.

tan feeding on aquatic invertebrates (Fig. 2.4). The other Mesozoic semiaquatic mammal in our sample, *Teinolophos* (#13), plots in a similar area of the **morphospace** to *Castorocauda*. Our extant sample also includes a semiaquatic carnivore, the water opossum (*Chironectes minimus*, #69), which plots in the middle of the carnivore morphospace, far away from *Castorocauda* and *Teinolophos*.

Docofossor (#7) has skeletal features indicative of a fossorial lifestyle and a dentition similar to those of extant mammals foraging underground, such as moles, solenodons, and tenrecs [123]. This **docodontan** has previously been considered an insectivore [30]. Here, *Docofossor* plots within the **morphospace** of extant carnivores; however, it plots close to the burrowing Hispaniolan solenodon (*Solenodon paradoxus*, #109), which has an insectivorous diet. Among the extant insectivores in our sample, the burrowing vermivores (e.g., the hairy-tailed mole, *Parascalops breweri* [#108], and the Hispaniolan solenodon) have more negative PC1 scores than other insectivores (similar to that of *Docofossor*), and their PC1 values are more similar to those of carnivores.

The dental morphology of *Haldanodon* (#6) is indicative of an insectivorous diet. Here, it plots within the carnivore **morphospace** (very near extant herbivores), because of its tall coronoid process and comparatively shorter jaw. *Docodon* (#8) likely ate insects and other small invertebrates [167] and, based on its diminutive size [247], *Microdocodon* (#10) was probably insectivorous. Both of these docodontans plot within the insectivore morphospace.

2.4.1.2 Non-therian crown mammals

The jaw shape of **non-therian crown mammals** varies widely, plotting mostly within the **morphospace** of insectivores and carnivores. *Fruitafossor* (#11), a fossorial mammal with teeth similar to extant armadillos, has been considered an omnivore eating insects, small invertebrates and some plants [124]. Here, it plots within the insectivore morphospace, closely to the insectivorous and fossorial hairy-tailed mole (*Parascalops breweri*, #108), and shares similar PC1 scores with other fossorial taxa, such as *Docofossor* (#7) and the Hispaniolan solenodon (#109).

Extant monotremes eat insects and other small invertebrates. It has been proposed that the Early Cretaceous monotreme *Teinolophos* (#13) had a semi-aquatic lifestyle and ate in a similar manner to the insectivorous *Kuehneotherium* [186]. Here, *Teinolophos* and the australosphenidan *Henosferus* (#12), have PC1 scores similar to insectivores and omnivores.

The eutriconodontans are a very diverse group of insectivores and carnivores which had a wide range of body sizes, including some of the largest Mesozoic mammals known [97]. Here all eutriconodontans fall within or very close to the extant carnivore **morphospace**. In particular, *Triconodon* (#16) and *Argentoconodon* (#19) plot within the carnivore morphospace, *Trioracodon* (#17) and *Volaticotherium* (#18) plot between the carnivore and insectivore morphospace, and *Yanoconodon* (#15) plots within the insectivore morphospace. Both gobiconodontids, *Gobiconodon* (#20) and *Repenomamus* (#21), have more negative PC1 scores and plot closer to the herbivore

morphospace, but still remain within or close to the carnivore morphospace. *Triconodon*, *Trioracodon*, *Gobiconodon* and *Repenomamus* are all considered carnivores based on craniodental morphology and body size [30, 98, 195]; additionally, there is direct evidence for the carnivorous diet of *Repenomamus* from fossilized stomach contents [88]. *Yanoconodon* and *Volaticotherium* are considered insectivores[30].

Symmetrodontans like *Spalacotherium* (#22), *Zhangheotherium* (#24) and *Maotherium* (#25) have often been considered insectivores based on their craniodental morphology [30, 98]. Here, all symmetrodontans plot within the insectivore **morphospace**. Dryolestids are also commonly considered insectivorous [98, 207]. Here, *Crusafontia* (#26) plots between the morphospace of extant carnivores and insectivores, while *Amblotherium* (#27) plots within the insectivore morphospace. *Vincelestes* (#29) has previously been considered a carnivore on the basis of jaw shape [80]. Here, it plots near the morphospaces of both omnivores and herbivores. Bonaparte [20] considered the incisor wear of *Vincelestes* reminiscent of Cenozoic carnivores, and Rougier [194] considered its jaw morphology indicative of a forceful bite enabling the incorporation of tough plant matter into a primarily carnivorous/insectivorous diet.

2.4.1.3 Therian crown mammals

While extant marsupials have a large diversity of diets, including herbivory, extinct **metatherians** are considered to have been limited in diet to insectivory and carnivory. Their jaw shape is very similar to that of extant carnivores and insectivores (Fig.2.4). Dental morphology indicates that *Eodelphis* (#32) and *Deltatheridium* (#30) were carnivores, *Didelphodon* (#31) durophagous or molluscivorous [39, 195], and *Alphadon* (#33) has been considered to be insectivorous, on the basis of its jaw shape and body size[80]. Here, *Eodelphis*, *Deltatheridium* and *Didelphodon* plot closely to the extant carnivores, while *Alphadon* plots closely to the extant insectivores.

Extant placentals also have a wide range of diets, but many of the extinct **eutherians** in this study (i.e., *Sinodelphys* [#34], *Juramaia* [#35], *Eomaia* [#36], *Kennalestes* [#40], *Barunlestes* [#44] and *Kulbeckia* [#43]) are considered insectivorous [30, 80]. Here, we corroborate this hypothesis (Fig. 2.4): all extinct eutherians plot within the insectivore **morphospace**, with the exception of *Asioryctes* (#38) which plots in the insectivore/carnivore morphospace, and *Juramaia* and *Sinodelphys*, which plot just outside the insectivore morphospace.

2.4.2 Mechanical advantage of the jaws of small mammals

We obtained mechanical advantage (**MA**) data to test whether extant mammals of different dietary groups have distinct MA values: while many dietary groups are statistically different from each other (Table 2.3), mechanical advantage values on their own do not obviously correspond to a particular dietary category. The mechanical advantage of the jaws was standardized across all jaws to account for differences in jaw morphology (e.g., presence or absence of the angular process) (Fig. 2.3b); the outlever was measured at the anterior end of the jaw and at the first lower molar

(**m1**). When measuring mechanical advantage at the jaw tip and considering extant taxa only, we find statistically significant differences in the mechanical advantage of the **masseter** (**MAM**) values in all pairwise dietary combinations except for carnivore-insectivore (Table 2.2). The mechanical advantage of the **temporalis** (**MAT**) is statistically distinct only between herbivores and insectivores, and carnivores and insectivores (Table 2.3). Herbivores and carnivores do not have statistically distinct MAT values. This may differ in a sample of larger (> 5kg) therians. When measuring the outlever at the m1, we find statistically significant differences in all pairwise comparisons of MAM between dietary groups, except for herbivore-omnivore and carnivore-insectivore. When considering MAT, we only find significant differences between omnivores and carnivores, insectivores and herbivores, and insectivores and carnivores.

	Measured at jaw tip			
	MAM			
F=6.664	**Insectivore**	**Herbivore**	**Omnivore**	**Carnivore**
Insectivore				
Herbivore	**0.001**			
Omnivore	**0.0295**	**0.04**		
Carnivore	0.7612	**0.0006**	**0.0309**	
F=3.314	**MAT**			
Insectivore				
Herbivore	**0.0045**			
Omnivore	0.2725	0.0847		
Carnivore	**0.0048**	0.4721	0.1139	
	Measured at m1			
	MAM			
F=6.813	**Insectivore**	**Herbivore**	**Omnivore**	**Carnivore**
Insectivore				
Herbivore	**0.0011**			
Omnivore	**0.0008**	0.189		
Carnivore	0.0603	**0.0093**	**0.0817**	
F=3.817	**MAT**			
Insectivore				
Herbivore	**0.0197**			
Omnivore	0.1682	0.3622		
Carnivore	**0.0022**	0.3922	**0.0376**	

Table 2.3: **Pairwise *p* values (uncorrected significance) of one way PERMANOVAs of the mechanical advantage values of the masseter (MAM) and temporalis (MAT) obtained in this study on extant taxa of known dietary preferences only (permutation N=9999).** Significant p values (<0.05) in **bold** letters.

With respect to mechanical advantage (measured at the jaw tip) and shape, our results show that generally, shorter jaws (negative PC1) have higher mechanical advantage and longer jaws

have lower mechanical advantage, as predicted by the lever-like nature of the system (Figs. 2.5a and 2.5b). Comparing Figs. 2.4 and 2.5, we can see that taxa with negative PC1 scores (i.e., those with shorter jaws and high **MA**) are largely herbivores and carnivores, while taxa with positive PC1 scores (i.e, those with longer jaws and low MA) are typically insectivores. Mesozoic mammals largely plot in areas of **morphospace** with low to intermediate **MAM** and **MAT**, with some exceptions (Fig. 2.5). For example, *Vincelestes* has some of the highest MAM and MAT values, congruent with an omnivorous diet consisting of meat and hard plant matter (or possibly durophagy) [20, 194], and putative carnivorous taxa, such as *Triconodon* and *Repenomamus*, have high MAT values congruent with their proposed diets (Fig. 2.4b) [88, 196].

Fig. 2.6 shows the mechanical advantage of the **masseter** (left) and **temporalis** (right), measured at the jaw tip, in a phylogenetic context (see also Fig. A.6 for individual taxon names). Phylogeny seems to play a large role on the mechanical advantage and diet of the jaws of small mammals.

Most Mesozoic taxa have low (blue) to intermediate (green) **MAM** values. Most stem mammals have intermediate (green) to high (red) MAM values and **non-therian crown mammals** have low MAM values, with the exception of *Fruitafossor* and *Vincelestes*, which has the highest MAM value of all taxa (both extinct and extant). Most **eutherians**, both extinct and extant, have intermediate to low MAM values, with the exception of the relatively high values (yellow to orange) seen in elephant shrews (order Macroscelidea) and the four-toed hedgehog (order Eulipotyphla, *Atelerix albiventris*). Some members of the orders Carnivora (including canids and euplerids) and Afrosoricida have some of the lowest MAM values. Metatherians have MAM values ranging from low to intermediate (in the orders Dasyuromorphia and Didelphimorphia, as well as in the Mesozoic **metatherians**) to some of the highest in the order Diprotodontia (e.g., the sugar glider [*Petaurus breviceps*], the woylie [*Bettongia penicillata*], the cuscus [*Phalanger orientalis*]).

Most taxa have intermediate **MAT** values (Fig. 2.6, A.6). Very low MAT values are seen in the extinct non-therian crown mammals *Teinolophos* and *Zhangheotherium* and a few extant taxa, including marsupials like the Western barred bandicoot (*Perameles bougainville*) and the numbat (*Myrmecobius fasciatus*), and placentals such as the striped treeshrew (*Tupaia dorsalis*) and the short-snouted elephant shrew (*Elephantulus brachyrhynchus*). The highest MAT values belong to members of the order Carnivora, including skunks (*Mephitis macroura* and *Conepatus humboldtii*), the least weasel (*Mustela nivalis*) and the tayra (*Eira barbara*). Some diprotodontians like the common ringtail possum (*Pseudocheirus peregrinus*) and the sugar glider (*Petaurus breviceps*) also have relatively high MAT values. Some extinct taxa also have relatively high MAT values, including the stem mammal *Docofossor*, and the non-therian crown mammals, *Triconodon* and *Vincelestes*.

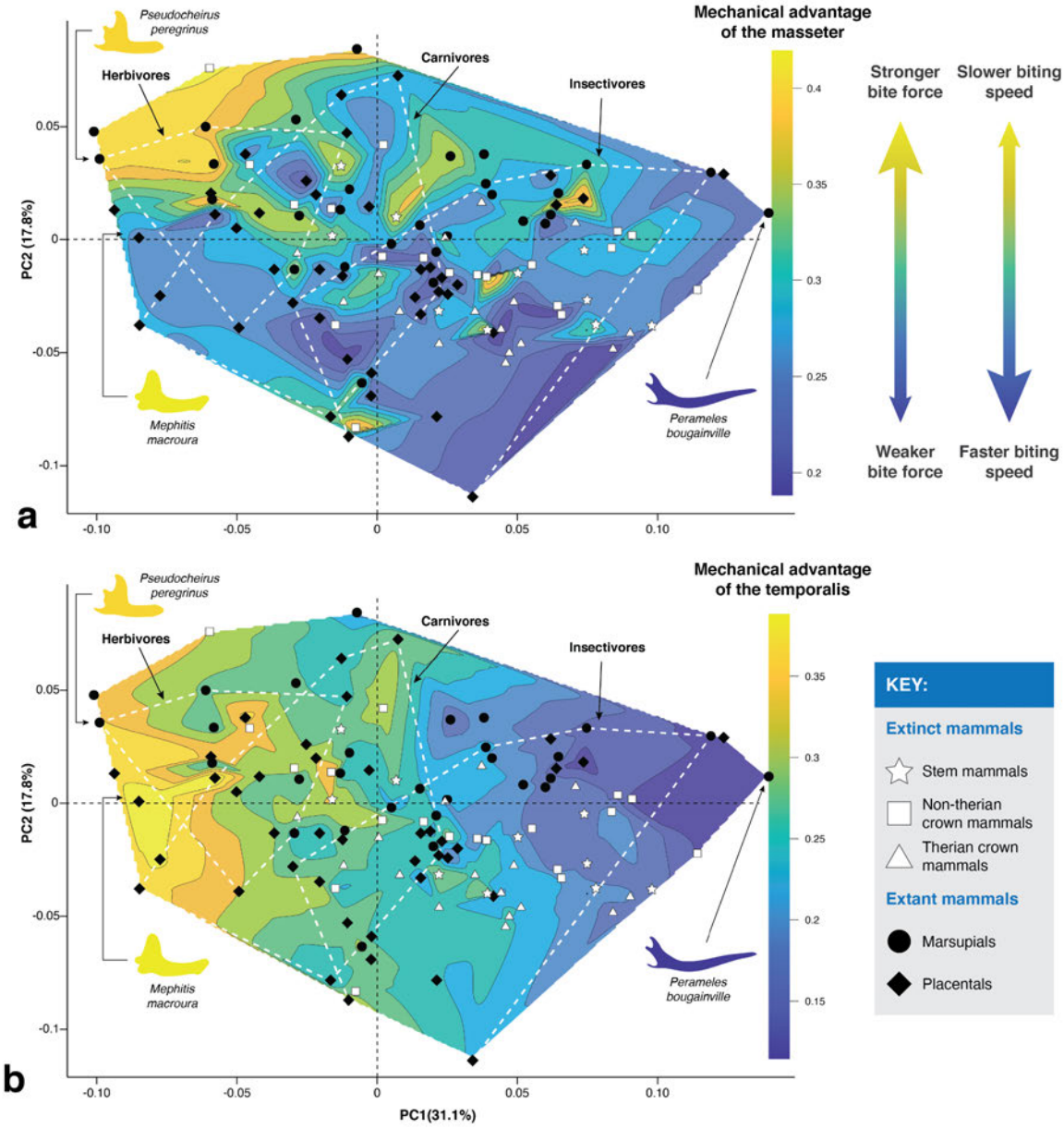

Figure 2.5: **Morphofunctional landscape comparing a functional metric (i.e., mechanical advantage of the masseter [a, MAM] and temporalis [b, MAT] when biting at the anterior end of the jaw) with jaw shape (PC1 and PC2 axes).** Silhouette colours are indicative of the mechanical advantage values of the taxa. Convex hulls in dashed lines as in Fig. 2.4

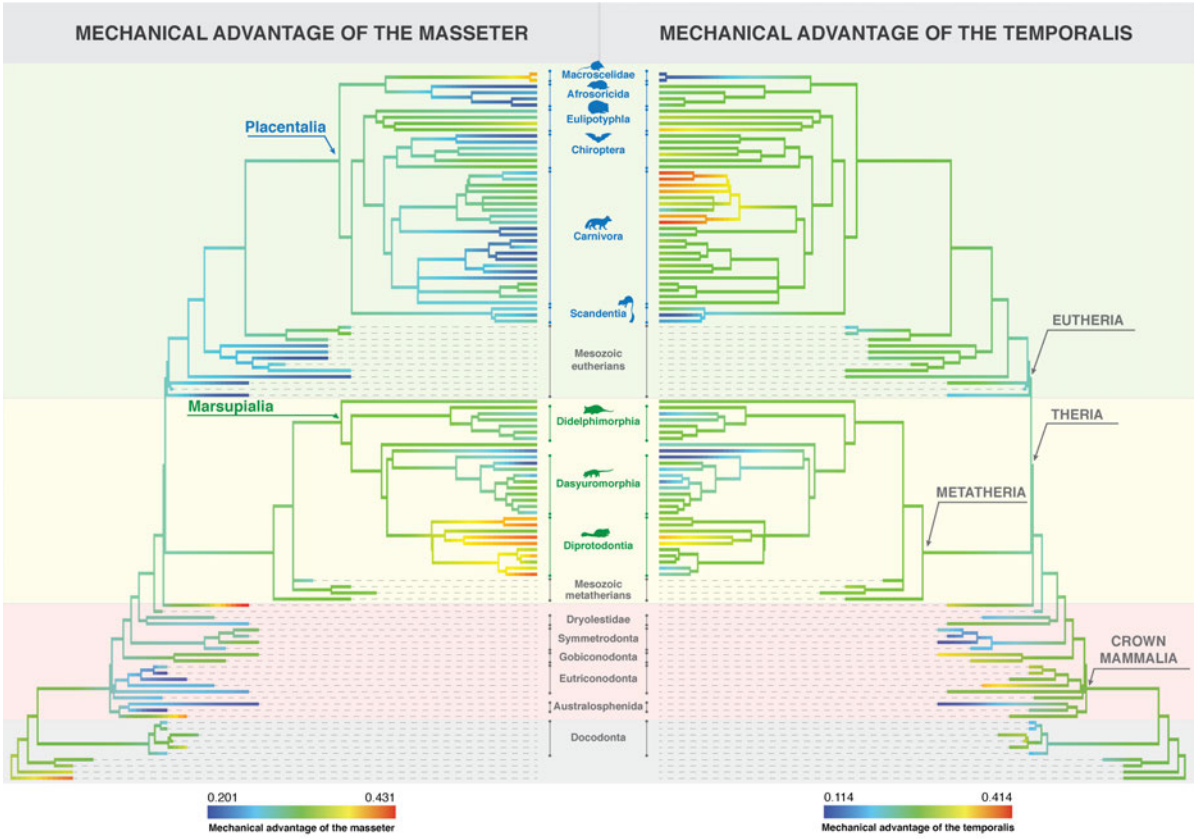

Figure 2.6: **Mechanical advantage values of the temporalis (left) and masseter (right) when biting at the jaw tip visualised in the context of the phylogeny used in this study.** See Supplementary Fig. S8 for individual taxon names.

2.4.3 The relationship between jaw shape, mechanical advantage and diet in small mammals

The relationship between jaw shape and mechanical advantage was tested in a phylogenetic context using a Phylogenetic Generalized Least Squares (**PGLS**) regression. There is a significant correlation between jaw shape and mechanical advantage of the **masseter** and **temporalis** (p=0.001) measured at the tip of the jaw in small mammals (Fig. 2.7 and 2.8). R^2 values are greater in the plot of jaw shape against mechanical advantage of the temporalis, implying a tighter predictive relationship between jaw shape and **MAT** than jaw shape and **MAM**: this might be a result of measuring the temporalis lever arm between two fixed landmarks (Fig. 2.3b). In Figures 2.7 and 2.8, the regression vector (axis y) shows differences in jaw shape. In Figure 2.7, jaws with taller and more robust ascending rami (and hence longer masseter lever arms) have more positive regression scores and jaws with shorter, more gracile ascending rami (and shorter masseter lever arms) have more negative regression scores. In Figure 2.8, jaws with more ventrally positioned condyles (and hence longer temporalis lever arms) have more positive

regression scores, and jaws with more dorsally positioned condyles (and shorter temporalis lever arms) have more negative regression scores. In both Figures 2.7 and 2.8, longer jaws tend have lower mechanical advantage values (i.e., when biting: less forcefulness, more speed), and shorter jaws tend to have higher mechanical advantage values (i.e., when biting: more forcefulness, less speed).

In Figures 2.7a and 2.8a, dietary categories among extant mammals can be roughly distinguished (with the exception of omnivores). In Figure 2.7a, carnivores and insectivores have similar **MAM** values (intermediate to low), while herbivores have intermediate to high MAM values. Carnivores tend to have higher regression scores than insectivores, and herbivores have the highest regression scores. Omnivores have low to high MAM values and regression scores.

In Figure 2.8a, insectivores have intermediate to low **MAT** values. Carnivores have intermediate MAT values, although some mustelids (i.e., the least weasel [*Mustela nivalis*, #99], the American badger [*Taxidea taxus*, #96], and the North American river otter [*Lontra canadensis*, #98]), have the highest MAT values among extant mammals. Herbivores have intermediate to high MAT values. Insectivores tend to have lower regression scores, and carnivores and herbivores tend to have higher regression scores.

We also found a significant relationship between jaw shape and mechanical advantage of the **masseter** and **temporalis** (p=0.001) measured at the first lower molar (**m1**) in small mammals (Figs. A.10, A.11). We made this alternative measurement because Grossnickle ([79]) found that the length of the posterior portion of the jaw (measured from the jaw joint to the m1) is a strong predictor of diet in mammals. Compared to the mechanical advantage (**MA**) measurements at the jaw tip (Fig. 2.7 and 2.8), we see a less clear distinction between dietary groups among extant mammals. There is considerable overlap between dietary groups in Fig. A.10 (jaw shape~**MAM** regression). In Fig. A.11 (jaw shape~**MAT** regression), there is a better separation between dietary groups.

In both cases, Mesozoic mammals have comparable regression and mechanical advantage scores to extant insectivores, carnivores and, in some instances, herbivores (Figs. 2.7b and 2.8b). Can we use a combination of jaw shape data and mechanical advantage values to infer diet in Mesozoic mammals?

2.4.4 Jaw shape and mechanical advantage as proxies for diet in Mesozoic mammals

We performed a phylogenetic flexible discriminant analysis using the regression scores of jaw shape on mechanical advantage (of both jaw tip and **m1** measurements) following Motani and Schmitz [152] to determine the posterior probability of the Mesozoic taxa of belonging to one of three dietary categories: insectivore, carnivore or herbivore. The results of the analysis can be seen in Figure 2.9 and the posterior probability values can be seen in S2 Data. For the most part, we see a good separation between dietary groups among extant mammals (Fig. 2.9a), with some

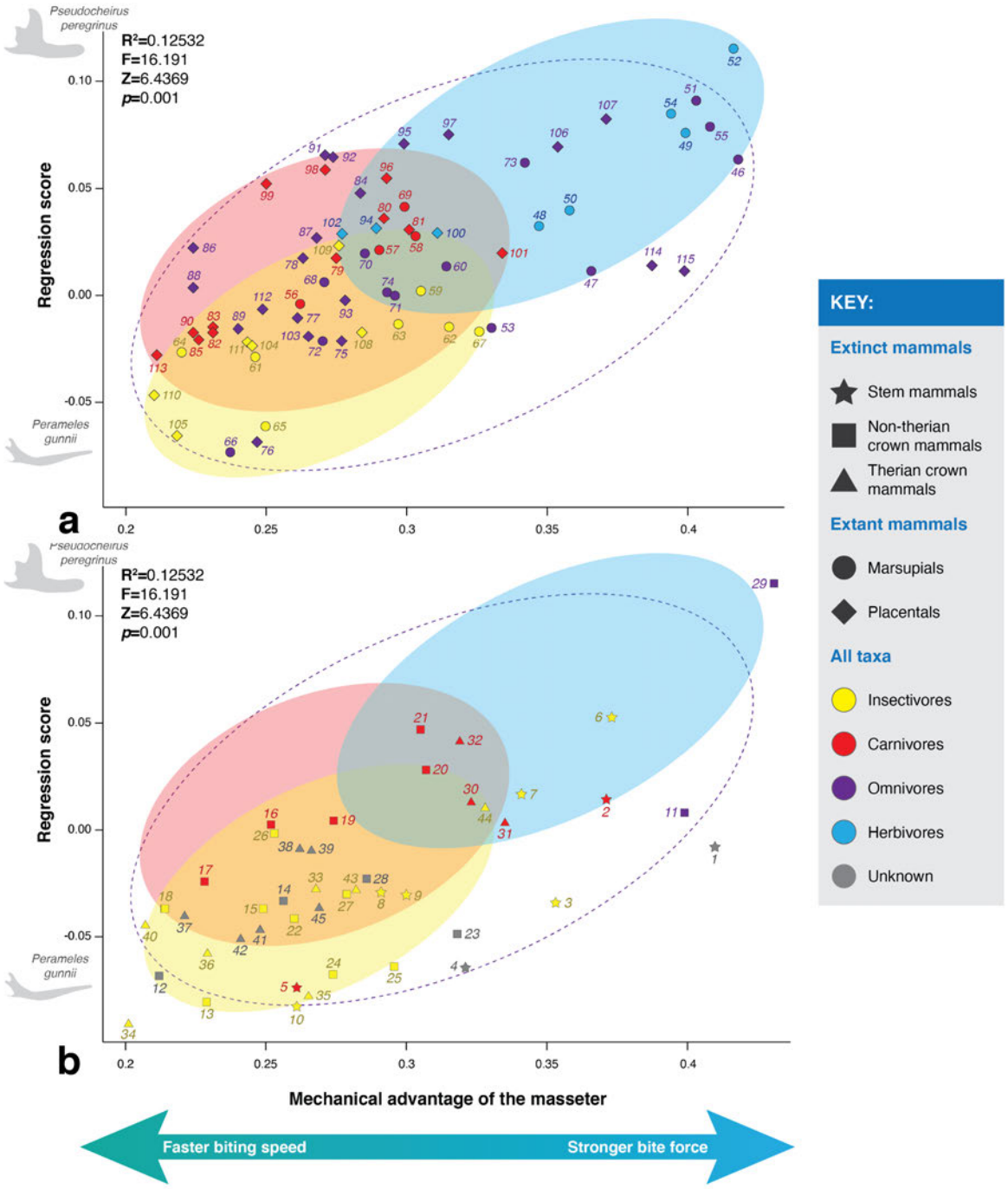

Figure 2.7: **Relationship between jaw shape and mechanical advantage of the masseter. PGLS** regression of Procrustes coordinates on mechanical advantage of the masseter on extant taxa (a) and extinct taxa (b). Colours indicate known dietary categories of extant mammals and suggested dietary categories for Mesozoic mammals (obtained from the literature). Ovals indicate where extant taxa of known dietary categories plot, as in part (a).

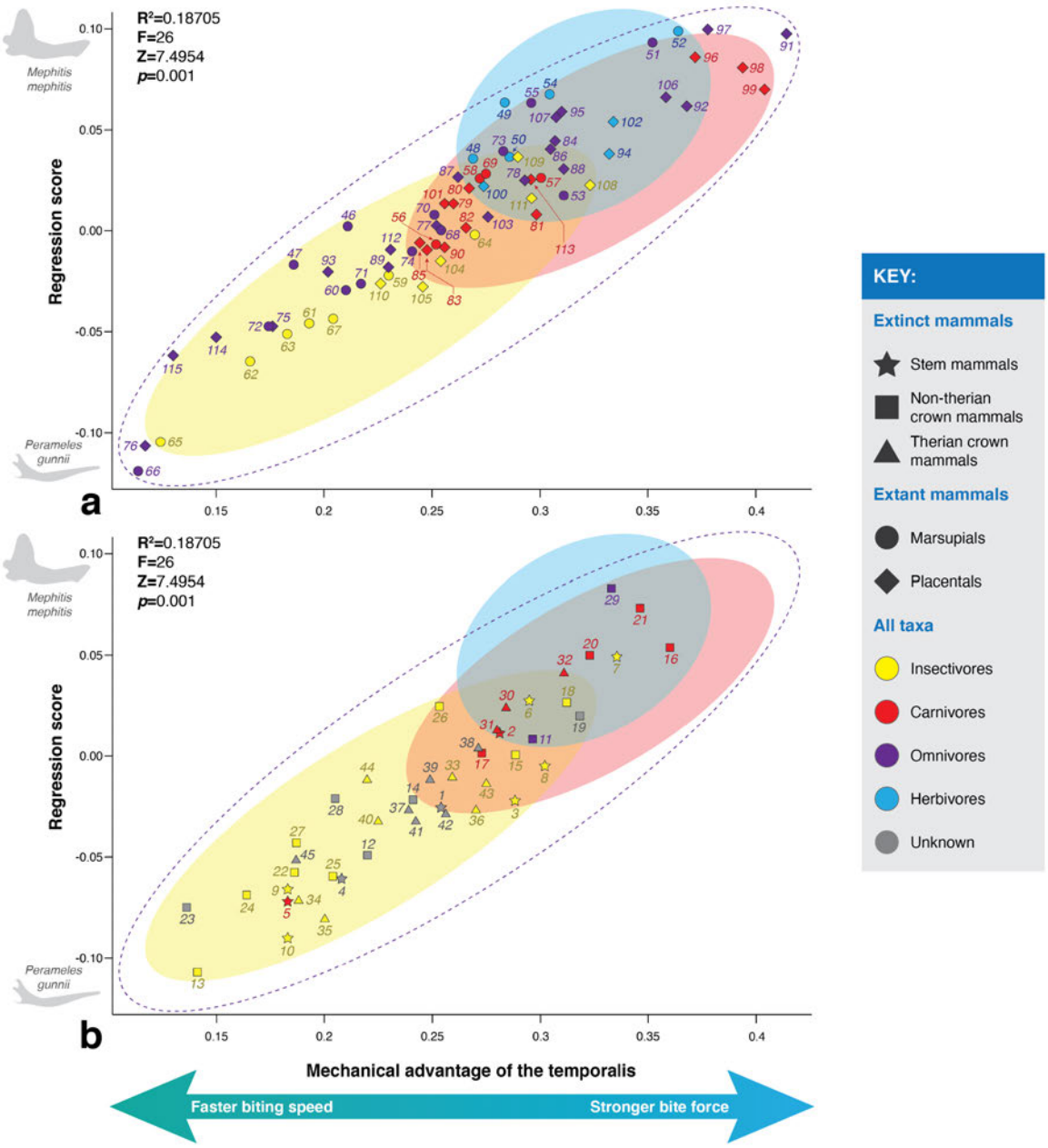

Figure 2.8: **Relationship between jaw shape and mechanical advantage of the temporalis. PGLS** regression of Procrustes coordinates on mechanical advantage of the **masseter** on extant taxa (a) and extinct taxa (b). Colours indicate known dietary categories of extant mammals and suggested dietary categories for Mesozoic mammals (obtained from the literature). Ovals indicate where extant taxa of known dietary categories plot, as in part (a).

exceptions: the primarily herbivorous olingo (*Bassaricyon gabbii*, #94) plots within the carnivores (although mainly frugivorous, it can consume small vertebrates), as does the insectivorous His-

paniolan solenodon (*Solenodon paradoxus*, #109).

The Mesozoic mammals included in our sample have largely been considered **faunivorous** and Figure 2.9b corroborates this hypothesis. The majority of them are classified as insectivorous, including most stem mammals, australophenidans, symmetrodonts and **eutherians**, among others. With the exception of *Phascolotherium* (#14), all eutriconodontans (including the gobiconodontids) were classified as carnivorous, alongside most **metatherians** in the sample (i.e., *Didelphodon* [#31], *Deltatheridium* [#30], *Eodelphis* [#32]), the stem mammal *Sinoconodon* (#2), the dryolestid *Crusafontia* (#26), and the **eutherian** *Sasayamamylos* (#39). Two taxa in the analysis were classified as herbivorous, because of their relatively tall ascending rami: *Vincelestes* (#29) and *Haldanodon* (#6). The dental morphology of *Vincelestes* points to a primarily **faunivorous** diet [20], but it has been noted before that its jaw morphology is indicative of a forceful bite; Rougier [194] suggested that this jaw morphology might have enabled *Vincelestes* to incorporate tough plant matter into its diet, but it might also be indicative of durophagy. The dental morphology [167] and body size of *Haldanodon* point towards an insectivorous diet; in this analysis, the posterior probability of *Haldanodon* being a herbivore is not high (only 50.3%). The evidence thus far suggests *Haldanodon* had a **faunivorous** diet; its jaw morphology might be indicative of the incorporation of tougher food sources into its diet.

2.5 Discussion

In this study we found that jaw shape is largely indicative of dietary category (with the exclusion of omnivores) in small extant mammals. This reflects the findings of Grossnickle and Polly [80]; however, we find a clearer discrimination of jaw shape between carnivores and insectivores, which might be related to our larger sample size and landmarking regime. In Fig. 2.4 there is some overlap between these two dietary categories but, in general, hypercarnivores such as the felids (#79, 80, 81) and the Tasmanian devil (*Sarcophilus harrisi*, #58) are clearly distinguished from the insectivores, while some mesocarnivores like the quolls (genus *Dasyurus*, #56, 57) and the Corsac fox (*Vulpes corsac*, #90) are more similar to the insectivores. This is in agreement with the study by ref. [175] who also found a clear separation of hypercarnivorous mammals from mesocarnivores and insectivores. As hypothesized by Prevosti et al., [175] and previous authors, hypercarnivores have shorter jaws to increase the mechanical advantage of the adductor musculature and deliver a stronger bite; alongside other morphological features, this configuration proves advantageous for prey subduing and meat consumption.

Generally, it is expected that herbivores would have a high mechanical advantage (i.e., increased bite force) of the **masseter** (**MAM**) and that carnivores would have a high mechanical advantage of the **temporalis** (**MAT**). Interestingly, we found that herbivores not only tend to have high MAM, but also high MAT, while carnivores have high MAT, but low MAM. A study on cranial morphology of rodents [200] found a similar pattern: herbivores have enlarged masseter

and temporalis muscles, while carnivores have and enlarged temporalis and a reduced masseter. Despite their different diets, the enlarged temporalis muscle in herbivores and carnivores might serve a similar function: to resist dislocating forces when biting at the front of the jaw, either when dealing with struggling prey (in carnivores) or biting hard plant material (in herbivores) [200]. On the other hand, insectivores have lower mechanical advantage (i.e., increased biting speed)

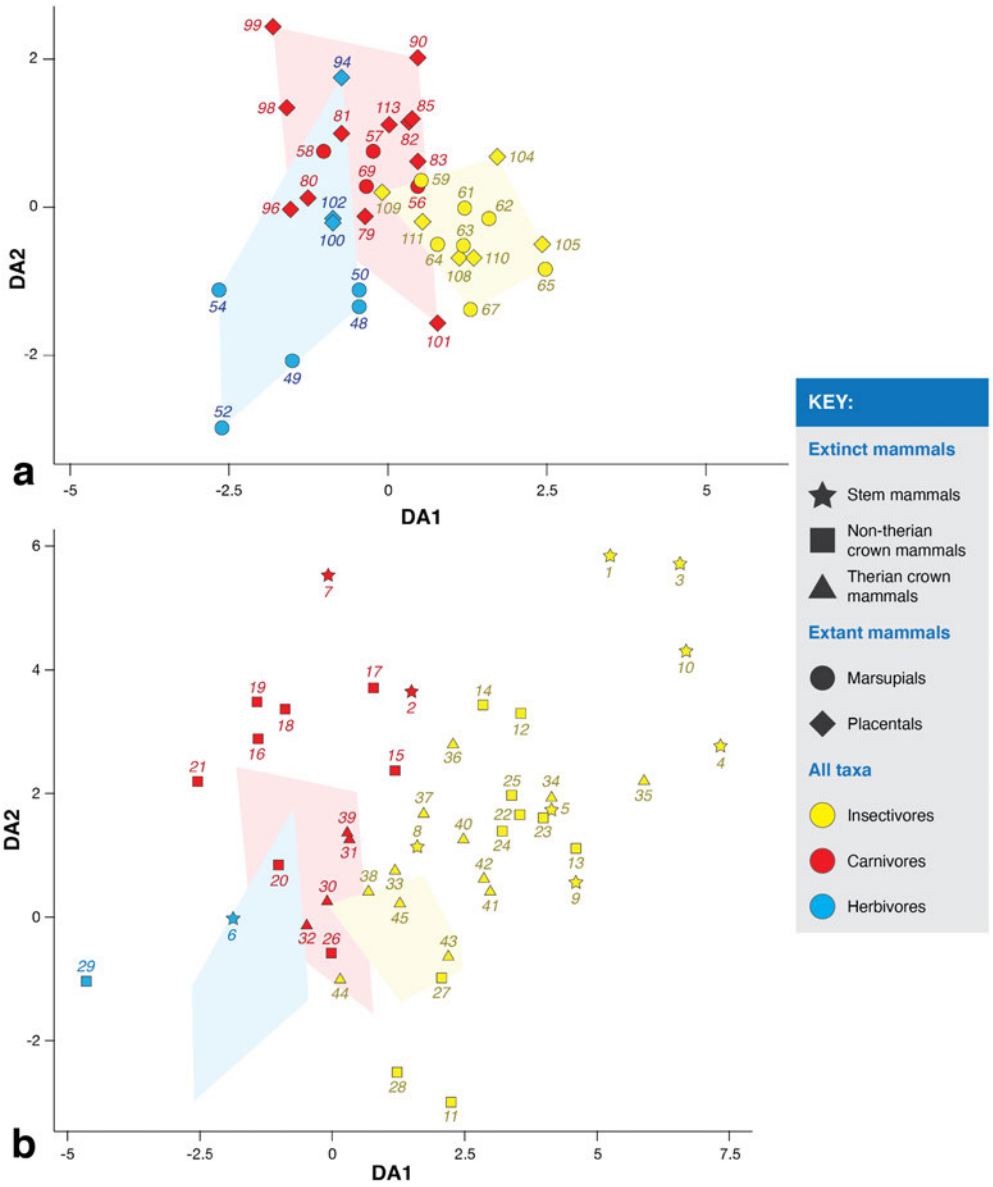

Figure 2.9: **Phylogenetic flexible discriminant analysis results**, showing discriminant axis one (DA1) and two (DA2), of extant mammals (a) and Mesozoic mammals (b). Extinct taxa are colour coded based on their posterior probability of belonging to one of the established dietary categories. Convex hulls show the position of the extant taxa in the plot and are colour coded based on their dietary categories. Note the different scale between the two plots.

in both muscles, which would be beneficial for catching fast moving prey. This low mechanical advantage is a byproduct of their long snouts, advantageous for both speedy jaw closure and for some foraging strategies (e.g., capturing prey inside holes or burrows).

Mechanical advantage values are closely related to jaw shape, which are in turn related to phylogeny. On their own, mechanical advantage values do not obviously correspond to particular dietary categories; however by combining jaw shape with mechanical advantage values of both the **masseter** and **temporalis**, we find a good correspondence with dietary categories in extant mammals. Herbivores tend to have shorter jaws and high mechanical advantage of both the masseter and temporalis; carnivores tend to have jaws intermediate in length, high mechanical advantage of the temporalis and low mechanical advantage of the masseter; and insectivores have longer jaws, and low mechanical advantage of both muscles.

The position of taxa in Figs. 2.4, 2.7 and 2.8 is related to both the length of the jaw and the length of the lever arms of the **temporalis** and **masseter**. Grossnickle [79] noted that the posterior portion of the jaw in non-rodents tends to be shorter in herbivores than in **faunivorous** taxa; while we did not include a similar measurement in our study, we can observe here that herbivores tend to have shorter jaws than faunivorous taxa (as well as higher mechanical advantage values).

Grossnickle [79] found that, among non-rodent therians, the jaw joint to angular process (JAPr) distance is longer in herbivores than in faunivorous taxa, consequently increasing the lever arm of the **masseter**. Our results corroborate these findings, and can be seen in the silhouettes along the regression score axis in Figure 2.7. We also found a tighter predictive relationship between **MAT** and jaw shape than between **MAM** and jaw shape. This is mainly related to two issues: 1) the lever arm of the **temporalis** was measured in between two fixed landmarks and 2) the differential presence of an angular process in jaws across the sample, which in turn affects the mechanical advantage of the masseter. Having explored the relationship between jaw shape, mechanical advantage and diet in small extant mammals, now we can evaluate whether these morphometric and functional metrics are good proxies for diet in Mesozoic mammals.

Overall, we found good correspondence between jaw shape, mechanical advantage and diet in Mesozoic mammals. We corroborate the hypothesis that most Mesozoic taxa were insectivorous and some clades, like eutriconodontans, had a carnivorous diet.

In Figure 2.7 we see that many stem mammals have higher **masseter** mechanical advantage values than 'expected' for their proposed dietary categories (also seen in Fig. 2.6). Stem mammals have a very anteriorly positioned angle of the mandible. This is related to the presence of retained postdentary bones (located posteriorly to the angle) that are incorporated into an enclosed middle ear to a greater or lesser extent in more derived mammals [114]. The anterior position of the angle in turn increases the lever arm of the masseter. In contrast, **non-therian crown mammals** that have not attained a fully-enclosed middle ear, such as *Yanoconodon* (#15) and *Maotherium* (#25), do not have longer masseter lever arms because their mandibles lack an anteriorly positioned

angular process, possibly related to the fact that the middle ear ossicles that have now become medially separated from the dentary [114]. Therian mammals with a fully enclosed middle ear do not have anteriorly positioned angular processes.

2.6 Conclusions

In this study, we analyzed the relationship between jaw shape and mechanical advantage of the **adductor muscles** in small extant mammals of known diets to determine whether there is a relationship between jaw shape, function and dietary ecology in extant taxa, and furthermore, whether these proxies can be useful to infer dietary categories in Mesozoic mammals. Jaw shape alone can be used as a good indicator to roughly distinguish among herbivores, carnivores and insectivores, but cannot distinguish omnivores. Overall, this holds true for most Mesozoic mammals.

Mechanical advantage values on their own cannot be used to confidently assign a taxon to a particular dietary category; phylogeny also plays an important role. However, by combining mechanical advantage data, of both the **masseter** and **temporalis**, with jaw shape we can distinguish between most dietary categories: herbivores have high **MAM** and **MAT** values, tall ascending rami and shorter jaws; carnivores have low MAM values, medium to high MAT values, medium to short ascending rami and jaw length; and insectivores have low to medium MAM and MAT values, short ascending rami and longer jaws.

These morphological and functional characteristics reflect the differential need of these animals for acquiring and processing particular types of food, which can be aided by having either stronger or faster jaw closure. Other factors, such as different foraging strategies and phylogenetic history, also play a role in determining the morphological configuration and functional traits of the mammalian jaws. The fact that the jaw shape and mechanical advantage of extant mammals could be successfully used as the basis for inferring the diet of mammals living during the Mesozoic (even those with retained postdentaries), highlights that ecological pressures and principles of jaw design were similar today and in the past.

We corroborate the hypothesis that most non-**allotherian** Mesozoic mammals had a **faunivorous** diet. Considering the taxa in our sample, most stem mammals, symmetrodonts, dryolestids, amphitheriids and **eutherians** seem to have had an insectivorous diet (or one consistent of aquatic invertebrates in the case of semi-aquatic mammals such as *Castorocauda* and *Teinolophos*), while the eutriconodontans and **metatherians** studied here probably had a more carnivorous diet. Fossorial or semi-fossorial mammals with a potentially vermivorous diet can also be distinguished from other insectivores as their jaw shape is more similar to that of carnivores.

CHAPTER 3

VALIDATING THE USE OF EXTRUDED FINITE-ELEMENT MODELS USING EARLY MAMMAL JAWS

This chapter has been previously published in Journal of the Royal Society Interface: **Morales-Garcia, N.M.**, Burgess, T.D., Hill, J.J., Gill, P.G., and Rayfield, E.J. 2019. The use of extruded finite-element models as a novel alternative to tomography-based models: a case study using early mammal jaws. Journal of the Royal Society Interface, 16: 20190674.

The idea of creating extruded models for their use in Finite Element Analysis (**FEA**) was originally proposed by Emily Rayfield. Initial validation experiments were carried out in extant animal jaws by Thomas Burgess during his MSc in Palaeobiology at the University of Bristol, under the supervision of Jennifer J. Hill and Emily Rayfield. Nuria Melisa Morales redesigned the process of making the models and created enhanced extruded models for their use in **FEA**. The use of these models was validated using the jaws of stem mammals *Morganucodon* and *Kuehneotherium*. Nuria Melisa Morales built all the models used in this paper, ran all the **FE** and sensitivity analyses and wrote the manuscript. This project was performed under the supervision of Pam Gill and Emily Rayfield, who contributed to the development of the method and commented on the manuscript.

3.1 Abstract

Finite Element Analysis (**FEA**) has been used in palaeobiology to assess the mechanical performance of the jaw. It uses two types of models: tomography-based 3D models (very accurate, not always accessible) and 2D models (quick and easy to build, good for broad scale studies, cannot obtain absolute stress and strain values). Here we introduce extruded **FE** models, which provide

fairly accurate mechanical performance results, while remaining low-cost, quick and easy to build. These are simplified 3D models built from lateral outlines of a relatively flat jaw and extruded to its average width. There are two types: extruded (flat mediolaterally) and enhanced extruded (accounts for width differences in the ascending ramus). Here we compare mechanical performance values resulting from four types of **FE** models (i.e., tomography-based 3D, extruded, enhanced extruded and 2D) in *Morganucodon* and *Kuehneotherium*. In terms of absolute values, both types of extruded model perform well in comparison to the tomography-based 3D models, but enhanced extruded models perform better. In terms of overall patterns all models produce similar results. Extruded **FE** models constitute a viable alternative to the use of tomography-based 3D models, particularly in relatively flat bones.

3.2 Introduction

Finite element analysis (**FEA**) is an engineering technique that reconstructs stress, strain and deformation patterns in digital structures [183, 249, 250]. This method allows for a complex 3D structure to be broken down into a finite number of elements of known material properties, size and shape whose response to a force can be readily quantified [183, 249, 250]. In vertebrates, FEA has mainly been used to assess feeding behaviour and mechanical performance of the skull in a wide array of groups, including cartilaginous fish [240], ray-finned fish [82], crocodilians [169], non-avian dinosaurs [184], birds [44], mammaliaforms [75], rodents [41, 42], primates [55, 219, 225], bats [56], ungulates [22], and carnivorous mammals [158, 212, 240, 241]. To a lesser extent it has been used in the study of locomotion and behaviour, for example to assess the loading regime of the metatarsus in a theropod dinosaur [214], to study the mechanical potential of the manual ungual of dromaeosaurids in prey dispatching [128], to simulate sauropod trackway formation [61] and theropod dinosaur locomotion [18, 18].

For its use in palaeontology, **FEA** has been validated using experimental approaches, including the in-vivo analysis of primate [192] and American alligator skulls [148, 171], ex-vivo studies using a domestic pig cranium [22] and the mandible of an ostrich [44], and in macaque mandibles using in-vitro data [136], as well as combined in-vivo and ex-vivo data [161]. Additionally, a comprehensive set of sensitivity analyses have been performed to improve **FE** models in terms of elastic properties and loading regimes [105, 193, 218, 227], boundary conditions [136], mesh density [22] and generation [133], as well as element size and homogeneity [130].

In palaeontology, finite element (**FE**) models are traditionally built using computed-tomography (**CT**) scan data. This method of data capture is widely used for **FEA** because it allows for the construction of very precise three-dimensional models and because it captures the internal anatomy of the structures of interest [183]. Other approaches to 3D data capture, like photogrammetry, laser scanning and mechanical digitisation, have been used to completely or partially build models for FEA [21, 68, 109, 110, 220] although these techniques are not able to capture internal

anatomy. Alternatively, 2D FE-models (also known as planar models) have been used to study feeding **biomechanics** across the fish-tetrapod transition [155], analyse the skull mechanics of temnospondyls [70, 71] and crocodilians [169], study the mechanical performance of dinosaur skulls [127, 182, 182] and cingulate xenarthrans [209], analyse the relationship between jaw shape and diet in primates [134] and assess the digestive physiology of ruminants using the robustness of their jaws [67], among others. It is simple, easy and quick to build 2D planar FE-models and they represent a first approximation for performing large scale studies and looking into general trends among clades [127, 134, 155, 169]. Additionally, they do not require CT scan data, which can sometimes be inaccessible or very expensive. The simplicity of 2D planar models can be problematic however, because they do not capture the three-dimensionality of the structure and the muscle configuration and the forces acting upon it, and must assume that the stresses and strains act only in the sagittal 2D plane [155]. It is therefore unclear to what extent 2D planar models can replicate the stress environment of a three-dimensional shape. Until this relationship is assessed, the utility of 2D planar models and the potential for studying large scale macroevolutionary trends cannot be fully realised.

Here we test the utility of simple 2D planar **FE** models and simplified 3D models, to predict the stress response of a complex three-dimensional structure. Recent 2D FE studies have focused on the vertebrate mandible, based on the assumption that it is a simple and largely planar structure that retains information about the feeding ecology of the individual. Here we create simplified FE models of relatively flat mandibles, built digitally using a lateral 2D outline of the jaw and data on its mediolateral width. We focus on the Early Jurassic mammaliaforms *Morganucodon* and *Kuehneotherium*, two of the earliest and most basal representatives of the total group Mammalia. The biomechanical performance of the jaws of these taxa has been previously studied using 3D FE models built from **CT** scan data, alongside other biomechanical techniques [75]; therefore, they constitute ideal subjects for the validation of novel FE models. We create three types of FE model of increasing complexity: a) 2D planar models, b) *extruded models*, which have been extruded to the average width of the jaw and maintain a uniform thickness, and c) *enhanced extruded models*, similar to extruded models, but where the ascending ramus has been modified to more closely resemble the 3D geometry of the jaw. We compare stress and strain within the jaws of these simplified FE models to the complex 3D models to assess the utility of simplified approaches. Given that these models were built using fossil material, no in-vivo validation was possible. Because these models represent isolated jaws only and the orientation of the adductor muscles cannot be accurately determined without a skull, we perform a series of sensitivity analyses to determine how the orientation of the muscle loads impacts the overall results when using the enhanced extruded models, as a means of helping us quantify uncertainty for incompletely preserved fossils.

3.3 Materials

We used the mandibles of two Early Jurassic (Hettangian–Early Sinemurian) stem mammals from Glamorgan, Wales, UK following [75]: *Morganucodon watsoni* [reconstructed from specimens UMZC Eo.D.61, UMZC Eo.D.45 (University Museum of Zoology in Cambridge, UK) and NHMUK PV M85507 (Natural History Museum, London, UK)] and *Kuehneotherium praecursoris* (reconstructed from specimens NHMUK PV M19766, NHMUK PV M19749, UMZC Sy.97 and NHMUK PV M92779). We used the **FE** models created by [75] as the basis for building 2D planar and extruded FE models and for comparison with the results from 3D **FEA**. The models in [75] are based on slightly incomplete specimens and the extruded models in this paper replicate this incomplete morphology.

3.4 Methods

3.4.1 Model creation

An example of all the models used in this study are shown in Figure 3.1 for *Morganucodon* and *Kuehneotherium*.

3.4.1.1 2D planar FE models

Lateral view screenshots of the mandibles were taken from Figure 1 in [75]. The mandibles were outlined in ImageJ v.1.46r [205] using the multi-point feature. The resulting data were processed in Microsoft Excel to include only the XY coordinates of the outline. These data were imported into the computer aided design (CAD) software Inventor Professional 2016 (Autodesk, USA) where a 2D model of the mandible was sketched using the spline function. The models (Figure 3.1D) were then exported to a .STEP file for later use in the **FEA** software, Abaqus v.6.14-1 (SIMULIA, USA).

3.4.1.2 Extruded FE models

2D planar **FE** models were constructed as above. These models were extruded medially to an average width in Inventor Professional 2016 (Autodesk, USA). The average width of the mandible was obtained from 10 equidistant measurements taken along the length of the mandible (in the 3D models used in [75]) in ImageJ v.1.46r [205]. For *Morganucodon*, the length of the mandible was 21.11 mm and the average width was 0.81 mm. For *Kuehneotherium*, the length of the mandible was 20.76 mm (incisor region missing from original model) and the average width was 0.85 mm. The resulting extruded FE models (Figure 3.1) were exported to a .STEP file for later use in the **FEA** software, Abaqus v.6.14-1 (SIMULIA, USA).

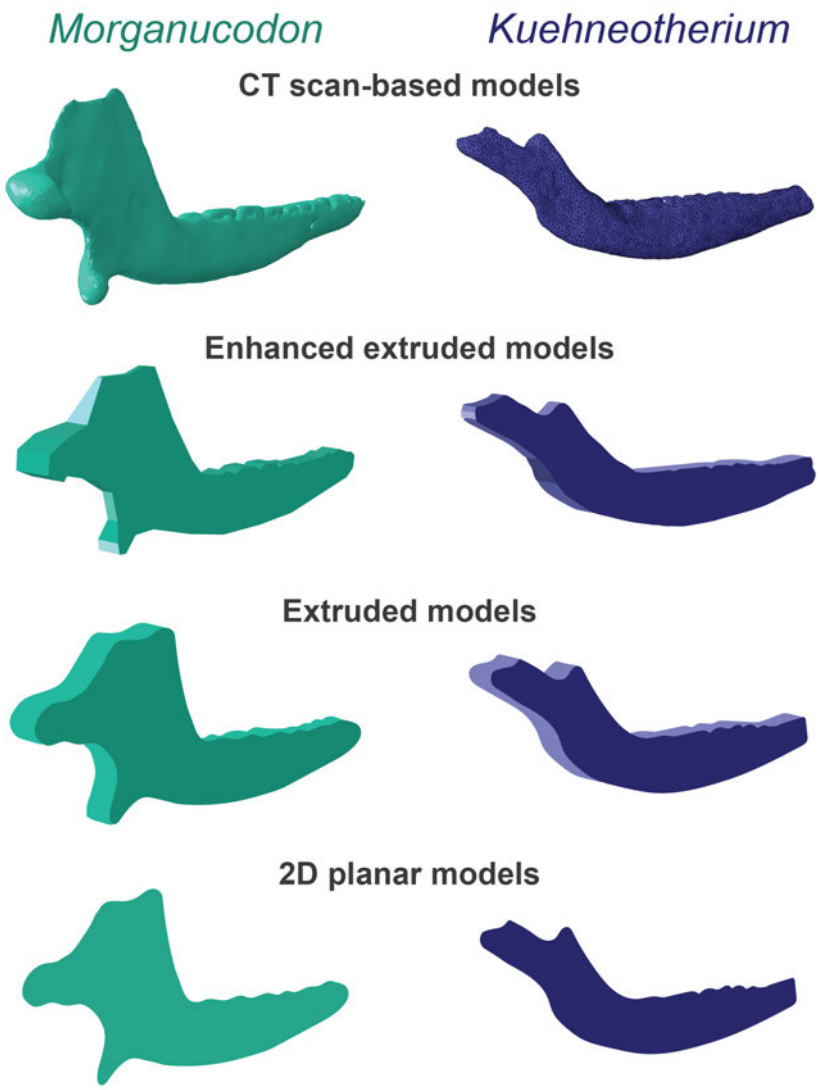

Figure 3.1: **FE models analysed in this paper.** *Morganucodon* on the left and *Kuehneotherium* on the right. From top to bottom: **CT** scan-based models, enhanced extruded models, extruded models and 2D planar models.

3.4.1.3 Enhanced extruded FE models

Alternative models to the simple, flat extruded **FE** models were generated. Using the 3D computer graphics software Blender v 2.78, the mandibles were outlined and transformed into simple extruded models. Posteriorly, the ascending rami of the mandibles were modified in width to account for a more complex geometry (as shown in Figure 3.1) in three main areas: the coronoid process, the condyle and the angular process (i.e., those regions in which the lateromedial width of the ascending ramus was markedly different from that of the horizontal ramus). The region between the condyle and the top of the coronoid process, as well as the concavity of the

angular, were likewise modified to obtain a gradual transition in width between areas. These structures were modified by taking additional width measurements from dorsal and posterior view screenshots of the 3D models of the jaws of *Morganucodon* and *Kuehneotherium* from [75] in ImageJ v.1.46r [205]. These models were exported into .STL in Blender and converted to .STEP using the CAD software FreeCAD v 0.16 for later use in the **FEA** software, Abaqus.

3.4.2 Meshing

Finite element analysis requires models to be meshed into a finite number of elements of known size and shape. For all models, meshing was performed in the **FEA** software, Abaqus v.6.14-1 (SIMULIA, USA). As in [75], the mesh of extruded and enhanced extruded **FE** models used linear four-noded tetrahedral (C3D4) elements; the mesh of 2D planar models used 3 node linear triangular (CPE3) elements. For a summary on the number of elements used in each mesh see Table 3.1.

	Morganucodon	*Kuehneotherium*
CT scan-based model	115,213	68,555
Enhanced extruded model	111,770	68,074
Extruded model	115,420	68,239
2D planar model	7,192	3,550

Table 3.1: **Summary of elements in the mesh of *Morganucodon* and *Kuehneotherium*.** Note that the **CT** scan-based, enhanced extruded and extruded models use linear four-noded tetrahedral (C3D4) elements, while the planar 2D model uses 3 node linear triangular (CPE3) elements.

3.4.3 Finite Element Analysis

3.4.3.1 Material properties

Mandibles were assigned isotropic and homogenous material properties of bone following [75], with a Young's modulus of 18 GPa and Poisson's ratio of 0.3. As in [75], none of the models created included tooth crowns because edentate jaw models have been shown to perform better than dentate ones [136] and because the fossil specimens lacked some or all of the teeth. However, the models by Gill et al. [75] did include the tooth roots which had the material properties of dentine (i.e., Young's modulus of 25 GPa and Poisson's ratio of 0.3). In order to test whether the inclusion of dentine had a significant effect on the **FEA** results, the original [75] models were re-run with only one material (i.e., bone) in both mandible and tooth roots. The summary of the results can be found in Table 3.2. The stress, strain and reaction forces produced by the set of models with only the material properties of bone was almost identical to those produced by models with two

different material properties (i.e., bone and dentine); therefore, the original models (with two material properties) do represent a good basis for validating the extruded models.

	Morganucodon		*Kuehneotherium*	
	A	B	A	B
von Mises stress (MPa)				
Mean	3.99	3.96	4.21	4.18
Median	3.00	2.93	2.08	2.04
Maximum	53.8	53.41	82.7	82.84
Maximum principal strain (microstrain)				
Mean	142	142	156	158
Median	102	101.5	73.5	75.1
Maximum	3,100	3,084	4,920	4,930
Reaction forces (N)				
Jaw joint	2.38	2.38	3.12	3.12
Bite	2.00	2.00	1.14	1.14

Table 3.2: **Comparative results of biomechanical analyses- *Morganucodon* and *Kuehneotherium* under the two different FE models:** A-Two material properties: bone and dentine (Young's modulus=25 GPa, Poisson's ratio=0.3), B-One material property: bone. Green: more than 75% similarity with values obtained from 3D model; Yellow: between 50-74%; Red: less than 50% similarity.

3.4.3.2 Constraints and boundary conditions

Following [75], multi-point constraints with master (i.e., a single point representing the muscle attachment area in the absent skull in which the lines of action of the slave nodes converge) and slave nodes (i.e., a set of points that represent the muscle attachment area in the jaw) were applied at the mandibular condyle and at the biting point: m2 in *Morganucodon* and m3 in *Kuehneotherium*. There were approximately 32 slave nodes constrained at the condyle and 26 slave nodes constrained at the biting point in *Morganucodon* and approximately 23 slave nodes constrained at the condyle and 31 slave nodes constrained at the biting point in *Kuehneotherium* (muscle attachment regions across models encompass comparable areas but have slightly different number of nodes). Boundary conditions in all taxa were constrained in four degrees of freedom at the mandibular condyle (U_1=U_2=U_3=U_{R1}=0) and in four degrees of freedom at the biting point (U_1=U_2=U_{R1}=U_{R2}=0). U1 is the mesiodistal axis, U2 is the dorsoventral axis and U3 is the axis along the length of the jaw; U refers to translational movement, UR refers to rotational movement.

3.4.3.3 Muscle attachment simulation

For *Morganucodon* and *Kuehneotherium*, four muscles were modeled: superficial **temporalis**, deep temporalis, superficial **masseter** and deep masseter (Figure 3.2). Multi-point constraints with master and slave nodes were used to simulate areas of muscle attachment at the mandible (slave nodes) and at the point they would attach to the skull (master nodes). Muscle loadings were different for each taxon and relative contributions of each muscle were calculated to obtain an overall bite force of 2N in *Morganucodon* and 1.14 N in *Kuehneotherium*. The actual loading forces, obtained from [75], were as follows: superficial temporalis, 2 N; deep temporalis, 1.6 N; superficial masseter, 1.6 N; deep masseter, 1.6 N.

3.4.3.4 Jaw performance

Reaction forces at the biting point and condyle were queried after running the model. Field output reports including maximum principal strain (i.e., tensile strain experienced by a bone following the application of a load [183]) and von Mises stress (i.e., parameter that predicts failure under ductile fracture [183]) were recorded for each model. Mesh-weighted arithmetic means were also calculated to account for differences in element size in the mesh following [130].

3.4.4 Sensitivity analyses

In order to evaluate the relevance of the accurate positioning of the master nodes of the muscle attachments (and the concomitant orientation of the muscle loads) in the absence of a skull, several sensitivity analyses were performed in the enhanced extruded **FE** models of *Morganucodon* and *Kuehneotherium*. These analyses involved moving the position of the master nodes of the **temporalis**, deep **masseter** and superficial masseter by 1%, 5% and 10% of the total jaw length in x, y and z, using a series of different transformation combinations (pictured in Figure 3.2 and fully described in Appendix B). A total of 156 analyses were performed: 78 for *Morganucodon* and 78 for *Kuehneotherium*. The full compendium of the resulting stress and strain values obtained from these analyses can be found in Table 3.3.

3.5 Results

3.5.1 Finite Element Analysis

The comparative stress, strain and reaction forces of *Morganucodon* and *Kuehneotherium* obtained from **FEA**, using the four different models are summarised in Table 3.4 and displayed as comparative plots in Figure 3.5. Figure 3.3 shows the the von Mises stress plots of all jaws. Particularly in Table 3.4, the mesh-weighted arithmetic mean (MWAM) values calculated to account for element size differences in the mesh, is fairly consistent to the arithmetic mean. This indicates that the size of the elements in the mesh is fairly homogeneous. Deformation patterns,

Analysis number	Change in x axis	Change in y axis	Change in x axis
1	0	Negative	0
2	0	Positive	0
3	Positive	0	0
4	Negative	0	0
5	Positive	Negative	0
6	Negative	Negative	0
7	Negative	Positive	0
8	Positive	Positive	0
9	0	Negative	Negative
10	0	Negative	Positive
11	0	Positive	Positive
12	0	Positive	Negative
13	Positive	0	Negative
14	Positive	0	Positive
15	Negative	0	Positive
16	Negative	0	Negative
17	0	0	Negative
18	0	0	Positive
19	Positive	Positive	Positive
20	Negative	Negative	Negative
21	Positive	Positive	Negative
22	Negative	Negative	Positive
23	Positive	Negative	Positive
24	Negative	Positive	Negative
25	Negative	Positive	Positive
26	Positive	Negative	Negative

Table 3.3: **Sensitivity analyses method.** The sensitivity analyses were carried out by moving the muscle loads 1%, 5% and 10% of the total length of the jaw in the x, y and z axis as described below. **x axis:** ***positive***=towards the anterior end of the jaw, ***negative***= towards the posterior end of the jaw; **y axis:** ***positive***= towards the dorsal end of the jaw, ***negative***= towards the ventral end of the jaw; **z axis:** ***positive***= towards the labial end of the jaw, ***negative***= towards the lingual end of the jaw.

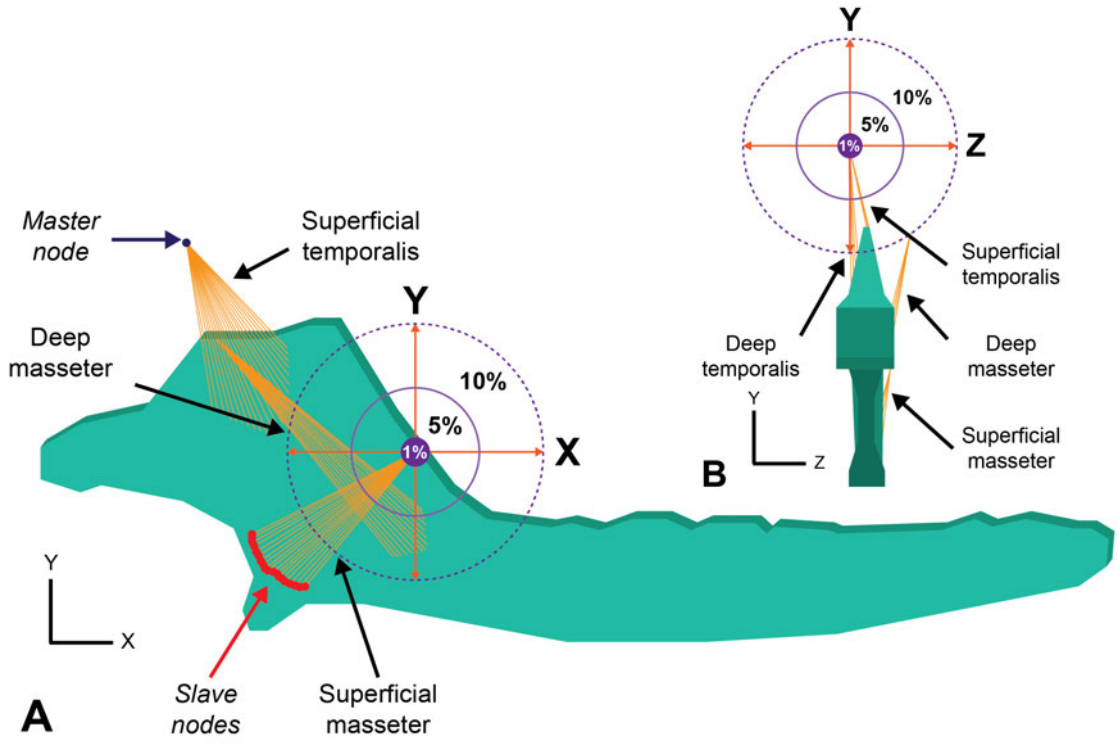

Figure 3.2: **Sensitivity analyses.** Jaw of *Morganucodon* in (a) lateral view, and (b) posterior view, depicting the range of distance (i.e., 1, 5, 10% of the total length of the jaw) the muscles were moved during the sensitivity analyses

fairly consistent across all models, are shown in Figure 3.4. In broad terms, the mean and median von Mises stress values resulting from both types of extruded **FE** models (enhanced and non-enhanced) were similar (75-92%) to those obtained from 3D models built from **CT** scan data. Particularly, enhanced extruded models produce more similar stress values to those obtained from the original 3D models, although they slightly overestimate (2.75%) the maximum stress experienced by the jaw. The mean and median von Mises stress values resulting from the 2D planar models were less than 0.05% similar to those obtained from 3D models built from CT scan data. Overall, the von Mises stress patterns in the jaws (Figure 3.3) are fairly consistent across models, including the 2D planar models, with most of the stress being experienced around the muscle attachments and the biting point in both *Morganucodon* and *Kuehneotherium*. In Figure 3.3 (B and F), this pattern is not evident in the enhanced extruded **FE** models because the von Mises stress scale was standardised for all 3D and extruded **FE** models, and the enhanced models experienced the lowest maximum stress values.

In terms of maximum strain magnitude, we obtained different results in both taxa. In the case of *Morganucodon*, the extruded **FE** model performed better than its enhanced counterpart,

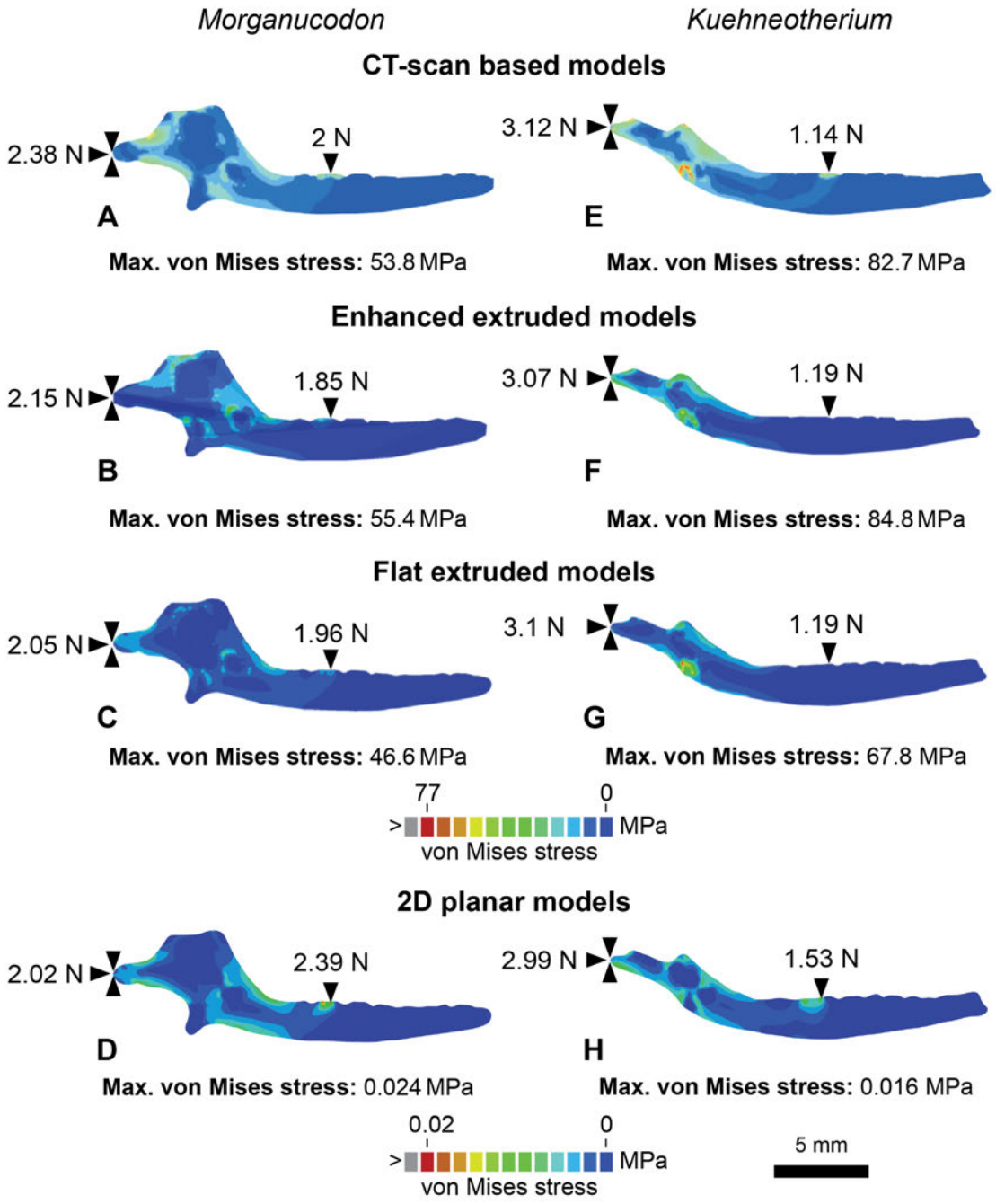

Figure 3.3: **Finite-element stress plots.** *Morganucodon* (a-d) and *Kuehneotherium* (e-h), using **CT** scan-based 3D models (a,e), extruded **FE** models: enhanced (b,f), and flat (c,g), and 2D models (d,h). Reaction forces (in N), depicted by black triangles, shown for the jaw joint and the bite point (m2 in *Morganucodon* and m3 in *Kuehneotherium*).

	Morganucodon				*Kuehneotherium*			
	A	B	C	D	A	B	C	D
von Mises stress (MPa)								
arithmetic mean	3.99	3.57	3.05	0.002	4.21	3.68	3.26	0.002
MWAM	4.03	3.44	3.04	0.002	4.20	3.55	3.38	0.002
median	3.00	2.77	2.34	0.001	2.08	1.65	1.56	0.001
max	53.8	55.4	46.6	0.024	82.7	84.8	67.8	0.016
Max. principal strain (microstrain)								
arithmetic mean	142	136	115	0.074	156	132	118	0.065
MWAM	149	131	115	0.073	153	128	122	0.063
median	102	90.8	82.7	0.036	73.5	55.8	53.6	0.032
max	3,100	2,590	2,830	0.89	4,920	5,400	4,250	0.79
Reaction forces (N)								
jaw joint	2.38	2.15	2.05	2.02	3.12	3.07	3.1	2.99
bite	2.00	1.85	1.96	2.39	1.14	1.19	1.19	1.53

Table 3.4: **Comparative results of biomechanical analyses.** *Morganucodon* and *Kuehneotherium* under the four different **FE** models: A, **CT** scan-based model; B, enhanced extruded model; C, extruded model; D, 2D planar model. MWAM, Mesh-weighted arithmetic mean (following [15] and [37]). Green, more than 75% similarity with values obtained from 3D model; yellow, between 50 and 74%; red, less than 50% similarity.

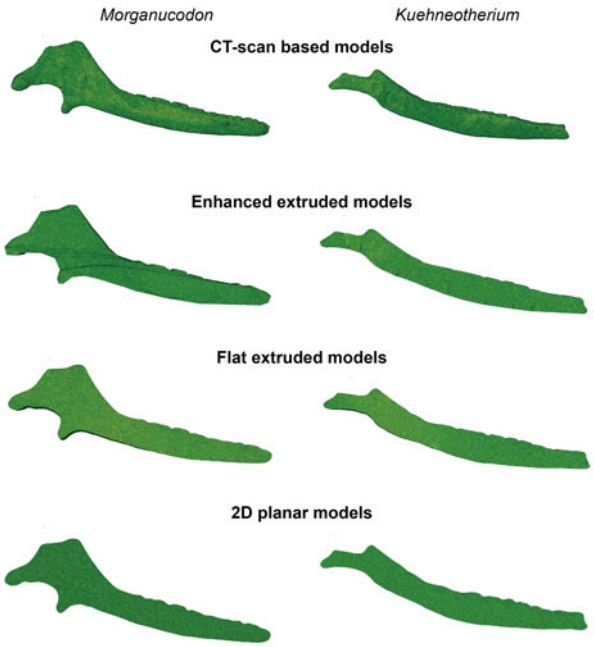

Figure 3.4: **Deformation patterns of all FE models evaluated in this study.** *Morganucodon* (left) and *Kuehneotherium* (right). From top to bottom: **CT** scan-based models, enhanced extruded models, extruded models, and 2D planar models

with the former achieving 91% of the original strain value and the latter only recovering 84%. In contrast, for *Kuehneotherium* the enhanced extruded FE model performed better than the simple extruded model, although it overestimated the maximum strain value by approximately 10%. In both taxa, the mean and median microstrain values were more similar between the original and enhanced extruded models, with the former recovering strain values of between 90-96% of the 3D model in *Morganucodon* and 76-85% in *Kuehneotherium*. In both taxa, the mean, median and maximum strain values resulting from the 2D planar models were less than 0.05% similar to those obtained from 3D models built from **CT** scan data.

The reaction forces experienced at the jaw joint were similar across all **FE** models. In *Morganucodon*, the enhanced model recovered 90% of the original reaction force value, the flat extruded model recovered only 86%, and the 2D planar model was 85% similar. In the case of *Kuehneotherium* both extruded FE models recovered approximately 99% of the original reaction force and the 2D model recovered 96%.

Both extruded **FE** models also performed well in terms of the reaction forces experienced at the biting point. In the case of *Morganucodon*, the flat extruded model produced a reaction force 98% similar to that produced by the original 3D model, while the reaction force produced by the enhanced extruded FE model was only 93% similar. For *Kuehneotherium*, the reaction forces in both models were identical, with both slightly overestimating the original value by approximately 4%. In the case of the 2D models, the reaction forces experienced at the biting point were overestimated in both models, by 20% in *Morganucodon* and 34% in *Kuehneotherium*.

3.5.2 Sensitivity Analyses

The summary of the results of the 156 sensitivity analyses, comparing the mean, median and maximum stress and strain values experienced in the enhanced extruded models with varying muscle positions to the original 3D models built from **CT** scan data, can be found in Table 3.5. However, not all of these models depict a realistic orientation of the adductor muscles. Muscles were moved by a value determined as a percentage of jaw length. In some cases, moving muscles by 5% or 10% of jaw length resulted in muscle lines of action that were impossible; for example passing through the ascending ramus of the jaw. In broad terms, the largest source of deviation from the original mean, median and maximum stress and strain values experienced by the jaw, can be attributed to the unrealistic modeling of the adductor muscles, as can be seen when comparing Table 3.5 (all iterations) with Table 3.6 (only realistic muscle iterations). Overall, this unrealistic positioning is largely related to moving the muscle loads in the z axis (Figure 3.2) past the anteroposterior axis of the jaw, effectively making the muscle pull in the opposite mediolateral direction of its natural orientation. Therefore, these models with unrealistic muscle orientations were removed, meaning that only 22 models were determined realistic for *Morganucodon* and 27 for *Kuehneotherium* (refer to Appendix B for detailed results). These results are summarised in Table 3.6 and graphically depicted in Figure 3.6.

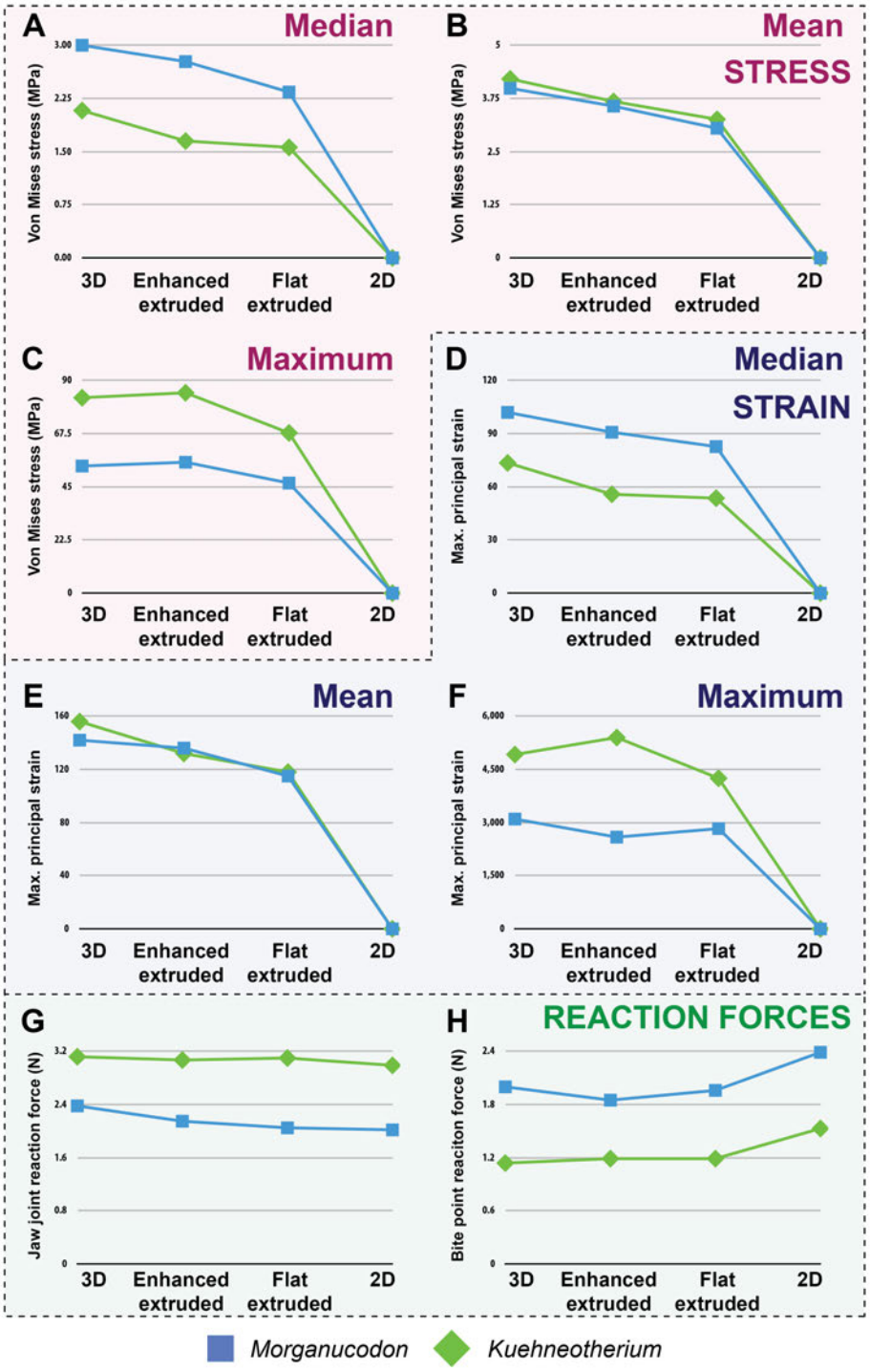

Figure 3.5: **Comparative performance of the different FE models,** in terms of von Mises stress (MPa) (a: median, b: mean, c: maximum), maximum principal strain (d: median, e: mean, f: maximum) and reaction forces (in newtons: N) at the jaw joint (g) and bite point (h). *Morganucodon* in blue and *Kuehneotherium* in green.

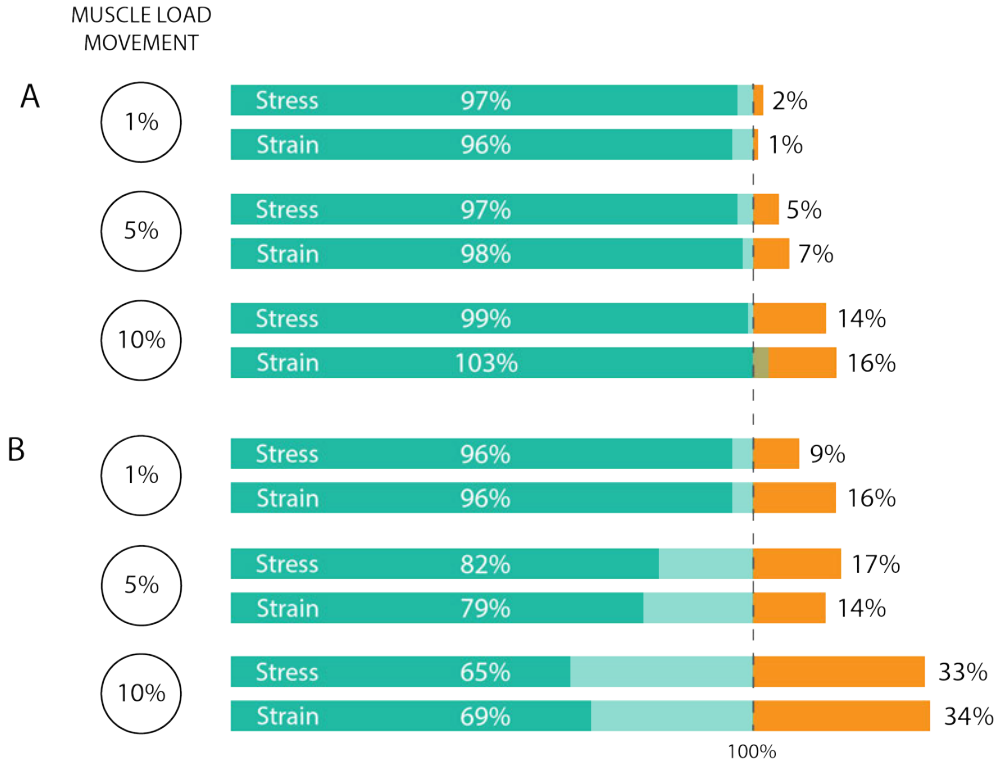

Figure 3.6: **Results of the sensitivity analyses.** Bar chart depicting the range of the mean and median stress and strain values observed in the sensitivity analyses for (a) *Morganucodon* and (b) *Kuehneotherium*. 100% line represents the original stress and strain results obtained from the enhanced extruded **FE** models, the green bar represents up to how much these results were underestimated in the sensitivity analyses, and the orange bar shows up to how much these results were overestimated.

When considering only the models with realistic muscle orientations (Figure 3.6) it is apparent that, in broad terms, the more the muscle loads are moved from their original position, the more the resulting stress and strain values deviate from the original values (i.e., those of the enhanced extruded **FE** models depicted in Table 3.4). However, in all cases these values proportionally deviate more in *Kuehneotherium* than in *Morganucodon*. Additionally, the mean and median stress and strain values tend to change fairly consistently throughout iterations, but the maximum values, particularly when moving the muscles over 5% of the total length of the jaw, deviate considerably (Table 3.6).

In *Morganucodon*, the mean and median stress and strain values resulting from the 1% muscle movement sensitivity analyses did not deviate more than 4% from the original values

	Morganucodon			*Kuehneotherium*		
	range (min-max)	s.d.	% similarity range	range (min-max)	s.d.	% similarity range
moving all muscles 1%						
von Mises stress (MPa)						
mean	3.5-3.8	0.1	97-106%	3.6-3.8	0.1	98-104%
median	2.7-2.9	0.04	99-104%	1.5-1.8	0.1	90-109%
max	54.7-56.1	0.4	99-101%	77.8-91.9	4.5	92-108%
maximum principal strain (microstrain)						
mean	131.1-146	5.3	96-107%	130.2-138.7	2.5	98-105%
median	90.1-96.2	2.04	99-106%	47.2-65.0	5.9	85-116%
max	2529.4-2968.2	121.01	98-115%	4952.9-5845	285.5	92-108%
moving all muscles 5%						
von Mises stress (MPa)						
mean	3.5-5.3	0.6	98-148%	3.5-5.6	0.7	95-153%
median	2.7-4.0	0.42	96-143%	1.4-4.0	0.9	82-246%
max	52-120	20	94-217%	65.4-121.1	17.4	77-143%
maximum principal strain (microstrain)						
mean	132.1-209.6	25.8	97-154%	125.9-214.9	29.6	95-162%
median	87.2-139.5	16.8	96-154%	43.9-151.2	35.5	79-271%
max	2760.7-5426.1	712.5	107-210%	3834.1-7794.5	1288.1	71-144%
moving all muscles 10%						
von Mises stress (MPa)						
mean	3.5-7.7	1.4	99-216%	3.5-8.8	1.8	95-238%
median	2.5-5.5	1.0	91-198%	1.1-6.8	2	65-414%
max	56.2-202.6	41.1	101-366%	63.8-187	32.8	75-220%
maximum principal strain (microstrain)						
mean	134-311.2	58.7	98-228%	125.8-343.6	75.4	95-259%
median	82.7-203.1	40.5	91-224%	38.7-259.8	74.4	69-465%
max	3108.3-8894.3	1560.9	120-343%	4064.2-11561.8	2026.5	75-214%

Table 3.5: **Comparative stress and strain results of the sensitivity analyses-** Includes: range (minimum and maximum values of all the iterations), standard deviation and % similarity range (percentual value that represents the range of how much the stress and strain values, in all iterations of the sensitivity analyses, deviated from the original results from the enhanced extruded **FE** models).

obtained from the enhanced extruded model. The 5% movement sensitivity analyses results did not deviate more than 7% and the 10% movement sensitivity analyses did not deviate by more than 16%. The sensitivity analyses models tended to overestimate the mean and median stress and strain values in this taxon.

In *Kuehneotherium*, the mean and median stress and strain values resulting from the 1% muscle movement sensitivity analyses deviated up to 16% from the original values obtained from the enhanced extruded model. The 5% movement sensitivity analyses results deviated up to 21% and the 10% movement sensitivity analyses deviated up to 34%. The sensitivity analyses models tended to both underestimate and overestimate the mean and median stress and strain values in this taxon.

	Morganucodon			*Kuehneotherium*		
	range (min-max)	s.d.	% similarity range	range (min-max)	s.d.	% similarity range
moving all muscles 1%						
von Mises stress (MPa)						
mean	3.5-3.6	0.1	97-101%	3.6-3.8	0.1	98-104%
median	2.7-2.8	0.02	99-102%	1.6-1.8	0.1	96-109%
max	54.7-55.7	0.3	99-101%	77.8-86.9	3	92-102%
maximum principal strain (microstrain)						
mean	131.3-137.7	2.5	96-101%	130-139	2.7	98-105%
median	90.1-92.1	0.7	99-101%	54.0-65.0	4	96-116%
max	2529.4-2735.8	66.8	98-106%	4952.9-5530.4	192.9	92-102%
moving all muscles 5%						
von Mises stress (MPa)						
mean	3.7-3.8	0.1	102-105%	3.6-4.1	0.2	97-112%
median	2.7-2.8	0.1	97-103%	1.4-1.9	0.3	82-117%
max	54.6-66	5	99-119%	75-99.7	9.8	88-117%
maximum principal strain (microstrain)						
mean	139.6-145.1	2.4	102-107%	127.8-150.9	8.6	96-114%
median	89.4-94.9	2.3	98-104%	43.9-62.5	8	79-112%
max	2985.1-3366.7	117.2	115-130%	4774.1-6065.8	623.6	88-112%
moving all muscles 10%						
von Mises stress (MPa)						
mean	3.78-4.06	0.12	106-114%	3.5-4.8	0.46	95-129%
median	2.74-3.02	0.11	99-109%	1.07-2.2	0.53	65-133%
max	58.87-92.91	14.09	106-168%	65.2-141.7	28.47	77-167%
maximum principal strain (microstrain)						
mean	145.8-157.9	5.46	106-116%	125.8-176.9	18.72	95-134%
median	93.23-102	3.85	103-113	38.7-70.4	15.39	69-126%
max	3399.8-4305.9	415.52	131-166%	4152.7-8022.6	1410.94	77-149%

Table 3.6: **Comparative stress and strain results of the sensitivity analyses with realistic muscle configurations-** Includes: range (minimum and maximum values of all the iterations), standard deviation and % similarity range (percentual value that represents the range of how much the stress and strain values, in all iterations of the sensitivity analyses, deviated from the original results from the enhanced extruded **FE** models).

3.6 Discussion and conclusions

The more the geometric configuration of the digitally built models resembles that of the most accurate 3D digital representation of the jaw (i.e., the 3D models built from **CT** scan data), the closer their stress and strain values. In descending order of similarity these are a) the enhanced extruded **FE** models, b) the extruded FE models, and finally c) the 2D planar FE models. Both types of extruded FE models produced results which, in most cases, recuperated more than 75% of the stress and strain values observed in the original 3D models. However, 2D planar FE models achieved less than 0.05% of these values. Regardless, the von Mises stress plots across all models show fairly similar patterns, and the reaction forces in the jaw joint and biting point are closely comparable in most cases, including in the 2D models.

2D planar **FE** models are a popular alternative to the use of 3D models built from **CT** scan data because of their efficiency when performing large scale studies and because they are valuable as a first approximation to evaluate the overall von Mises stress patterns experienced in the jaw [127, 155, 169]. However, as previously mentioned by these authors and further demonstrated here, 2D planar models cannot replicate the absolute stress and strain magnitudes experienced by the jaw because they represent an oversimplification of the geometry of the jaw and of the line of action of the adductor muscles. 2D models can, however, represent reaction forces and comparative patterns of stress and strain, presumably so long as muscle lines of action do not deviate far from the 2D plane of the model (although this remains to be tested). The use of extruded FE models can better approximate the 3D geometry of the jaw and its muscle configuration and produce similar stress and strain values to those obtained from 3D models built with CT scan data, while still preserving the economy and efficiency of 2D models. In terms of replicating absolute stress and strain magnitudes, enhanced extruded FE models constitute one of the best alternatives to the use of 3D models when no CT scan or photogrammetry data is available. Extruded FE models also constitute a viable alternative because they are easier and quicker to build than their enhanced counterparts, while still producing similar stress and strain values. Similar results have been obtained from Rahman and Lautenschlager's box models [179] in Finite Element Analysis (**FEA**) using a skull of *Allosaurus* and a vertebra of *Stegosaurus*. Their models, which also represent a 3D simplification of the geometry of bone, have been assessed qualitatively (e.g., von Mises stress plots) and quantitatively (e.g., stress, strain, deformation) and perform in a similar manner to extruded models.

A large number of **FE** analyses evaluating the mechanical performance of the jaw have been performed without the cranium (e.g., [75, 127, 130, 136, 155, 171, 209, 209]). Given that both types of extruded FE models presented here are only built for the jaw and not the cranium, we cannot be certain we are realistically modelling muscle lines of action. Therefore, sensitivity analyses were performed in the enhanced extruded models to evaluate how much the resulting stress and strain values would change if the muscle loads were moved in various directions. As previously mentioned, the unrealistic modelling of the muscle loads in the z direction was

the largest source of deviation from the original stress and strain values, as well as moving the muscle loads by more than 10% of the total length of the jaw in both *Morganucodon* and *Kuehneotherium*; therefore, the understanding of how the adductor muscles attach to the cranium should be as thorough as possible.

The stress and strain values resulting from both types of extruded **FE** models represent a close approximation to the results obtained from 3D FE models built from **CT** scan data in relatively flat bones, particularly jaws. These models are still subject to the same assumptions as any other biological FE-model, in terms of estimating material properties and boundary conditions such as muscle loads and constraints. The economy and efficiency with which they can be both built and analysed, while still providing reliable approximations of the stress and strain magnitudes experienced in the jaw, makes them a good alternative to the use of 2D planar models when performing large scale studies where questions of comparative shape performance are warranted. Given the nature of how these models are built, reconstructions based upon a number of incomplete specimens is possible in a relatively easy manner, which is advantageous when dealing with fossil material. The use of early mammal jaws for building extruded FE models has proven useful since they are relatively flat and lack considerable anterior or other curvature along their length. How more three-dimensionally complex jaws may lend themselves to the extruded approach deserves further attention. Likewise, and to explore the full potential of this method, further studies can be made on the validation of extruded FE models on different morphologies (e.g., skull, limb bones, etc.). Enhanced extruded models, which provide more accurate results than simple extruded models, can be made as geometrically complex as needed; however, this can be a time-consuming process and could generate problems with meshing (further validation is needed). Other tools, like photogrammetry, can be performed at low cost to obtain 3D structure; however, other factors, like the size of the specimen, can present considerable obstacles to this technique. Additionally, the presence of an obscuring matrix around the fossil can be challenging for both photogrammetry and for building extruded models. While extruded models can be built from the reconstruction of several specimens, it is important to understand the limitations of the technique (e.g., must have a dorsal view picture to accurately estimate width of the jaw). On the other hand, enhanced extruded FE models are advantageous because they can be built using only a reduced number of pictures (i.e., lateral view, dorsal view, posterior view and, optionally, ventral view) as opposed to photogrammetry. Enhanced or simple extruded FE models therefore offer an alternative to 2D planar and CT scan-based 3D models for representing the mechanical behaviour of relatively flat geometric structures, such as the mammalian mandible.

CHAPTER 4

FUNCTIONAL PERFORMANCE OF THE JAWS OF MESOZOIC MAMMALS AS REVEALED BY FINITE ELEMENT ANALYSIS

This chapter is in review at *PLoS One* as: **Morales-Garcia, N.M.**, Tang, K.L., Gill, P.G., Janis, C.M., and Rayfield, E.J. Functional performance of the jaws of Mesozoic mammals as revealed by finite element analysis.

This project was performed in collaboration with former Palaeobiology MSc student Kit Lam Tang. He built the original **FE** models of extant mammals and performed the corresponding analyses; he also updated the method to build the enhanced extruded FE models I devised and validated in Chapter 3 and contributed to the manuscript. Nuria Melisa Morales designed the study, built the Mesozoic mammal models, updated the extant mammal models, performed the Finite Element Analysis and posterior analyses on all taxa, and wrote the manuscript. Pam Gill, Christine Janis and Emily Rayfield supervised the project and commented on the manuscript.

4.1 Abstract

[redacted]

4.2 Introduction

4.3 Materials and methods

4.3.1 Materials

[redacted]

4.3.2 Model construction

[redacted]

[redacted].

4.3.3 Finite Element Analysis

[redacted]

[redacted]

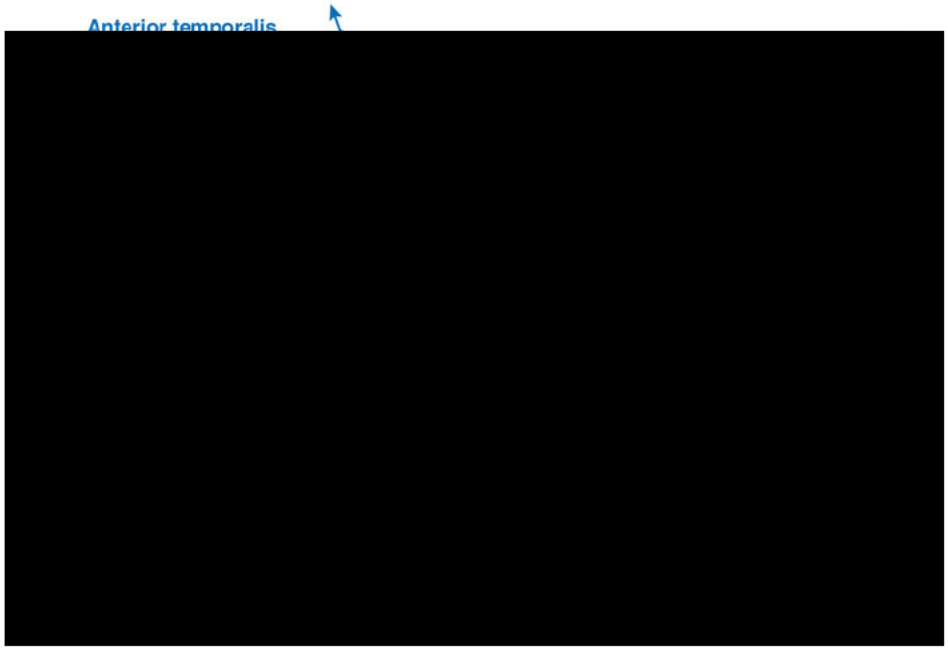

[redacted]

4.3.4 Intervals Method

[redacted]

4.3.5 Linear measurements

[redacted]

4.3.6 Geometric morphometrics

[redacted]

4.4 Results

Geometric Morphometrics

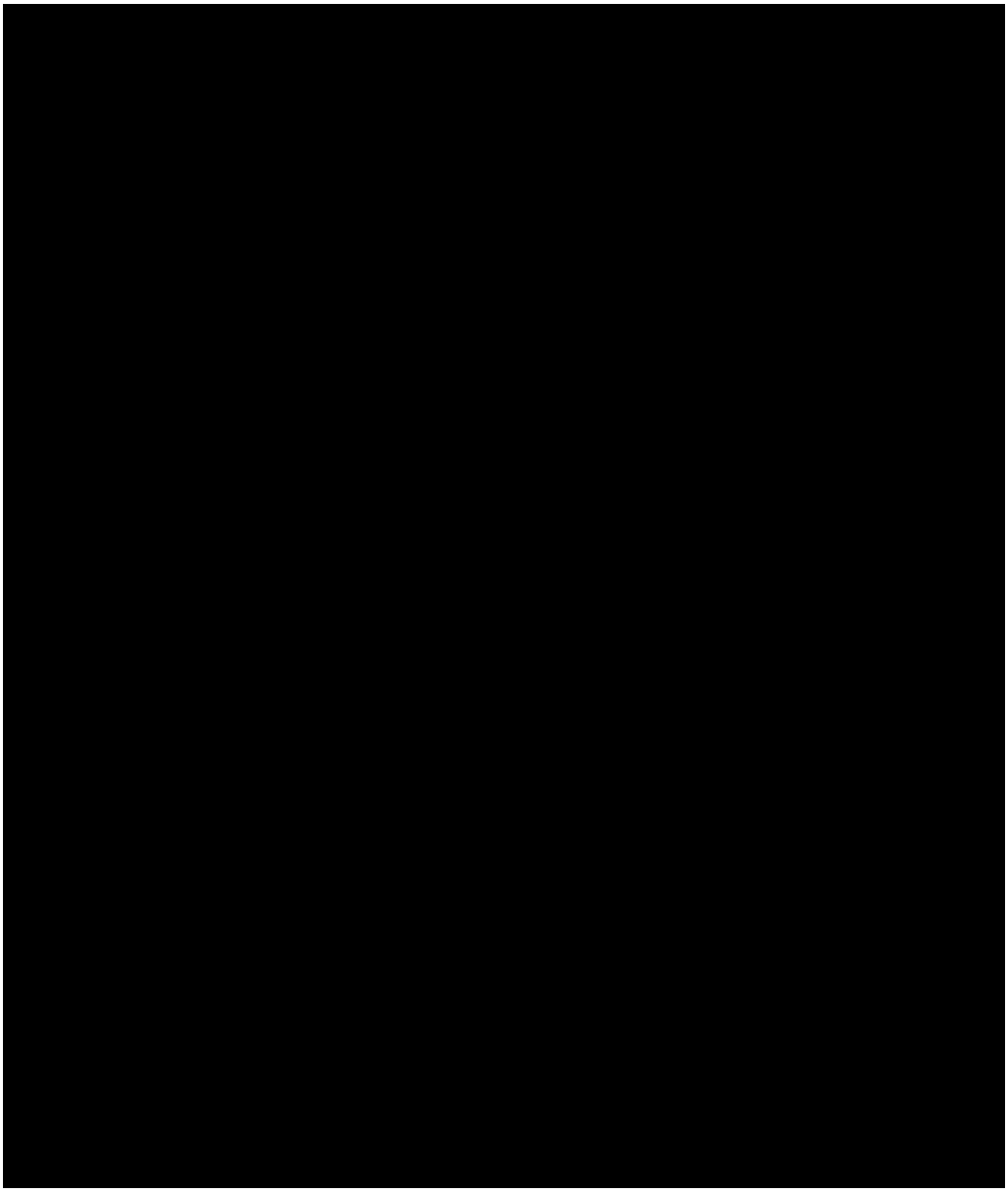

4.4.1 Finite Element Analysis

[redacted]

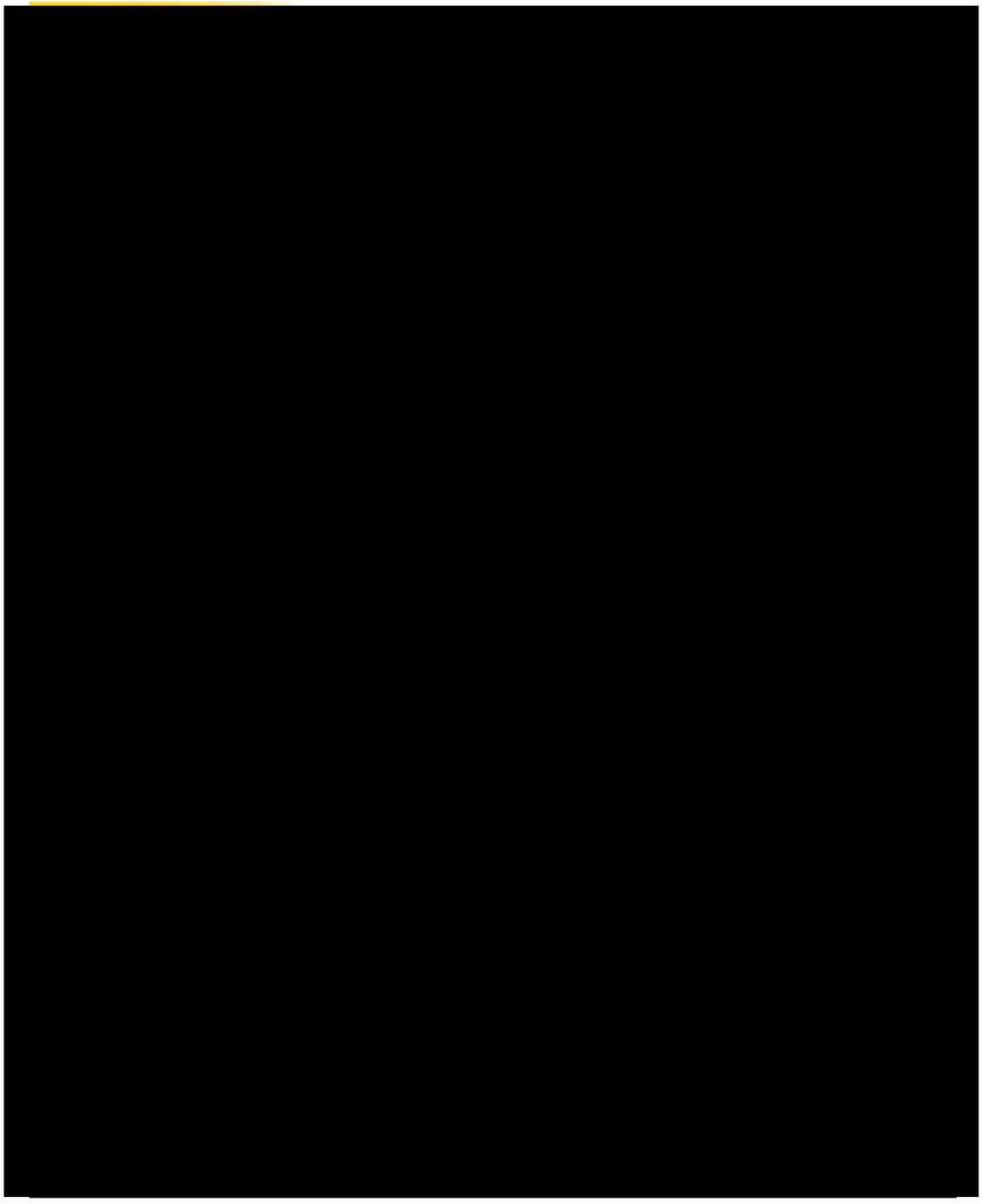

4.4.2 Intervals Method

4.4.2.1 Convergence study

Table 4.1:

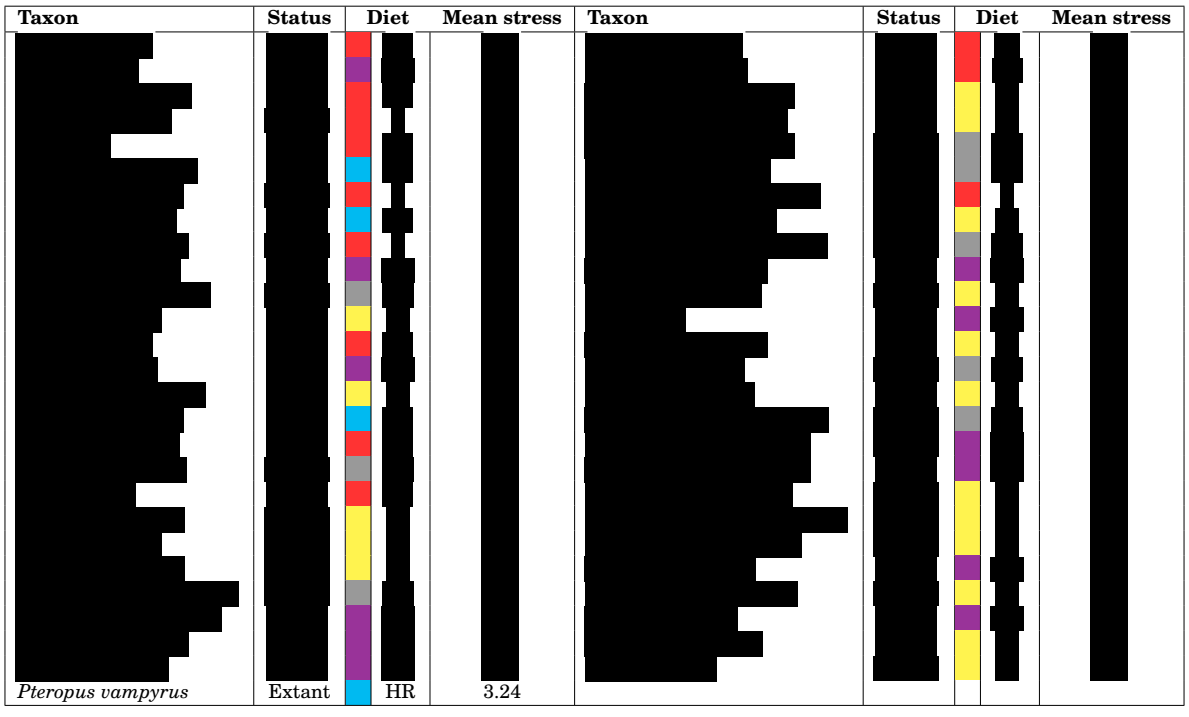

Principal Components Analysis

[redacted]

[redacted]

4.5 Discussion

[redacted]

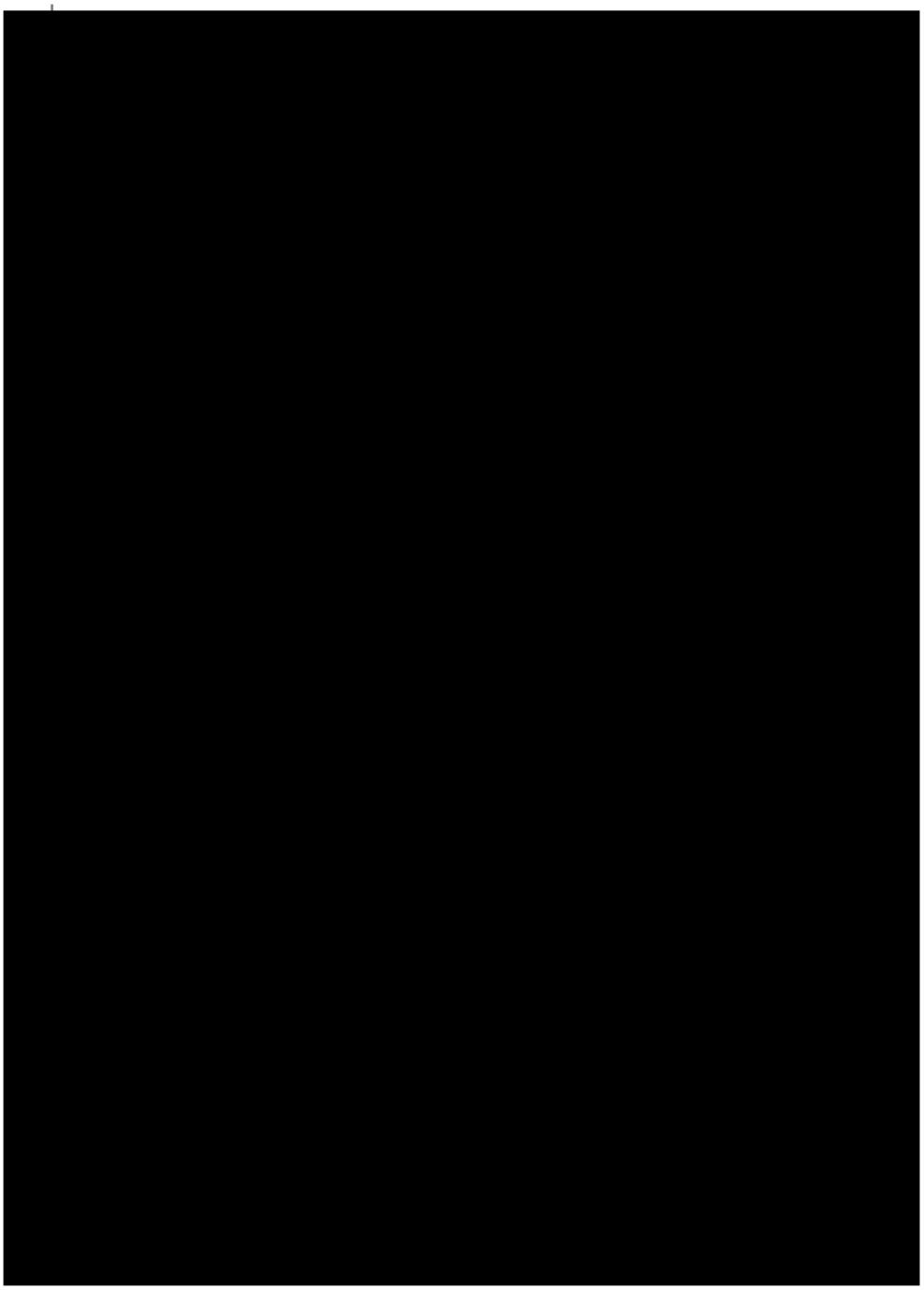

Figure 4.6:

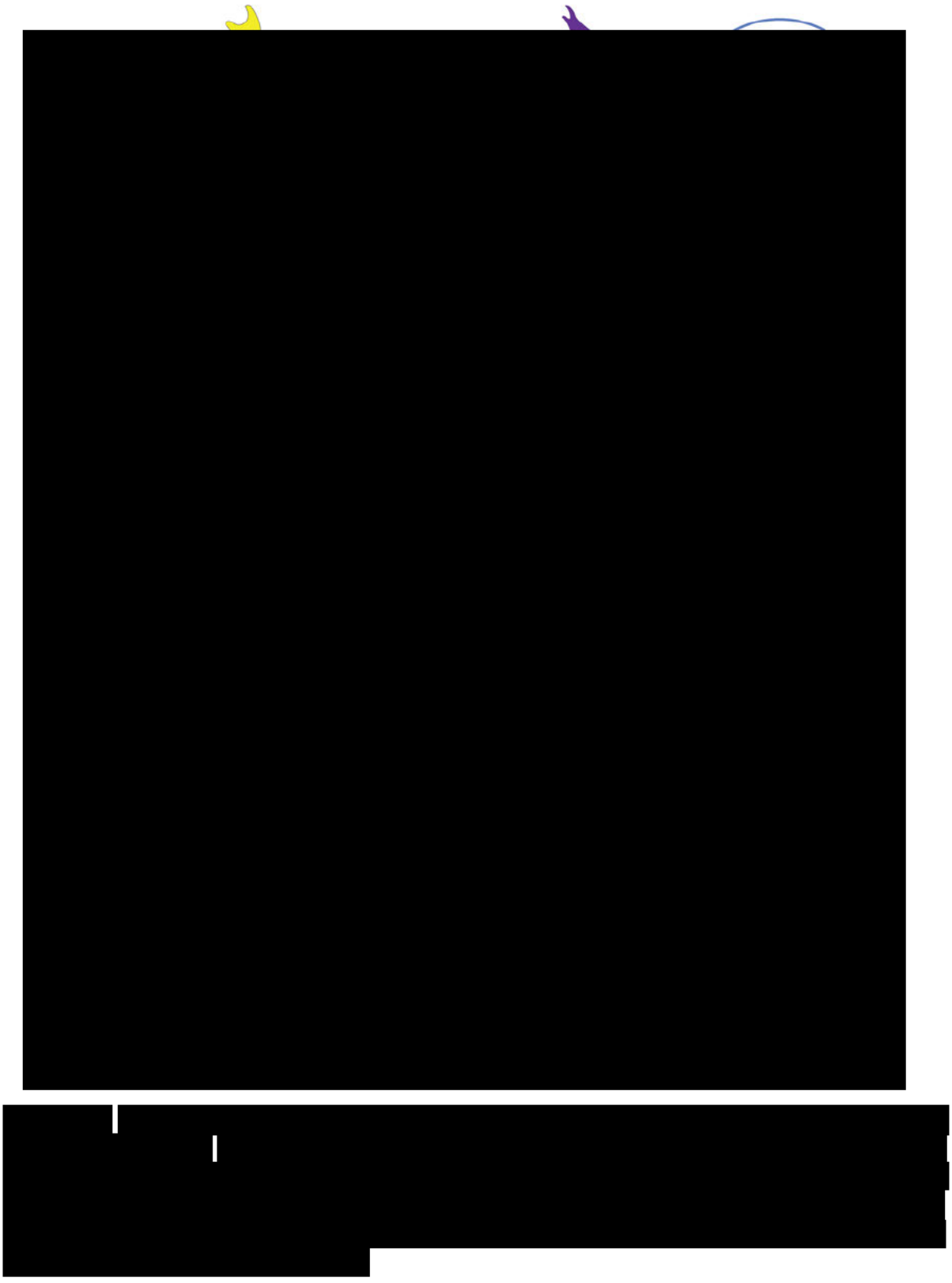

[redacted]

[redacted]

[redacted]

[redacted]

4.6 Conclusion

[redacted]

[redacted]

CHAPTER 5

CONCLUSIONS

The main aim of this thesis was to analyse the relationship between jaw morphology, functional performance and diet in Mesozoic mammals. To do so, I used a robust sample of modern mammals of known diets as a comparative basis and I employed a variety of techniques, including **geometric morphometrics**, mechanical advantage, finite element analysis, and **phylogenetic comparative methods**. I also developed a new technique to aid in the biomechanical analysis of fossil jaws. I found clear differences in the morphology and functional performance of the jaws of small mammals of different diets, and used this knowledge to infer diet in Mesozoic mammals. Below, I summarise the findings of each chapter.

5.1 Jaw shape and mechanical advantage are indicative of diet in Mesozoic mammals

Chapter 2 involved analysing the relationship between 2D jaw shape, mechanical advantage (i.e., a functional metric describing jaw leverage), and diet in small extant mammals, to later infer diet in Mesozoic mammals. I decided to use this 2D approach, based on photographic data, for several reasons: 1) after teeth, jaws are one of the most commonly preserved fossils of Mesozoic mammals; 2) lateral view photographs of mammal jaws, both extinct and extant, are ubiquitous in the literature and they are also easy to access in museum collections; 3) this allowed me to gather a considerable sample size, which I would not have been able to do with other types of data; 4) jaw morphology is intertwined with diet and, because I was able to gather a substantial sample of both extinct and extant mammals, I had the opportunity of investigating how jaw form and function related to the feeding ecology of small mammals; and finally 5) jaw shape analysis of Mesozoic mammals already existed [80], but functional studies of their jaws were lacking.

Differences in jaw morphology, which in turn relates to differences in function, between carnivorous and herbivorous mammals have long been highlighted in the literature. For example, the position of the condyle with respect to the tooth is a common difference observed when comparing carnivorans with herbivorous ungulates. The condyle of carnivores tends to be in line with the tooth row and, together with shearing teeth and large areas for the insertion of the **temporalis** muscle in the jaw and, the skull and jaw morphology of carnivores allows them to have a large gape and delivers a strong bite for slicing and crushing [43]. In contrast, ungulates have a very dorsally positioned condyles, which increases the mechanical advantage of their main adductor muscle: the **masseter**. Likewise, the tall ascending ramus of herbivorous ungulates allows for a larger attachment area for the **masseter**. Together with their specialised dentition, these traits prove ideal for grinding tough plant material [43]. Based on these ideas and, following on from the results of Grossnickle and Polly, [80], I was hoping to find clear differences in jaw shape between **faunivorous** and herbivorous extant mammals (note Grossnickle and Polly, [80] did not find differences between the jaw shapes of carnivores and insectivores).

In contrast to Grossnickle and Polly, [80], I used a more detailed landmarking regime and a bigger sample size, which allowed me to find a better separation between herbivores, carnivores, and insectivores. I was also expecting that most Mesozoic mammals would have similar jaw shapes to insectivores, and only a few specialised clades would resemble carnivores (e.g., eutriconodontans). I was surprised to find an extremely good correspondence between the proposed diets of Mesozoic mammals (which were largely based on skull and dental morphology, as well as body size, e.g., [30, 80, 98]) and the results of my study, and my findings also contributed further evidence to support or reject the proposed diets of some Mesozoic mammals. For example, the diet of *Agilodocodon* has been a matter of debate. Meng et al., [146] suggested this **docodontan** had dental adaptations for an exudativorous feeding behaviour, while Wible and Burrows, [234] refuted this hypothesis and suggested an insectivorous diet for this taxon; the latter hypothesis is fully supported by my results.

I also expected to find a clear separation between the mechanical advantage values of the different dietary categories, with carnivores having high mechanical advantage of the **temporalis** (**MAT**) and herbivores high mechanical advantage of the **masseter** (**MAM**). My results were not so straightforward: I found that mechanical advantage values on their own do not obviously correspond to a particular dietary category and rather should be used in a comparative manner, alongside jaw shape. I was surprised to find that carnivores are not the only dietary group with high **MAT**, but that herbivores do as well, highlighting the fact that certain morphological and functional traits can have more than one purpose. In both herbivores and carnivores, an enlarged **temporalis** muscle is key in avoiding dislocating forces when feeding but as a result of widely different needs (i.e., struggling prey in carnivores and biting hard plant material in herbivores) [200].

Based on the results of this chapter, I believe the methodology I used to be effective in dis-

tinguishing dietary categories among small mammals and has the potential to be used in, not only Mesozoic mammals, but also in other Cenozoic small mammals. It would be interesting to analyse how this relationship between jaw shape, function and diet changes when using larger mammals, and analyse how it changes throughout the evolution of mammals. There is room for improvement in this study, including analysing a larger sample size of extant mammals for further discriminant analyses of jaw shape. A limitation of this study lies on the quality of the jaw reconstructions of some Mesozoic mammals; however, some studies that have re-evaluated old reconstructions of fossil material using more recently developed techniques. For example, Schultz et al., [206] re-examined the jaw morphology of *Docodon victor* and found that manual reconstructions of its jaw from previous decades were incorrect; with the use of **CT** scan data, a more accurate reconstruction of its jaw was achieved (and this jaw reconstruction was used in the analyses of Chapter 2 and 4). This type of data is useful in uncovering morphology hidden in matrix and reconstructing distorted material (see [108])

5.2 Validating the use of extruded finite-element models using early mammal jaws

Having analysed jaw function using a 2D metric (i.e., mechanical advantage), I was interested in analysing the three-dimensional functional performance of the jaws of small mammals using Finite Element Analysis (**FEA**). However, building finite element models using tomographic data is expensive and time-consuming, particularly because I wanted to analyse a large sample of mammalian jaws. Building on from the MSc project of Thomas Burgess, I decided to validate the use of simplified 3D models of early mammal jaws built from photographs for their use in FEA. This idea, while novel in palaeontology, is common in engineering as FEA is used as a technique to evaluate the performance of structures before they are built- paraphrasing Colin Palmer “engineers do not **CT** scan bridges and perform FEA on structures that are already operational”.

When performing this study, I anticipated that the results of these simplified 3D models, which I called “enhanced extruded FE models” would be somewhat similar to those produced by tomography based models: I expected the stress distribution heatmaps to be similar, but the numerical values of stress and strain to not be identical. However, when analysing the output of the enhanced extruded FE models, I was surprised to find that their resulting stress and strain absolute values very closely resembled those produced by tomography-based FE models, making enhanced extruded models a viable alternative. I believe this to be of paramount importance regarding accessibility to techniques such as **FEA**. When building tomography-based models, one needs the monetary resources to pay for at least **CT** scanning, segmentation software, and finite element analysis software, which could very well amount to thousands of pounds. Hailing from a developing country myself, I fully understand and support the need to make these cutting-edge

techniques more accessible, and I believe the use of extruded FE models can at least reduce the cost of performing **FEA** by eliminating the costs of **CT** scanning and segmentation software. Extruded FE models are built in freely available software such as ImageJ and Blender, and I will make the protocol for building these models available when publishing Chapter 4 (see Appendix D).

Overall, I found the use of extruded FE models to be a viable alternative to the use of tomography-based models. An extruded FE model can be built in under an hour, which makes them ideal for performing large scale studies (as seen in Chapter 4). When compared to 2D FE models, extruded models might take longer to build, but produce more accurate results. So far, extruded models have only been tested on mammal jaws, but it would be relevant to test whether other structures, like long bones or teeth, could be accurately analysed using simplified 3D models such as these. The complexity the model is built with depends on the user, but I would advise against building overly-complicated models because 1) it would partly defeat the purpose of the model by taking a long time to build, and 2) errors with meshing might occur. Finally, I must highlight a couple of limitations of this technique: 1) internal structures cannot be accounted for, and 2) if a fossil is flattened and preserved within a slab, it might not be possible to acquire the measurements needed for building the model. However, in general, extruded FE models can be very useful when analysing the three-dimensional functional performance of simple structures like the mammalian jaw.

5.3 Functional performance of the jaws of Mesozoic mammals as revealed by Finite Element Analysis

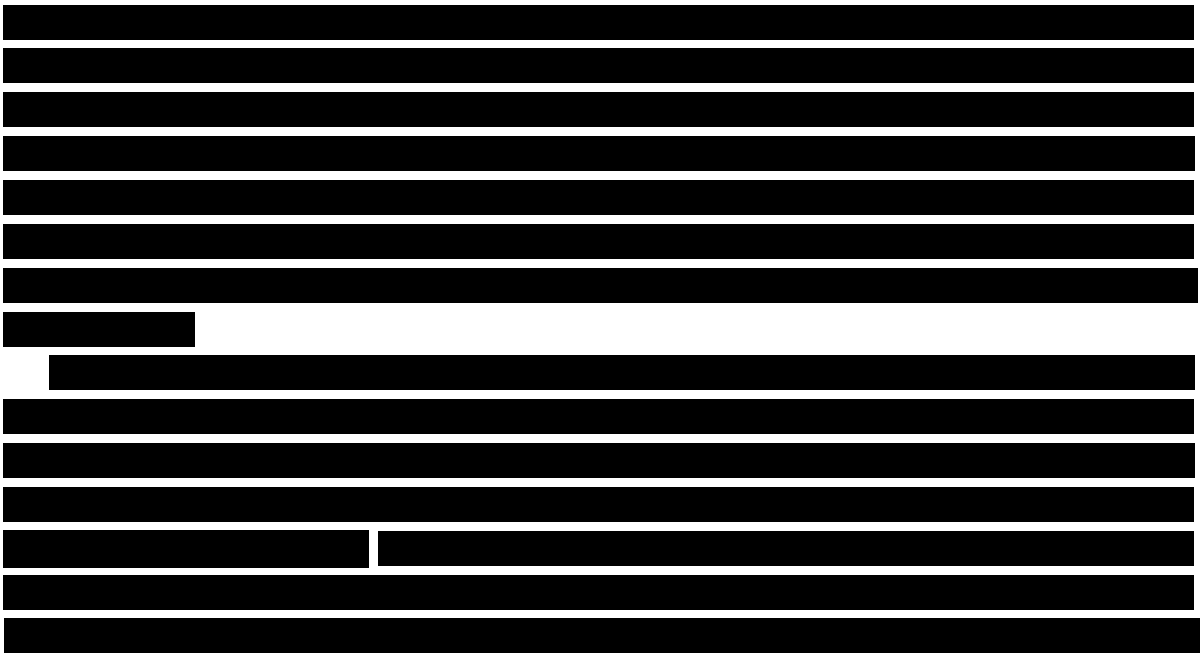

[redacted]

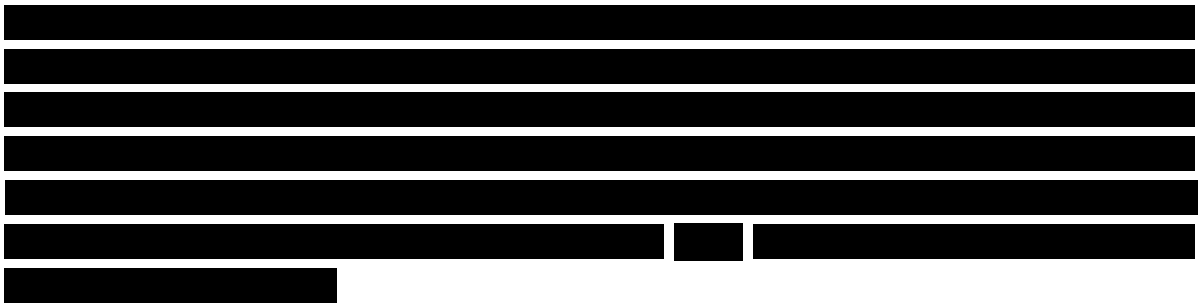

5.4 Future avenues of research

As with any PhD, my project began with a number of goals which I did not have the time to achieve, but are still very much viable avenues of research including 1) quantifying the jaw functional diversity and disparity of individual Mesozoic mammal faunas, bearing in mind that there are not a large number of faunas with pristine jaw preservation, 2) performing macroevolutionary studies of the functional evolution of the mammalian jaw, 3) studying the functional performance and evolution of the teeth of Mesozoic mammals, and 4) analysing the dynamics of Mesozoic terrestrial communities and their evolution in the context of the changing environmental conditions of the Mesozoic and relevant events like the Cretaceous Terrestrial Revolution.

5.5 Summary

In summary, this thesis has used functional, morphometric, and phylogenetic tools to identify differences among extant small mammals of known diets, and used that knowledge to infer diet in Mesozoic mammals. I highlighted the advantages and limitations of the approaches taken and the level of resolution one might expect from using these techniques. Finally, I introduced a new tool for building finite element models which I hope contributes to the accessibility of this technique and furthers the use of large scale finite element analysis studies. Lastly, I would like to finish with a graphic summarising the results of my thesis:

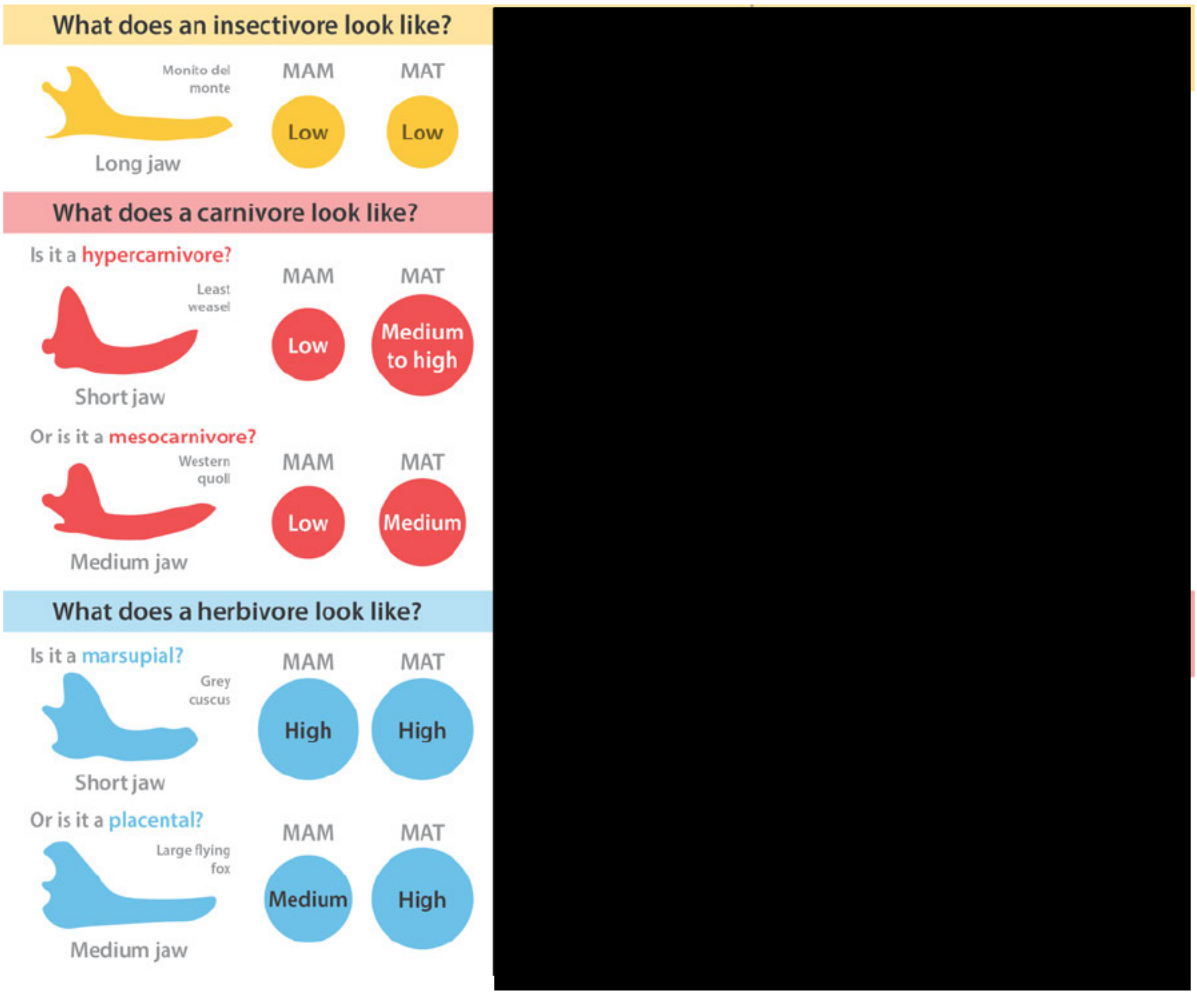

Figure 5.1: **Summary figure highlighting morphological and functional traits of different dietary categories among small mammals. MAM**=Mechanical advantage of the **masseter**, **MAT**=Mechanical advantage of the **temporalis**.

APPENDIX A

APPENDIX A

This appendix has the supplementary information of Chapter 2.

S2 Data Supplementary Data Chapter 2. All the supporting data used in this manuscript can be found in the following link: `https://data.bris.ac.uk/webshare/Palaeobiology_Users/ae9909fc-f5e4-48ac-82db-4a97cc12728d/`.

This appendix includes the following figures and tables:

1. Complete list of taxa used in this study, and their diets (Tables A.1, A.2 and A.3).
2. Genus-level phylogenies of placentals, marsupials, and Mesozoic mammals (Figs. A.1, A.2,A.3)
3. Time-scaled phylogeny of all the taxa considered in this study (Fig. A.4)
4. PCA and PGLS plots including allotherians (Figures A.5 and A.9)
5. All **MA** values obtained in this study (Table A.4)
6. Visualisations of **MA** values on the time-scaled phylogeny used here (Figs. A.6, A.7)
7. Morphofunctional landscape showing **MA** values (m1 outlever) in the context of jaw shape (Fig. A.8)
8. PGLS plots of jaw shape and **MA** of the masseter and temporalis (m1 outlever) (Figs. A.10, A.11)

Order	Common name	Species name	Diet
Afrosoricida	Short-tailed shrew tenrec	*Microgale brevicaudata*	Insectivore
	Cowan's shrew tenrec	*Microgale cowani*	Insectivore
	Giant otter shrew	*Potamogale velox*	Carnivore
	Tailless tenrec	*Tenrec ecaudatus*	Omnivore
Carnivora	Northern olingo	*Bassaricyon gabbii*	Herbivore
	Humboldt's hog-nosed skunk	*Conepatus humboldtii*	Omnivore
	Common kusimanse	*Crossarchus obscurus*	Omnivore
	Tayra	*Eira barbara*	Omnivore
	Sand cat	*Felis margarita*	Carnivore
	Malagasy civet	*Fossa fossana*	Carnivore
	Ring-tailed vontsira	*Galidia elegans*	Omnivore
	Common genet	*Genetta genetta*	Carnivore
	Javan mongoose	*Herpestes javanicus*	Omnivore
	Margay	*Leopardus wiedii*	Carnivore
	South American gray fox	*Lycalopex griseus*	Omnivore
	Hooded skunk	*Mephitis macroura*	Omnivore
	Least weasel	*Mustela nivalis*	Carnivore
	African palm civet	*Nandinia binotata*	Omnivore
	White-nosed coati	*Nasua narica*	Omnivore
	Asian palm civet	*Paradoxurus hermaphroditus*	Omnivore
	Spotted linsang	*Prionodon pardicolor*	Carnivore
	Corsac fox	*Vulpes corsac*	Carnivore
Chiroptera	Jamaican fruit bat	*Artibeus jamaicensis*	Herbivore
	Big-eared woolly bat	*Chrotopterus auritus*	Omnivore
	Little brown bat	*Myotis lucifugus*	Insectivore
	Greater bulldog bat	*Noctilio leporinus*	Carnivore
	Brown long-eared bat	*Plecotus auritus*	Insectivore
	Large flying fox	*Pteropus vampyrus*	Herbivore
Eulipotyphla	Four-toed hedgehog	*Atelerix albiventris*	Omnivore
	Northern short-tailed shrew	*Blarina brevicauda*	Omnivore
	Hairy-tailed mole	*Parascalops breweri*	Insectivore
	Hispaniolan solenodon	*Solenodon paradoxus*	Insectivore
Macroscelidea	Short-snouted elephant shrew	*Elephantulus brachyrhynchus*	Omnivore
	Rufous elephant shrew	*Elephantulus rufescens*	Omnivore
Scandentia	Striped treeshrew	*Tupaia dorsalis*	Omnivore
	Common treeshrew	*Tupaia glis*	Omnivore
	Ruddy treeshrew	*Tupaia splendidula*	Omnivore

Table A.1: **List of extant placental taxa used in this study and their dietary categories.** Dietary information obtained from [153]. Yellow=Insectivore; Red= Carnivore; Purple= Omnivore; Blue= Herbivore

Order	Common name	Species name	Diet
Dasyuromorphia	Yellow-footed antechinus	*Antechinus flavipes leucogaster*	Insectivore
	Dusky antechinus	*Antechinus swainsonii*	Insectivore
	Western quoll	*Dasyurus geoffroii*	Carnivore
	Northern quoll	*Dasyurus hallucatus*	Carnivore
	Numbat	*Myrmecobius fasciatus*	Insectivore
	Dibbler	*Parantechinus apicalis*	Insectivore
	Brushed-tailed phascogale	*Phascogale tapoatafa*	Omnivore
	Long-tailed planigale	*Planigale ingrami*	Insectivore
	Fat-tailed dunnart	*Sminthopsis crassicaudata*	Insectivore
Didelphimorphia	Derby's woolly opossum	*Caluromys derbianus*	Omnivore
	Water opossum	*Chironectes minimus*	Carnivore
	Robinson's mouse opossum	*Marmosa robinsoni*	Omnivore
	Brown four-eyed opossum	*Metachirus nudicaudatus*	Omnivore
	Northern three-striped opossum	*Monodelphis americana*	Omnivore
	Anderson's four-eyed opossum	*Philander andersoni*	Omnivore
Diprotodontia	Feathertail glider	*Acrobates pygmaeus*	Omnivore
	Woylie	*Bettongia penicillata*	Omnivore
	Goodfellow's tree kangaroo	*Dendrolagus goodfellowi*	Herbivore
	Small dorcopsis	*Dorcopsulus vanheurni*	Herbivore
	Sugar glider	*Petaurus breviceps*	Omnivore
	Northern common cuscus	*Phalanger orientalis*	Herbivore
	Long-nosed potoroo	*Potorous tridactylus*	Omnivore
	Common ringtail possum	*Pseudocheirus peregrinus*	Herbivore
	Tasmanian pademelon	*Thylogale billardierii*	Herbivore
	Common brushtail possum	*Trichosurus vulpecula*	Omnivore
Microbiotheria	Monito del monte	*Dromiciops gliroides*	Insectivore
Paucituberculata	Long-nosed caenolestid	*Rhyncholestes raphanurus*	Omnivore
Peramelemorphia	Western barred bandicoot	*Perameles bougainville*	Omnivore

Table A.2: **List of extant marsupial taxa used in this study and their dietary categories.** Dietary information obtained from [153]. Yellow=Insectivore; Red= Carnivore; Purple= Omnivore; Blue= Herbivore

Higher clade	Genus	Suggested diet	Source
	Stem mammals		
	Haramiyavia	Herbivore/omnivore	[117]
	Sinoconodon	Carnivore/scavenger	[97, 98]
Morganucodonta	*Morganucodon*	Insectivore	[75]
	Dinnertherium	Unknown	
Docodonta	*Agilodocodon*	Omnivore	[30]
	Castorocauda	Carnivore	[30]
	Haldanodon	Insectivore	[167]
	Docodon	Insectivore	[167]
	Docofossor	Insectivore	[30]
	Agilodocodon	Insectivore	[234]
	Microdocodon	Unknown	
	Non-therian crown mammals		
	Fruitafossor	Omnivore	[124]
Australosphenida	*Henosferus*	Unknown	
	Teinolophos	Invertivore	[186]
Eutriconodonta	*Volaticotherium*	Insectivore	[30]
	Phascolotherium	Unknown	
	Yanoconodon	Insectivore	[30]
	Triconodon	Carnivore	[98, 195]
	Trioracodon	Carnivore	[98, 195]
	Argentoconodon	Unknown	
	Gobiconodon	Carnivore	[30]
	Repenomamus	Carnivore	[30, 88]
"Symmetrodonta"	*Spalacotherium*	Unknown	
	Origolestes	Unknown	
	Zhangheotherium	Insectivore	[30]
	Maotherium	Insectivore	[30]
Dryolestidae	*Crusafontia*	Unknown	
	Amblotherium	Unknown	
	Amphitherium	Unknown	
	Vincelestes	Carnivore/omnivore	[20, 194]
	Therian crown mammals		
Eutheria	*Sinodelphys*	Insectivore	[30]
	Juramaia	Insectivore	[30]
	Eomaia	Insectivore	[30]
	Maelestes	Unknown	
	Asioryctes	Unknown	
	Sasayamamylos	Unknown	
	Kennalestes	Insectivore	[80]
	Daulestes	Unknown	
	Uchkudukodon	Unknown	
	Kulbeckia	Insectivore	[80]
	Barunlestes	Insectivore	[80]
	Zalambdalestes	Unknown	
Metatheria	*Deltatheridium*	Carnivore	[195]
	Alphadon	Insectivore	[80]
	Didelphodon	Carnivore	[39, 195]
	Eodelphis	Carnivore	[39]

Table A.3: **List of extinct taxa used in this study and their suggested dietary categories.** Dietary information obtained from [20, 30, 39, 75, 80, 88, 97, 98, 117, 124, 167, 186, 194, 195, 234]. Yellow=Insectivore; Red= Carnivore; Purple= Omnivore; Blue= Herbivore.

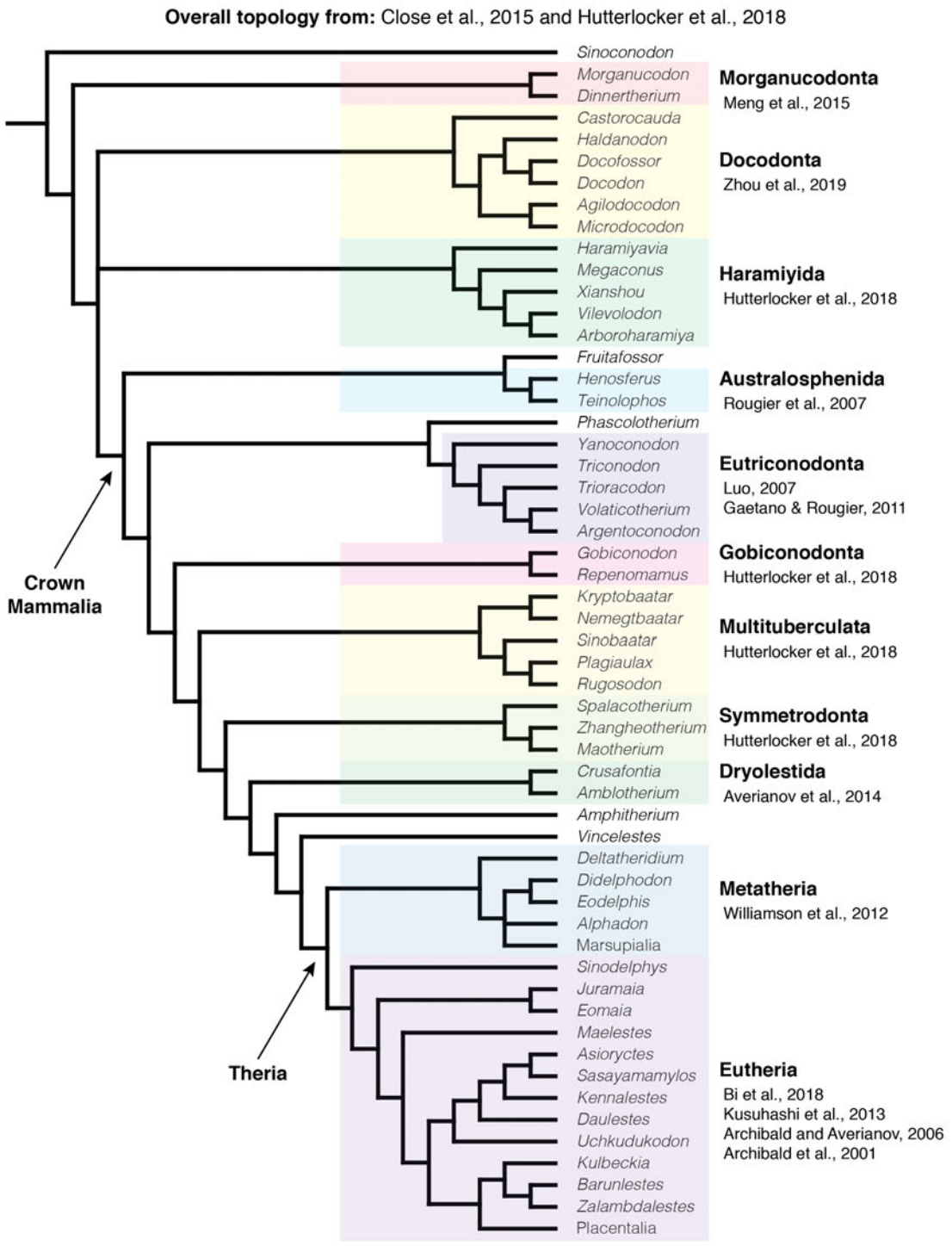

Figure A.1: **Genus-level phylogeny of the Mesozoic taxa used in this study.** Phylogeny assembled from [38, 91] (overall topology), [99] (*Haramiyavia*), [146] (Morganucodonta), [247] (Docodonta), [197] (Australosphenida), [73, 113] (Eutriconodonta), [129] (Symmetrodonta) [11] (Dryolestidae), [237] (Metatheria), [7, 8, 17, 106] (Eutheria)

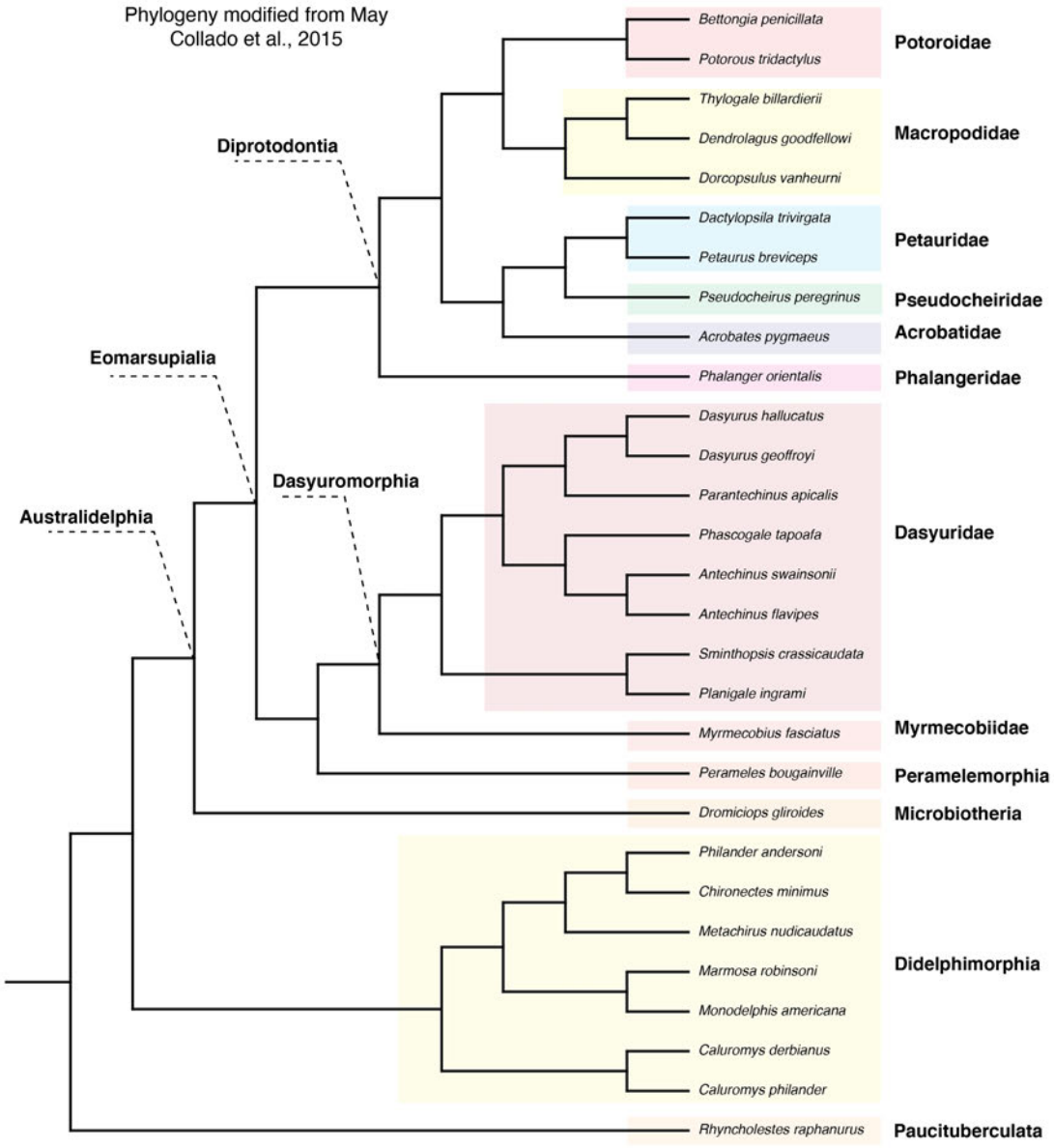

Figure A.2: **Species level phylogeny of the marsupial taxa used in this study.** Phylogeny modified from [137]

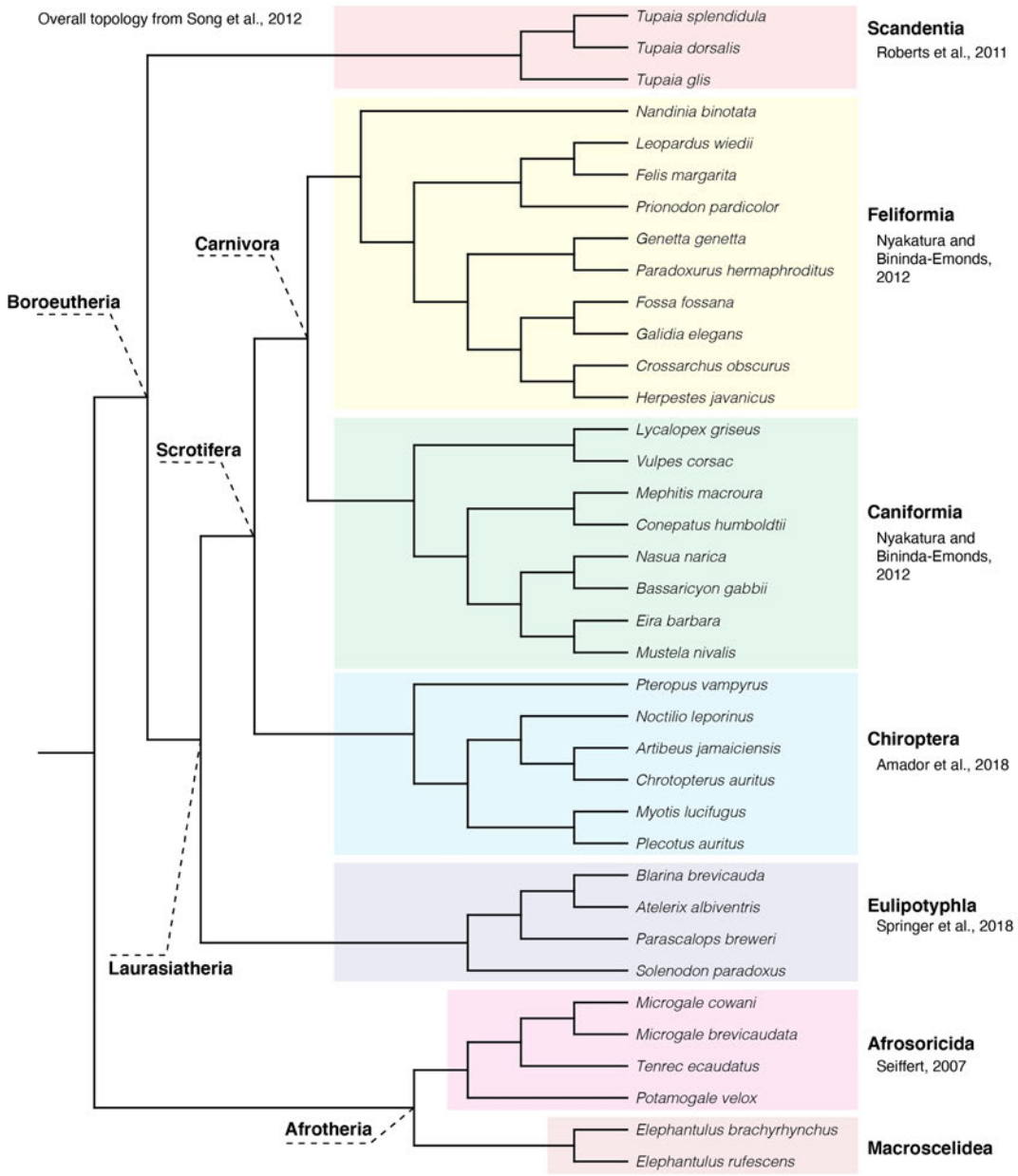

Figure A.3: **Species level phylogeny of the placental taxa used in this study.** Phylogeny assembled from [215] (overall topology), [190] (Scandentia), [157] (Carnivora), [3] (Chiroptera), [216] (Eulipotyphla), [208] (Afrosoricida).

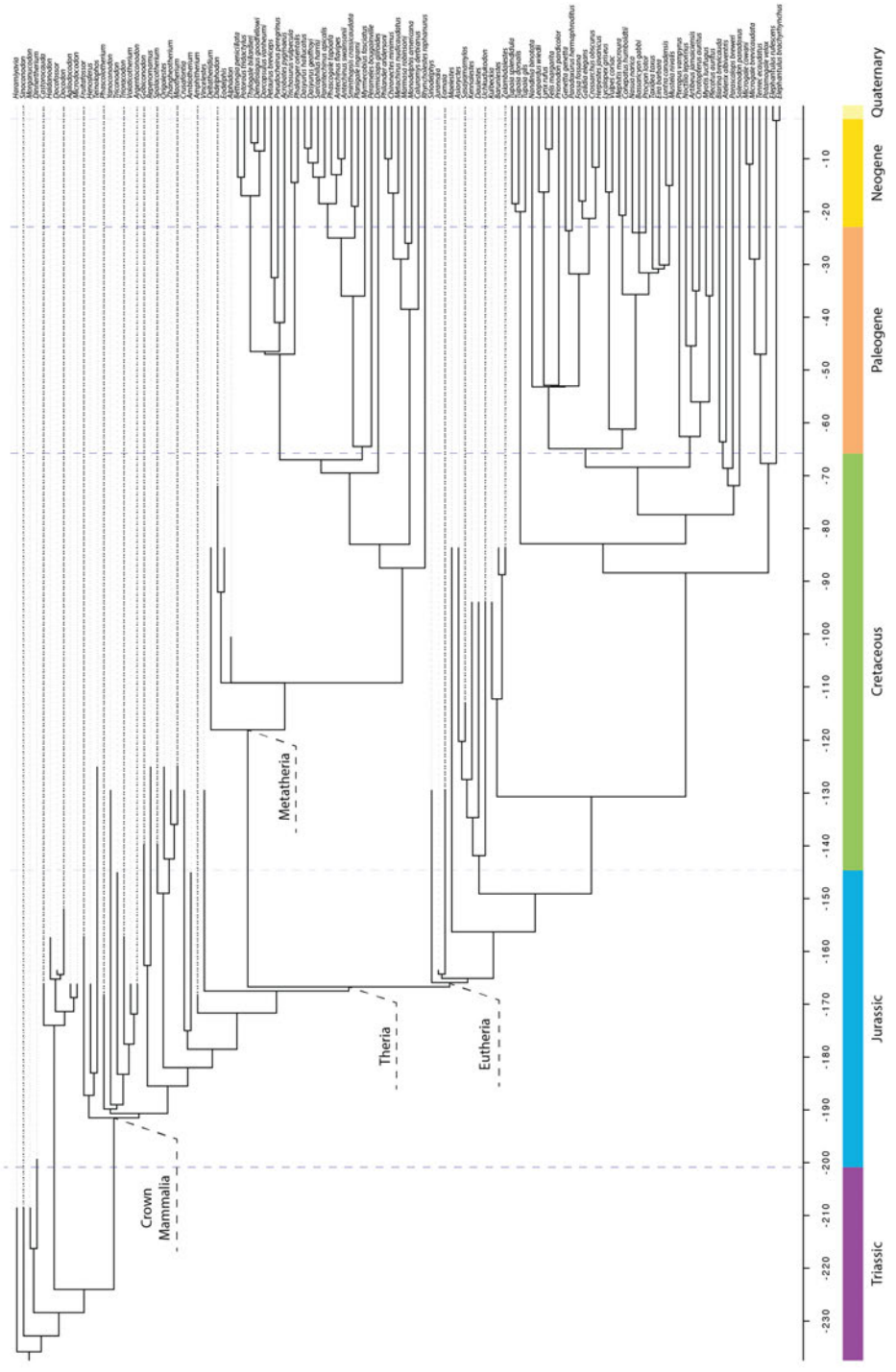

Figure A.4: **Time scaled phylogeny.** Dated using the 'equal' method of [24]. Phylogeny assembled using sources detailed in Figs. A.1, A.2, A.3

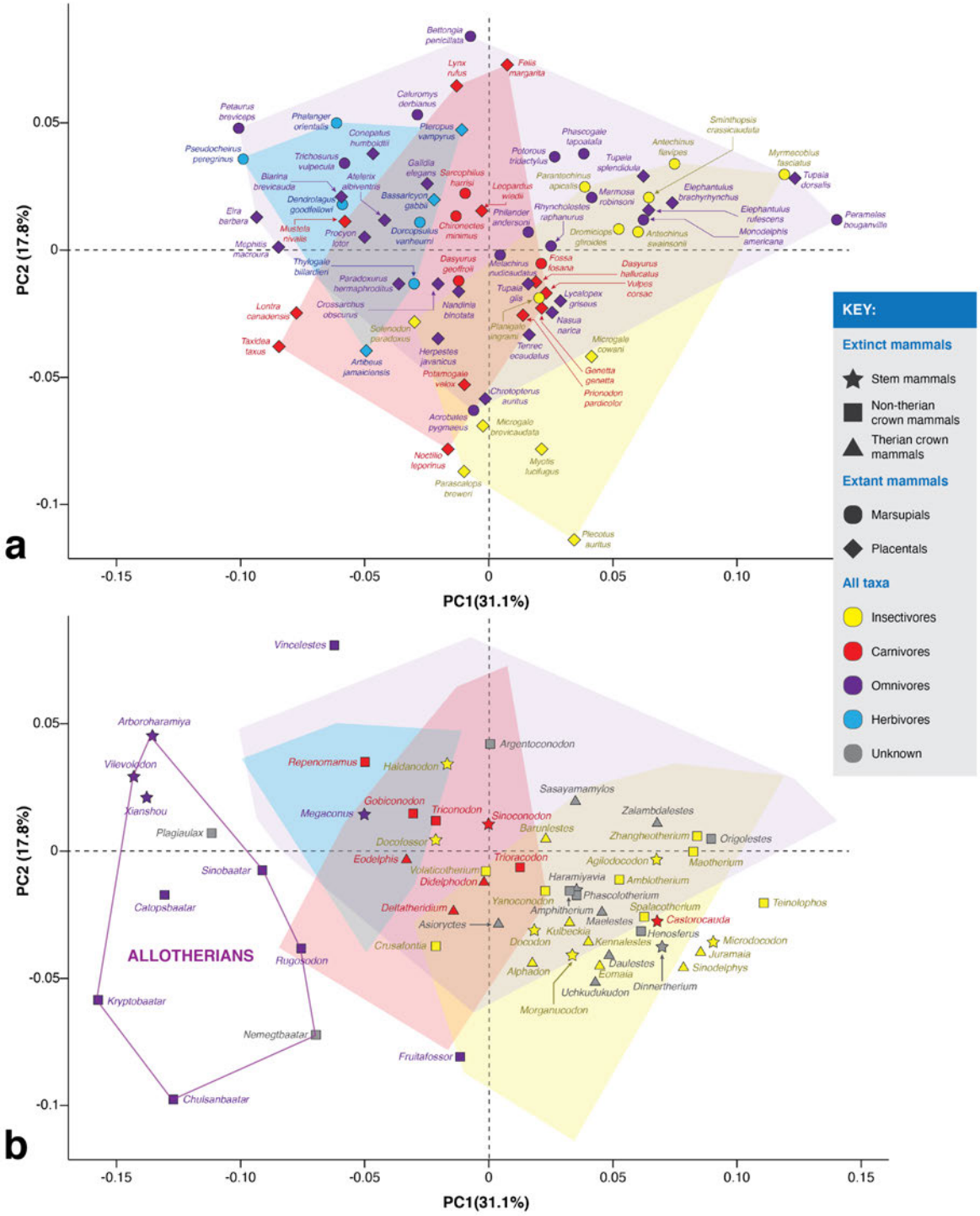

Figure A.5: **Scatter plots of the Principal Component Analysis (PCA) results (PC1 vs PC2), including allotherians (i.e., multituberculates and haramiyids).** a) Extant taxa, b) Extinct taxa. Convex hulls shown for extant insectivores (yellow), carnivores (red), omnivores (purple) and herbivores (blue). Icon colours indicate known dietary categories of extant mammals and suggested dietary categories for Mesozoic mammals (obtained from the literature).

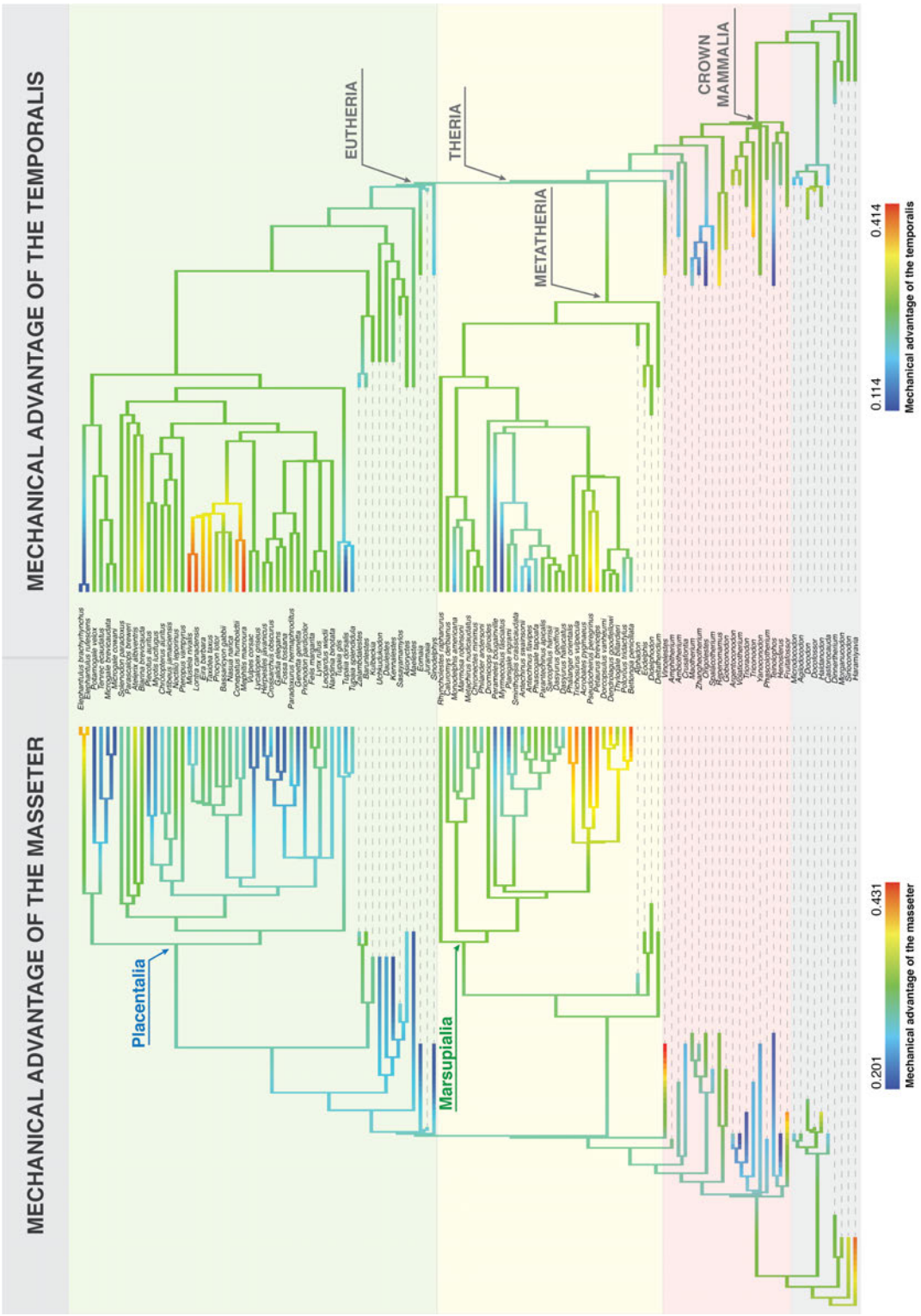

Figure A.6: **Mechanical advantage values of the temporalis (left) and masseter (right) visualised in the context of the phylogeny used in this study**, with taxa names. Moment arm of resistance measured at the jaw tip. Taxon numbers as in Figure 2.1

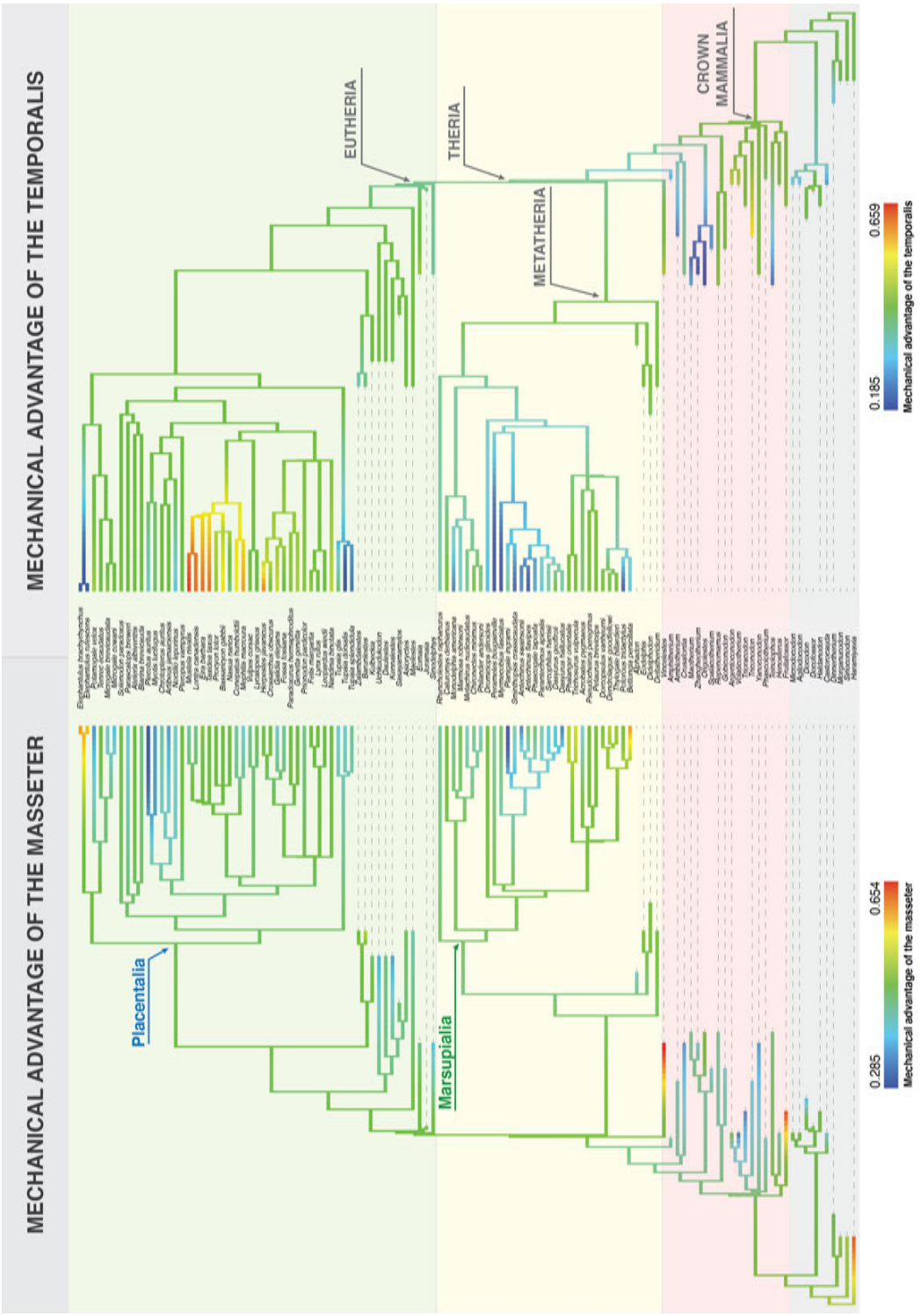

Figure A.7: **Mechanical advantage values of the temporalis (left) and masseter (right) visualised in the context of the phylogeny used in this study**, with taxa names. Moment arm of resistance measured at the m1.

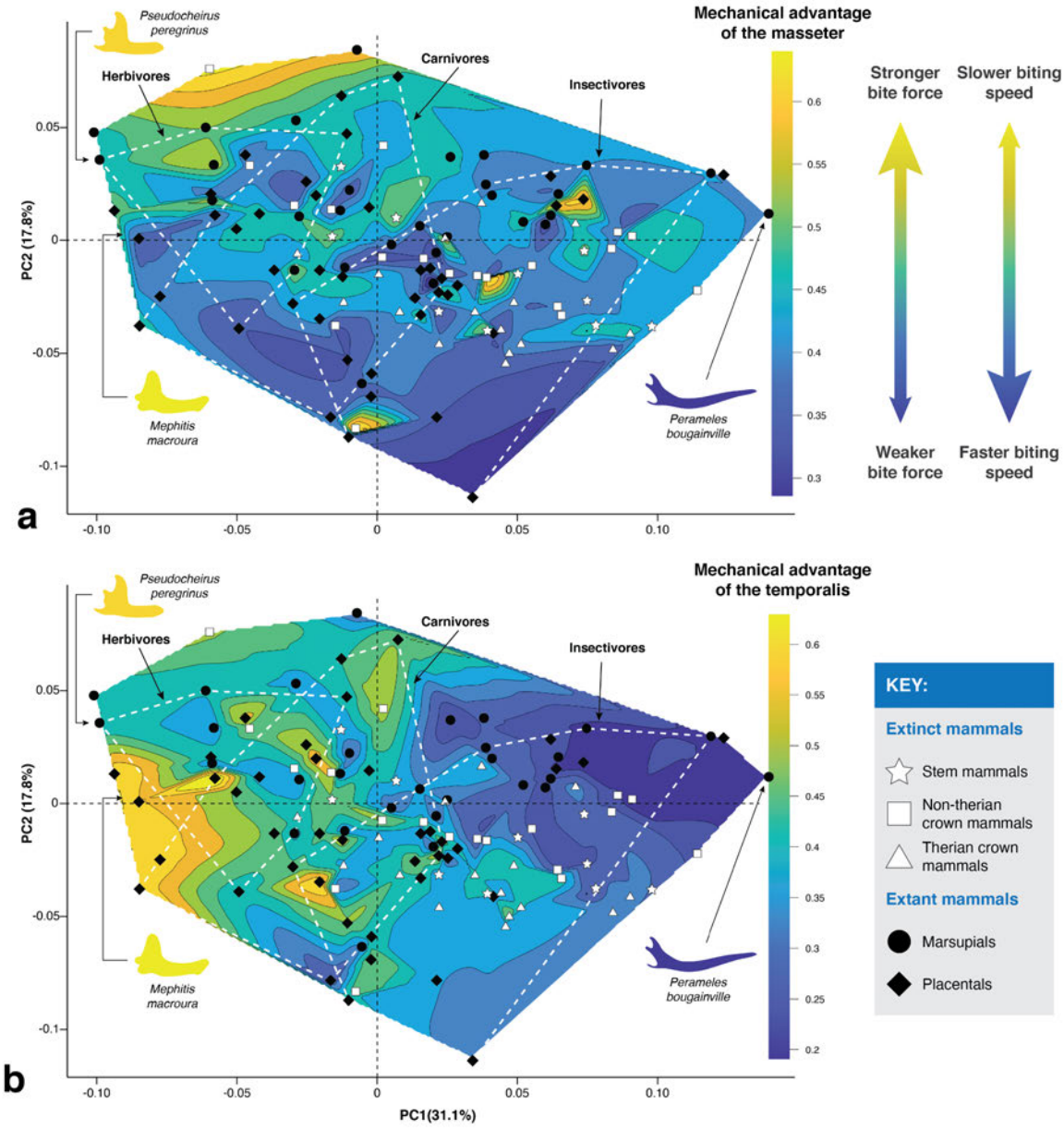

Figure A.8: **Morphofunctional landscape comparing a functional metric (i.e., mechanical advantage of the masseter [A, MAM] and temporalis [B, MAT]) with jaw shape (PC1 and PC2 axes). Moment arm of resistance for mechanical advantage measured at the m1.** Silhouette colours are indicative of the mechanical advantage values of the taxa.

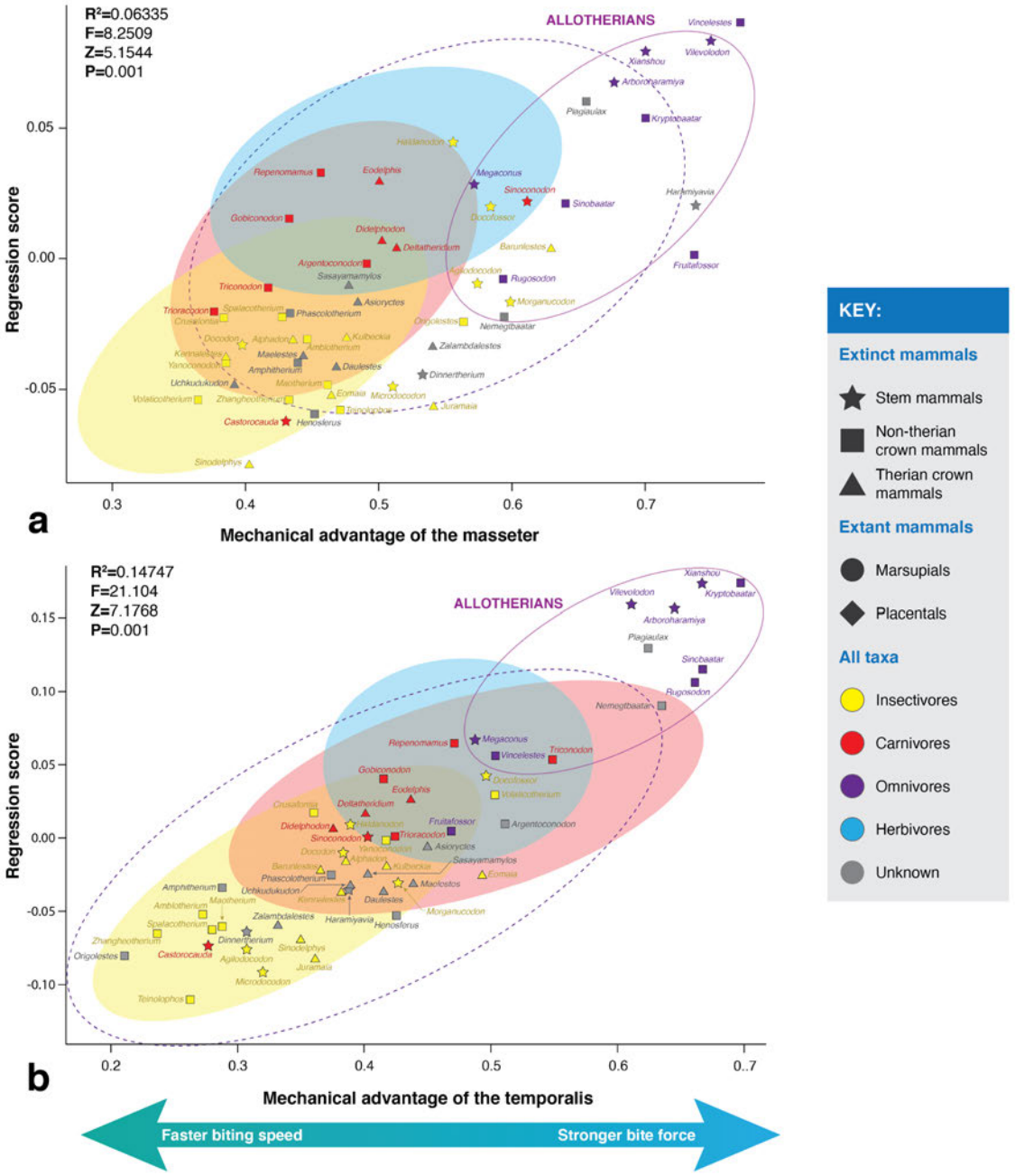

Figure A.9: **PGLS regression of Procrustes coordinates (i.e., jaw shape) on mechanical advantage of the masseter (a) and temporalis (b). Only extinct taxa are shown; includes allotherians.** Colours indicate suggested dietary categories for Mesozoic mammals (obtained from the literature). Colored ovals indicate where extant taxa of known dietary categories plot.

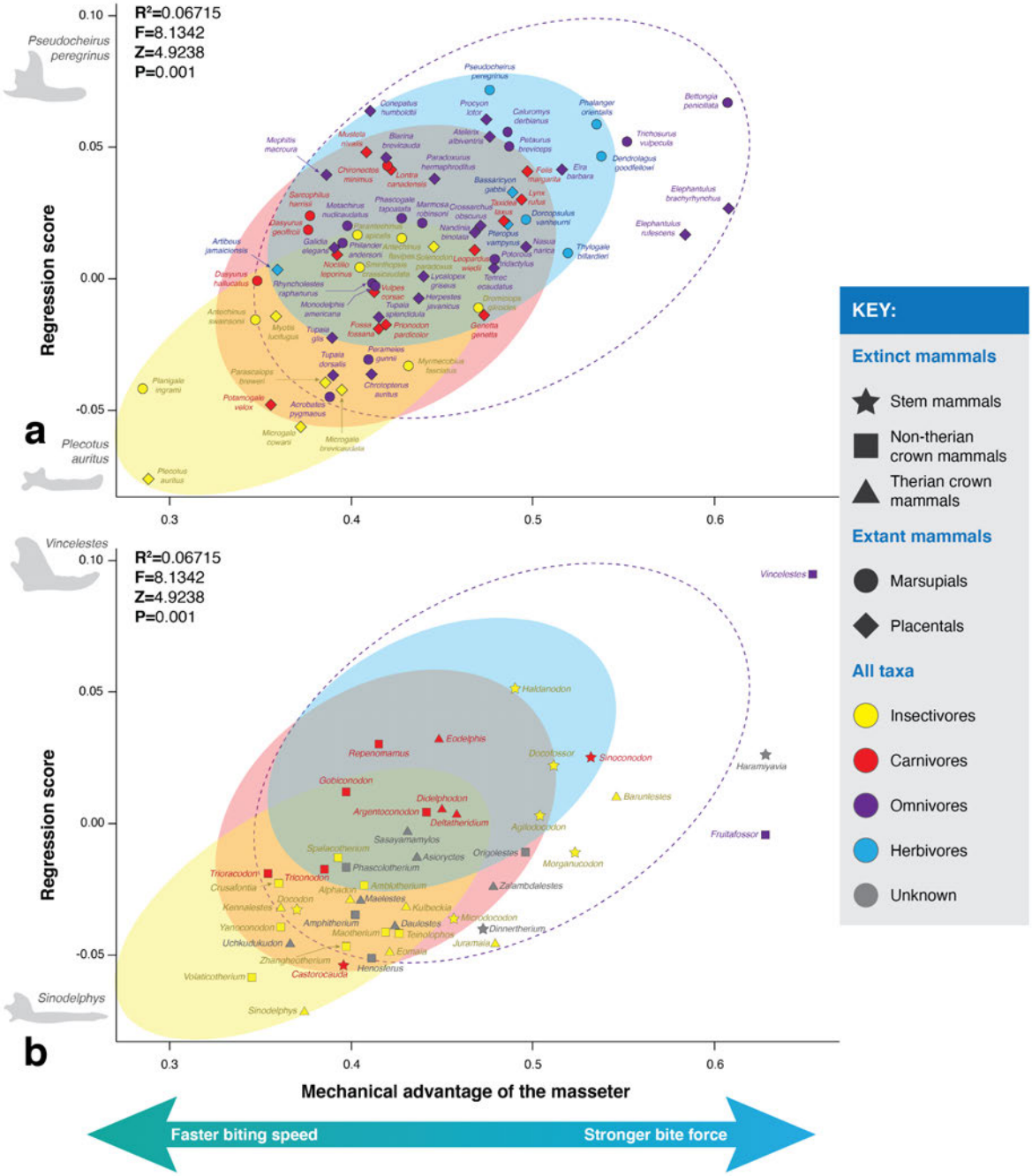

Figure A.10: **Relationship between jaw shape and mechanical advantage of the masseter measured at the m1.** PGLS regression of Procrustes coordinates on mechanical advantage of the masseter on extant taxa (a) and extinct taxa (b). Colours indicate known dietary categories of extant mammals and suggested dietary categories for Mesozoic mammals (obtained from the literature). Ovals indicate where extant taxa of known dietary categories plot.

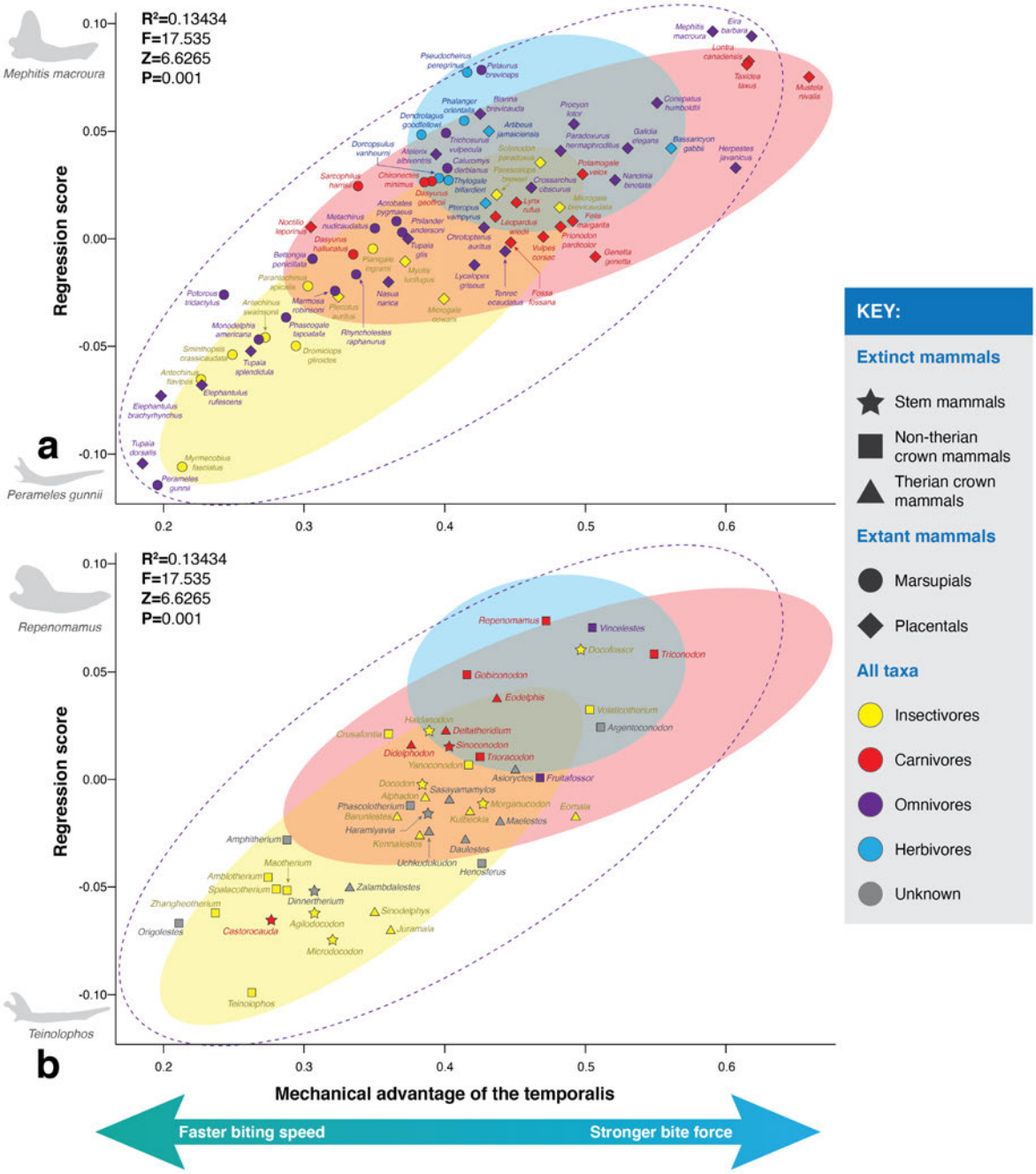

Figure A.11: **Relationship between jaw shape and mechanical advantage of the temporalis measured at the m1.** PGLS regression of Procrustes coordinates on mechanical advantage of the temporalis on extant taxa (a) and extinct taxa (b). Colours indicate known dietary categories of extant mammals and suggested dietary categories for Mesozoic mammals (obtained from the literature). Ovals indicate where extant taxa of known dietary categories plot.

	Taxon	**MAT (m1)**	**MAM (m1)**	**MAT (jaw tip)**	**MAM (jaw tip)**
1	*Haramiyavia*	0.388	0.628	0.254	0.410
2	*Sinoconodon*	0.403	0.532	0.281	0.371
3	*Morganucodon*	0.427	0.523	0.288	0.353
4	*Dinnetherium*	0.307	0.473	0.208	0.321
5	*Castorocauda*	0.277	0.395	0.183	0.261
6	*Haldanodon*	0.389	0.490	0.295	0.373
7	*Docofossor*	0.496	0.511	0.335	0.341
8	*Docodon*	0.384	0.370	0.302	0.291
9	*Agilodocodon*	0.307	0.504	0.183	0.300
10	*Microdocodon*	0.320	0.456	0.183	0.261
11	*Fruitafossor*	0.468	0.628	0.297	0.399
12	*Henosferus*	0.426	0.411	0.220	0.212
13	*Teinolophos*	0.263	0.426	0.141	0.229
14	*Phascolotherium*	0.375	0.397	0.241	0.256
15	*Yanoconodon*	0.417	0.361	0.289	0.249
16	*Triconodon*	0.549	0.385	0.360	0.252
17	*Trioracodon*	0.425	0.354	0.273	0.228
18	*Volaticotherium*	0.503	0.345	0.312	0.214
19	*Argentoconodon*	0.511	0.441	0.318	0.274
20	*Gobiconodon*	0.416	0.397	0.323	0.307
21	*Repenomamus*	0.472	0.415	0.346	0.305
22	*Spalacotherium*	0.281	0.393	0.186	0.260
23	*Origolestes*	0.211	0.496	0.136	0.318
24	*Zhangheotherium*	0.237	0.397	0.164	0.274
25	*Maotherium*	0.288	0.419	0.204	0.296
26	*Crusafontia*	0.360	0.360	0.253	0.253
27	*Amblotherium*	0.273	0.407	0.187	0.279
28	*Amphitherium*	0.288	0.402	0.205	0.286
29	*Vincelestes*	0.505	0.654	0.333	0.431
30	*Deltatheridium*	0.401	0.458	0.284	0.323
31	*Didelphodon*	0.376	0.450	0.280	0.335
32	*Eodelphis*	0.437	0.448	0.311	0.319
33	*Alphadon*	0.386	0.399	0.259	0.268
34	*Sinodelphys*	0.350	0.374	0.188	0.201
35	*Juramaia*	0.361	0.479	0.200	0.265
36	*Eomaia*	0.493	0.421	0.270	0.229
37	*Maelestes*	0.439	0.405	0.239	0.221
38	*Asioryctes*	0.450	0.436	0.271	0.262
39	*Sasayamamylos*	0.403	0.431	0.249	0.266
40	*Kennalestes*	0.382	0.361	0.225	0.207
41	*Daulestes*	0.415	0.424	0.242	0.248

42	*Uchkudukudon*	0.389	0.366	0.256	0.241
43	*Kulbeckia*	0.418	0.430	0.275	0.282
44	*Barunlestes*	0.366	0.546	0.220	0.328
45	*Zalambdalestes*	0.332	0.478	0.187	0.269
46	*Bettongia penicillata*	0.306	0.607	0.211	0.418
47	*Potorous tridactylus*	0.243	0.479	0.186	0.366
48	*Thylogale billardierii*	0.403	0.519	0.269	0.347
49	*Dendrolagus goodfellowi*	0.383	0.538	0.284	0.399
50	*Dorcopsulus vanheurni*	0.396	0.496	0.286	0.358
51	*Petaurus breviceps*	0.426	0.487	0.352	0.403
52	*Pseudocheirus peregrinus*	0.416	0.476	0.364	0.416
53	*Acrobates pygmaeus*	0.366	0.388	0.311	0.330
54	*Phalanger orientalis*	0.414	0.535	0.304	0.394
55	*Trichosurus vulpecula*	0.401	0.552	0.296	0.408
56	*Dasyurus hallucatus*	0.335	0.348	0.252	0.262
57	*Dasyurus geoffroii*	0.391	0.376	0.301	0.290
58	*Sarcophilus harrisi*	0.339	0.377	0.272	0.303
59	*Parantechinus apicalis*	0.303	0.403	0.230	0.305
60	*Phascogale tapoatafa*	0.287	0.428	0.210	0.314
61	*Antechinus swainsonii*	0.273	0.347	0.193	0.246
62	*Antechinus flavipes*	0.227	0.428	0.166	0.315
63	*Sminthopsis crassicaudata*	0.249	0.404	0.183	0.297
64	*Planigale ingrami*	0.349	0.285	0.270	0.220
65	*Myrmecobius fasciatus*	0.214	0.431	0.124	0.250
66	*Perameles bougainville*	0.197	0.409	0.114	0.237
67	*Dromiciops gliroides*	0.294	0.470	0.204	0.326
68	*Philander andersoni*	0.370	0.395	0.254	0.271
69	*Chironectes minimus*	0.386	0.420	0.275	0.299
70	*Metachirus nudicaudatus*	0.350	0.398	0.251	0.285
71	*Marmosa robinsoni*	0.322	0.439	0.217	0.296
72	*Monodelphis americana*	0.268	0.413	0.175	0.270
73	*Caluromys derbianus*	0.402	0.486	0.283	0.342
74	*Rhyncholestes raphanurus*	0.337	0.411	0.241	0.293
75	*Tupaia splendidula*	0.262	0.415	0.175	0.277
76	*Tupaia dorsalis*	0.185	0.390	0.117	0.247
77	*Tupaia glis*	0.374	0.389	0.252	0.261
78	*Nandinia binotata*	0.521	0.468	0.293	0.263
79	*Leopardus wiedii*	0.436	0.468	0.256	0.275
80	*Lynx rufus*	0.451	0.494	0.267	0.292
81	*Felis margarita*	0.491	0.497	0.298	0.301
82	*Prionodon pardicolor*	0.482	0.419	0.266	0.231
83	*Genetta genetta*	0.507	0.473	0.248	0.231
84	*Paradoxurus hermaphroditus*	0.482	0.446	0.307	0.284

85	*Fossa fossana*	0.447	0.415	0.244	0.226
86	*Galidia elegans*	0.530	0.390	0.305	0.224
87	*Crossarchus oscurus*	0.461	0.471	0.262	0.268
88	*Herpestes javanicus*	0.607	0.437	0.311	0.224
89	*Lycalopex griseus*	0.421	0.440	0.230	0.240
90	*Vulpes corsac*	0.470	0.412	0.256	0.224
91	*Mephitis macroura*	0.590	0.386	0.414	0.271
92	*Conepatus humboldtii*	0.551	0.410	0.368	0.274
93	*Nasua narica*	0.360	0.496	0.202	0.278
94	*Bassaricyon gabbii*	0.561	0.489	0.332	0.289
95	*Procyon lotor*	0.492	0.474	0.310	0.299
96	*Taxidea taxus*	0.615	0.484	0.372	0.293
97	*Eira barbara*	0.618	0.516	0.378	0.315
98	*Lontra canadensis*	0.616	0.422	0.394	0.271
99	*Mustela nivalis*	0.659	0.408	0.404	0.250
100	*Pteropus vampyrus*	0.429	0.486	0.274	0.311
101	*Noctilio leporinus*	0.305	0.392	0.260	0.334
102	*Artibeus jamaiciensis*	0.432	0.359	0.334	0.277
103	*Chrotopterus auritus*	0.428	0.411	0.276	0.265
104	*Myotis lucifugus*	0.372	0.358	0.254	0.245
105	*Plecotus auritus*	0.324	0.288	0.246	0.218
106	*Blarina brevicauda*	0.425	0.419	0.358	0.354
107	*Atelerix albiventris*	0.394	0.476	0.307	0.371
108	*Parascalops breweri*	0.437	0.385	0.323	0.284
109	*Solenodon paradoxus*	0.467	0.445	0.290	0.276
110	*Microgale cowani*	0.399	0.372	0.226	0.210
111	*Microgale brevicaudata*	0.481	0.394	0.296	0.243
112	*Tenrec ecaudatus*	0.443	0.478	0.231	0.249
113	*Potamogale velox*	0.498	0.355	0.295	0.211
114	*Elephantulus rufescens*	0.227	0.584	0.150	0.387
115	*Elephantulus brachyrhynchus*	0.198	0.608	0.130	0.399

Table A.4: **Mechanical advantage values of the temporalis (MAT) and masseter (MAM) obtained in this study.** Outlever measured at the m1 and the jaw tip.

APPENDIX B

APPENDIX B

This appendix has the detailed results of the sensitivity analyses (Subsection 3.5.2) of Chapter 3. It includes 6 tables with the raw strain and stress values of across all iterations, and 6 tables which depict these results using percentages (of how they compare to the original values).

For the supporting data of this Chapter, refer to:

S3 Data Supplementary Data Chapter 3. All the supporting data used in this paper can be found in the following link: `https://www.doi.org/10.5523/bris.2b5w9l61qc6vl2rrkhv0sdex6v`. It includes all the finite element models and field output reports used to validate the use of extruded finite element models.

	Strain			Stress			Validity
	Mean	Median	Max	Mean	Median	Max	
1	137.2	90.9	2722.7	3.6	2.8	55.5	Valid
2	135.5	90.9	2719.1	3.6	2.8	55.3	Invalid
3	136.8	91.5	2665.0	3.6	2.8	55.2	Valid
4	135.8	90.4	2610.1	3.6	2.7	55.6	Valid
5	136.0	91.5	2797.9	3.6	2.8	55.2	Invalid
6	135.0	90.5	2641.3	3.6	2.8	55.5	Invalid
7	136.7	90.2	2735.8	3.6	2.7	55.7	Valid
8	137.7	91.4	2718.5	3.6	2.8	55.3	Valid
9	142.9	94.5	2805.2	3.7	2.9	55.7	Invalid
10	131.6	92.0	2637.4	3.5	2.8	54.9	Valid
11	132.3	90.5	2641.1	3.5	2.8	55.1	Valid
12	145.4	95.6	2942.7	3.8	2.9	55.9	Invalid
13	144.7	95.7	2829.8	3.8	2.9	55.7	Invalid
14	132.2	91.5	2583.3	3.5	2.8	54.8	Valid
15	131.6	90.9	2581.5	3.5	2.8	55.2	Valid
16	143.6	94.4	2787.5	3.7	2.8	56.0	Invalid
17	144.1	95.1	2805.0	3.8	2.9	55.8	Invalid
18	131.9	91.2	2529.4	3.5	2.8	55.0	Valid
19	132.7	90.8	2600.8	3.5	2.8	54.9	Valid
20	142.4	93.9	2725.4	3.7	2.8	55.9	Invalid
21	146.0	96.2	2968.2	3.8	2.9	55.8	Invalid
22	131.3	91.8	2561.9	3.5	2.8	55.1	Valid
23	131.9	92.1	2714.0	3.5	2.8	54.7	Valid
24	144.9	95.1	2924.1	3.8	2.8	56.1	Invalid
25	132.0	90.1	2689.6	3.5	2.8	55.3	Valid
26	143.5	95.1	2885.8	3.7	2.9	55.6	Invalid
Original	136.3	90.9	2590.0	3.6	2.8	55.4	
Min	131.3	90.1	2529.4	3.5	2.7	54.7	
Max	146.0	96.2	2968.2	3.8	2.9	56.1	
STD	5.3	2.0	121.0	0.1	0.04	0.4	

Table B.1: **Raw stress (MPa) and strain (microstrain) results of the sensitivity analyses:** *Morganucodon*, moving all muscles 1%. Min= minimum, Max= maximum, STD= standard deviation.

	Strain			Stress			Validity
	Mean	Median	Max	Mean	Median	Max	
1	100.67	100.04	105.13	100.45	99.56	100.20	Valid
2	99.41	99.96	104.98	99.63	100.30	99.85	Invalid
3	100.38	100.63	102.89	100.33	100.54	99.73	Valid
4	99.67	99.51	100.78	99.72	99.12	100.33	Valid
5	99.79	100.69	108.03	99.96	100.97	99.55	Invalid
6	99.09	99.54	101.98	99.35	99.54	100.16	Invalid
7	100.34	99.27	105.63	100.16	98.90	100.50	Valid
8	101.05	100.56	104.96	100.79	100.38	99.90	Valid
9	104.87	104.03	108.31	104.22	103.07	100.63	Invalid
10	96.57	101.25	101.83	97.46	101.75	99.08	Valid
11	97.09	99.52	101.97	97.59	100.02	99.43	Valid
12	106.70	105.23	113.62	105.59	103.29	100.98	Invalid
13	106.21	105.30	109.26	105.29	103.84	100.50	Invalid
14	97.04	100.64	99.74	97.70	101.22	98.95	Valid
15	96.59	100.04	99.67	97.31	100.24	99.56	Valid
16	105.35	103.84	107.63	104.51	102.45	101.10	Invalid
17	105.75	104.60	108.30	104.87	103.07	100.80	Invalid
18	96.79	100.36	97.66	97.48	100.93	99.25	Valid
19	97.36	99.92	100.42	97.81	100.53	99.13	Valid
20	104.47	103.28	105.23	103.86	102.44	100.93	Invalid
21	107.15	105.82	114.60	106.00	103.86	100.68	Invalid
22	96.37	100.96	98.91	97.29	101.36	99.38	Valid
23	96.82	101.36	104.79	97.68	102.06	98.78	Valid
24	106.31	104.58	112.90	105.23	102.74	101.28	Invalid
25	96.88	99.08	103.84	97.41	99.52	99.73	Valid
26	105.33	104.61	111.42	104.63	103.73	100.33	Invalid

Table B.2: **Comparative stress (MPa) and strain (microstrain) results of the sensitivity analyses, represented in percentages:** *Morganucodon*, moving all muscles 1%. Min= minimum, Max= maximum, STD= standard deviation.

	Strain			Stress			Validity
	Mean	Median	Max	Mean	Median	Max	
1	141.9	92.1	3269.1	3.7	2.8	58.9	Valid
2	133.4	91.9	3255.4	3.5	2.9	54.9	Invalid
3	139.6	93.0	2985.1	3.7	2.8	54.6	Valid
4	134.8	87.2	2760.7	3.5	2.7	56.3	Invalid
5	136.5	92.7	3668.4	3.6	2.9	58.8	Invalid
6	132.1	88.7	2858.1	3.5	2.7	55.8	Invalid
7	140.5	89.4	3366.7	3.7	2.7	56.7	Valid
8	145.1	94.9	3350.9	3.8	2.8	66.0	Valid
9	185.2	122.8	3741.3	4.7	3.6	77.6	Invalid
10	159.8	118.5	3142.6	4.2	3.4	59.3	Invalid
11	145.0	104.0	3706.4	3.8	3.0	57.7	Invalid
12	205.2	136.5	5068.0	5.2	3.9	110.0	Invalid
13	199.2	132.4	4738.0	5.1	3.8	104.0	Invalid
14	151.1	109.6	2829.3	4.0	3.2	52.4	Invalid
15	152.6	108.9	3947.9	4.0	3.1	69.1	Invalid
16	191.5	127.3	4028.7	4.9	3.7	83.0	Invalid
17	194.5	129.3	4363.6	4.9	3.7	93.0	Invalid
18	150.8	109.2	3376.9	4.0	3.1	57.2	Invalid
19	145.5	105.2	3186.8	3.8	3.0	52.9	Invalid
20	181.9	120.4	3339.0	4.6	3.5	66.2	Invalid
21	209.6	139.5	5426.1	5.3	4.0	120.0	Invalid
22	161.6	118.5	3712.8	4.2	3.4	71.4	Invalid
23	160.0	118.6	3222.6	4.2	3.5	52.0	Invalid
24	202.5	134.3	4749.9	5.1	3.8	101.1	Invalid
25	146.6	102.8	4260.1	3.9	2.9	69.7	Invalid
26	190.1	126.2	4175.8	4.9	3.7	89.7	Invalid
Original	136.3	90.9	2590.0	3.6	2.8	55.4	
Min	132.1	87.2	2760.7	3.5	2.7	52.0	
Max	209.6	139.5	5426.1	5.3	4.0	120.0	
STD	25.8	16.8	712.5	0.6	0.42	20.0	

Table B.3: **Raw stress (MPa) and strain (microstrain) results of the sensitivity analyses:** *Morganucodon*, moving all muscles 5%. Min= minimum, Max= maximum, STD= standard deviation.

	Strain			Stress			Validity
	Mean	Median	Max	Mean	Median	Max	
1	104.10	101.35	126.22	103.02	99.60	106.35	Valid
2	97.86	101.15	125.69	98.97	102.99	99.16	Invalid
3	102.42	102.37	115.25	102.15	102.71	98.54	Valid
4	98.90	95.91	106.59	99.03	95.97	101.55	Invalid
5	100.14	101.98	141.64	100.91	103.19	106.12	Invalid
6	96.91	97.55	110.35	98.11	98.94	100.68	Invalid
7	103.08	98.38	129.99	102.10	96.71	102.42	Valid
8	106.50	104.38	129.38	105.23	102.75	119.18	Valid
9	135.89	135.09	144.45	132.06	130.00	140.02	Invalid
10	117.30	130.38	121.34	117.43	122.55	106.99	Invalid
11	106.40	114.47	143.10	106.74	107.84	104.18	Invalid
12	150.61	150.21	195.67	144.79	139.97	198.62	Invalid
13	146.19	145.62	182.93	141.25	137.82	187.64	Invalid
14	110.85	120.62	109.24	111.52	114.83	94.67	Invalid
15	111.96	119.86	152.43	112.00	111.89	124.64	Invalid
16	140.54	140.01	155.55	135.78	131.79	149.79	Invalid
17	142.76	142.28	168.48	137.92	134.95	167.89	Invalid
18	110.66	120.10	130.38	111.12	113.23	103.28	Invalid
19	106.75	115.78	123.04	107.07	109.01	95.55	Invalid
20	133.47	132.44	128.92	129.78	127.20	119.45	Invalid
21	153.83	153.54	209.50	147.95	142.90	216.53	Invalid
22	118.62	130.43	143.35	118.18	121.06	128.82	Invalid
23	117.39	130.49	124.43	117.90	124.55	93.80	Invalid
24	148.61	147.72	183.39	142.84	137.77	182.44	Invalid
25	107.55	113.13	164.48	107.68	106.37	125.90	Invalid
26	139.53	138.82	161.23	135.53	133.09	161.91	Invalid

Table B.4: **Comparative stress (MPa) and strain (microstrain) results of the sensitivity analyses, represented in percentages:** *Morganucodon*, moving all muscles 5%. Min= minimum, Max= maximum, STD= standard deviation.

	Strain			Stress			Validity
	Mean	Median	Max	Mean	Median	Max	
1	149.9	96.5	3999.5	3.9	2.9	78.8	Valid
2	134.0	95.0	3938.1	3.6	3.0	62.7	Invalid
3	144.8	95.6	3399.8	3.8	2.9	58.9	Valid
4	135.0	82.7	3108.3	3.5	2.5	57.1	Invalid
5	141.3	90.4	4788.6	3.7	2.8	77.9	Invalid
6	134.0	87.6	3130.0	3.6	2.7	56.2	Invalid
7	149.5	93.2	4254.2	3.8	2.7	73.2	Valid
8	157.9	102.3	4305.9	4.1	3.0	92.9	Valid
9	254.7	169.3	5427.7	6.4	4.7	121.3	Invalid
10	246.8	182.6	4815.6	6.3	5.0	114.3	Invalid
11	201.3	148.5	5653.2	5.2	4.1	103.2	Invalid
12	300.9	197.6	8086.2	7.5	5.3	181.8	Invalid
13	287.4	188.7	7566.3	7.2	5.1	172.4	Invalid
14	218.8	155.5	3947.4	5.6	4.4	79.3	Invalid
15	228.2	166.4	6345.2	5.8	4.5	130.2	Invalid
16	269.8	175.8	5918.8	6.7	4.9	127.7	Invalid
17	275.9	183.2	6718.8	6.9	5.0	149.1	Invalid
18	220.4	162.6	5138.7	5.6	4.5	104.6	Invalid
19	199.4	143.3	4469.2	5.1	4.0	77.1	Invalid
20	247.5	162.7	4584.3	6.2	4.6	96.4	Invalid
21	311.2	203.1	8894.3	7.7	5.5	202.6	Invalid
22	253.3	186.0	5986.8	6.4	5.0	139.3	Invalid
23	246.2	177.5	4214.1	6.3	5.0	89.8	Invalid
24	295.9	190.7	7336.5	7.4	5.2	163.1	Invalid
25	209.6	150.2	6856.3	5.4	4.2	129.4	Invalid
26	267.4	175.0	6307.3	6.7	4.8	147.3	Invalid
Original	136.3	90.9	2590.0	3.6	2.8	55.4	
Min	134.0	82.7	3108.3	3.5	2.5	56.2	
Max	311.2	203.1	8894.3	7.7	5.5	202.6	
STD	58.7	40.5	1560.9	1.4	1.00	41.1	

Table B.5: **Raw stress (MPa) and strain (microstrain) results of the sensitivity analyses:** *Morganucodon*, moving all muscles 10%. Min= minimum, Max= maximum, STD= standard deviation.

	Strain			Stress			Validity
	Mean	Median	Max	Mean	Median	Max	
1	110.01	106.18	154.42	107.86	102.95	142.28	Valid
2	98.35	104.54	152.05	100.20	106.74	113.25	Invalid
3	106.25	105.22	131.27	105.67	104.57	106.26	Valid
4	99.11	90.97	120.01	99.16	90.64	103.10	Invalid
5	103.68	99.43	184.89	104.68	100.16	140.60	Invalid
6	98.31	96.36	120.85	99.69	96.53	101.38	Invalid
7	109.70	102.57	164.25	107.49	98.97	132.06	Valid
8	115.90	112.56	166.25	113.50	108.96	167.72	Valid
9	186.89	186.27	209.56	178.71	170.19	218.97	Invalid
10	181.13	200.88	185.93	175.46	181.14	206.28	Invalid
11	147.70	163.43	218.27	144.41	148.58	186.29	Invalid
12	220.82	217.35	312.21	209.10	192.91	328.13	Invalid
13	210.93	207.66	292.14	200.65	185.75	311.20	Invalid
14	160.56	171.06	152.41	157.33	159.33	143.15	Invalid
15	167.48	183.05	244.99	162.00	162.34	235.02	Invalid
16	197.98	193.44	228.52	188.29	175.22	230.51	Invalid
17	202.45	201.58	259.41	192.50	181.05	269.16	Invalid
18	161.73	178.90	198.40	157.41	161.10	188.84	Invalid
19	146.37	157.69	172.55	143.77	144.24	139.24	Invalid
20	181.62	178.99	177.00	173.79	165.25	174.03	Invalid
21	228.39	223.50	343.41	216.40	197.97	365.67	Invalid
22	185.90	204.59	231.15	178.95	180.39	251.46	Invalid
23	180.68	195.27	162.71	176.10	181.44	162.09	Invalid
24	217.19	209.85	283.26	205.70	187.79	294.45	Invalid
25	153.81	165.29	264.72	149.56	150.50	233.64	Invalid
26	196.25	192.52	243.52	187.63	174.37	265.88	Invalid

Table B.6: **Comparative stress (MPa) and strain (microstrain) results of the sensitivity analyses, represented in percentages:** *Morganucodon*, moving all muscles 10%. Min= minimum, Max= maximum, STD= standard deviation.

	Strain			Stress			Validity
	Mean	Median	Max	Mean	Median	Max	
1	133.9	55.2	5405.7	3.7	1.7	85.0	Valid
2	131.3	56.3	5387.5	3.7	1.6	84.7	Valid
3	133.8	57.3	5272.0	3.7	1.7	82.9	Valid
4	131.3	54.2	5521.2	3.7	1.6	86.8	Valid
5	132.5	57.6	5263.0	3.7	1.7	82.7	Valid
6	130.2	54.6	5512.1	3.6	1.6	86.6	Valid
7	132.7	53.7	5530.4	3.7	1.6	86.9	Valid
8	135.3	56.6	5281.1	3.8	1.7	83.0	Valid
9	132.0	48.9	5701.7	3.7	1.5	89.7	Invalid
10	136.7	64.2	5077.1	3.8	1.8	79.8	Valid
11	137.7	61.5	5094.9	3.8	1.7	80.1	Valid
12	136.4	49.8	5720.2	3.8	1.6	90.0	Invalid
13	135.7	50.8	5586.1	3.7	1.6	87.8	Invalid
14	138.0	63.8	4961.7	3.8	1.8	78.0	Valid
15	136.4	61.8	5210.2	3.8	1.7	81.9	Valid
16	132.7	47.6	5835.8	3.7	1.5	91.8	Invalid
17	134.1	49.3	5710.9	3.7	1.5	89.8	Invalid
18	137.1	62.8	5086.0	3.8	1.7	79.9	Valid
19	138.7	62.9	4970.6	3.8	1.8	78.1	Valid
20	130.7	47.2	5826.5	3.6	1.5	91.6	Invalid
21	138.0	51.5	5595.3	3.8	1.6	88.0	Invalid
22	136.1	63.4	5201.3	3.8	1.7	81.7	Valid
23	137.4	65.0	4952.9	3.8	1.8	77.8	Valid
24	134.9	48.1	5845.0	3.7	1.5	91.9	Invalid
25	136.9	60.5	5219.2	3.8	1.7	82.0	Valid
26	133.6	50.6	5576.9	3.7	1.6	87.7	Invalid
Original	132.5	55.8	5396.6	3.7	1.6	84.8	
Min	130.2	47.2	4952.9	3.6	1.5	77.8	
Max	138.7	65.0	5845.0	3.8	1.8	91.9	
STD	2.5	5.9	285.5	0.1	0.10	4.5	

Table B.7: **Raw stress (MPa) and strain (microstrain) results of the sensitivity analyses:** *Kuehneotherium*, moving all muscles 1%. Min= minimum, Max= maximum, STD= standard deviation.

	Strain			Stress			Validity
	Mean	Median	Max	Mean	Median	Max	
1	101.08	98.94	100.17	100.91	100.67	100.17	Valid
2	99.06	100.80	99.83	99.22	99.82	99.83	Valid
3	100.99	102.59	97.69	100.93	103.30	97.69	Valid
4	99.11	97.02	102.31	99.16	96.81	102.31	Valid
5	99.99	103.19	97.52	100.11	103.36	97.51	Valid
6	98.23	97.82	102.14	98.42	96.31	102.14	Valid
7	100.14	96.18	102.48	100.02	97.18	102.49	Valid
8	102.12	101.38	97.86	101.89	103.83	97.86	Valid
9	99.66	87.53	105.65	99.35	92.80	105.71	Invalid
10	103.15	115.03	94.08	103.08	107.30	94.04	Valid
11	103.95	110.23	94.41	103.70	105.01	94.38	Valid
12	102.94	89.19	106.00	102.17	94.14	106.07	Invalid
13	102.40	91.03	103.51	101.79	95.92	103.57	Invalid
14	104.14	114.36	91.94	103.98	108.17	91.91	Valid
15	102.93	110.69	96.55	102.76	103.55	96.52	Valid
16	100.14	85.24	108.14	99.68	90.03	108.21	Invalid
17	101.22	88.28	105.82	100.70	92.96	105.89	Invalid
18	103.47	112.43	94.24	103.32	105.67	94.21	Valid
19	104.70	112.60	92.11	104.42	107.81	92.08	Valid
20	98.61	84.59	107.97	98.36	89.54	108.03	Invalid
21	104.15	92.17	103.68	103.29	97.17	103.75	Invalid
22	102.70	113.55	96.38	102.58	105.21	96.35	Valid
23	103.73	116.41	91.78	103.67	109.37	91.74	Valid
24	101.82	86.11	108.31	101.14	91.11	108.39	Invalid
25	103.32	108.30	96.71	103.07	102.25	96.69	Valid
26	100.80	90.65	103.34	100.42	96.07	103.39	Invalid

Table B.8: **Comparative stress (MPa) and strain (microstrain) results of the sensitivity analyses, represented in percentages:** *Kuehneotherium*, moving all muscles 1%. Min= minimum, Max= maximum, STD= standard deviation.

	Strain			Stress			Validity
	Mean	Median	Max	Mean	Median	Max	
1	141.4	52.1	5442.2	3.9	1.6	90.6	Valid
2	128.4	57.9	5351.3	3.6	1.6	84.1	Invalid
3	140.7	62.5	4774.1	3.9	1.9	75.0	Valid
4	127.8	47.3	6020.0	3.6	1.4	94.6	Valid
5	134.8	63.7	4729.1	3.8	1.9	74.3	Invalid
6	125.9	52.3	5974.3	3.5	1.4	93.9	Invalid
7	135.0	43.9	6065.8	3.7	1.4	99.7	Valid
8	150.9	60.0	4819.2	4.1	1.9	82.5	Valid
9	170.1	101.7	7033.5	4.5	2.9	109.6	Invalid
10	203.9	146.8	4236.0	5.4	4.0	76.2	Invalid
11	191.8	123.9	4614.3	5.1	3.4	85.4	Invalid
12	205.2	128.7	7158.7	5.4	3.7	115.2	Invalid
13	196.1	117.9	6460.0	5.2	3.4	100.6	Invalid
14	196.5	132.1	3834.1	5.2	3.7	65.4	Invalid
15	199.7	137.9	4529.2	5.3	3.7	81.8	Invalid
16	180.4	110.8	7731.7	4.8	3.1	120.3	Invalid
17	186.8	115.8	7095.8	4.9	3.3	110.4	Invalid
18	196.5	135.7	4124.8	5.2	3.7	71.4	Invalid
19	193.4	121.9	4011.9	5.1	3.4	71.0	Invalid
20	164.1	95.5	7669.5	4.4	2.7	119.4	Invalid
21	214.9	131.7	6799.7	5.6	3.8	112.2	Invalid
22	208.2	151.2	4528.5	5.5	4.0	82.1	Invalid
23	202.6	141.5	3987.9	5.4	3.9	70.2	Invalid
24	198.4	125.6	7794.5	5.2	3.6	121.1	Invalid
25	193.5	124.0	5259.0	5.1	3.4	100.4	Invalid
26	179.3	105.7	6397.6	4.8	3.0	99.7	Invalid
Original	132.5	55.8	5396.6	3.7	1.6	84.8	
Min	125.9	43.9	3834.1	3.5	1.4	65.4	
Max	214.9	151.2	7794.5	5.6	4.0	121.1	
STD	29.6	35.5	1288.1	0.7	0.93	17.4	

Table B.9: **Raw stress (MPa) and strain (microstrain) results of the sensitivity analyses:** *Kuehneotherium*, moving all muscles 5%. Min= minimum, Max= maximum, STD= standard deviation.

	Strain			Stress			Validity
	Mean	Median	Max	Mean	Median	Max	
1	106.71	93.26	100.84	105.77	99.16	106.78	Valid
2	96.91	103.80	99.16	97.57	97.91	99.13	Invalid
3	106.21	112.00	88.46	105.63	116.68	88.44	Valid
4	96.42	84.69	111.55	96.55	82.17	111.58	Valid
5	101.76	114.03	87.63	102.11	112.88	87.58	Invalid
6	95.00	93.65	110.70	95.48	86.97	110.70	Invalid
7	101.91	78.60	112.40	101.25	83.03	117.52	Valid
8	113.90	107.42	89.30	112.14	115.36	97.22	Valid
9	128.40	182.12	130.33	123.15	175.16	129.20	Invalid
10	153.88	263.05	78.49	145.67	243.04	89.78	Invalid
11	144.76	222.01	85.50	138.12	206.24	100.72	Invalid
12	154.90	230.65	132.65	146.31	224.34	135.78	Invalid
13	148.00	211.25	119.70	140.40	207.04	118.56	Invalid
14	148.32	236.65	71.05	141.45	221.52	77.11	Invalid
15	150.72	246.97	83.93	142.65	225.84	96.41	Invalid
16	136.15	198.58	143.27	129.62	189.43	141.80	Invalid
17	140.95	207.51	131.49	134.03	199.52	130.18	Invalid
18	148.32	243.13	76.43	140.99	224.77	84.17	Invalid
19	145.96	218.38	74.34	139.61	204.71	83.69	Invalid
20	123.87	171.13	142.12	118.88	162.73	140.83	Invalid
21	162.17	235.89	126.00	152.77	231.11	132.31	Invalid
22	157.14	270.78	83.91	148.14	245.60	96.85	Invalid
23	152.91	253.51	73.90	145.25	237.39	82.72	Invalid
24	149.74	224.94	144.43	141.69	215.98	142.77	Invalid
25	146.01	222.13	97.45	138.72	205.17	118.33	Invalid
26	135.31	189.27	118.55	129.42	183.89	117.59	Invalid

Table B.10: **Comparative stress (MPa) and strain (microstrain) results of the sensitivity analyses, represented in percentages:** *Kuehneotherium*, moving all muscles 5%. Min= minimum, Max= maximum, STD= standard deviation.

	Strain			Stress			Validity
	Mean	Median	Max	Mean	Median	Max	
1	154.4	54.9	6687.8	4.2	1.7	124.3	Valid
2	130.6	66.2	5306.1	3.7	1.8	83.4	Invalid
3	152.3	68.7	4152.7	4.2	2.2	65.2	Valid
4	125.8	38.7	6643.9	3.5	1.1	104.5	Valid
5	144.8	73.0	4064.2	4.0	2.1	63.8	Invalid
6	133.1	62.6	6552.2	3.7	1.7	103.0	Invalid
7	141.9	38.9	8022.6	3.9	1.2	141.7	Valid
8	177.0	70.4	5959.4	4.8	2.2	110.3	Valid
9	250.0	173.8	8832.9	6.5	4.7	139.5	Invalid
10	320.8	245.1	6940.3	8.2	6.6	116.4	Invalid
11	283.7	199.9	6736.7	7.3	5.5	129.6	Invalid
12	322.8	220.4	10873.6	8.2	6.3	179.4	Invalid
13	303.4	201.4	8743.9	7.8	5.7	144.4	Invalid
14	296.2	206.1	6409.1	7.6	5.8	94.9	Invalid
15	311.3	237.7	6416.8	7.9	6.3	132.4	Invalid
16	274.0	199.3	10232.9	7.0	5.3	161.6	Invalid
17	283.3	195.0	8968.9	7.3	5.5	142.2	Invalid
18	298.6	222.5	6411.6	7.6	6.1	106.8	Invalid
19	285.2	188.8	5881.3	7.3	5.4	108.7	Invalid
20	242.0	171.5	10098.4	6.3	4.5	158.9	Invalid
21	343.6	228.2	11083.1	8.8	6.6	179.1	Invalid
22	335.7	259.8	6943.5	8.5	6.8	131.5	Invalid
23	315.8	226.4	6939.6	8.1	6.3	104.5	Invalid
24	311.5	222.7	11561.8	8.0	6.1	187.0	Invalid
25	292.6	211.7	8045.2	7.5	5.6	159.2	Invalid
26	269.0	175.6	8806.6	6.9	4.9	138.5	Invalid
Original	132.5	55.8	5396.6	3.7	1.6	84.8	
Min	125.8	38.7	4064.2	3.5	1.1	63.8	
Max	343.6	259.8	11561.8	8.8	6.8	187.0	
STD	75.4	74.4	2026.5	1.8	1.98	32.8	

Table B.11: **Raw stress (MPa) and strain (microstrain) results of the sensitivity analyses:** *Kuehneotherium*, moving all muscles 10%. Min= minimum, Max= maximum, STD= standard deviation.

	Strain			Stress			Validity
	Mean	Median	Max	Mean	Median	Max	
1	116.51	98.37	123.93	114.25	103.84	146.61	Valid
2	98.54	118.53	98.32	99.15	108.98	98.27	Invalid
3	114.96	123.04	76.95	113.19	131.59	76.91	Valid
4	94.96	69.40	123.11	95.02	65.17	123.17	Valid
5	109.30	130.75	75.31	108.63	127.90	75.24	Invalid
6	100.44	112.11	121.41	99.77	103.76	121.41	Invalid
7	107.13	69.60	148.66	105.48	72.63	167.07	Valid
8	133.58	126.13	110.43	129.02	133.29	130.00	Valid
9	188.70	311.28	163.67	175.60	287.73	164.42	Invalid
10	242.09	439.15	128.60	221.56	400.10	137.23	Invalid
11	214.09	358.07	124.83	197.19	333.69	152.80	Invalid
12	243.59	394.76	201.49	223.92	382.55	211.56	Invalid
13	228.98	360.71	162.03	211.22	347.43	170.25	Invalid
14	223.55	369.15	118.76	205.86	350.61	111.88	Invalid
15	234.95	425.86	118.90	214.96	380.50	156.07	Invalid
16	206.78	357.11	189.62	191.30	320.92	190.50	Invalid
17	213.83	349.36	166.19	197.62	331.57	167.64	Invalid
18	225.37	398.56	118.81	206.86	367.71	125.90	Invalid
19	215.24	338.28	108.98	198.99	324.93	128.20	Invalid
20	182.65	307.14	187.12	170.27	273.68	187.33	Invalid
21	259.30	408.79	205.37	237.76	398.00	211.18	Invalid
22	253.34	465.45	128.66	231.38	413.76	155.00	Invalid
23	238.31	405.58	128.59	218.51	380.80	123.22	Invalid
24	235.06	398.96	214.24	216.56	368.47	220.43	Invalid
25	220.86	379.23	149.08	202.54	339.29	187.64	Invalid
26	203.05	314.62	163.19	188.47	299.12	163.30	Invalid

Table B.12: **Comparative stress (MPa) and strain (microstrain) results of the sensitivity analyses, represented in percentages:** *Kuehneotherium*, moving all muscles 10%. Min= minimum, Max= maximum, STD= standard deviation.

APPENDIX C

APPENDIX C

This appendix has the supplementary figures and tables of Chapter 4. It includes details on the convergence of the mesh used in the finite element analysis study and on the convergence of the intervals used for principal components analysis following the Intervals' Method of [131].

S4 Data Supplementary Data Chapter 4. All the supporting data used in this manuscript can be found in the following link: `https://data.bris.ac.uk/webshare/Palaeobiology_Users/6638439a-2000-4e84-bf60-c916680de9d1/` It includes information on the list of taxa used in this study, basic data on the finite element models, a detailed protocol on how to build the enhanced extruded FE models, the code used to run the Intervals' Method and all the finite element models analysed in this study.

Table C.1: **Convergence test results**, showing number of elements per model, approximate size of elements in the mesh, average and median von Mises stress values (in MPa), and computational time (in seconds) needed to solve the finite element model. Depicted graphically in Figure C.1a-d

Model	Number of elements	Element size	Average stress	Median stress	Computational time
Model 1	30402	0.000255	4040573	2579320	45
Model 2	37171	0.000234	3850000	2490000	45
Model 3	46982	0.000213	3740000	3430000	45
Model 4	61714	0.00019125	3880000	3500000	49
Model 5	84619	0.00017	3830000	3560000	55
Model 6	121363	0.00014875	3860000	3550000	71
Model 7	180966	0.0001275	3890000	3580000	82
Model 8	297063	0.00010625	3900000	3580000	116
Model 9	536200	0.000085	3940000	3660000	186
Model 10	1109562	0.00006375	4110000	3790000	420
Model 11	3023174	0.0000425	4090000	3760000	1565

Table C.2: **Comparison of stress values** between subsequent pairs of finite element models, showing average and median von Mises stress in MPa. Expressed as a percentage of how similar subsequent pairs of models are. Depicted graphically in Figure C.1e

	Average stress similarity	**Median stress similarity**
Model 1 vs 2	95.28 %	96.54 %
Model 2 vs 3	97.14 %	62.25 %
Model 3 vs 4	96.26 %	97.96 %
Model 4 vs 5	98.71 %	98.29 %
Model 5 vs 6	99.22 %	99.72 %
Model 6 vs 7	99.22 %	99.15 %
Model 7 vs 8	99.74 %	100.00 %
Model 8 vs 9	98.97 %	97.77 %
Model 9 vs 10	95.69 %	96.45 %
Model 10 vs 11	99.51 %	99.21 %

Table C.3: **Coefficient of determination (R^2) values,** obtained by regressing sequential pairs of PC scores. Scores obtained from Principal Components Analyses performed using correlation and variance-covariance matrices of different numbers of intervals (i.e., 5, 10, 15, 25, 50, 75, 100, 125, 150). Convergence was determined when PC1 and PC2 has R^2) values higher than 0.99.

Intervals	**Correlation matrix**		**Variance-covariance matrix**	
	PC1	PC2	PC1	PC2
PCA 5 vs PCA 10	0.99654	0.218498	0.765913	0.069078
PCA 10 vs PCA 15	0.997948	0.940289	0.988337	0.563946
PCA 15 vs PCA 25	0.998931	0.984767	0.978646	0.61307
PCA 25 vs PCA 50	0.999345	0.987628	0.000888	0.000902
PCA 50 vs PCA 75	0.999941	0.999724	0.993213	0.995853
PCA 75 vs PCA 100	0.999988	0.999724	0.99876	0.99998
PCA 100 vs PCA 125	0.999996	0.999984	0.999271	0.999986
PCA 125 vs PCA 150	0.999998	0.999993	0.999509	0.999977

Table C.4: **m1 position along the dentary**, as a percentage of the total length of the dentary. Higher numbers indicate m1 more posteriorly located, while lower numbers indicate m1 more anteriorly located. Dietary information sources as in Table 1 of the main text.

Extant taxa			Extinct taxa		
Taxon	**Observed diet**	**m1 position**	**Taxon**	**Proposed diet**	**m1 position**
Lynx rufus	Hypercarnivore	81.61	*Zalambdalestes lechei*	Unknown	73.77
Genetta genetta	Hypercarnivore	79.64	*Peramus tenuirostris*	Unknown	73.49
Herpestes javanicus	Hypercarnivore	79.56	*Vincelestes neuquenianus*	Omnivore	72.64
Tenrec ecaudatus	Omnivore	77.83	*Barunlestes butleri*	Insectivore	70.58
Petrogale lateralis	Herbivore	75.52	*Maelestes gobiensis*	Unknown	70.24
Mustela nivalis	Hypercarnivore	75.29	*Sasayamamylos kawaii*	Unknown	67.41
Taxidea taxus	Omnivore	74.75	*Kennalestes gobiensis*	Insectivore	67.41
Bassaricyon gabbii	Herbivore	71.71	*Teinolophos trusleri*	Invertivore	67.04
Vulpes vulpes	Mesocarnivore	70.32	*Montanalestes keeblerorum*	Unknown	63.97
Lontra canadensis	Hypercarnivore	68.71	*Triconodon mordax*	Carnivore	62.32
Pteropus vampyrus	Herbivore	66.86	*Phascolotherium bucklandi*	Unknown	61.47
Macrotis lagotis	Omnivore	65.96	*Trioracodon ferox*	Carnivore	61.39
Microgale longicaudata	Insectivore	64.92	*Morganucodon watsoni*	Insectivore	60.34
Solenodon paradoxus	Vermivore	64.37	*Alphadon aetoni*	Insectivore	58.86
Perameles gunnii	Omnivore	61.10	*Laolestes eminens*	Unknown	55.07
Elephantulus rufescens	Omnivore	60.21	*Amblotherium soricinum*	Unknown	54.00
Petrodomus tetradactylus	Omnivore	59.77	*Amphitherium prevostii*	Insectivore	52.55
Tupaia glis	Omnivore	56.52	*Kuehneotherium praecursoris*	Insectivore	52.29
Dromiciops gliroides	Insectivore	55.65	*Didelphodon vorax*	Carnivore	51.61
Myotis lucifugus	Insectivore	54.99	*Dryolestes leirensis*	Insectivore	50.82
Monodelphis theresa	Omnivore	54.51	*Haldanodon exspectatus*	Insectivore	49.00
Philander opossum	Omnivore	53.30	*Gobiconodon haozhouensis*	Carnivore	47.40
Phalanger orientalis	Herbivore	52.97	*Docodon victor*	Insectivore	39.30
Parascalops breweri	Vermivore	49.93			
Atelerix albiventris	Insectivore	49.30			
Sminthopsis macroura	Insectivore	46.47			
Petaurus breviceps	Omnivore	44.45			
Dasyurus geoffroii	Mesocarnivore	42.77			
Blarina brevicauda	Omnivore	40.17			
Noctilio leporinus	Piscivore	33.77			

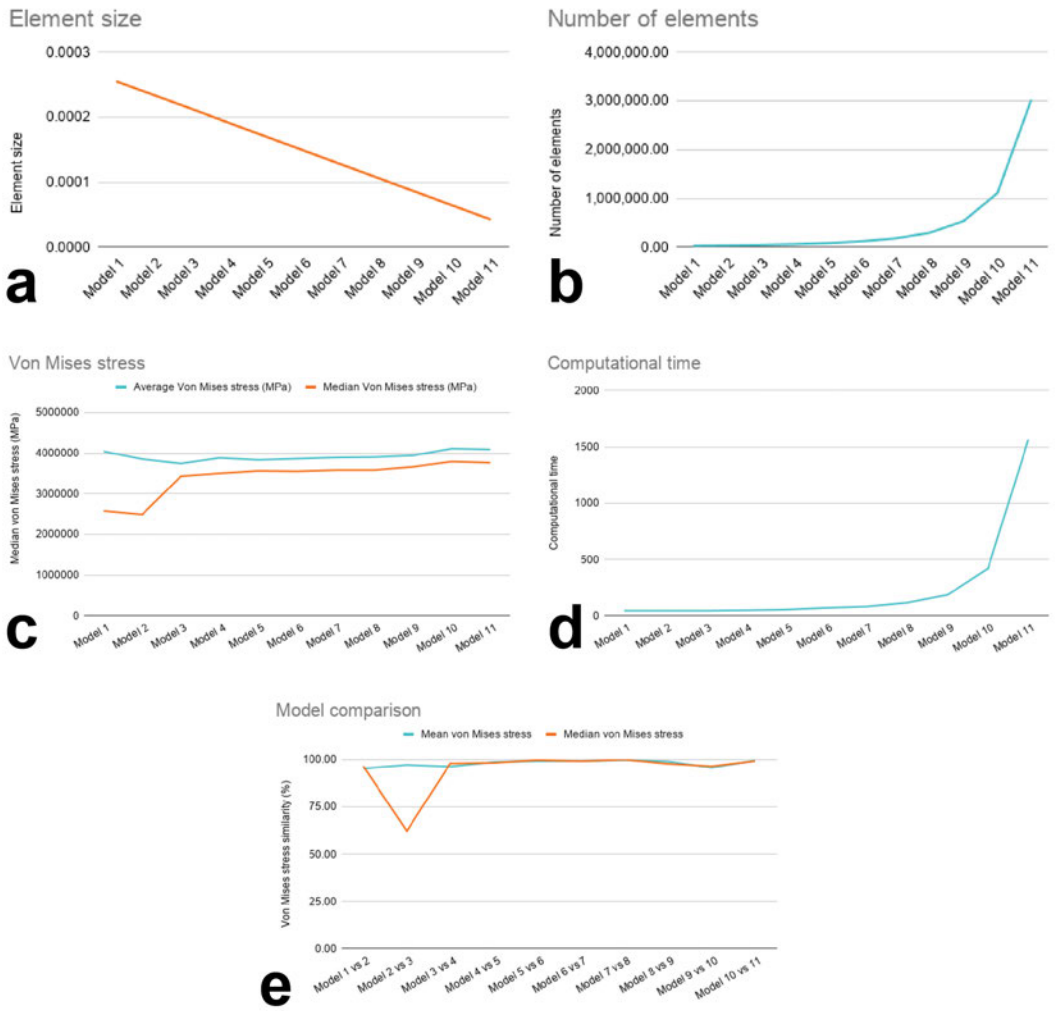

Figure C.1: **Mesh convergence study**, showing a) element size of the models (note that it decreases in a linear fashion) b) number of elements in the mesh (note it increases exponentially), c) average and median von Mises stress (MPa) in each model, d) computational time needed to solve the finite element models, and e) similarity in average and median stress values when comparing subsequent pairs of models (expressed as a percentage).

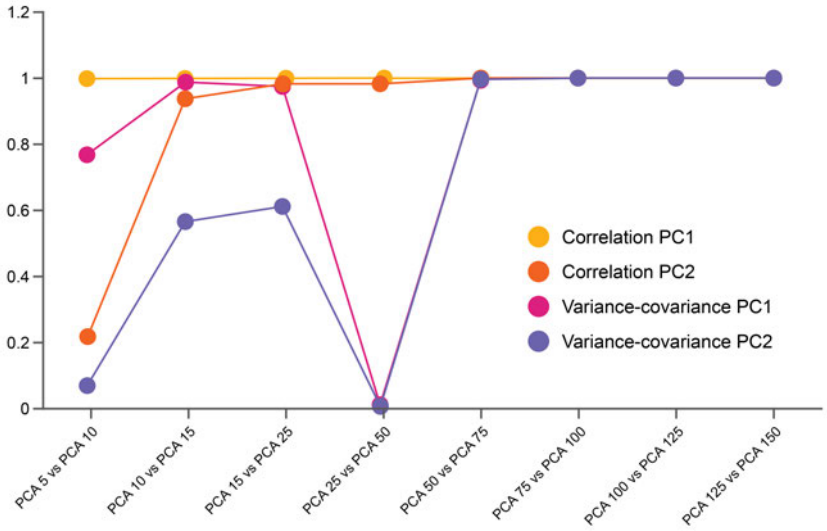

Figure C.2: **Convergence of the R^2 values of the PC scores,** using both correlation and variance-covariance matrices. Values shown in Table C.3. Convergence determined at the number of intervals where the R^2 values reached a plateau (and when the R^2 values of both PCs were over 0.99).

Figure C.3: **Correlation matrix PCA plots**, showing different intervals (5, 10, 15, 25, 50, 75, 100, 125, and 150) used to determine the convergence of the data in this study.

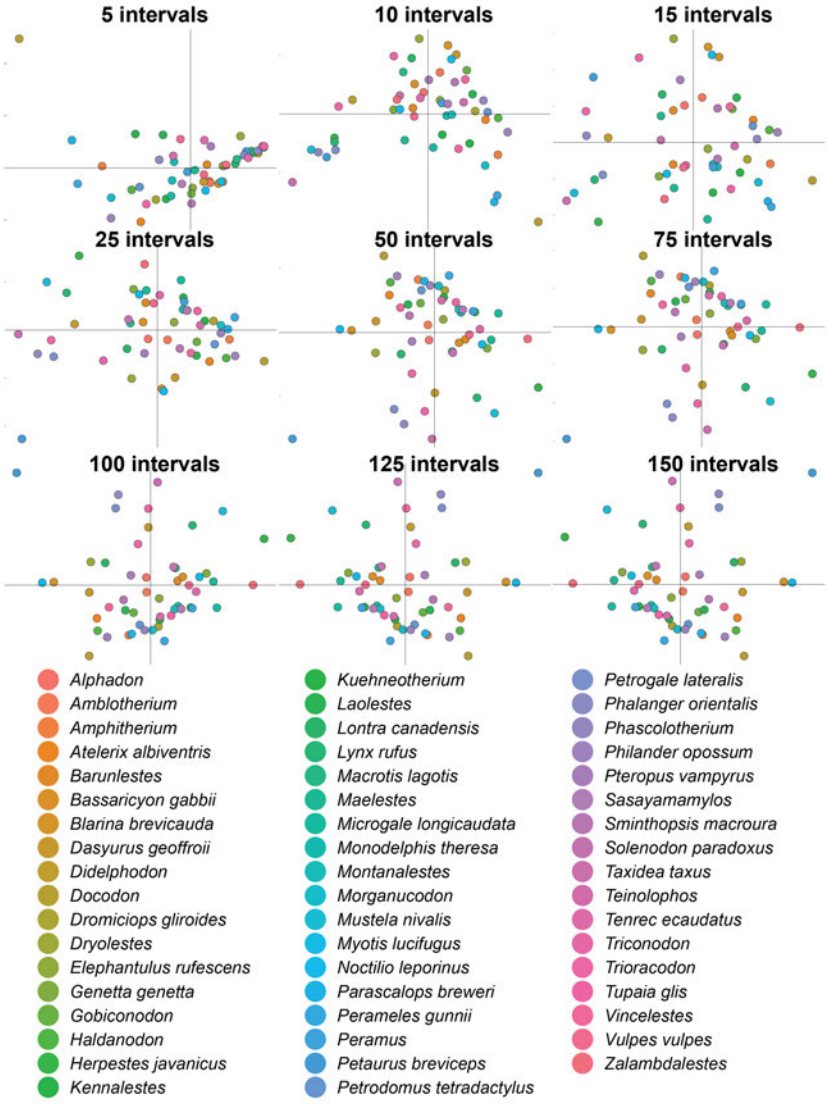

Figure C.4: **Variance-covariance matrix PCA plots**, showing different intervals (5, 10, 15, 25, 50, 75, 100, 125, and 150) used to determine the convergence of the data in this study.

APPENDIX D

APPENDIX D

This appendix has the detailed protocol on how to build enhanced extruded FE models. It was designed by Nuria Melisa Morales Garcia and modified by Kit Lam Tang. This protocol was used to build the models in Chapter 4 and it is a slightly updated version of the models validated in Chapter 3.

D.1 Building enhanced extruded FE models

This protocol describes in detail how to build enhanced extruded finite element models, first validated in Morales-Garcia et al., (2019) and used in Morales-Garcia et al., (in prep). For this protocol, we will be using a mammalian jaw which is relatively flat mediolaterally. Enhanced extruded FE models are built using freely available software: Image J/Fiji, Blender and FreeCAD, for their posterior analysis using the finite element method (FEM). Here is a list of FEM software, many of which are free: https://en.wikipedia.org/wiki/List_of_finite_element_software_packages

D.1.1 Choosing the right photographs

Extruded FE models are simplified 3D models built "by hand" using photographs, rather than using tomographic data. To do so, first we need to choose the right photographs. We need at least lateral and dorsal view photos (in the case of jaws) with a scale bar visible. You might be using photographs you have taken, but there are many free online resources where you might find such photos such as:

1. Animal Diversity Web of the University of Michigan (https://animaldiversity.org/)

2. Natural History Museum online database (https://data.nhm.ac.uk/)

Figure D.1: Lateral view picture of *Procyon lotor*

3. Field Museum online database (https://collections-zoology.fieldmuseum.org/)

4. University of Florida online collections (https://www.floridamuseum.ufl.edu/collections/databases/)

5. American Museum of Natural History online database (https://www.amnh.org/research/paleontology/collections/database)

For this protocol, we will be using the jaw of the Guadeloupe raccoon, *Procyon lotor* (Figures D.1 and D.2). These pictures were obtained from the Animal Diversity Web (University of Michigan Museum of Zoology 98905).

D.1.2 ImageJ

ImageJ and Fiji are free image processing programs that we will use to obtain measurements. Either can be used for helping us build extruded FE models. They can be found in the following links:

1. https://imagej.net/Welcome.

2. https://imagej.net/Fiji

We will be taking a series of measurements along the jaw of *Procyon*, starting with the lateral view picture (Figure D.3):

1. Open the file of the lateral view photo of the jaw (File>Open...)

Figure D.2: Dorsal view picture of *Procyon lotor*

2. Using the "Straight Line" tool, draw a line that represents the length of your scale bar.

3. Go to Analyze>Set Scale. In the "Known distance box" indicate the length of your scale bar. Make sure to also indicate the unit of length in the appropriate box. It is important that you always use the same units of length when measuring different jaws (and later when building the model in Blender)

4. Using the "Straight Line" tool, draw a line that represents the maximum length of the jaw (i.e., from its posteriormost point to its anteriormost point, not including teeth)

5. Go to Analyze>Measure. Write down the length of the jaw (this measurement will be useful later on).

6. Make a note of the dimensions of the picture (we will use this when we are making our model in Blender). You can find them in the top left corner of the image (not pictured in Figure D.3).

Now for the dorsal view photo (Figure D.4):

1. Repeat the first three steps taken with the lateral view picture (i.e., open the photo and set the scale)

Figure D.3: Summary of how to take measurements in ImageJ/Fiji using a lateral view photograph of the jaw of *Procyon lotor*

2. Take a series of measurements of the width of the dentary. Here I measure the width in between each tooth, but you decide how many measurements you will take. Record these measurements and average them.

3. Take a series of width measurements along the back of the jaw (e.g., along the coronoid process, the condyle, and, if visible, the angular process). You can also have ImageJ/Fiji open while you are building the model in Blender to take as many measurements as needed. Record these measurements.

D.1.3 Blender

Blender is the free 3D computer graphics software where we will be building our models. The following instructions are based on Blender v 2.90; if you are using a previous version of Blender, some of these instructions might not work for you. You can download the most recent version here: https://www.blender.org/

To start up Blender:

1. Open Blender. Click anywhere to dismiss the welcome window. You will see three objects on the screen: the camera, the cube and the lamp. Click on each of them and delete them by using the "x" key of your keyboard and then clicking OK or Enter. If you are using older versions of Blender you might have to select them with your right mouse button. The most recent version of Blender allows you to select objects with the left button of your mouse.

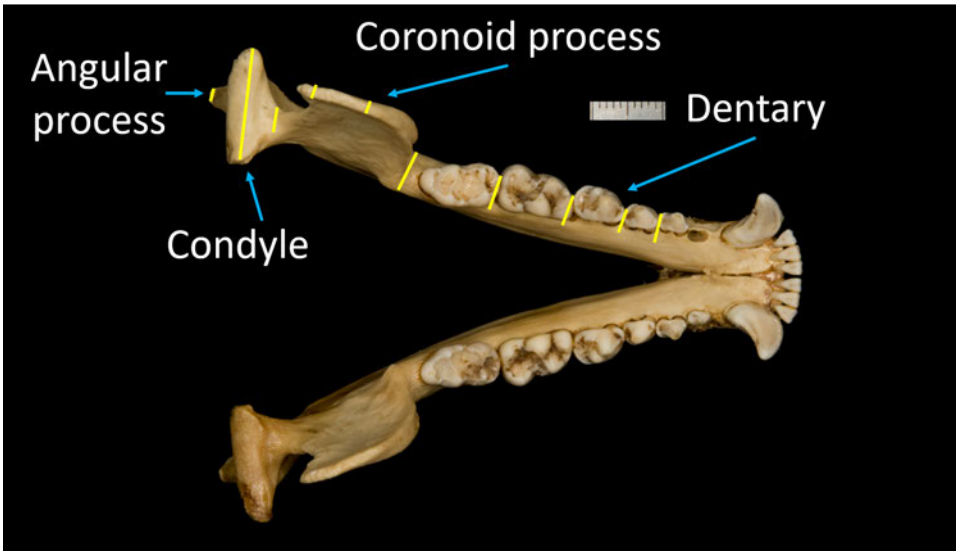

Figure D.4: Example of measurements taken in ImageJ/Fiji using a dorsal view picture of the jaw of *Procyon lotor*

2. Go to View>Viewpoint>Top on the top left corner, next to where it says "Object Mode". It is very important to do this, especially if you are using Abaqus to perform FEA, because it will make it easier to manipulate your model later on.

The first thing we will do to start building our model is to upload the lateral view picture of the jaw (Figure D.1) as reference (Figure D.6). To do so:

1. Drag and drop your image file into Blender. Hit the key "G" on your keyboard or go to Object>Move to move your object and center it at the cross-hairs of the grid.

2. On the panel on the bottom right of the screen, click on the Scene tab (it looks like a white cone, with a sphere on the front, and a white circle on the top right corner). Under Units>Length, change the units to millimeters (or to whatever units you used in ImageJ/Fiji).

3. On the same panel, click on the "Object Data Properties" tab (it is a red icon, with a triangle on the bottom left corner and a circle on the top right corner). Under Empty>Size, indicate the length of your image (remember you made a note of the dimensions of your image in Image J- this is NOT the length of the jaw, but of the entire image). Click Enter

4. Your image might have disappeared because it might be very small. Zoom in until you find it! You can use the middle scroll wheel of a mouse, or pinch out with two fingers using a track pad.

We will now start tracing the outline of the jaw (Figure D.7). To do so:

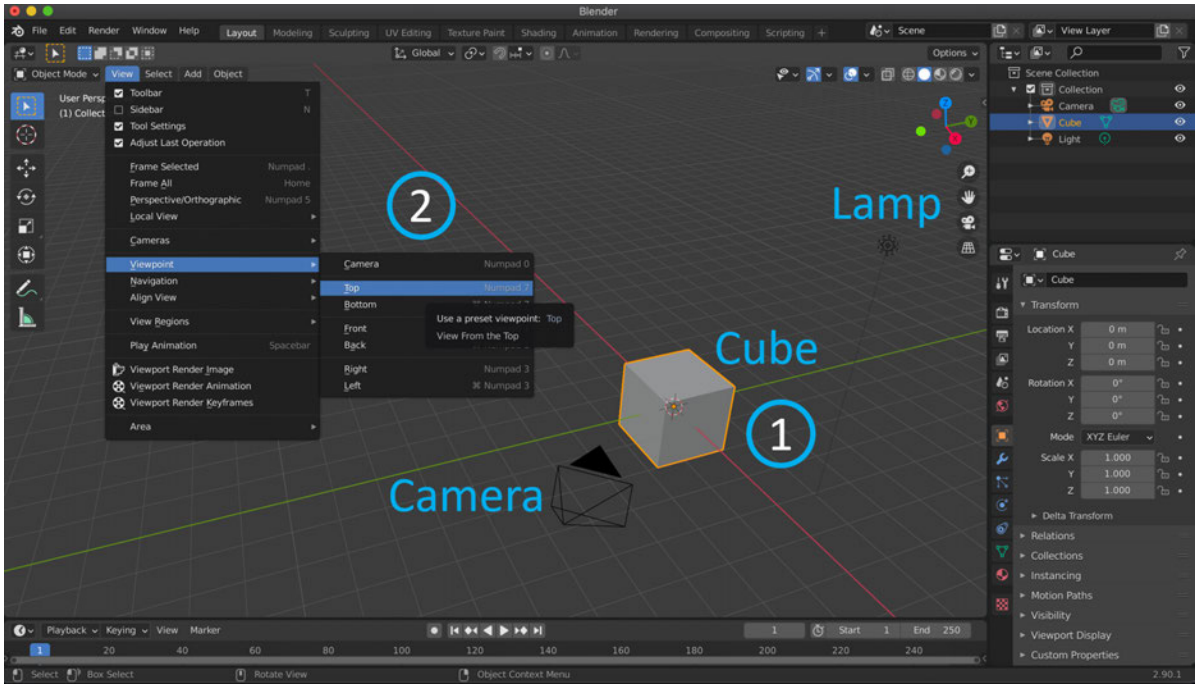

Figure D.5: Starting instructions for Blender

1. Go to Add>Mesh>Plane. This will add a square on top of your image. Chances are, it's a really big square. To make it smaller, hit they key "S" on your keyboard and move your mouse towards the center of the cube. The size of the square does not really matter, we just need it to be small enough to manipulate. Click once on it to stop scaling.

2. Go to Edit Mode. To do so, click on the arrow next to "Object Mode" and select "Edit Mode". This is located towards the top left corner of the window.

3. Next to "Edit Mode" you will see three squares. The first one, "Vertex Select" should be selected by default. If not, click on it.

4. We are going to select one of the vertices of our square. It does not matter which one. When you do so, that vertex will be highlighted in white, while the others will be black.

5. Press "P" on your keyboard. A pop-up menu will appear, make sure "Selection" is highlighted and hit "Enter" on your keyboard. This will separate one vertex from the rest of the square.

6. Switch back to "Object Mode". On the "Scene Collection" panel on the top right corner you will see three items: 1) Empty (this is your reference picture), 2) Plane (this is the square), and 3) Plane.001 (this is the vertex you just separated from the rest of the square). Right-click on "Plane" and select "Delete".

7. Select "Plane.001". Go to Object>Set Origin>Geometry to Origin

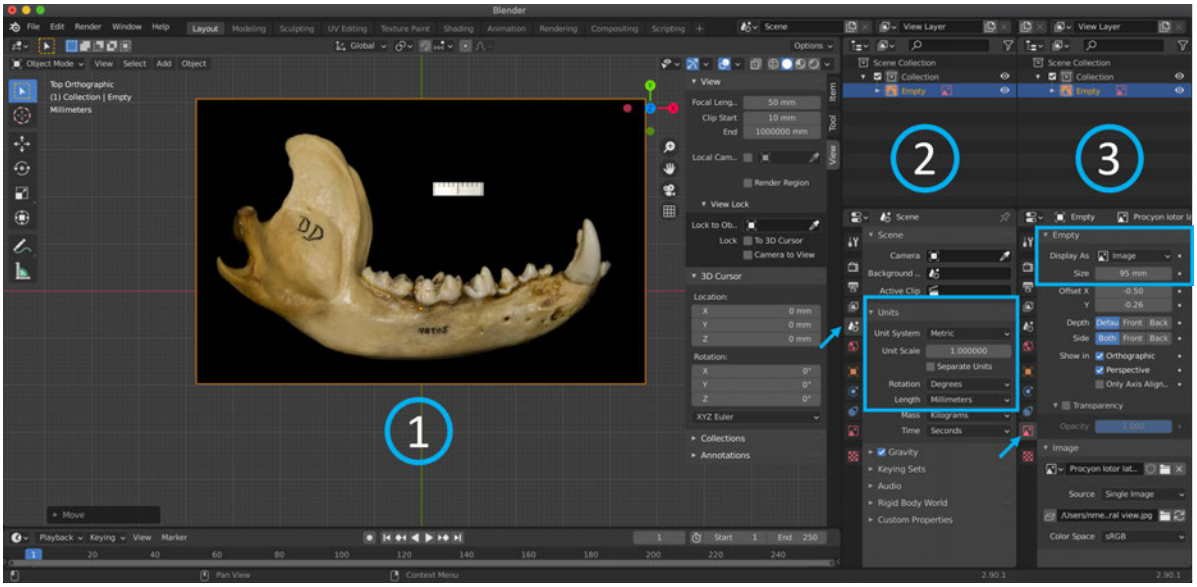

Figure D.6: Uploading a reference image to Blender

8. Hit "G" on your keyboard or go to Object>Transform>Move. Move the vertex to your preferred place along the outline of the jaw to start outlining.

Now we will properly outlining the jaw (Figure D.8).

1. Go to Edit Mode. Make sure your vertex is selected (i.e., highlighted in white). Press "E" to extrude, click wherever you want to set the next vertex. This will allow you to start tracing the jaw. Keep in mind that we need to do this using as few vertices as possible, while still capturing the shape of the jaw; otherwise, our outline will be too complicated to convert to 3D. Make sure to ignore the teeth.

2. Keep on pressing "E" until you have outlined the whole jaw. If at any point you want to delete a vertex, hit "X" of your keyboard, make sure "Vertices" is selected and hit Enter. You can also move the vertices after you finish outlining by hitting the "G" key.

3. Right before you finish outlining the jaw, you'll notice that you need to join the first and last vertices. To join them, while still in Edit Mode, select both vertices using "Shift" on your keyboard. Go to Mesh>Edges>Make Edge/Face or hit "F" on the keyboard. The vertices should now be connected.

4. We are now going to fill the outline. To do this, we must select all the vertices in the outline. While in Edit Mode, go to Select>All, or Hit "A" on your keyboard.

5. Click on any vertex and drag the cursor around the outline of the jaw until you have selected all the vertices. The selected vertices will be highlighted in orange. Hit Esc on your keyboard.

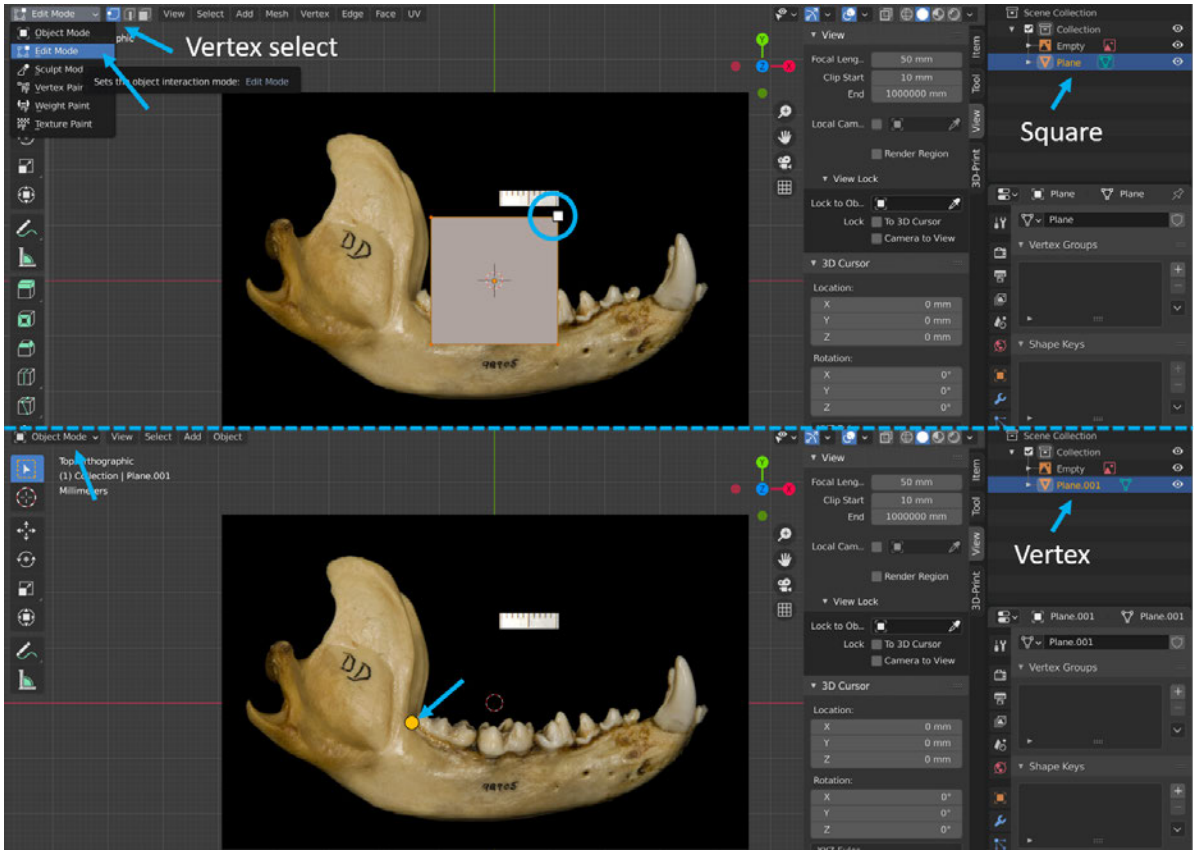

Figure D.7: How to isolate a vertex in Blender: this is the first step to start outlining a jaw

6. While in Edit Mode, press "F" on your keyboard to fill the outline.

Let's make sure the dimensions of our object are correct (Figure D.9):

1. Go to Object Mode. Hit "N" on your keyboard to bring out the sidebar. Under Item>Transform, you will find two important things: the scale and the dimensions.

2. We want the "Scale" to be at 1 in X, Y and Z. If it's not, go to Object>Apply>Scale.

3. Check the dimensions of your jaw are roughly the same as the measurements you took in ImageJ/Fiji.

We will now add additional vertices and edges to simulate muscle attachment areas. It is up to you how precise you want to be, but keep in mind: with extruded FE models less is more. If you make a model too complicated, you might have meshing issues later on and the model will take too long to make. Here I will only make a simple outline:

1. While in "Object Mode", hit "Z" in your keyboard and choose "Wireframe", so you can see the image behind.

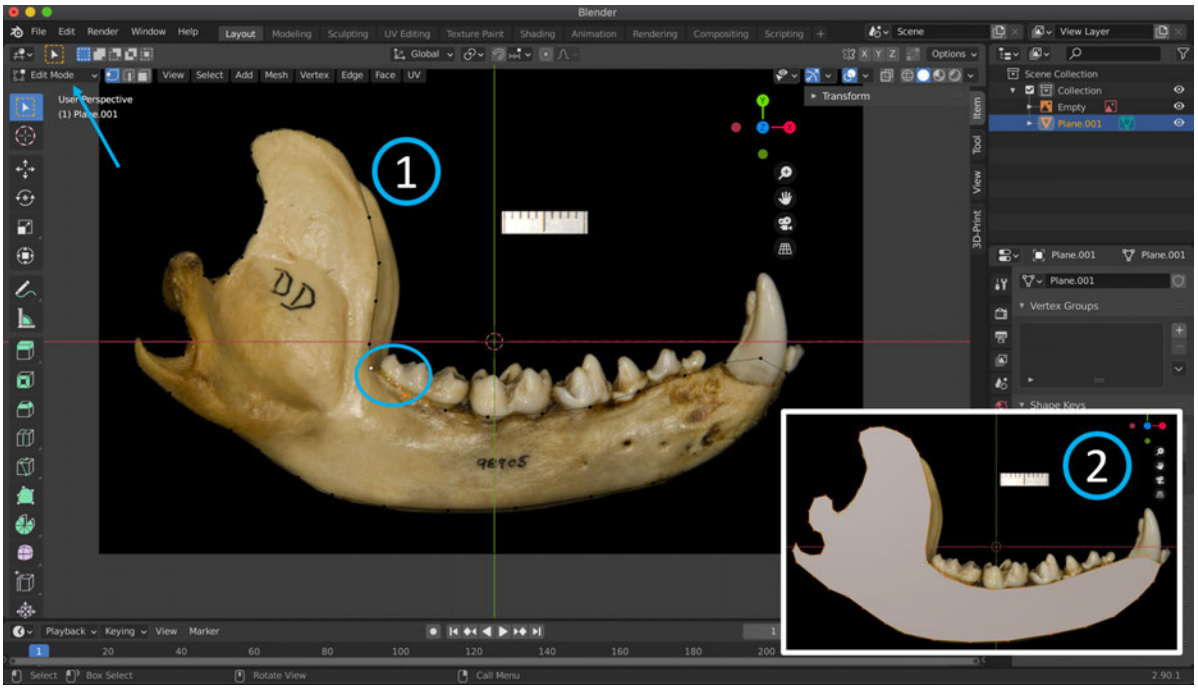

Figure D.8: How to outline and fill a jaw in Blender

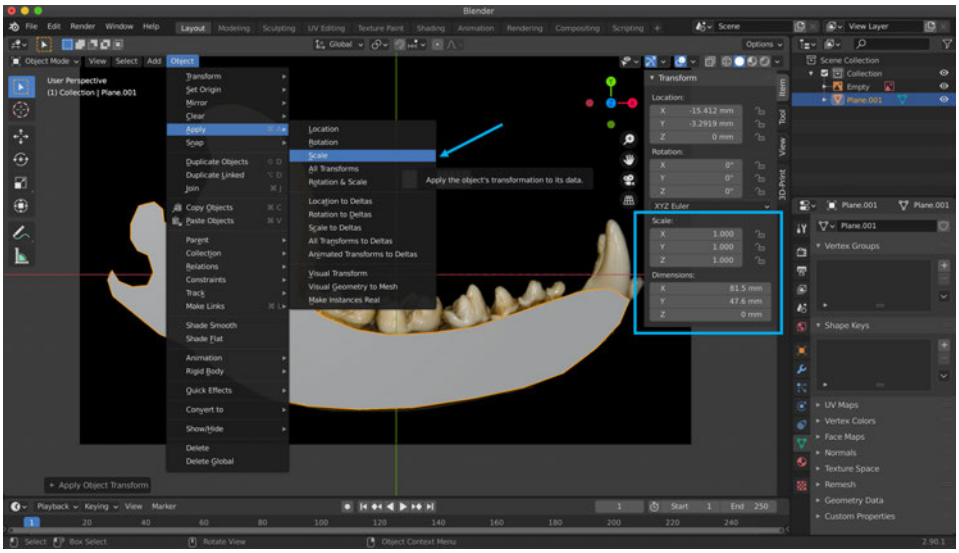

Figure D.9: How to check the dimensions of your object in Blender

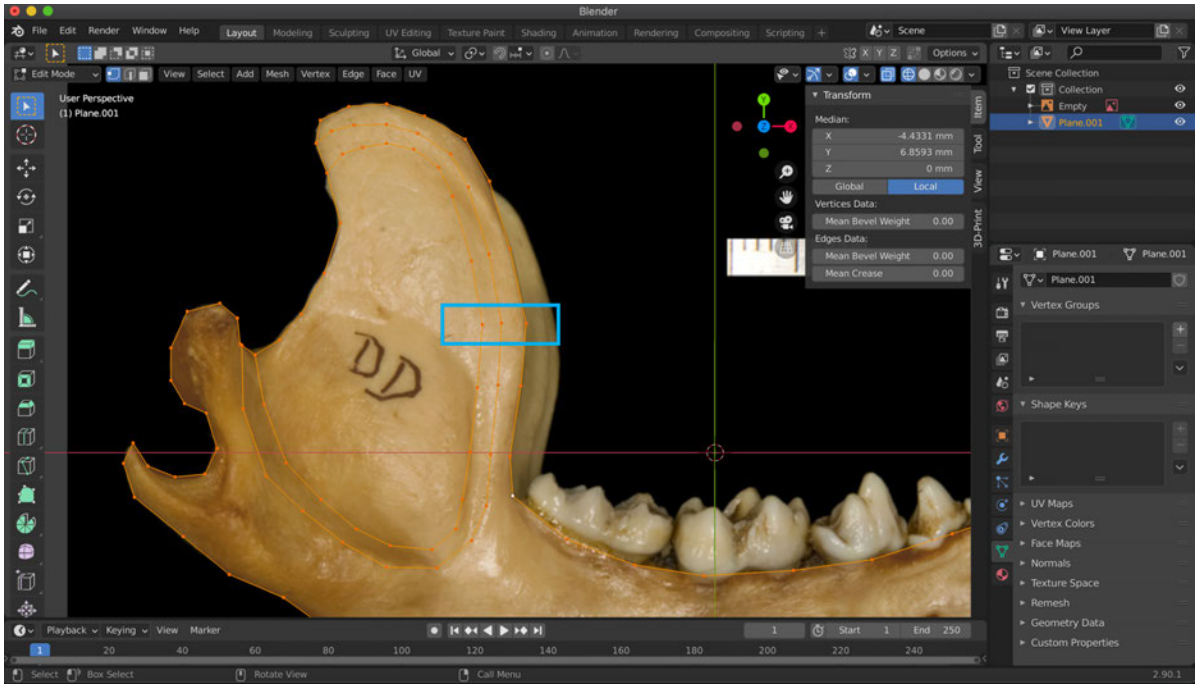

Figure D.10: How to use the knife tool to indicate the area of muscle attachment. See in blue box how the new vertices we create are in line with the original outline

2. Go to "Edit Mode". Hit "K" in your keyboard to activate the knife tool. This will allow us to "cut" through the model.

3. Starting from an existing vertex, let's trace a line around the area of muscle attachment, try to add the same (or a similar) number of vertices as in the outline, as they will be connected later; finish outlining by connecting to an existing vertex (make sure you are actually clicking on the vertex, otherwise you might inadvertently add new vertices to the outline that cause you meshing troubles later on). Again, try to not make this too complex. Hit Enter when you are done.

4. Draw a parallel line towards the inside of the jaw, with the same number of vertices. Remember to start and finish at existing outline vertices.

5. We can now hide the reference picture. In the Scene Collection Panel on the top right corner, click on the eye icon next to "Empty" to hide the picture. You can click on this icon again if you wish to use the picture for reference later on.

We are now going to extrude the model into 3D (Figure D.11):

1. While in Edit Mode, go to View>Front so you can see the jaw in dorsal view (it will appear as a line as it's currently in 2D).

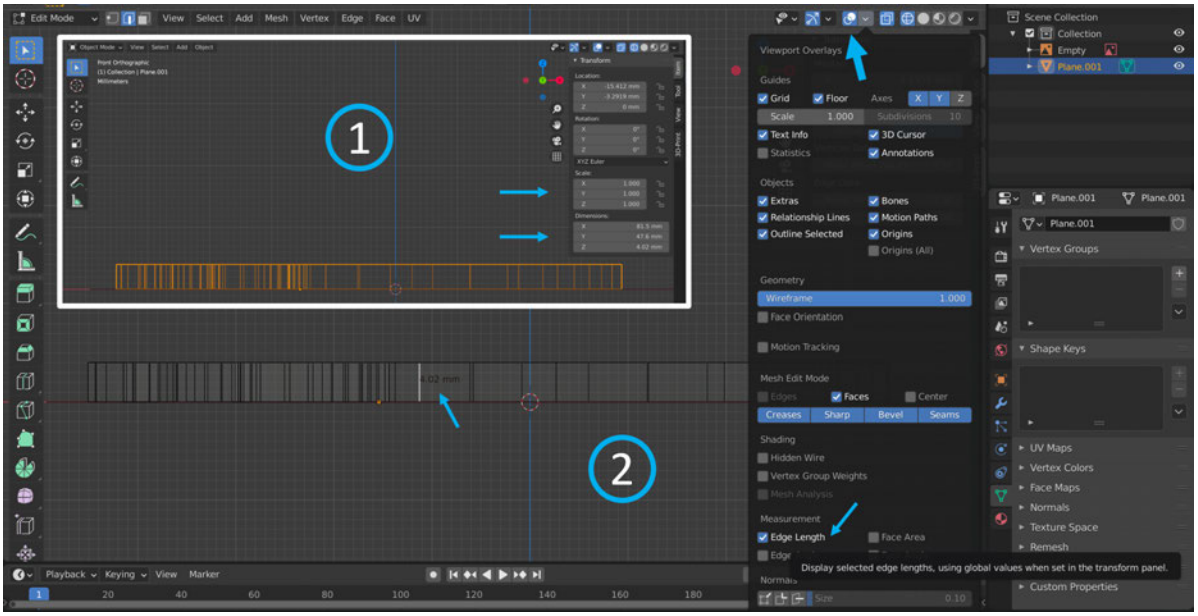

Figure D.11: How to extrude a 2D jaw in Blender (1) and how to check the lengths of edges (2)

2. Make sure the jaw is selected (highlighted in orange), go to Mesh>Extrude>Extrude Faces, or hit "E" on your keyboard.

3. Drag the cursor up to extrude the jaw. At this point it is irrelevant how much you extrude it, just click anywhere to release it.

4. Go to Object Mode. In the properties panel (press N to show), under "Dimensions", change the Z value to the average width of the dentary you calculated beforehand (after taking the measurements in ImageJ/Fiji)

5. Go to Object>Apply>Scale to apply the scale. In the properties panel, under scale, X,Y and Z should now all say 1.000. This is very important, so do not skip this step! Otherwise, all the edits we'll make later will be wrong.

6. You can also make sure the width of your jaw is accurate by displaying the "Edge Length" of whichever edge is selected. To do so, go to "Edit Mode" and click on Overlays (you can find this above the Properties Panel, it looks like two circles intersecting each other). Under Measurement, activate "Edge Length".

We are now going to create temporary edges linking the extra vertices we created using the knife tool (Figure D.12).

1. In Object Mode, go to View>Viewpoint>Top.

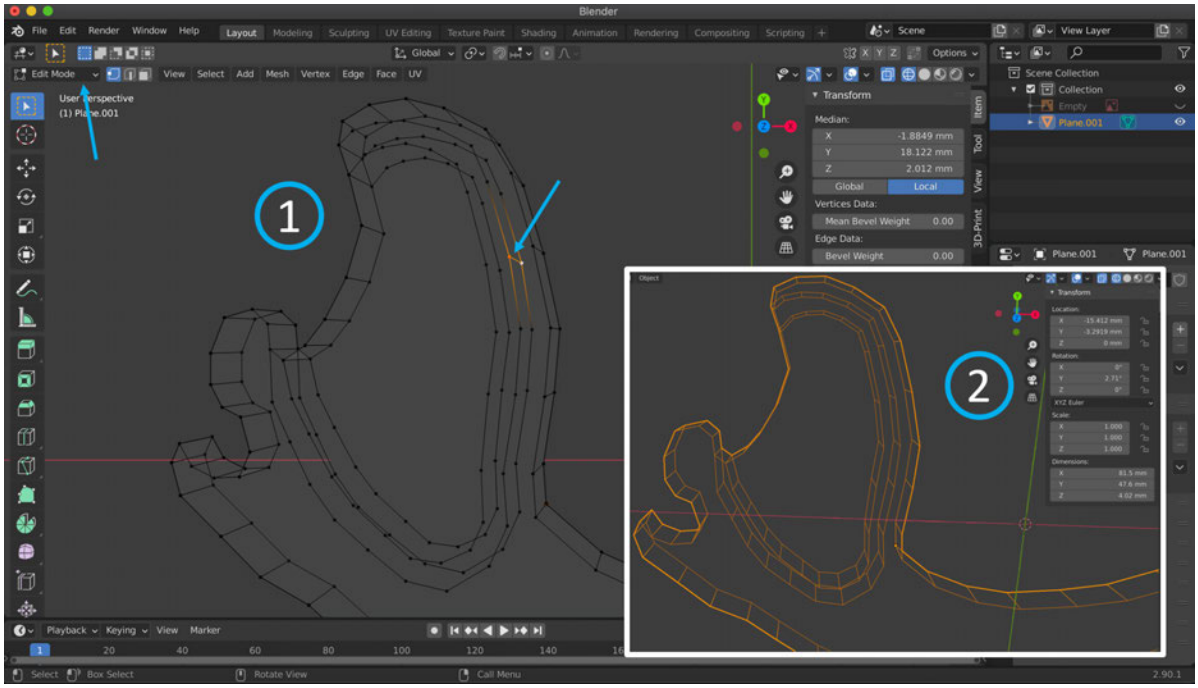

Figure D.12: How to join opposing vertices in Blender: 1) Identifying opposing vertices and joining them, 2) Finished product

2. Hit "R" and then "Y" on your keyboard to rotate your object along the y axis. We want to make sure we can see the opposing pairs of vertices we created with the knife tool (i.e., vertices with the same XY coordinates, but located in different places along the Z axis).

3. Using shift select opposing pairs of vertices and hit "F" on your keyboard to create an edge. You can make sure you are joining the right vertices by having the "Edge Length" tool activated: it should display the average width of your jaw; if it's anything else, you are joining the wrong vertices.

4. Repeat this for every single pair of opposing vertices that were created with the knife tool.

5. Please note: if you want to rotate the object, do so in "Object Mode", if you try to do so in "Edit Mode" you won't rotate the object, but whatever edge or vertex you have selected. You can also pan the object across the screen by holding Shift while moving the object with your mouse/trackpad.

You now have a flat extruded model. However, jaws are not completely flat and we must account for the differences in width at the ascending ramus. To do this, we are going to use the width measurements we obtained in ImageJ/Fiji (it's also handy to have ImageJ/Fiji open for any extra measurements) (Figure D.13):

1. In Object Mode, rotate the jaw (hit "R" on your keyboard to rotate, plus "X" if you are rotating on the x axis, "Y" if you are rotating on the y axis, and "Z" if you are rotating on the Z axis. You can hit Alt-R or Option-R to reset the rotation of the jaw.

2. We are going to be modifying the length of the edges along the ascending ramus of the jaw (i.e., along the the coronoid process, condyle and angular process).

3. To modify the length of the edges we need to activate a Blender add-on. Go to Edit>Preferences (on the top left corner of the window). Select the "Add-ons" tab. In the search bar, type "mesh". Check the box next to "Mesh: Edit Mesh Tools", and close the window.

4. In Edit Mode, click on the "Edge Select" icon (next to Edit Mode, it is the second square on the right).

5. Select any edge you want, I like starting with the edge representing the widest point of the condyle. When you select it, if you have the "Edge Length" tool activated, you will see the average width of the jaw displayed.

6. Look at the sidebar on the top right, you will have a new tab that says "Edit". Click on it and then on the arrow next to "Mesh Tools". Under Manual>Target Length, indicate the maximum width of the condyle you obtained in ImageJ/Fiji (or any other measurement fit for the edge you selected). Click OK.

7. As you see, the length of your edge has changed (the length is displayed next to the edge if you activated the Edge Length tool). Of course it looks odd, as it is the only one which is different. Using measurements obtained from ImageJ/Fiji modify the length of the rest of the edges along the ascending ramus so you have a "natural-looking" jaw. There might be places where you don't have exact measurements: for example, with a dorsal view picture you can measure the base and the top of the back of the coronoid process, but you do not have the measurements in-between. You can use both measurements to interpolate the length of the edges in between. The more you practice, the easier it will be to build these models.

We are now going to modify the length of the internal edges (Figure D.14):

1. Once you are done modifying the length of the outer edges of the ascending ramus, you need to modify the internal edges we created beforehand. Of course, because we are working with pictures, we don't know exactly how much the jaw slopes inwards. But the purpose of outlining the muscle attachment area is just we have an idea where the muscles attache when we are loading our model in an FEA software later on, and to avoid meshing problems. Therefore, we only need to make these internal edges slightly shorter than the outer edges. We want the jaw to look as if it was slightly sloping inwards.

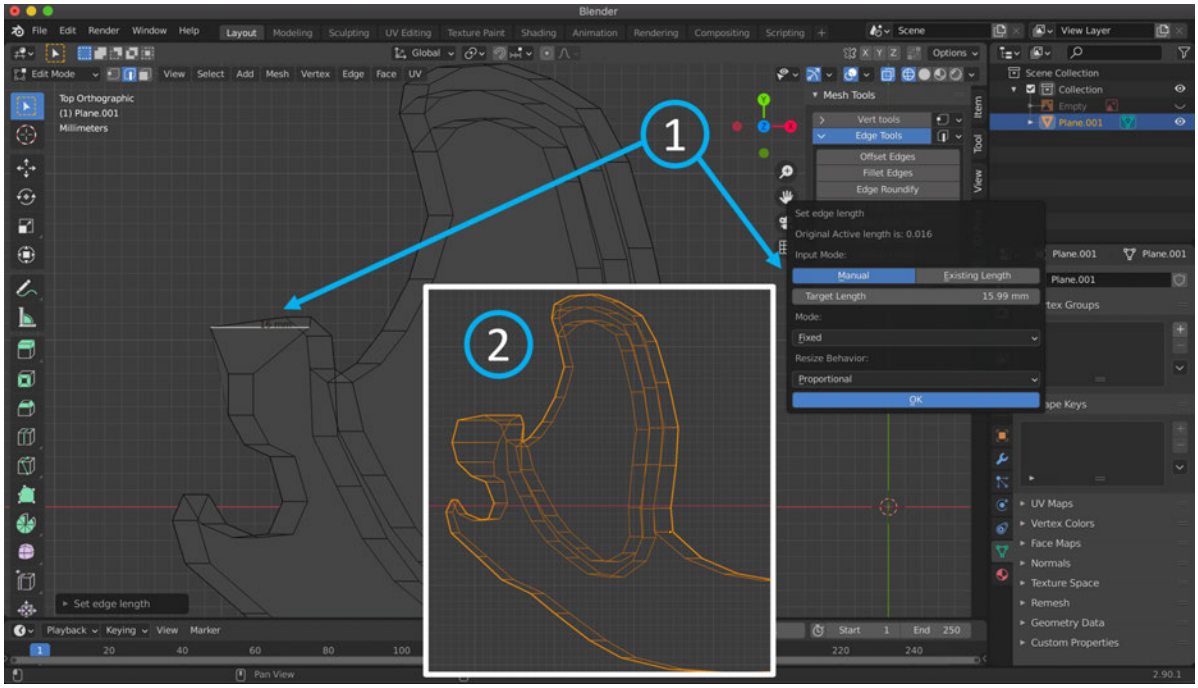

Figure D.13: How to modify the length of the edges in Blender using Edge Length Tools (1). Part 2 of the image shows how outer edges look after changing their length.

2. Once you are done modifying the length of these internal edges, select them, hit "X" on your keyboard, and hit Enter to delete them.

We are now going to join the muscle attachment vertices with the vertices outlining the jaw (Figure D.15):

1. In Object Mode, make sure you are looking at your jaw from the top (View>Viewpoint>Top) and that any rotation has been reset (Alt+R or Option+R)

2. Go to Edit Mode and make sure "Vertex select" is selected. Hit "K" to activate the Knife tool. Because we are now working with a 3D model, hit the key "Z" to activate cut-through (this means that any cut you make on one side of the jaw is reflected on the other).

3. Use the knife tool to join the vertices along the ascending ramus. This tool will allow you to connect the outer and inner vertices to generate a gently sloping effect and remove any artefacts caused by abrupt changes in width along the jaw. This is not necessary to do in flat parts of the model (e.g., the dentary). Make sure you are actually connecting existing vertices and not creating any new ones by mistake. If you make any mistakes just hit "Esc" on your keyboard. When you are done hit "Enter".

We are done! Let's see the finished model (Figure D.16):

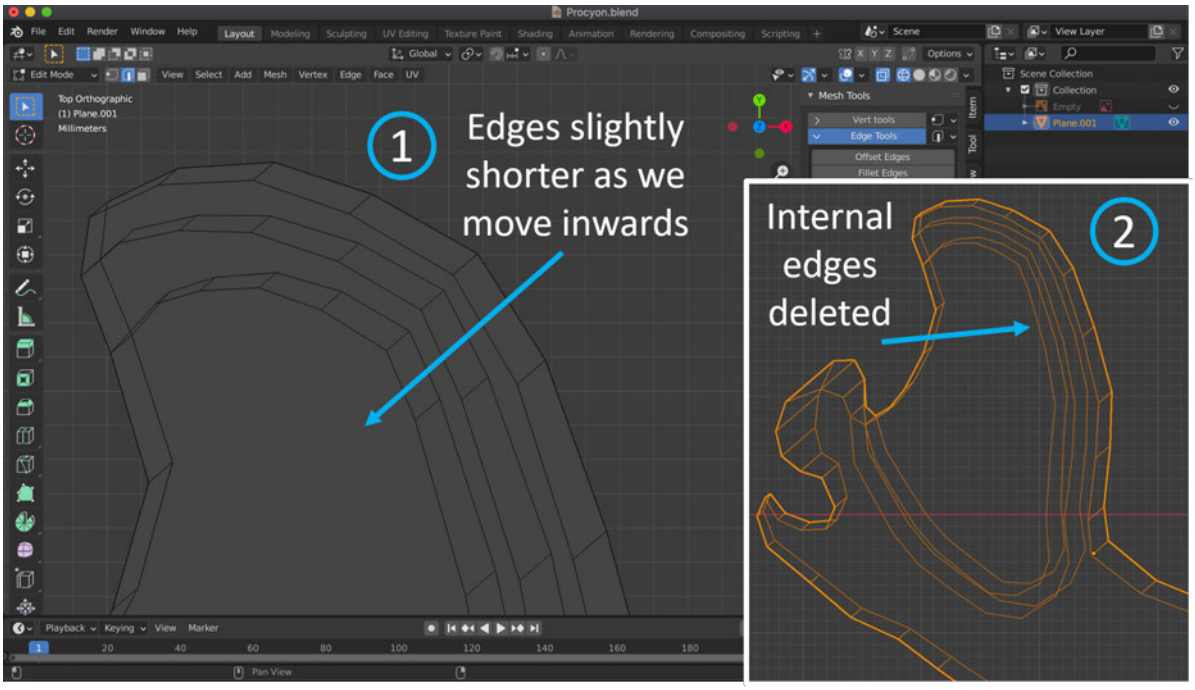

Figure D.14: How to modify the length of the internal edges (1) and then delete them (2)

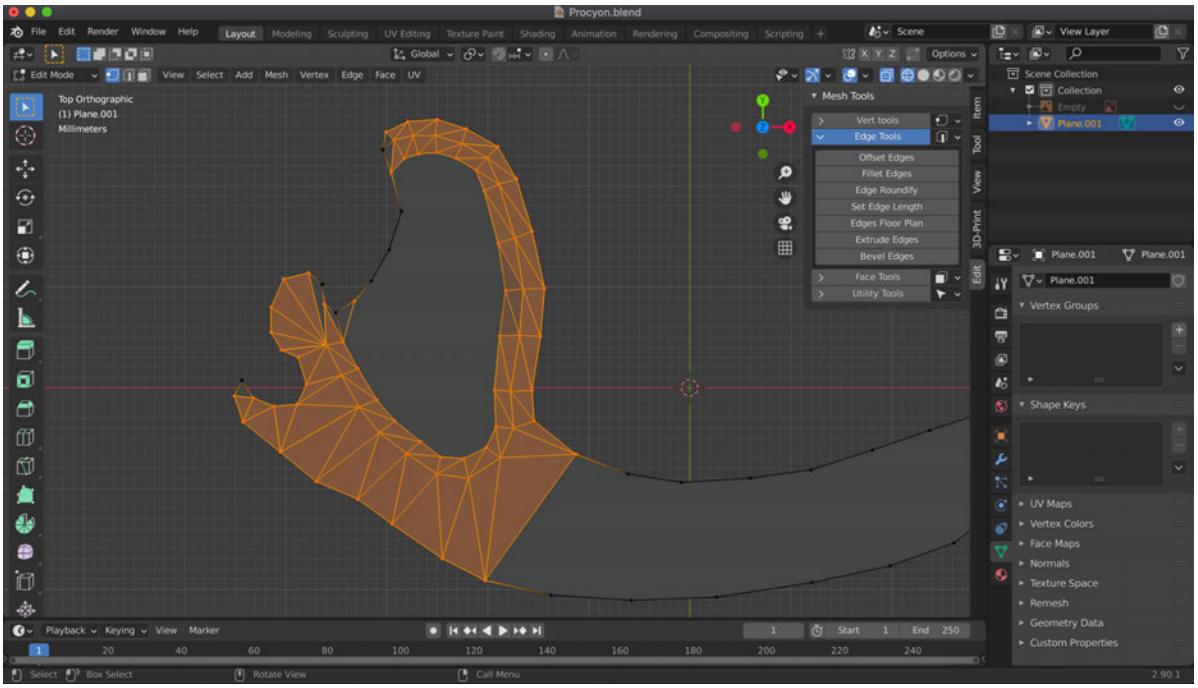

Figure D.15: How to join "inner" and "outer" vertices to smooth surface of the jaw

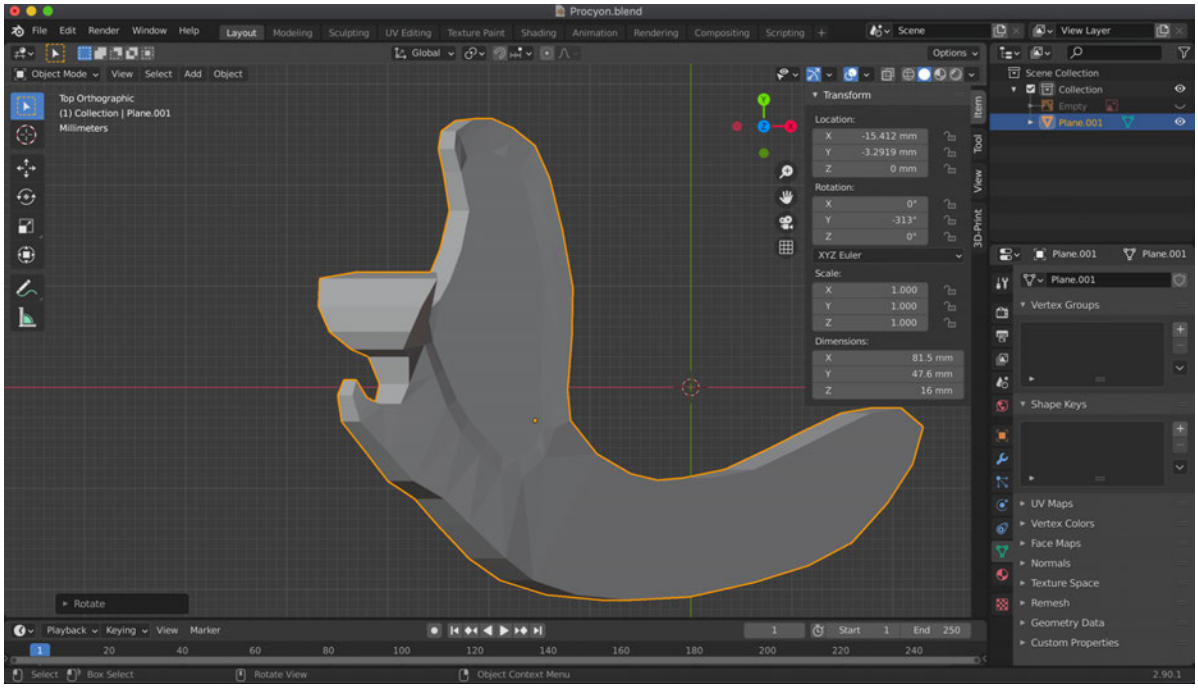

Figure D.16: The finished enhanced extruded model built in Blender

1. Go to Object Mode. Hit the "Z" key in your keyboard and select "Solid"

2. Your model is not ready to export as an STL, if you wish to scale it to a particular surface area or volume you have to install the add-on "3D-Print". Go to Edit>Preferences, and under the Add-on tab search for 3D-Print and check the box next to it.

3. On the sidebar to the right you can click on "3D-Print" and click on "Volume" or "Surface Area" to obtain this information. While in Object Mode, hit "S" to scale the model up or down, and query the surface area or volume again until you obtain the size you desire.

4. Under 3D print, you can also export your model as an STL

A few extra recommendations:

1. If you are building a large number of models, it good to work in "batches". That is: do all the outlines first, then all the extruding, then all the modification of edge lengths, and so on.

2. If you are going to use Abaqus to perform FEA, you have to convert your STL model to STEP first. This is done in the freely available software FreeCAD, the instructions for doing so are here: https://www.bantamtools.com/blog/convert-stl-to-step

APPENDIX E

APPENDIX E

This appendix has the detailed protocol on how to perform Finite Element Analysis (FEA) in Abaqus. This protocol was described extensively by Nuria Melisa Morales Garcia, but is based on the short protocol of Jennifer J. Hill and Thomas Burgess. This protocol was used to build run the FEA models in Chapters 3 and 4.

E.1 Performing finite element analysis in Abaqus

This protocol was made with the purpose of performing finite element analysis (FEA) in Abaqus using enhanced extruded FE models (see Morales-Garcia et al., 2019). However, this protocol is also useful if you are performing FEA on 3D models built with tomographic data or photogrammetry. Using Abaqus, we will recreate the material properties of bone and simulate the condutions under which the adductor muscles of the jaw work. We will then analyse the model using FEA and observe the stress and strain patterns along the jaw at the moment of biting.

The first thing we will do is import our model into Abaqus (Figure E.1). To do so:

1. Open Abaqus CAE. A window called "Start Session" will pop up. Choose Create Model Database with standard/explicit model.

2. Go to File>Import>Part. Expand the "File Filter" menu at the bottom of the screen and choose STEP (*.stp*,*.step*). You can now choose your STEP model and click OK.

3. A window called "Create part from STEP file" will appear. Under "Name-Repair" select "Combine into single part", and under "Part Attributes" make sure "3D" is selected under "Modelling Space" and "Deformable" is selected under "Type".

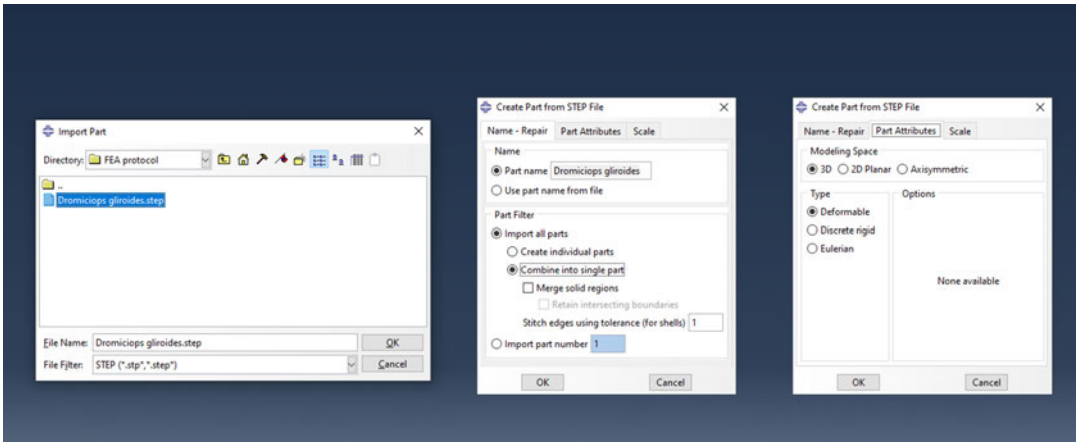

Figure E.1: How to export a STEP file into Abaqus

4. If you need to scale your model, go to the tab "Scale" and multiply all lengths by the number of your choice. If you followed my protocol on how to build enhanced extruded FE models in Blender, this step should not be necessary.

The first thing we are going to do is generate a mesh of our model (Figures E.2 and E.3). To do so:

1. Change the module to Mesh (you were previously in the Part module)

2. Click "Show Mesh Seeds"

3. Click "Seed Edges" on the lateral toolbar (it's an L-shaped figure with red dots at the bottom) or go to Seed>Edges on the top menu bar. Drag a box around the object of interest to complete this action. Click done at the bottom of the graphics window when you are done.

4. A window called "Local Seeds" will appear. Under the "Basic" tab, make sure "Method" is "By size" and "Bias" is "None". Under sizing controls, indicate the approximate size you wish the elements in your mesh will have. If it's your first time making a model, you probably won't know which value to put in, that's ok! To determine the size of the elements in your mesh, you will have to perform a convergence test (more on this later on), but for now let's just choose 0.0001. Click OK.

5. Click on "Assign Mesh Controls" on the lateral toolbar (it's right underneath "Seed Edges") or go to Mesh>Controls on the top menu bar. A window called "Mesh Controls" will pop up, select "Tet" and click OK.

6. Click on "Assign Element Type" on the lateral toolbar (it's a meshed L-shape with the letters S4R written on red above it). Under "Element Library" select Standard, under "Geometric Order" select "Linear", and under "Family" select 3D stress. The tab "Tet" should be activated and at the bottom it should say "C3D4: a 4-node linear tetrahedron".

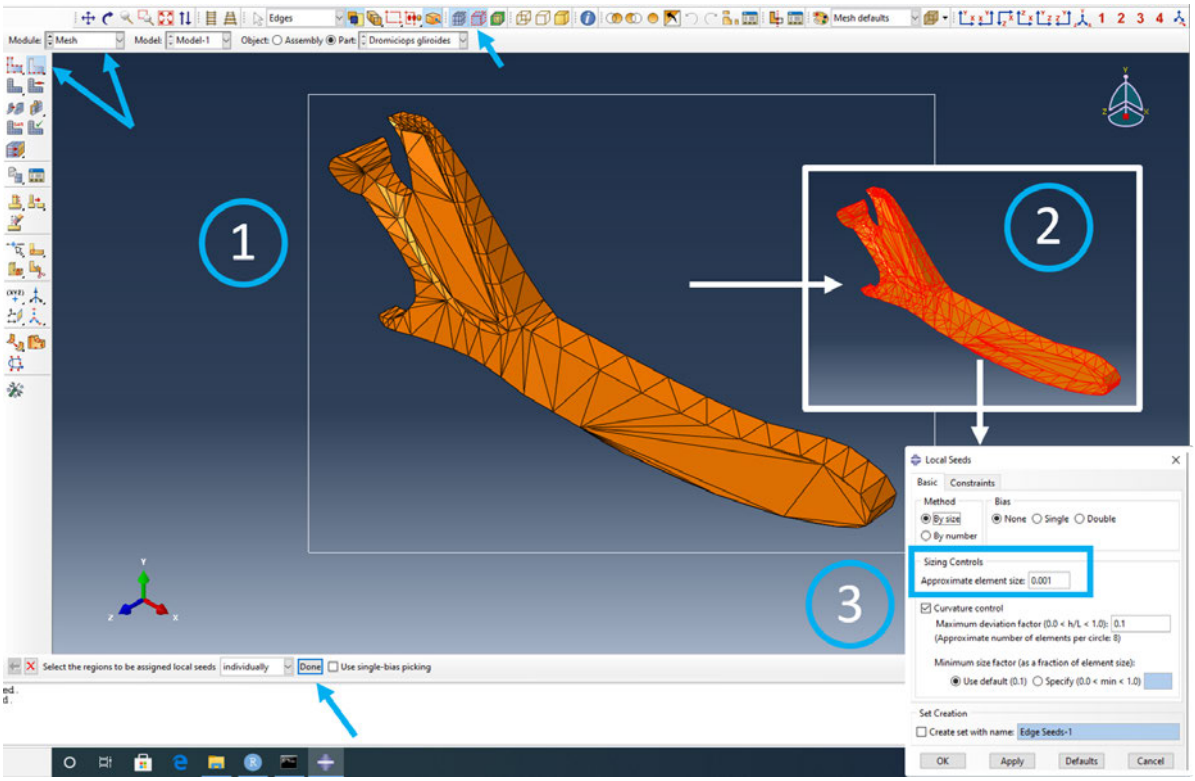

Figure E.2: How to export start the meshing process and assign element size in Abaqus

Click OK. Please note, this type of element suits 3D jaw models, but depending on the model you are building, the desired element type might be different.

7. Click on "Mesh Part" on the lateral toolbar (it's a meshed L-shaped icon) or go to Mesh>Part on the top menu bar. Once you do this, a prompt will appear at the bottom of the graphics window asking you if it's okay to mesh the part. Click on yes.

8. You have successfully meshed your jaw. At the bottom of the screen you will get a message telling you how many elements have been generated in your mesh. If you want to further query the mesh properties, click on the "Query Information" icon on one of the top toolbars (it's a white "i" within a blue circle), you can also find it in the top menu bar under Tools>Query. Click on "Mesh". At the bottom of the screen, there will be a prompt asking you whether you want to query the entire part. Click Done. Below, you will see the number of nodes and elements in your mesh, as well as the element type.

9. If you click on "Verify Mesh" on the lateral toolbar (it looks like a meshed L-shape with a green arrow on top), you will be able to check if you mesh has any errors.

We will now assign material properties to our jaw (Figure E.4). That is, the physical properties of bone that describe its stiffness and elasticity. You can find these values in the literature. To do so:

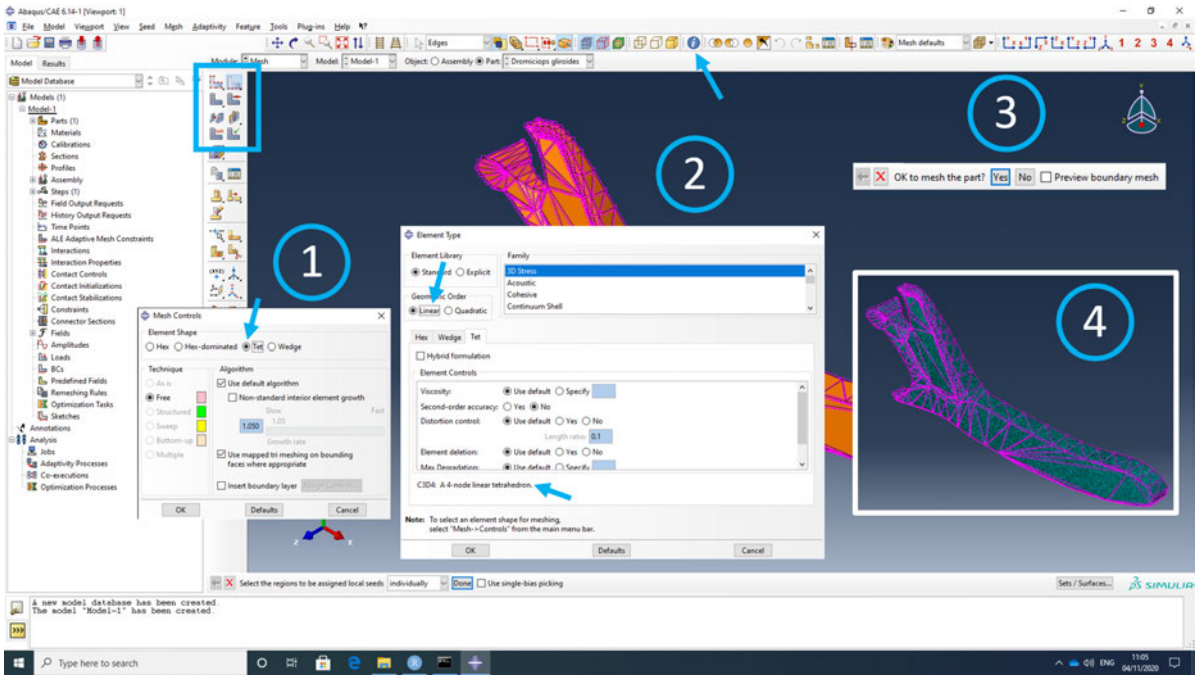

Figure E.3: How to assign element type and finish the meshing process in Abaqus

1. Change the module to "Property"
2. Click on "Create Material" (it's the very first icon on the lateral toolbar, it looks like a graph) or go to Material>Create on the top menu bar.
3. A window called "Edit Material" will pop up. Assign a name to you material and then select Mechanical>Elasticity>Elastic. You will then be able to assign the desired values of Young's Modulus in MPa and Poisson's ratio. Bone has a a Young's Modulus of 18,000 and Poison's ratio of 0.3. Click OK.
4. Please note that from now on, you will constantly need to assign names to the features you create, I strongly suggest that you give them easily recognisable names and keep them uniform if you are making several models.
5. Actions like the above (i.e., creating a new material) can be very repetitive if you are building a large number of models. You can make python scripts that will help you perform these actions effortlessly and quickly (I will talk about how to do this at the end of the protocol).
6. Click on "Create Section" on the lateral bar (it is a yellow beam icon, located right underneath the Create Material icon) or go to Section>Create.
7. A window called "Create Section" will appear. You don't need to change anything here, just make sure "Solid" and "Homogeneous" are selected. Click Continue.

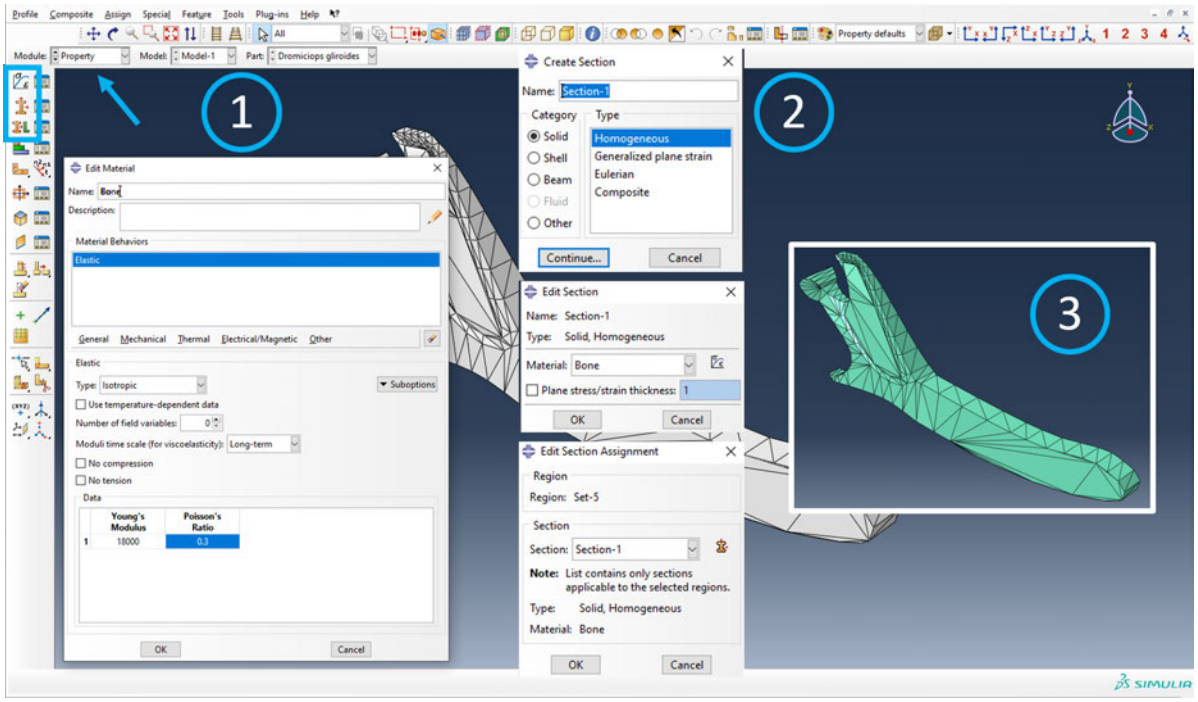

Figure E.4: How to create a material and assign it to the jaw

8. A window called "Edit Section" will appear. Make sure the material you just created is selected under "Material" and click OK.

9. Click on "Assign Section" on the lateral toolbal (it is located underneath "Create Section" and looks like a yellow beam pointing with a red arrow at a green L-shape), or go to Assign>Section on the top menu bar. Select your jaw by dragging a box around it and when you are finished click "Done" at the bottom of the graphics window.

10. A window called "Edit Section Assignment" will appear. Select the section you created from the drop down menu and click OK. Your jaw will change colour. This means that your material (i.e., bone) has been assigned to your model.

We will now create an instance, a step and a field output report request (Figure E.5)

1. Change the module to "Assembly". Don't worry if your object suddenly disappears after you do this.

2. Click on "Create Instance" from the lateral toolbar (it looks like a 3D L-shape with a red arrow on top) or go to Instance>Create on the top menu bar. Make sure "Parts" is selected under "Create instances from:". Select the part you are working with on the list and click OK.

3. Change the module to "Step".

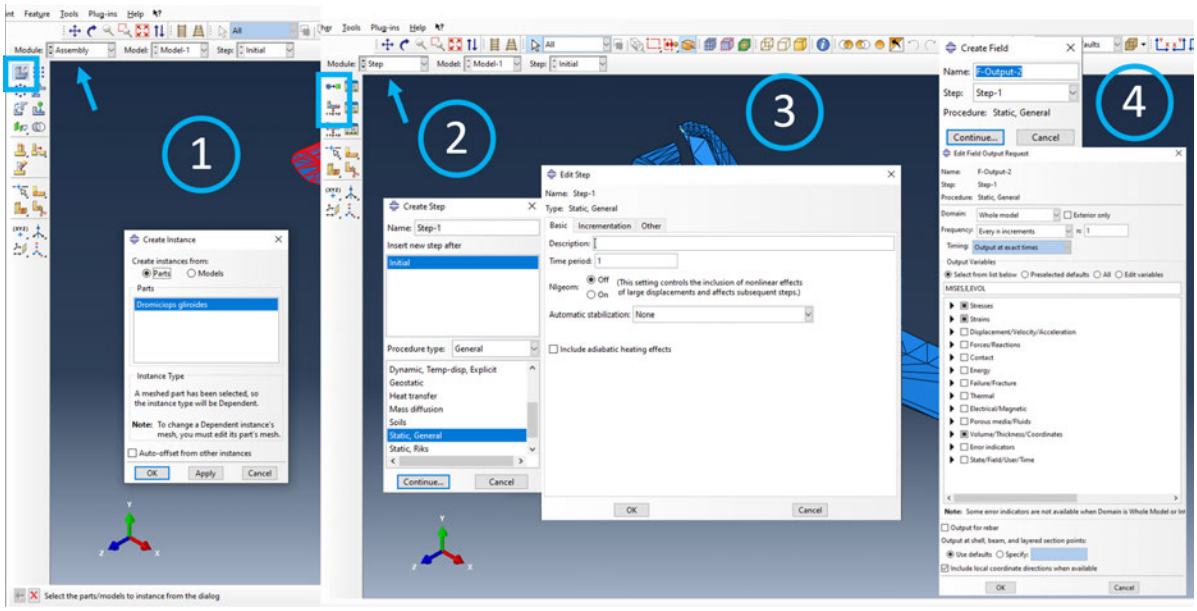

Figure E.5: How to create an instance, a step and request a field output report in Abaqus

4. Click on "Create Step" on the lateral toolbar (it looks like a blue circle and a black arrow pointing to a green square) or go to Step>Create on the top menu bar.

5. A window called "Create Step" will appear. You don't need to change anything, just make sure "Static, General" is selected under "Procedure type". Click continue.

6. A new window called "Edit Step" will appear. Default options should be fine in this case, so just click OK.

7. Click on "Create field output" on the lateral toolbar (it's right underneath Create Step) or go to Output>Field Output Requests>Create.

8. A window called "Create Field" will appear, click Continue

9. A window called "Edit Field Output Request" will appear. Here you can select all the variables you'd like information on upon completion of the FEA job. I usually choose the following: MISES, Mises equivalent stress (under Stresses); E, Total strain components (under Strains), and EVOL, Element Volume (under Volume/Thickness/Coordinates). Click OK when you are done

We will now create the boundary conditions of the model. That is, we are going to indicate where movement should be impaired along the jaw. For example, is a jaw we might want to restrict the movement of the condyle (i.e., the articulation with the skull) and the biting point. There are several ways of doing this. You might choose to select some nodes and apply the boundary conditions to all of them individually. Here I show you how to constrain a number of nodes on

the surface of the jaw to a single point "floating in space", where the boundary condition is then applied upon (Figures E.6, E.7 and E.8). To do so:

1. Change the module to Interaction

2. In the top menu bar, go to Tools>Set>Create.

3. A window called "Create Set" will appear. We are going to start creating a set to include nodes along the condyle. Therefore, I am going to name this set "Condyle set" (again, these names should be evident and you should keep them constant throughout). Select "Node" under "Type" and click OK.

4. You can now see the mesh. Click on "Apply Left View" on one of the top tool bars (the icon is a set of perpendicular arrows with the letter Y on top and the letter Z facing to the right). You should now be able to see the back of the jaw. Zoom in and select the nodes along the condyle where you will be imparing the movement. To select more than one node hold down the Shift key, to deselect a node hold down the Ctrl key and click on the node of interest. You can use the Pan (looks like two intersecting arrows) and Rotate (looks like a curved arrow) tools on one of the top tool bars to help you manipulate the model.

5. Make sure you only select nodes on the surface of the model. To do so, find an icon on one of the top toolbars that looks like a long orange box (it's the second icon to the right of the word "Nodes"). Click on the arrow on the bottom corner and pick the option "Select from Exterior Entities". When you activate this option, you will only be able to select nodes on the surface of the model, but be careful! You might still be selecting nodes on the opposite end of the jaw, rotate your model a little bit to make sure you've only selected nodes on the desired surface.

6. When you are done, click "Done" at the bottom of the screen (where it says "Select nodes from the set individually". You can also select multiple nodes at once by switching from "individually" to "by angle" or "by feature edge". However, be careful not to overconstrain your model, this might lead to very unrealistic results!

7. We will now create a single point that unites the individual nodes. This point is where the boundary conditions will be applied upon. We want to position this point just hovering above the surface of the condyle. To do so, we will query the position of one of the points which already exist on the model. Click on Query Information and select Point/Node. Choose the point which is located approximately at the middle point of the nodes you just selected. Click done at the bottom of the screen. Just below, you will see the coordinates.

8. Click on "Create Reference Point" on the lateral toolbar (it looks like a blue cross with the letters RP above). Fill out the coordinates of the node you just queried and click OK.

9. Go to the model tree on the left side of the screen. Under Assembly>Features, you will find the reference point you just created. It will be called RP-1. Right-click on it and change its name to something recognisable: I changed it to Condyle RP.

10. Now we are going to modify the X coordinates of this point, so that it's just hovering above the condyle. Double-click on Condyle RP and edit the X coordinate, so to achieve the desired effect. Click OK when you are done.

11. We now need to transform this reference point into a set. Go to Tools>Set>Create. Change the name of the set (I will call it Condyle reference set), make sure "Geometry" is selected under "Type" and click Continue.

12. At the bottom of the screen you will see "Select the geometry for the set". Click on the Condyle RP we just created and click Done at the bottom of the screen.

13. We will now create a constraint to join the nodes on the surface to the point hovering above the condyle. To do so, click on "Create Constraint" on the lateral toolbar (it looks like a blue square tied up to a yellow rectangle) or go to Constraint>Create on the top menu bar. Rename your constraint (I called it Constraint-condyle) and choose MPC constraint from the list. Click on Continue.

14. A window might appear automatically, but if it does not, click on Sets... on the bottom right corner of the screen. You are first going to select the point that will tie all the nodes together, so choose your Condyle reference set. Click on continue

15. Next, you are going to select the nodes on the surface. Choose "Condyle set", click on Continue.

16. A windown called "Edit Constraint" will appear, double-check everything is fine, and click OK.

17. Repeat these steps to create a constraint for the biting point.

18. Now that we have created the MPC constraints of the condyle and biting point, we can now create the boundary constraints.

19. Change the module to "Load". Click on "Create Boundary Condition" on the lateral toolbar (it's on the left of the second row, looks like an L-shape with a series of red lines underneath), or go to BC>Create on the top menu bar.

20. Rename the boundary condition (I called it BC-Condyle), and choose "Mechanical" under "Category", and "Displacement/Rotation" under "Types for Selected Step". Click continue.

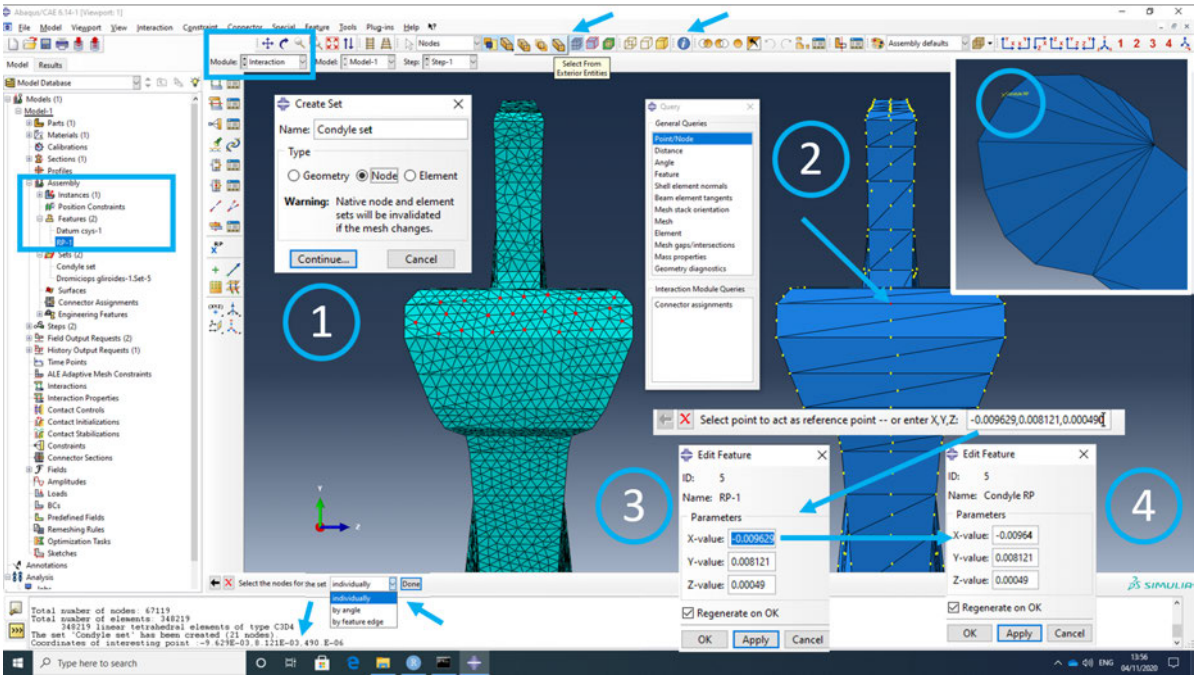

Figure E.6: How to create a node set and a reference point in Abaqus

21. Click on "Sets..." on the bottom right corner of the window. Select the point hovering above the jaw (i.e., Condyle reference set), and click continue. Choose what degrees of freedom you'd like the point to be constrained on. U1 is the mesodistal axis, U2 the dorsoventral axis, and U3 the axis along the length of the jaw; U refers to translational movement and UR refers to rotational movement. Click Ok when you are done.

22. Repeat for the biting point.

Now that we have created the boundary constraints, we need to simulate the pull of the adductor muscles on the jaw (Figures E.9 and E.10). This step is very similar to what we just did with the boundary conditions, but there are some important differences. To do this:

1. Change the module to "Interaction"

2. Follow the same steps as above (steps 2-6) to create node sets for each muscle (i.e., go to the top menu: Tools>Set>Create, rename the set and choose "Node" under type). You will end up with several node sets (I usually have external anterior temporalis, internal anterior temporalis, external posterior temporalis, internal anterior temporalis, superficial masseter and deep masseter). Make sure you do not use any of the same nodes in different muscle node sets, otherwise you will have problems later on.

3. Follow the same steps as above (steps 7-12) to create a point that will unite all the nodes in a set. By uniting all these nodes in a single point, we are simulating the direction the fibers

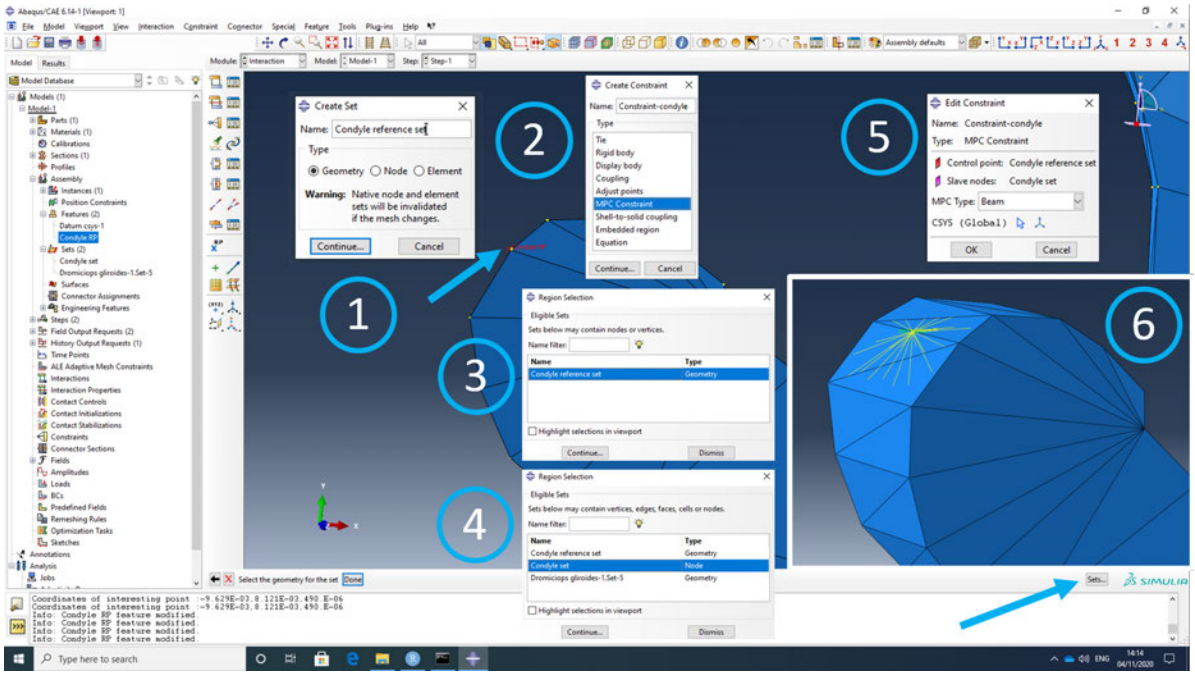

Figure E.7: How to create an MPC constraint in Abaqus

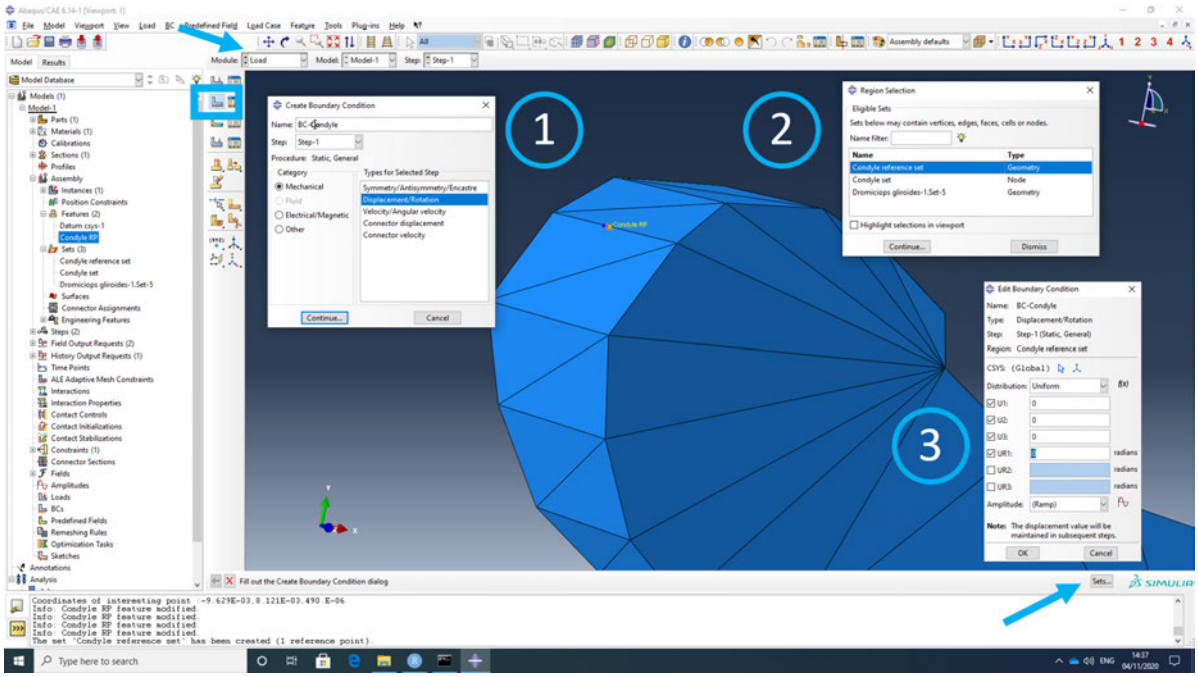

Figure E.8: How to create a boundary condition in Abaqus

of the muscles would be oriented in real life. We don't have a skull to attach these muscles to and we don't want to make a very long constraint that simulates precisely where the most dorsal attachment of the muscles on the skull would be. We just want this point to hover relatively close to the jaw (more so than with the condyle and biting point). More importantly, we want to mimic the direction of the muscle fibers in X,Y and Z (see Figure E.10 for an example).

4. Before we move on to make the constraint, we need to create a new coordinate system. If you click on Apply Front View (icon on one of the top toolbars that looks like perpendicular arrows, with a Y on top and an X facing to the right), you will see that the X axis points to the right, the Y axis points upwards, and the Z axis points towards you. If we were to create a load now, said load would only be able to point along these axes. If, for example, we want our load to pull diagonally, we have to create a new coordinate system.

5. To do so, click on Create Datum CSYS (3 points) on the lateral toolbar (it is the bottom right icon, looks like 3 arrows with 3 red crosses), or go to Tools>Datum>CSYS>3 points.

6. Rename your coordinate system. I call mine based on the muscle I will be applying them on (for example, Anterior temporalis CSYS). Make sure "Rectangular" is chosen.

7. On the bottom of the screen, you will be prompted to enter the origin of your coordinate system. You will notice that there is already a CSYS in place, whose origin is at 0,0,0. I like having all my CSYSs on a row, so I will enter the origin of this new one slightly to the right (i.e., more positive values in X).

8. Then you will be prompted to choose a point the X axis will be pointing towards. I want X to face to the top right of my screen, so I will make it a bit more positive on X and also in Y.

9. Finally, it will ask you to choose a point the XY plane will be facing. I am happy to have it parallel to the jaw, but if I wanted to tilt it a little, I would modify the Z axis.

10. If you are unhappy with your CSYS, you can always delete it from the Model Tree, under Assembly>Features. You can also insert reference points to allow you to play around with the coordinates, until you find some that you are happy with.

11. Create a new CSYS for every muscle you want to load.

12. Repeat the same steps to create an MPC constraint (steps 13-16) as before, but now when the window "Edit constraint" appears, make sure to indicate the CSYS you created for each muscle. Select them by clicking on the white arrow next to CSYS (Global).

Now we can load the model, by simulating the force the adductor muscles of the jaw pull with (Figure E.11). To do so:

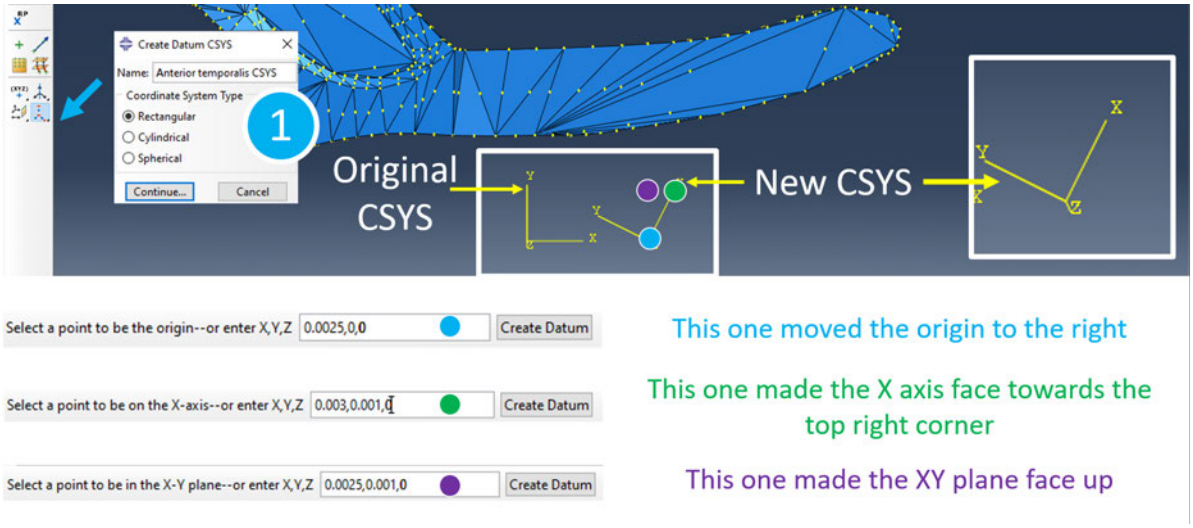

Figure E.9: How to create a new CSYS in Abaqus

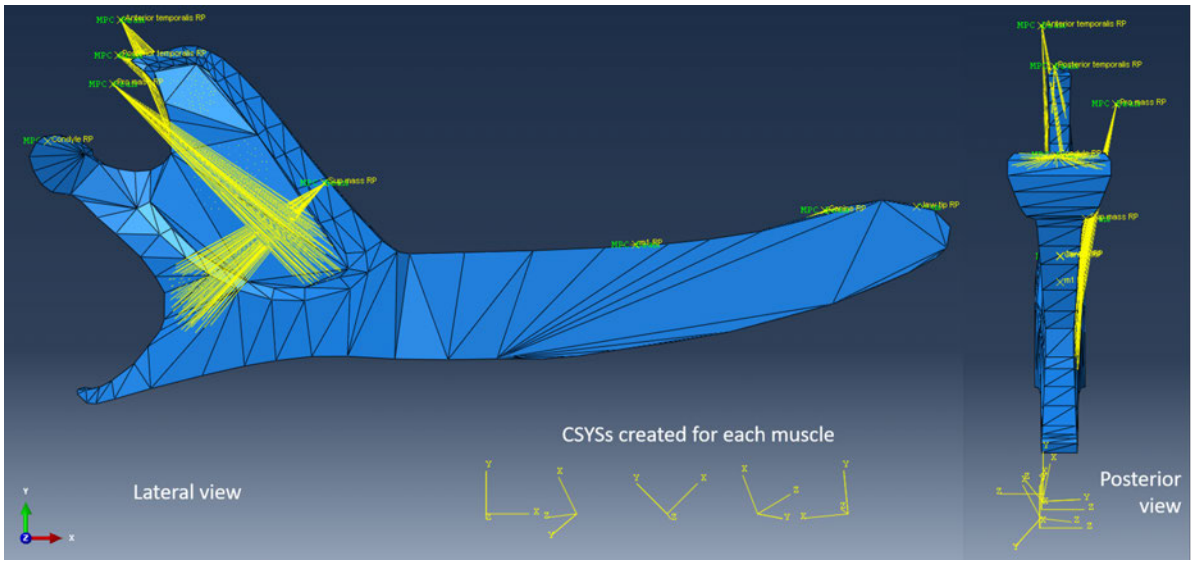

Figure E.10: Lateral and posterior view of the jaw of *Dromiciops gliroides* with all the muscle nodes constrained, and with unique CSYSs

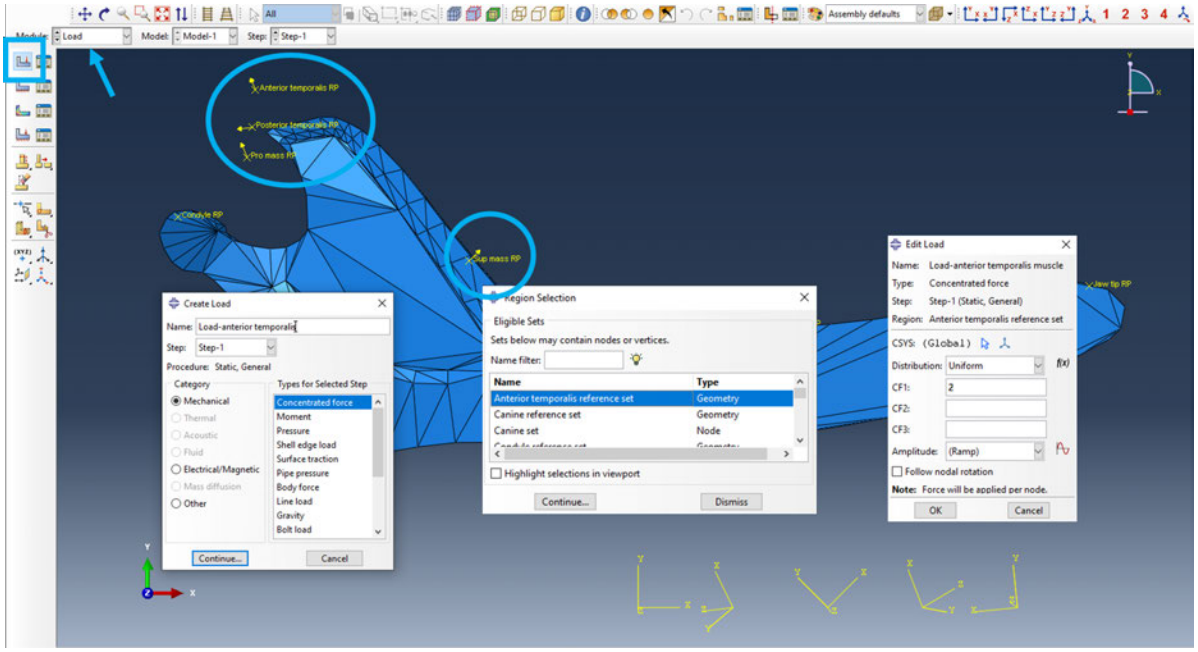

Figure E.11: How to load an FE model in Abaqus

1. Change the module to Load.
2. Click on "Create Load" on the lateral toolbar (it looks like an L-shape with a red arrow facing down at the end), or go to Load>Create on the top menu bar.
3. A window called "Create Load" will appear. Choose a name for the load (e.g., Load-Anterior temporalis) and select the step you defined earlier (do not choose Initial).
4. A set of options will now appear in the window. Make sure "Mechanical" is selected under category and "Concentrated force" is selected under "Type of Selected Step". Click Continue
5. Choose the set that represents the points that anchors all respective muscle nodes together (do not choose the individual muscle nodes).
6. A window called "Edit Load" will pop up. Input the force component CF1 (i.e., load on the x axis), CF2 (i.e., load on the y axis), or CF3 (i.e., load on the z axis). Choose the corresponding CSYS. For example, if you choose the original CSYS and write "2" in CF2, your load will point upwards, if you write "-2" it will face downwards. Click OK when you are done.
7. Repeat this for all the muscles.

The last step is to run your model (Figure E.12). To do so:

1. Go to File>Set Working Directory and choose the folder your CAE file is stored. This is important because all the files associated with the job will be stored here

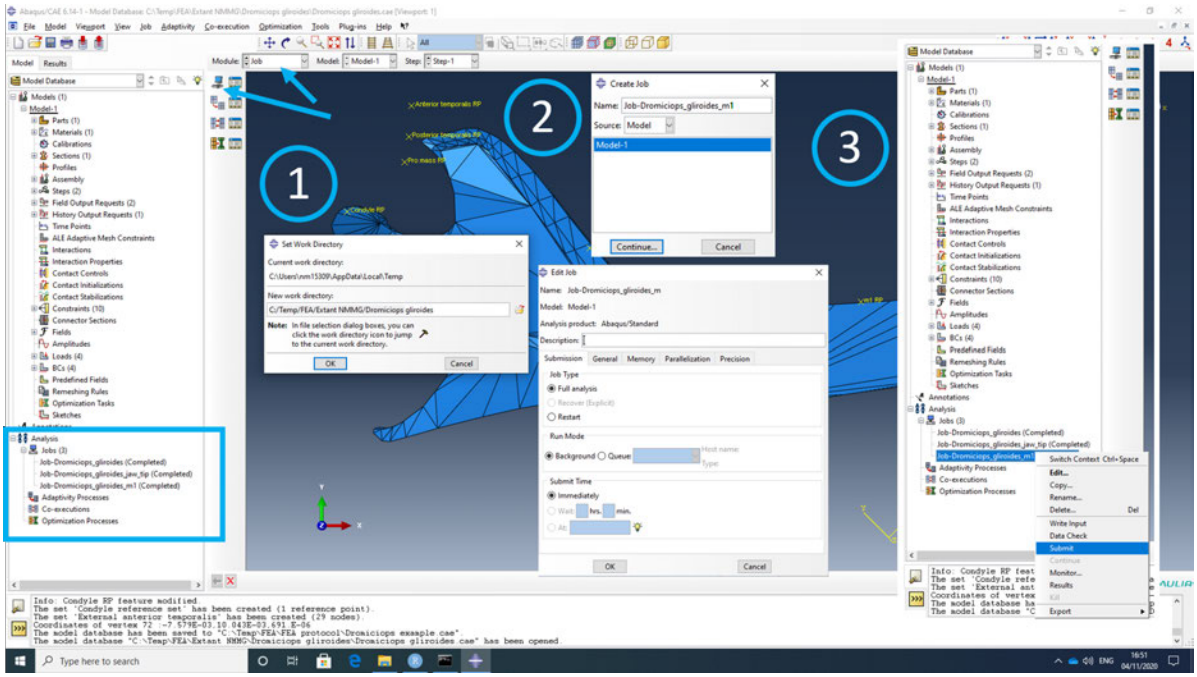

Figure E.12: How to run a job in Abaqus

2. Change the module to Job.
3. Click on the icon "Create Job" on the lateral toolbar (it is the first icon and it looks like a computer), or go to Job>Create on the top menu bar.
4. Name your job and click Continue. A new window will appear, change nothing and click OK.
5. Go to Job>Submit and choose your job name from the list. Click OK.
6. Wait for the model to finish running. Look at the Model tree on the left, under Analysis>Jobs, you will see the status of your job. It will change to "Completed" when it's done.
7. Right-click on the job and choose "Results", or go to Job>Results on the top menu bar and choose the name of your job.

You are now in the visualisation modfule and can see the results of your analysis (Figure E.13). There are many things you can do in this module

1. Plot contours on deformed/undeformed shape: shows you the von Mises stress (or other metrics) as a heatmap on your jaw. Click on the colorful L-shaped icon on the lateral toolbar to activate or go to Plot>Contours on the top menu bar and choose one of the options
2. You can hide the mesh by going to Options>Common>Basic and choose "No edges" under "Visible Edges"

3. You can modify the limits of the stress scale by going to Options>Contour>Limits. There you can specify the minimum and maximum values you want to see on your scale. This is handy for when you want to compare several models with different stress values.

4. You can generate your field output report (i.e., get a detailed spreadsheet telling you the stress, strain and volume values per element of your mesh). Go to Report>Field Output to write an RPT file (which can be imported into Excel). Choose Stress and Strain under Integration Point Position, and Element Volume under Whole Element Position.

5. You can also save the heatmap by going to File>Print. Under Settings>Destination, choose file, indicate the file name, and format of your image file (I recommend PNG).

6. You can revisit your job files any time you like, just make sure Abaqus is set to the right working directory.

You have now analysed a 3D jaw model using FEA! I have a few extra tips:

E.2 Convergence tests

To perform a convergence test to determine the size of the mesh, you need to run a series of analyses in which the models are loaded identically, but the element size changes. Because the number of elements in your mesh is going to increase exponentially (while the element size decreases in a linear fashion), perform a rule of three to determine how many nodes you should select per model. For example, you have 2 models: model 1 has a mesh with an element size of 1 and has 10,000 elements, model 2 has an element size of 0.75 and a mesh size of 20,000. As you see the element size only decreased by 25% but the number of elements has doubled. So, if you chose 10 nodes for the condyle in model 1, you have to choose 20 for model 2 (because the number of elements in the mesh has doubled). So, you have to perform a rule of three based on the number of elements in your mesh, not the element size.

E.3 Python scripts

If you are going to be analysing a large number of analyses which are built in a similar way, python scripts are going to make your like much easier (for example, when performing the convergence tests). Abaqus will basically generate the script for us, we only have to modify it (Figure E.14). Follow these steps:

1. When you start building a model, set your working directory to wherever folder it is stored

2. Go to File>Macro Manager and click on "Create". Name your macro and choose "Work" under "Directory".

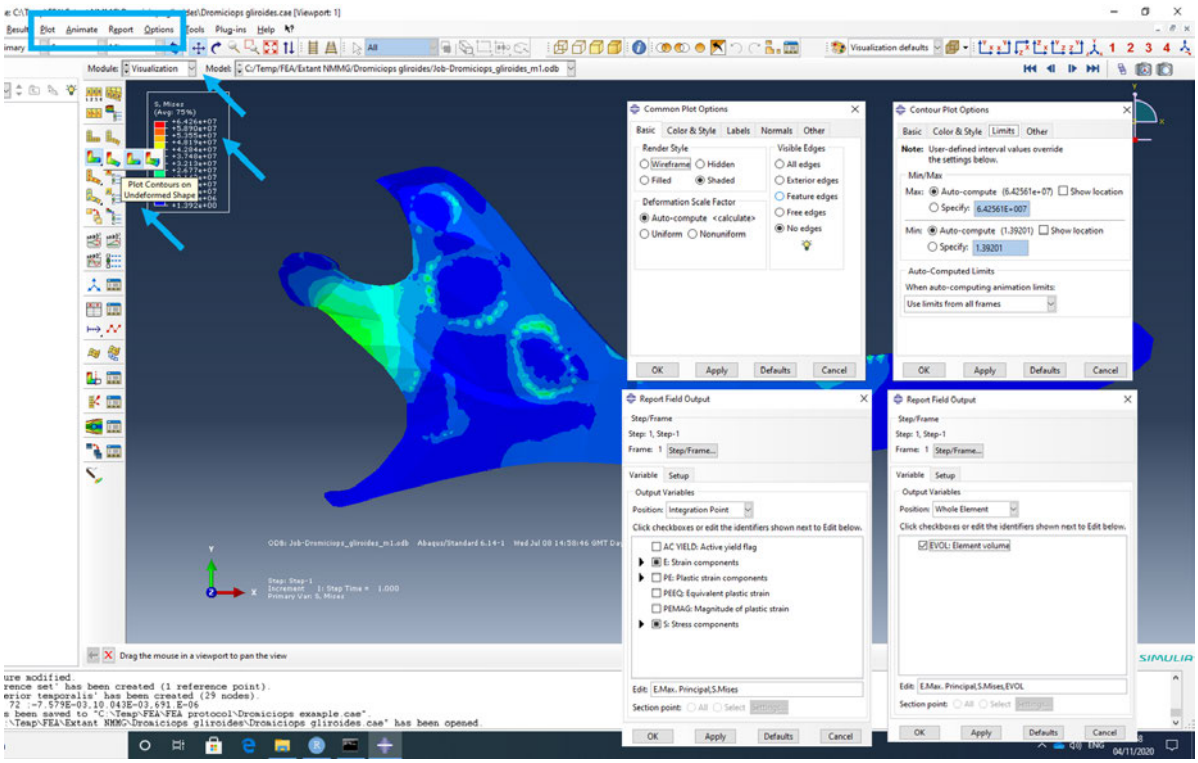

Figure E.13: How to visualise the results of FEA in Abaqus

3. Perform whatever repetitive action you would have to do across multiple models, for example, create a material and assign it to a section. Stop recording the macro when you are ready.

4. On your work directory, you will find a python script called abaqusMacros.py, that you can open on a text editor (just double-click it to open).

5. Delete the line that says "def name of your script():"

6. Delete any blank spaces before the start of a line (hit delete/backspace 4 times in all cases)

7. Save your file and copy across to the other folders where you have your other FE models/CAE files

8. Open another CAE file which, in this example, does not have assigned material properties. Set the working directory, and go to File>Run Script and open your script.

9. Automatically, whatever instructions were in your script have now been reproduced in this new model. In this case the material properties have been assigned to your jaw, without you manually needing to do it.

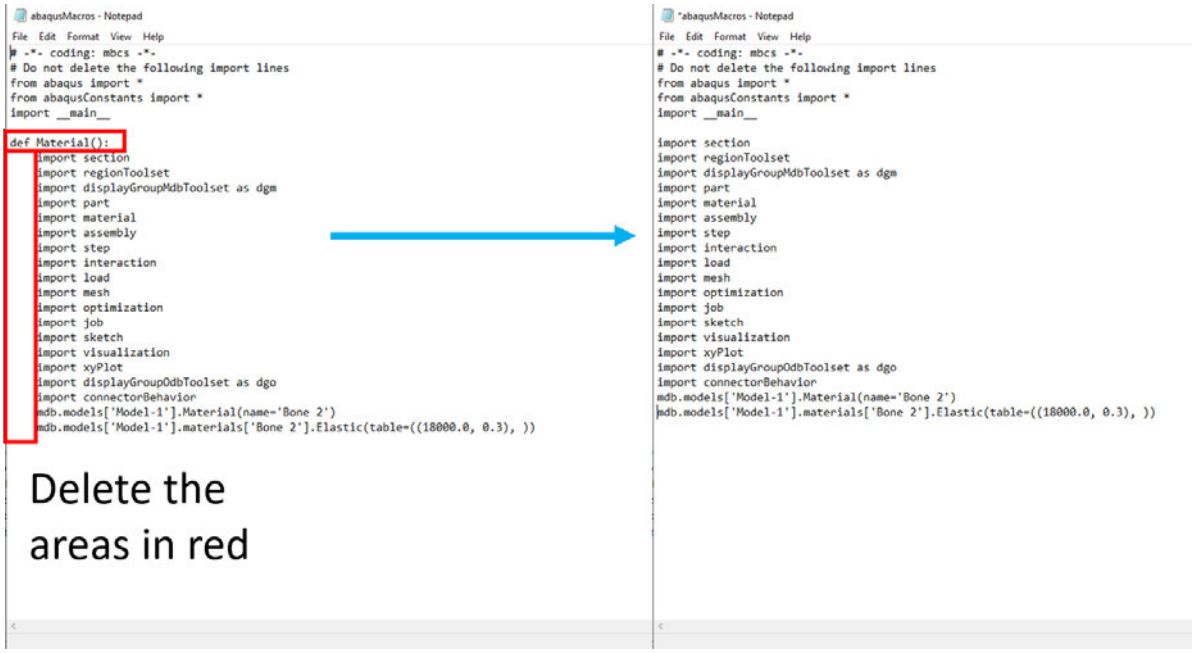

Figure E.14: How to edit python scripts for their use in Abaqus

10. I use python scripts for creating and assigning material properties, constraining, loading, generating new CSYSs, writing field output reports and saving the von Mises stress heatmaps. Some scripts do not need to be modified on a case by case basis and can be copied across multiple models (like creating and assigning material properties) but some others, like loading and constraining muscles and saving field output reports need to be "personalised". In the case of the field outputs, you need to modify the script to change the directory your file will be stored in. In the case of loading and constraining the muscles you need to check the "ID" of the corresponding CSYSs before running the script, you can get this ID with the Query Information tool in the toolbar and then update it accordingly in the script.

BIBLIOGRAPHY

[1] Adams, D. C. and Otárola-Castillo, E. (2013).
Geomorph: An r package for the collection and analysis of geometric morphometric shape data.
Methods in Ecology and Evolution, 4(4):393–399.

[2] Adams, N. F., Rayfield, E. J., Cox, P. G., Cobb, S. N., and Corfe, I. J. (2019).
Functional tests of the competitive exclusion hypothesis for multituberculate extinction.
Royal Society Open Science, 6:181536.

[3] Amador, L. I., Moyers Arévalo, R. L., Almeida, F. C., Catalano, S. A., and Giannini, N. P. (2018).
Bat Systematics in the Light of Unconstrained Analyses of a Comprehensive Molecular Supermatrix.
Journal of Mammalian Evolution, 25:37–70.

[4] Anantharaman, S., Wilson, G. P., Das Sarma, D., and Clemens, W. A. (2006).
A possible Late Cretaceous "Haramiyidan" from India.
Journal of Vertebrate Paleontology, 26(2):488–490.

[5] Anyonge, W. and Baker, A. (2006).
Craniofacial morphology and feeding behavior in *Canis dirus*, the extinct Pleistocene dire wolf.
Journal of Zoology, 269(3):309–316.

[6] Archer, M., Flannery, T. F., Ritchie, A., and Molnar, R. E. (1985).
First Mesozoic mammal from Australia - An early Cretaceous monotreme.
Nature, 318:363–366.

[7] Archibald, J. D. and Averianov, A. O. (2006).
Late Cretaceous asioryctitherian eutherian mammals from Uzbekistan and phylogenetic analysis of Asioryctitheria.
Acta Palaeontologica Polonica, 51(2):351–376.

[8] Archibald, J. D., Averianov, A. O., and Ekdale, E. G. (2001).
Late Cretaceous relatives of rabbits, rodents, and other extant eutherian mammals.
Nature, 414:62–65.

[9] Attard, M. R., Chamoli, U., Ferrara, T. L., Rogers, T. L., and Wroe, S. (2011).
Skull mechanics and implications for feeding behaviour in a large marsupial carnivore guild: The thylacine, Tasmanian devil and spotted-tailed quoll.
Journal of Zoology, 285(4):292–300.

[10] Averianov, A. O. (2002).
Early Cretaceous "symmetrodont" mammal *Gobiotheriodon* from Mongolia and the classification of "Symmetrodonta".
Acta Palaeontologica Polonica, 47(4):705–716.

[11] Averianov, A. O., Martin, T., and Lopatin, A. (2014).
The oldest dryolestid mammal from the Middle Jurassic of Siberia.
Journal of Vertebrate Paleontology, 34(4):924–931.

[12] Averianov, A. O., Martin, T., and Lopatin, A. V. (2013).
A new phylogeny for basal Trechnotheria and Cladotheria and affinities of South American endemic Late Cretaceous mammals.
Naturwissenschaften, 100(4):311–326.

[13] Bapst, D. W. (2012).
Paleotree: An R package for paleontological and phylogenetic analyses of evolution.
Methods in Ecology and Evolution, 3(5):803–807.

[14] Bell, F. (1998).
Principles of mechanics and biomechanics.
Stanley Thornes, United Kingdom.

[15] Ben-David, M. and Flaherty, E. A. (2012).
Stable isotopes in mammalian research: A beginner's guide.
Journal of Mammalogy, 93(2):312–328.

[16] Benevento, G. L., Benson, R. B., and Friedman, M. (2019).
Patterns of mammalian jaw ecomorphological disparity during the Mesozoic/Cenozoic transition.
Proceedings of the Royal Society B: Biological Sciences, 286:20190347.

[17] Bi, S., Zheng, X., Wang, X., Cignetti, N. E., Yang, S., and Wible, J. R. (2018).
An Early Cretaceous eutherian and the placental-marsupial dichotomy.
Nature, 558:390–395.

[18] Bishop, P. J., Hocknull, S. A., Clemente, C. J., Hutchinson, J. R., Barrett, R. S., and Lloyd, D. G. (2018a).

Cancellous bone and theropod dinosaur locomotion. Part II—a new approach to inferring posture and locomotor biomechanics in extinct tetrapod vertebrates.
PeerJ, 6:e5779.

[19] Bishop, P. J., Hocknull, S. A., Clemente, C. J., Hutchinson, J. R., Farke, A. A., Barrett, R. S., and Lloyd, D. G. (2018b).
Cancellous bone and theropod dinosaur locomotion. Part III—Inferring posture and locomotor biomechanics in extinct theropods, and its evolution on the line to birds.
PeerJ, 6:e5777.

[20] Bonaparte, J. (1986).
Sobre *Mesungulatum houusayi* y nuevos mamíferos Cretácicos de Patagonia, Argentina [On *Mesungulatum houssayi* and new Cretaceous mammals from Patagonia, Argentina].
Actas del IV Congreso Argentino de Paleontología y Biostratigrafía, 2:48–61.

[21] Bright, J. A. (2014).
A review of paleontological finite element models and their validity.
Journal of Paleontology, 88(4):760–769.

[22] Bright, J. A. and Rayfield, E. J. (2011a).
Sensitivity and ex vivo validation of finite element models of the domestic pig cranium.
Journal of Anatomy, 219(4):456–471.

[23] Bright, J. A. and Rayfield, E. J. (2011b).
The Response of Cranial Biomechanical Finite Element Models to Variations in Mesh Density.
Anatomical Record, 294(4):610–620.

[24] Brusatte, S. L., Benton, M. J., Ruta, M., and Lloyd, G. T. (2008).
Superiority, competition, and opportunism in the evolutionary radiation of dinosaurs.
Science, 321(5895):1485–1488.

[25] Butler, P. M., Sigogneau-Russell, D., and Ensom, P. C. (2012).
Possible persistence of the morganucodontans in the Lower Cretaceous Purbeck Limestone Group (Dorset, England).
Cretaceous Research, 33:135–145.

[26] Calandra, I. and Merceron, G. (2016).
Dental microwear texture analysis in mammalian ecology.
Mammal Review, 46(3):215–228.

[27] Casanovas-Vilar, I. and van Dam, J. (2013).
Conservatism and Adaptability during Squirrel Radiation: What Is Mandible Shape Telling Us?

PLoS ONE, 8(4):e61298.

[28] Cassini, G. H. and Vizcaíno, S. F. (2012).
An Approach to the Biomechanics of the Masticatory Apparatus of Early Miocene (Santacrucian Age) South American Ungulates (Astrapotheria, Litopterna, and Notoungulata): Moment Arm Estimation Based on 3D Landmarks.
Journal of Mammalian Evolution, 19:9–25.

[29] Chang, Y., Tambe, A. A., Maeda, Y., Wada, M., and Gonda, T. (2018).
Finite element analysis of dental implants with validation: to what extent can we expect the model to predict biological phenomena? A literature review and proposal for classification of a validation process.
International Journal of Implant Dentistry, 4:7.

[30] Chen, M., Strömberg, C. A., and Wilson, G. P. (2019).
Assembly of modern mammal community structure driven by Late Cretaceous dental evolution, rise of flowering plants, and dinosaur demise.
Proceedings of the National Academy of Sciences of the United States of America, 116(20):9931–9940.

[31] Chen, M. and Wilson, G. P. (2015).
A multivariate approach to infer locomotor modes in Mesozoic mammals.
Paleobiology, 41(2):280–312.

[32] Chimento, N., Agnolin, F., and Novas, F. (2012).
The Patagonian fossil mammal *Necrolestes*: a Neogene survivor of Dryolestoidea.
Revista del Museo Argentino de Ciencias Naturales, 14(2):261–306.

[33] Christiansen, P. and Wroe, S. (2007).
Bite forces and evolutionary adaptations to feeding ecology in carnivores.
Ecology, 88(2):347–358.

[34] Cifelli, R. L. (1999).
Tribosphenic mammal from the North American Early Cretaceous.
Nature, 401:363–366.

[35] Clemens, W. A., Goodwin, M. B., Hutchison, J. H., Schaff, C. R., Wood, C. B., and Colbert, M. W. (2007).
First record of a Jurassic mammal (?"Peramura") from Ethiopia.
Acta Palaeontologica Polonica, 52(3):433–439.

[36] Clemente, C. J., Dick, T. J., Glen, C. L., and Panagiotopoulou, O. (2020).
Biomechanical insights into the role of foot pads during locomotion in camelid species.

Scientific Reports, 10:3856.

[37] Clementz, M. T. (2012).
New insight from old bones: Stable isotope analysis of fossil mammals.
Journal of Mammalogy, 93(2):368–380.

[38] Close, R. A., Friedman, M., Lloyd, G. T., and Benson, R. B. (2015).
Evidence for a mid-Jurassic adaptive radiation in mammals.
Current Biology, 25(16):2137–2142.

[39] Cohen, J. E. (2018).
Earliest Divergence of Stagodontid (Mammalia: Marsupialiformes) Feeding Strategies from the Late Cretaceous (Turonian) of North America.
Journal of Mammalian Evolution, 25(2):165–177.

[40] Cox, P. G. (2017).
The jaw is a second-class lever in *Pedetes capensis* (Rodentia: Pedetidae).
PeerJ, 5:e3741.

[41] Cox, P. G., Rayfield, E. J., Fagan, M. J., Herrel, A., Pataky, T. C., and Jeffery, N. (2012).
Functional evolution of the feeding system in rodents.
PLoS ONE, 7(4):e36299.

[42] Cox, P. G., Rinderknecht, A., and Blanco, R. E. (2015).
Predicting bite force and cranial biomechanics in the largest fossil rodent using finite element analysis.
Journal of Anatomy, 226(3):215–223.

[43] Crompton, A. W., Lieberman, D. E., and Aboelela, S. (2006).
Tooth orientation during occlusion and the functional significance of condylar translation in primates and herbivores.
In Carrano, M., Gaudin, T., W., B. R., and R., W. J., editors, *Amniote Paleobiology: Perspectives on the Evolution of Mammals, Birds and Reptiles.*, chapter 11, pages 367–388. University of Chicago Press.

[44] Cuff, A. R., Bright, J. A., and Rayfield, E. J. (2015).
Validation experiments on finite element models of an ostrich (*Struthio camelus*) cranium.
PeerJ, 3:e1294.

[45] Datta, P. and Das, D. (1996).
Discovery of the oldest fossil mammal from India.
India Minerals, 50:217–222.

[46] Davis, B. M. (2012).
Micro-computed tomography reveals a diversity of Peramuran mammals from the Purbeck Group (Berriasian) of England.
Palaeontology, 55(4):789–817.

[47] Davis, B. M., Cifelli, R. L., and Kielan-Jaworowska, Z. (2008).
Earliest Evidence of Deltatheroida (Mammalia: Metatheria) from the Early Cretaceous of North America.
In *Mammalian Evolutionary Morphology*, pages 3–24. Springer Netherlands, Dordrecht.

[48] De Iuliis, G., Bargo, M., and Vizcaíno, S. (2001).
Variation in skull morphology and mastication in the fossil giant armadillos *Pampatherium spp.* and allied genera (Mammalia: Xenarthra: Pampatheriidae), with comments on their systematics and distribution.
Journal of Vertebrate Paleontology, 20(4):743–754.

[49] Debuysschere, M. (2017).
The Kuehneotheriidae (Mammaliaformes) from Saint-Nicolas-de-Port (Upper Triassic, France): a Systematic Review.
Journal of Mammalian Evolution, 24(2):127–146.

[50] Debuysschere, M., Gheerbrant, E., and Allain, R. (2015).
Earliest known European mammals: A review of the Morganucodonta from Saint-Nicolas-de-Port (Upper Triassic, France).
Journal of Systematic Palaeontology, 13(10):825–855.

[51] Degrange, F. J., Tambussi, C. P., Moreno, K., Witmer, L. M., and Wroe, S. (2010).
Mechanical Analysis of Feeding Behavior in the Extinct "Terror Bird" *Andalgalornis steulleti* (Gruiformes: Phorusrhacidae).
PLoS ONE, 5(8):e11856.

[52] Desai, Y. M., Eldho, T., and Shah, A. H. (2011).
Finite element method with applications in engineering.
Doring Kindersley, India.

[53] DeSantis, L. R. (2016).
Dental microwear textures: Reconstructing diets of fossil mammals.
Surface Topography: Metrology and Properties, 4:023002.

[54] Dickinson, A. S., Steer, J. W., and Worsley, P. R. (2017).
Finite element analysis of the amputated lower limb: A systematic review and recommendations.
Medical Engineering and Physics, 43:1–18.

[55] Dumont, E. R., Davis, J. L., Grosse, I. R., and Burrows, A. M. (2011).
Finite element analysis of performance in the skulls of marmosets and tamarins.
Journal of Anatomy, 218:151–162.

[56] Dumont, E. R., Piccirillo, J., and Grosse, I. R. (2005).
Finite-element analysis of biting behavior and bone stress in the facial skeletons of bats.
Anatomical Record - Part A Discoveries in Molecular, Cellular, and Evolutionary Biology, 283(2):319–330.

[57] Dumont, E. R., Samadevam, K., Grosse, I., Warsi, O. M., Baird, B., and Davalos, L. M. (2014).
Selection for mechanical advantage underlies multiple cranial optima in new world leaf-nosed bats.
Evolution, 68(5):1436–1449.

[58] Echarri, S., Ercoli, M. D., Amelia Chemisquy, M., Turazzini, G., and Prevosti, F. J. (2017).
Mandible morphology and diet of the South American extinct metatherian predators (Mammalia, Metatheria, Sparassodonta).
Earth and Environmental Science Transactions of the Royal Society of Edinburgh, 106(4):277–288.

[59] Emerson, S. B. and Radinsky, L. (1980).
Functional Analysis of Sabertooth Cranial Morphology.
Paleobiology, 6(3):295–312.

[60] Evans, A. R., Wilson, G. P., Fortelius, M., and Jernvall, J. (2007).
High-level similarity of dentitions in carnivorans and rodents.
Nature, 445:78–81.

[61] Falkingham, P. L., Bates, K. T., Margetts, L., and Manning, P. L. (2011).
Simulating sauropod manus-only trackway formation using finite-element analysis.
Biology Letters, 7:142–145.

[62] Falkingham, P. L., Margetts, L., Smith, I. M., and Manning, P. L. (2009).
Reinterpretation of palmate and semi-palmate (webbed) fossil tracks; insights from finite element modelling.
Palaeogeography, Palaeoclimatology, Palaeoecology, 271:69–76.

[63] Feilich, K. L. and López-Fernández, H. (2019).
When Does Form Reflect Function? Acknowledging and Supporting Ecomorphological Assumptions.
Integrative and Comparative Biology, 59(2):358–370.

[64] Figueirido, B., Macleod, N., Krieger, J., Renzi, M. D., Pérez-Claros, A., and Palmqvist, P. (2011).
Constraint and adaptation in the evolution of carnivoran skull shape.
Paleobiology, 37(3):490–518.

[65] Figueirido, B., Serrano-Alarcón, F. J., Slater, G. J., and Palmqvist, P. (2010).
Shape at the cross-roads: Homoplasy and history in the evolution of the carnivoran skull towards herbivory.
Journal of Evolutionary Biology, 23(12):2579–2594.

[66] Figueirido, B., Tseng, Z. J., Serrano-Alarcón, F. J., Martín-Serra, A., and Pastor, J. F. (2014).
Three-dimensional computer simulations of feeding behaviour in red and giant pandas relate skull biomechanics with dietary niche partitioning.
Biology Letters, 10:20140196.

[67] Fletcher, T. M., Janis, C. M., and Rayfield, E. J. (2010).
Finite element analysis of ungulate jaws: Can mode of digestive physiology be determined?
Palaeontologia Electronica, 13(3):1–15.

[68] Foffa, D., Cuff, A. R., Sassoon, J., Rayfield, E. J., Mavrogordato, M. N., and Benton, M. J. (2014).
Functional anatomy and feeding biomechanics of a giant Upper Jurassic pliosaur (Reptilia: Sauropterygia) from Weymouth Bay, Dorset, UK.
Journal of Anatomy, 225(2):209–219.

[69] Forasiepi, A. M. and Sánchez-Villagra, M. R. (2014).
Heterochrony, dental ontogenetic diversity, and the circumvention of constraints in marsupial mammals and extinct relatives.
Paleobiology, 40(2):222–237.

[70] Fortuny, J., Marcé-Nogué, J., De Esteban-Trivigno, S., Gil, L., and Galobart, A. (2011).
Temnospondyli bite club: Ecomorphological patterns of the most diverse group of early tetrapods.
Journal of Evolutionary Biology, 24(9):2040–2054.

[71] Fortuny, J., Marcé-Nogué, J., Gil, L., and Galobart, A. (2012).
Skull Mechanics and the Evolutionary Patterns of the Otic Notch Closure in Capitosaurs (Amphibia: Temnospondyli).
Anatomical Record, 295(7):1134–1146.

[72] Fox, R. C. (1969).
Studies of Late Cretaceous vertebrates. III. A triconodont mammal from Alberta.
Canadian Journal of Zoology, 47(6):1253–1256.

[73] Gaetano, L. C. and Rougier, G. W. (2011).
New materials of *Argentoconodon fariasorum* (Mammaliaformes, Triconodontidae) from the Jurassic of Argentina and its bearing on triconodont phylogeny.
J. Vertebr. Paleontol., 31(4):829–843.

[74] Gill, P. G. (2004).
Kuehneotherium from the Mesozoic fissure fillings of South Wales.
Phd thesis, University of Bristol.

[75] Gill, P. G., Purnell, M. A., Crumpton, N., Brown, K. R., Gostling, N. J., Stampanoni, M., and Rayfield, E. J. (2014).
Dietary specializations and diversity in feeding ecology of the earliest stem mammals.
Nature, 512:303–305.

[76] Godefroit, P. (1997).
Reptilian, therapsid and mammalian teeth from the Upper Triassic of Varangéville (northeastern France).
Bulletin de l'Institut Royal des Sciences Naturelles de Belqique, Sciences de la Terre, 67:83–102.

[77] Goussard, F., Germain, D., Delmer, C., and Moreno, K. (2010).
Finite element analysis: A promising tool for the reconstruction of extinct vertebrate graviportal taxa. A preliminary study based on the metacarpal arrangement of Elephas maximus.
Comptes Rendus - Palevol, 9:455–461.

[78] Grossnickle, D. M. (2017).
The evolutionary origin of jaw yaw in mammals.
Scientific Reports, 7:45094.

[79] Grossnickle, D. M. (2020).
Feeding ecology has a stronger evolutionary influence on functional morphology than on body mass in mammals.
Evolution, 74(3):610–628.

[80] Grossnickle, D. M. and David Polly, P. (2013).
Mammal disparity decreases during the Cretaceous angiosperm radiation.
Proceedings of the Royal Society B: Biological Sciences, 280:20132110.

[81] Grossnickle, D. M., Smith, S. M., and Wilson, G. P. (2019).
Untangling the Multiple Ecological Radiations of Early Mammals.
Trends in Ecology and Evolution, 34(10):936–949.

[82] Grubich, J. R., Huskey, S., Crofts, S., Orti, G., and Porto, J. (2012).
Mega-Bites: Extreme jaw forces of living and extinct piranhas (Serrasalmidae).

Scientific Reports, 2:1009.

[83] Haddoumi, H., Allain, R., Meslouh, S., Metais, G., Monbaron, M., Pons, D., Rage, J. C., Vullo, R., Zouhri, S., and Gheerbrant, E. (2016).
Guelb el Ahmar (Bathonian, Anoual Syncline, eastern Morocco): First continental flora and fauna including mammals from the Middle Jurassic of Africa.
Gondwana Research, 29:290–319.

[84] Hammer, Ø., Harper, D. A. T., and Ryan, P. D. (2001).
PAST: Paleontological statistics software package for education and data analysis.
Palaeontologia Electronica, 4(1):1–9.

[85] Hampton, P. M. (2011).
Comparison of cranial form and function in association with diet in natricine snakes.
Journal of Morphology, 272(12):1435–1443.

[86] Hastie, T., Tibshirani, R., Leisch, F., Hornik, K., and Ripley, B. (2017).
mda: Mixture and Flexible Discriminant Analysis.

[87] Hiiemae, K. and Houston, W. J. B. (1971).
The structure and function of the jaw muscles in the rat (*Rattus norvegicus* L.).
Zoological Journal of the Linnean Society, 50(1):75–99.

[88] Hu, Y., Meng, J., Wang, Y., and Li, C. (2005).
Large Mesozoic mammals fed on young dinosaurs.
Nature, 433:149–152.

[89] Huiskes, R. and Chao, E. Y. (1983).
A survey of finite element analysis in orthopedic biomechanics: The first decade.
Journal of Biomechanics, 16(6):385–409.

[90] Hutchins, M., Kleiman, D. G., Geist, V., and McDade, M. C., editors (2004).
Grzimek's Animal Life Encyclopedia, Volume 13: Mammals II.
Gale Group, Farmingtom Hills, MI, 2nd edition.

[91] Huttenlocker, A. K., Grossnickle, D. M., Kirkland, J. I., Schultz, J. A., and Luo, Z. X. (2018).
Late-surviving stem mammal links the lowermost Cretaceous of North America and Gondwana.
Nature, 558:108–123.

[92] Janis, C. (2008).
An Evolutionary History of Browsing and Grazing Ungulates.
In Gordon, I. and Prins, H., editors, *The Ecology of Browsing and Grazing. Ecological Studies 195*, pages 21–45. Springer.

[93] Janis, C. M. (1995).
Correlations Between Craniodental Morphology and Feeding Behavior in Ungulates: Reciprocal Illumination Between Living and Fossil Taxa.
In Thomason, J., editor, *Functional Morphology in Vertebrate Paleontology*, pages 76–98. Cambridge University Press.

[94] Ji, Q., Luo, Z. X., Yuan, C. X., and Tabrum, A. R. (2006).
A Swimming Mammaliaform from the Middle Jurassic and Ecomorphological Diversification of Early Mammals.
Science, 311(5764):1123–1127.

[95] Joyce, W. G. and Bandyopadhyay, S. (2020).
A reevaluation of the basal turtle *Indochelys spatulata* from the Early-Middle Jurassic (Toarcian-Aalenian) of India, with descriptions of new material.
PeerJ, 8:e8542.

[96] Kemp, T. (2005).
The Origin and Evolution of Mammals.
Oxford University Press.

[97] Kielan-Jaworowska, Z. (2013).
In Pursuit of Early Mammals.
Indiana University Press.

[98] Kielan-Jaworowska, Z., Cifelli, R. L., and Luo, Z.-X. (2004).
Mammals from the Age of Dinosaurs.
Columbia University Press.

[99] King, B. and Beck, R. M. (2020).
Tip dating supports novel resolutions of controversial relationships among early mammals.
Proceedings of the Royal Society B: Biological Sciences, 287:20200943.

[100] Koutromanos, I. (2018).
Fundamentals of Finite Element Analysis: Linear Finite Element Analysis.
John Wiley & Sons.

[101] Koyabu, D. B. and Endo, H. (2010).
Craniodental mechanics and diet in Asian colobines: Morphological evidence of mature seed predation and sclerocarpy.
American Journal of Physical Anthropology, 142:137–148.

[102] Koyabu, D. B., Oshida, T., Dang, N. X., Can, D. N., Kimura, J., Sasaki, M., Motokawa, M., Son, N. T., Hayashida, A., Shintaku, Y., and Endo, H. (2009).

Craniodental mechanics and the feeding ecology of two sympatric callosciurine squirrels in Vietnam.
Journal of Zoology, 279(4):372–380.

[103] Krause, D. W. (1982).
Jaw movement, dental function, and diet in the Paleocene multituberculate *Ptilodus*.
Paleobiology, 8(3):265–281.

[104] Krause, D. W., Hoffmann, S., and Werning, S. (2017).
First postcranial remains of Multituberculata (Allotheria, Mammalia) from Gondwana.
Cretaceous Research, 80:91–100.

[105] Kupczik, K., Dobson, C. A., Fagan, M. J., Crompton, R. H., Oxnard, C. E., and O'Higgins, P. (2007).
Assessing mechanical function of the zygomatic region in macaques: Validation and sensitivity testing of finite element models.
Journal of Anatomy, 210:41–53.

[106] Kusuhashi, N., Tsutsumi, Y., Saegusa, H., Horie, K., Ikeda, T., Yokoyama, K., and Shiraishi, K. (2013).
A new Early Cretaceous eutherian mammal from the Sasayama Group, Hyogo, Japan.
Proceedings of the Royal Society B: Biological Sciences, 280:20130142.

[107] Kusuhashi, N., Wang, Y. Q., Li, C. K., and Jin, X. (2016).
Two new species of *Gobiconodon* (Mammalia, Eutriconodonta, Gobiconodontidae) from the Lower Cretaceous Shahai and Fuxin formations, northeastern China.
Historical Biology, 28(1-2):14–26.

[108] Lautenschlager, S. (2016).
Reconstructing the past: Methods and techniques for the digital restoration of fossils.
Royal Society Open Science, 3:160342.

[109] Lautenschlager, S., Gill, P., Luo, Z. X., Fagan, M. J., and Rayfield, E. J. (2017).
Morphological evolution of the mammalian jaw adductor complex.
Biological Reviews, 92(4):1910–1940.

[110] Lautenschlager, S., Gill, P. G., Luo, Z. X., Fagan, M. J., and Rayfield, E. J. (2018).
The role of miniaturization in the evolution of the mammalian jaw and middle ear.
Nature, 561:533–537.

[111] Lisiak-Myszke, M., Marciniak, D., Bieliński, M., Sobczak, H., Garbacewicz, L., and Drogoszewska, B. (2020).
Application of finite element analysis in oral and maxillofacial surgery-A literature review.

Materials, 13:3063.

[112] Lucas, S. G. and Luo, Z. (1993).
Adelobasileus from the Upper Triassic of West Texas: the oldest mammal.
Journal of Vertebrate Paleontology, 13(3):309–334.

[113] Luo, Z. X. (2007).
Transformation and diversification in early mammal evolution.
Nature, 450:1011–1019.

[114] Luo, Z.-X. (2011).
Developmental Patterns in Mesozoic Evolution of Mammal Ears.
Annual Review of Ecology, Evolution, and Systematics, 42:355–380.

[115] Luo, Z. X., Cifelli, R. L., and Kielan-Jaworowska, Z. (2001).
Dual origin of tribosphenic mammals.
Nature, 409:53–57.

[116] Luo, Z.-X., Crompton, A. W., and Lucas, S. G. (1995).
Evolutionary Origins of the Mammalian Promontorium and Cochlea.
Journal of Vertebrate Paleontology, 15(1):113–121.

[117] Luo, Z. X., Gatesy, S. M., Jenkins, F. A., Amaral, W. W., and Shubin, N. H. (2015a).
Mandibular and dental characteristics of Late Triassic mammaliaform *Haramiyavia* and their ramifications for basal mammal evolution.
Proceedings of the National Academy of Sciences of the United States of America, 112(51):E7101–E7109.

[118] Luo, Z. X., Ji, Q., Wible, J. R., and Yuan, C. X. (2003).
An Early Cretaceous Tribosphenic Mammal and Metatherian Evolution.
Science, 302(5652):1934–1940.

[119] Luo, Z. X., Ji, Q., and Yuan, C. X. (2007).
Convergent dental adaptations in pseudo-tribosphenic and tribosphenic mammals.
Nature, 450:93–97.

[120] Luo, Z. X., Kielan-Jaworowska, Z., and Cifelli, R. L. (2002).
In quest for a phylogeny of Mesozoic mammals.
Acta Palaeontologica Polonica, 47(1):1–78.

[121] Luo, Z.-X., Kielan-Jaworowska, Z., and Cifelli, R. L. (2004).
Evolution of dental replacement in mammals.
Bulletin of the Carnegie Museum of Natural History, 36:159–175.

[122] Luo, Z. X., Meng, Q. J., Grossnickle, D. M., Liu, D., Neander, A. I., Zhang, Y. G., and Ji, Q. (2017).
New evidence for mammaliaform ear evolution and feeding adaptation in a Jurassic ecosystem.
Nature, 548:326–329.

[123] Luo, Z. X., Meng, Q. J., Ji, Q., Liu, D., Zhang, Y. G., and Neander, A. I. (2015b).
Evolutionary development in basal mammaliaforms as revealed by a docodontan.
Science, 347(6223):760–764.

[124] Luo, Z. X. and Wible, J. R. (2005).
A late Jurassic digging mammal and early mammalian diversification.
Science, 308(5718):103–107.

[125] Luo, Z. X., Yuan, C. X., Meng, Q. J., and Ji, Q. (2011).
A Jurassic eutherian mammal and divergence of marsupials and placentals.
Nature, 476:442–445.

[126] Macho, G. A., Shimizu, D., Jiang, Y., and Spears, I. R. (2005).
Australopithecus anamensis: A finite-element approach to studying the functional adaptations of extinct hominins.
Anatomical Record - Part A Discoveries in Molecular, Cellular, and Evolutionary Biology, 283(2):310–318.

[127] Maiorino, L., Farke, A. A., Kotsakis, T., Teresi, L., and Piras, P. (2015).
Variation in the shape and mechanical performance of the lower jaws in ceratopsid dinosaurs (Ornithischia, Ceratopsia).
Journal of Anatomy, 227(5):631–646.

[128] Manning, P. L., Margetts, L., Johnson, M. R., Withers, P. J., Sellers, W. I., Falkingham, P. L., Mummery, P. M., Barrett, P. M., and Raymont, D. R. (2009).
Biomechanics of dromaeosaurid dinosaur claws: Application of X-ray microtomography, nanoindentation, and finite element analysis.
Anatomical Record, 292(9):1397–1405.

[129] Mao, F., Hu, Y., Li, C., Wang, Y., Chase, M. H., Smith, A. K., and Meng, J. (2020).
Integrated hearing and chewing modules decoupled in a Cretaceous stem therian mammal.
Science, 367(6475):305–308.

[130] Marcé-Nogué, J., de Esteban-Trivigno, S., Escrig, C., and Gil, L. (2016).
Accounting for differences in element size and homogeneity when comparing finite element models: Armadillos as a case study.
Palaeontologia Electronica, 19(2):1–22.

[131] Marcé-Nogué, J., De Esteban-Trivigno, S., Püschel, T. A., and Fortuny, J. (2017a).
The intervals method: A new approach to analyse finite element outputs using multivariate statistics.
PeerJ, 5:e3793.

[132] Marcé-Nogué, J., DeMiguel, D., Fortuny, J., de Esteban-Trivigno, S., and Gil, L. (2013).
Quasi-homothetic transformation for comparing the mechanical performance of planar models in biological research.
Palaeontologia Electronica, 16(3):1–15.

[133] Marcé-Nogué, J., Fortuny, J., Gil, L., and Sanchez, M. (2015).
Improving mesh generation in finite element analysis for functional morphology approaches.
Spanish Journal of Paleontology, 30(1):117–132.

[134] Marcé-Nogué, J., Püschel, T. A., and Kaiser, T. M. (2017b).
A biomechanical approach to understand the ecomorphological relationship between primate mandibles and diet.
Scientific Reports, 7:8364.

[135] Margetts, L., Leng, J. M., Smith, I. M., and Manning, P. L. (2006).
Parallel three dimensional finite element analysis of dinosaur trackway formation.
Proceedings of the 6th European Conference on Numerical Methods in Geotechnical Engineering - Numerical Methods in Geotechnical Engineering, pages 743–749.

[136] Marinescu, R., Daegling, D. J., and Rapoff, A. J. (2005).
Finite-element modeling of the anthropoid mandible: The effects of altered boundary conditions.
Anatomical Record - Part A Discoveries in Molecular, Cellular, and Evolutionary Biology, 283(2):300–309.

[137] May-Collado, L. J., Kilpatrick, C. W., and Agnarsson, I. (2015).
Mammals from 'down under': A multi-gene species-level phylogeny of marsupial mammals (Mammalia, Metatheria).
PeerJ, 3:e805.

[138] McLester, J. and St Pierre, P. (2008).
Applied biomechanics: Concepts and connections.
Thomson Wadsworth, Canada.

[139] McMenamin, M. A. (2018).
Deep Time Analysis.
Springer.

[140] Meloro, C. (2011).
Feeding habits of Plio-Pleistocene large carnivores as revealed by the mandibular geometry.
Journal of Vertebrate Paleontology, 31(2):428–446.

[141] Meloro, C., Raia, P., Piras, P., Barbera, C., and O'Higgins, P. (2008).
The shape of the mandibular corpus in large fissiped carnivores: Allometry, function and phylogeny.
Zoological Journal of the Linnean Society, 154(4):832–845.

[142] Meng, J. (2014).
Mesozoic mammals of China: Implications for phylogeny and early evolution of mammals.
National Science Review, 1(4):521–542.

[143] Meng, J., Bi, S., Wang, Y., Zheng, X., and Wang, X. (2014).
Dental and mandibular morphologies of *Arboroharamiya* (Haramiyida, Mammalia): A comparison with other haramiyidans and *Megaconus* and implications for mammalian evolution.
PLoS ONE, 9(12):e113847.

[144] Meng, J., Hu, Y., Wang, Y., Wang, X., and Li, C. (2006).
A Mesozoic gliding mammal from northeastern China.
Nature, 444:889–893.

[145] Meng, Q. J., Grossnickle, D. M., Liu, D., Zhang, Y. G., Neander, A. I., Ji, Q., and Luo, Z. X. (2017).
New gliding mammaliaforms from the Jurassic.
Nature, 548:291–296.

[146] Meng, Q. J., Ji, Q., Zhang, Y. G., Liu, D., Grossnickle, D. M., and Luo, Z. X. (2015).
An arboreal docodont from the jurassic and mammaliaform ecological diversification.
Science, 347(6223):764–768.

[147] Merceron, G., Escarguel, G., Angibault, J. M., and Verheyden-Tixier, H. (2010).
Can dental microwear textures record inter-individual dietary variations?
PLoS ONE, 5(3):e9542.

[148] Metzger, K. A., Daniel, W. J., and Ross, C. F. (2005).
Comparison of beam theory and finite-element analysis with in vivo bone strain data from the alligator cranium.
Anatomical Record - Part A Discoveries in Molecular, Cellular, and Evolutionary Biology, 283(2):331–348.

[149] Minas (Web developer) (2020).
MapChart (www.mapchart.net).

[150] Morales-García, N. M., Burgess, T. D., Hill, J. J., Gill, P. G., and Rayfield, E. J. (2019).
The use of extruded finite-element models as a novel alternative to tomography-based models: A case study using early mammal jaws.
Journal of the Royal Society Interface, 16:20190674.

[151] Morales-García, N. M., Gill, P. G., Janis, C. M., and Rayfield, E. J. (In Review).
Jaw shape and mechanical advantage are indicative of diet in Mesozoic mammals.
Nature Communications Biology.

[152] Motani, R. and Schmitz, L. (2011).
Phylogenetic versus functional signals in the evolution of form-function relationships in terrestrial vision.
Evolution, 65(8):2245–2257.

[153] Myers, P., Espinosa, R., Parr, C. S., Jones, T., Hammond, G. S., and Dewey, T. A. (2020).
The Animal Diversity Web.

[154] Navalón, G., Bright, J. A., Marugán-Lobón, J., and Rayfield, E. J. (2019).
The evolutionary relationship among beak shape, mechanical advantage, and feeding ecology in modern birds.
Evolution, 73(3):422–435.

[155] Neenan, J. M., Ruta, M., Clack, J. A., and Rayfield, E. J. (2014).
Feeding biomechanics in *Acanthostega* and across the fish-tetrapod transition.
Proceedings of the Royal Society B: Biological Sciences, 281:20132689.

[156] Nowak, R. (2018).
Walker's Mammals of the World. Monotremes, Marsupials, Afrotherians, Xenarthrans, and Sundatherians.
Johns Hopkins University Press, Baltimore.

[157] Nyakatura, K. and Bininda-Emonds, O. R. (2012).
Updating the evolutionary history of Carnivora (Mammalia): a new species-level supertree complete with divergence time estimates.
BMC Biology, 10:12.

[158] Oldfield, C. C., Mchenry, C. R., Clausen, P. D., Chamoli, U., Parr, W. C., Stynder, D. D., and Wroe, S. (2012).
Finite element analysis of ursid cranial mechanics and the prediction of feeding behaviour in the extinct giant *Agriotherium africanum*.
Journal of Zoology, 286(2):171–171.

[159] O'Meara, R. N. and Thompson, R. S. (2014).
Were There Miocene Meridiolestidans? Assessing the Phylogenetic Placement of *Necrolestes patagonensis* and the Presence of a 40 Million Year Meridiolestidan Ghost Lineage.
Journal of Mammalian Evolution, 21(3):271–284.

[160] Panagiotopoulou, O. (2009).
Finite element analysis (FEA): Applying an engineering method to functional morphology in anthropology and human biology.
Annals of Human Biology, 36(5):609–623.

[161] Panagiotopoulou, O., Iriarte-Diaz, J., Wilshin, S., Dechow, P. C., Taylor, A. B., Mehari Abraha, H., Aljunid, S. F., and Ross, C. F. (2017).
In vivo bone strain and finite element modeling of a rhesus macaque mandible during mastication.
Zoology, 124:13–29.

[162] Panagiotopoulou, O., Pataky, T. C., and Hutchinson, J. R. (2019).
Foot pressure distribution in White Rhinoceroses (*Ceratotherium simum*) during walking.
PeerJ, 7:e6881.

[163] Paradis, E. and Schliep, K. (2019).
Ape 5.0: An environment for modern phylogenetics and evolutionary analyses in R.
Bioinformatics, 35(3):526–528.

[164] Parmar, V., Prasad, G. V., and Kumar, D. (2013).
The first multituberculate mammal from India.
Naturwissenschaften, 100(6):515–523.

[165] Pascual, R., Goin, F. J., Balarino, L., and Sauthier, D. E. U. (2002).
New data on the Paleocene monotreme *Monotrematum sudamericanum*, and the convergent evolution of triangulate molars.
Acta Palaeontologica Polonica, 47(3):487–492.

[166] Pennell, M. W., Eastman, J. M., Slater, G. J., Brown, J. W., Uyeda, J. C., Fitzjohn, R. G., Alfaro, M. E., and Harmon, L. J. (2014).
Geiger v2.0: An expanded suite of methods for fitting macroevolutionary models to phylogenetic trees.
Bioinformatics, 30(15):2216–2218.

[167] Pfretzschner, H. U., Martin, T., Maisch, M. W., Matzke, A. T., and Sun, G. (2005).
A new docodont mammal from the Late Jurrasic of the Junggar Basin in Northwest China.
Acta Palaeontologica Polonica, 50(4):799–808.

[168] Pian, R., Archer, M., Hand, S. J., Beck, R. M., and Cody, A. (2016).
The upper dentition and relationships of the enigmatic Australian Cretaceous mammal *Kollikodon ritchiei*.
Memoirs of Museum Victoria, 74:97–105.

[169] Pierce, S. E., Angielczyk, K. D., and Rayfield, E. J. (2008).
Patterns of morphospace occupation and mechanical performance in extant crocodilian skulls: A combined geometric morphometric and finite element modeling approach.
Journal of Morphology, 269(7):840–864.

[170] Pineda-Munoz, S., Lazagabaster, I. A., Alroy, J., and Evans, A. R. (2017).
Inferring diet from dental morphology in terrestrial mammals.
Methods in Ecology and Evolution, 8(4):481–491.

[171] Porro, L. B., Metzger, K. A., Iriarte-Diaz, J., and Ross, C. F. (2013).
In vivo bone strain and finite element modeling of the mandible of *Alligator mississippiensis*.
Journal of Anatomy, 223(3):195–227.

[172] Poux, C., Madsen, O., Glos, J., De Jong, W. W., and Vences, M. (2008).
Molecular phylogeny and divergence times of Malagasy tenrecs: Influence of data partitioning and taxon sampling on dating analyses.
BMC Evolutionary Biology, 8:102.

[173] Prasad, G. V. and Manhas, B. K. (2002).
Triconodont mammals from the Jurassic Kota Formation of India.
Geodiversitas, 24(2):445–464.

[174] Prasad, G. V. and Manhas, B. K. (2007).
A new docodont mammal from the Jurassic Kota formation of India.
Palaeontologia Electronica, 10(2):1–11.

[175] Prevosti, F. J., Turazzini, G. F., Ercoli, M. D., and Hingst-Zaher, E. (2012).
Mandible shape in marsupial and placental carnivorous mammals: A morphological comparative study using geometric morphometrics.
Zoological Journal of the Linnean Society, 164(4):836–855.

[176] Price, S. A., Hopkins, S. S., Smith, K. K., and Roth, V. L. (2012).
Tempo of trophic evolution and its impact on mammalian diversification.
Proceedings of the National Academy of Sciences of the United States of America, 109(18):7008–7012.

[177] Purnell, M. A., Crumpton, N., Gill, P. G., Jones, G., and Rayfield, E. J. (2013).

Within-guild dietary discrimination from 3-D textural analysis of tooth microwear in insectivorous mammals.
Journal of Zoology, 291(4):249–257.

[178] Püschel, T. A., Marcé-Nogué, J., Gladman, J., Patel, B. A., Almécija, S., and Sellers, W. I. (2020).
Getting Its Feet on the Ground: Elucidating *Paralouatta*'s Semi-Terrestriality Using the Virtual Morpho-Functional Toolbox.
Frontiers in Earth Science, 8(79):1–15.

[179] Rahman, I. A. and Lautenschlager, S. (2016).
Applications of the three-dimensional box modelling to paleontological functional analysis.
The Paleontological Society Papers, 22:119–132.

[180] Rayfield, E. J. (2004).
Cranial mechanics and feeding in *Tyrannosaurus rex*.
Proceedings of the Royal Society B: Biological Sciences, 271:1451–1459.

[181] Rayfield, E. J. (2005a).
Aspects of comparative cranial mechanics in the theropod dinosaurs *Coelophysis*, *Allosaurus* and *Tyrannosaurus*.
Zoological Journal of the Linnean Society, 144(3):309–316.

[182] Rayfield, E. J. (2005b).
Using finite-element analysis to investigate suture morphology: A case study using large carnivorous dinosaurs.
Anatomical Record - Part A Discoveries in Molecular, Cellular, and Evolutionary Biology, 283(2):349–365.

[183] Rayfield, E. J. (2007).
Finite Element Analysis and Understanding the Biomechanics and Evolution of Living and Fossil Organisms.
Annual Review of Earth and Planetary Sciences, 35:541–576.

[184] Rayfield, E. J., Norman, D. B., Horner, C. C., Horner, J. R., Smith, P. M., Thomason, J. J., and Upchurch, P. (2001).
Cranial design and function in a large theropod dinosaur.
Nature, 409:1033–1037.

[185] Revell, L. J. (2012).
phytools: An R package for phylogenetic comparative biology (and other things).
Methods in Ecology and Evolution, 3(2):217–223.

[186] Rich, T. H., Hopson, J. A., Gill, P. G., Trusler, P., Rogers-Davidson, S., Morton, S., Cifelli, R. L., Pickering, D., Kool, L., Siu, K., Burgmann, F. A., Senden, T., Evans, A. R., Wagstaff, B. E., Seegets-Villiers, D., Corfe, I. J., Flannery, T. F., Walker, K., Musser, A. M., Archer, M., Pian, R., and Vickers-Rich, P. (2016).
The mandible and dentition of the Early Cretaceous monotreme *Teinolophos trusleri*.
Alcheringa, 40(4):475–501.

[187] Rich, T. H. and Vickers-Rich, P. (2004).
Diversity of early cretaceous mammals from Victoria, Australia.
Bulletin of the American Museum of Natural History, 285:36–53.

[188] Rich, T. H., Vickers-Rich, P., Flannery, T. F., Kear, B. P., Cantrill, D. J., Komarower, P., Kool, L., Pickering, D., Trusler, P., Morton, S., Van Klaveren, N., and Fitzgerald, E. M. (2009).
An Australian multituberculate and its palaeobiogeographic implications.
Acta Palaeontologica Polonica, 54(1):1–6.

[189] Ripley, B. and Venables, W. (2002).
Modern Applied Statistics with S.
Springer New York, New York, 4th edition.

[190] Roberts, T. E., Lanier, H. C., Sargis, E. J., and Olson, L. E. (2011).
Molecular phylogeny of treeshrews (Mammalia: Scandentia) and the timescale of diversification in Southeast Asia.
Molecular Phylogenetics and Evolution, 60(3):358–372.

[191] Rohlf, F. J. (2015).
The tps series of software.
Hystrix, 26(1):9–12.

[192] Ross, C. F., Berthaume, M. A., Dechow, P. C., Iriarte-Diaz, J., Porro, L. B., Richmond, B. G., Spencer, M., and Strait, D. (2011).
In vivo bone strain and finite-element modeling of the craniofacial haft in catarrhine primates.
Journal of Anatomy, 218:112–141.

[193] Ross, C. F., Patel, B. A., Slice, D. E., Strait, D. S., Dechow, P. C., Richmond, B. G., and Spencer, M. A. (2005).
Modeling masticatory muscle force in finite element analysis: Sensitivity analysis using principal coordinates analysis.
Anatomical Record - Part A Discoveries in Molecular, Cellular, and Evolutionary Biology, 283(2):288–299.

[194] Rougier, G. W. (1993).

Vincelestes neuquenianus Bonaparte (Mammalia, Theria) un Primitivo Mamífero del Cretacico Inferior de la Cuenca Neuquina.
Phd thesis, Universidad de Buenos Aires.

[195] Rougier, G. W., Davis, B. M., and Novacek, M. J. (2015).
A deltatheroidan mammal from the Upper Cretaceous Baynshiree Formation, eastern Mongolia.
Cretaceous Research, 52:167–177.

[196] Rougier, G. W., Garrido, A., Gaetano, L., Puerta, P. F., Corbitt, C., and Novacek, M. J. (2007a).
First Jurassic triconodont from South America.
American Museum Novitates, 3580:1–17.

[197] Rougier, G. W., Martinelli, A. G., Forasiepi, A. M., and Novacek, M. J. (2007b).
New Jurassic Mammals from Patagonia, Argentina: A Reappraisal of Australosphenidan Morphology and Interrelationships.
American Museum Novitates, 3566:1–54.

[198] Rupin, F., Saied, A., Dalmas, D., Peyrin, F., Haupert, S., Barthel, E., Boivin, G., and Laugier, P. (2008).
Experimental determination of Young modulus and Poisson ratio in cortical bone tissue using high resolution scanning acoustic microscopy and nanoindentation.
The Journal of the Acoustical Society of America, 123(5):3785–3785.

[199] Sacco, T. and Van Valkenburgh, B. (2004).
Ecomorphological indicators of feeding behaviour in the bears (Carnivora: Ursidae).
Journal of Zoology, 263:41–54.

[200] Samuels, J. X. (2009).
Cranial morphology and dietary habits of rodents.
Zoological Journal of the Linnean Society, 156(4):864–888.

[201] Santana, S. E. (2016).
Quantifying the effect of gape and morphology on bite force: Biomechanical modelling and in vivo measurements in bats.
Functional Ecology, 30(4):557–565.

[202] Santana, S. E., Grosse, I. R., and Dumont, E. R. (2012).
Dietary hardness, loading behavior, and the evolution of skull form in bats.
Evolution, 66(8):2587–2598.

[203] Santana, S. E., Strait, S., and Dumont, E. R. (2011).
The better to eat you with: Functional correlates of tooth structure in bats.
Functional Ecology, 25(4):839–847.

[204] Sarkar, D. (2008).
Lattice: Multivariate Data Visualization with R.
Springer New York, New York.

[205] Schneider, C. A., Rasband, W. S., and Eliceiri, K. W. (2012).
NIH Image to ImageJ: 25 years of image analysis.
Nature Methods, 9(7):671–675.

[206] Schultz, J. A., Bhullar, B. A. S., and Luo, Z. X. (2019).
Re-examination of the Jurassic Mammaliaform *Docodon victor* by Computed Tomography and Occlusal Functional Analysis.
Journal of Mammalian Evolution, 26:9–38.

[207] Schultz, J. A. and Martin, T. (2011).
Wear pattern and functional morphology of dryolestoid molars (Mammalia, Cladotheria).
Palaontologische Zeitschrift, 85(3):269–285.

[208] Seiffert, E. R. (2007).
A new estimate of afrotherian phylogeny based on simultaneous analysis of genomic, morphological, and fossil evidence.
BMC Evolutionary Biology, 7:224.

[209] Serrano-Fochs, S., De Esteban-Trivigno, S., Marcé-Nogué, J., Fortuny, J., and Fariña, R. A. (2015).
Finite element analysis of the Cingulata jaw: An ecomorphological approach to armadillo's diets.
PLoS ONE, 10(4):e0120653.

[210] Sigogneau-Russell, D. (2003).
Holotherian mammals from the Forest Marble (Middle Jurassic of England).
Geodiversitas, 25(3):501–537.

[211] Simpson, G. G. (1925).
Mesozoic Mammalia, II; Tinodon and its allies.
American Journal of Science, 59:451–470.

[212] Slater, G. J., Figueirido, B., Louis, L., Yang, P., and van Valkenburgh, B. (2010).
Biomechanical consequences of rapid evolution in the polar bear lineage.
PLoS ONE, 5(11):e13870.

[213] Smit, H. A., Jansen van Vuuren, B., O'Brien, P. C., Ferguson-Smith, M., Yang, F., and Robinson, T. J. (2011).
Phylogenetic relationships of elephant-shrews (Afrotheria, Macroscelididae).
Journal of Zoology, 284(2):133–143.

[214] Snively, E. and Russell, A. (2002).
The Tyrannosaurid metatarsus: Bone strain and inferred ligament function.
Senckenbergiana lethaea, 82(1):35–42.

[215] Song, S., Liu, L., Edwards, S. V., and Wu, S. (2012).
Resolving conflict in eutherian mammal phylogeny using phylogenomics and the multispecies coalescent model.
Proceedings of the National Academy of Sciences of the United States of America, 109(37):14942–14947.

[216] Springer, M. S., Murphy, W. J., and Roca, A. L. (2018).
Appropriate fossil calibrations and tree constraints uphold the Mesozoic divergence of solenodons from other extant mammals.
Molecular Phylogenetics and Evolution, 121:158–165.

[217] Stayton, C. T. (2006).
Testing Hypotheses of Convergence With Multivariate Data: Morphological and Functional Convergence Among Herbivorous Lizards.
Evolution, 60(4):824–841.

[218] Strait, D. S., Wang, Q., Dechow, P. C., Ross, C. F., Richmond, B. G., Spencer, M. A., and Patel, B. A. (2005).
Modeling elastic properties in finite-element analysis: How much precision is needed to produce an accurate model?
Anatomical Record - Part A Discoveries in Molecular, Cellular, and Evolutionary Biology, 283(2):275–287.

[219] Strait, D. S., Weber, G. W., Neubauer, S., Chalk, J., Richmond, B. G., Lucas, P. W., Spencer, M. A., Schrein, C., Dechow, P. C., Ross, C. F., Grosse, I. R., Wright, B. W., Constantino, P., Wood, B. A., Lawn, B., Hylander, W. L., Wang, Q., Byron, C., Slice, D. E., and Smith, A. L. (2009).
The feeding biomechanics and dietary ecology of *Australopithecus africanus*.
Proceedings of the National Academy of Sciences of the United States of America, 106(7):2124–2129.

[220] Sutton, M. D., Rahman, I. A., and Garwood, R. J. (2013).
Surface-Based Methods.

In *Techniques for Virtual Palaeontology*, pages 115–129. John Wiley & Sons Ltd, Oxford.

[221] Tarquini, S. D., Chemisquy, M. A., and Prevosti, F. J. (2020).
Evolution of the Carnassial in Living Mammalian Carnivores (Carnivora, Didelphimorphia, Dasyuromorphia): Diet, Phylogeny, and Allometry.
Journal of Mammalian Evolution, 27:95–109.

[222] Taylor, M. and Prendergast, P. J. (2015).
Four decades of finite element analysis of orthopaedic devices: Where are we now and what are the opportunities?
Journal of Biomechanics, 48(5):767–778.

[223] Timm-Davis, L. L., DeWitt, T. J., and Marshall, C. D. (2015).
Divergent skull morphology supports two trophic specializations in otters (lutrinae).
PLoS ONE, 10(12):e0143236.

[224] Toyohara, R., Kurosawa, D., Hammer, N., Werner, M., Honda, K., Sekiguchi, Y., Izumi, S. I., Murakami, E., Ozawa, H., and Ohashi, T. (2020).
Finite element analysis of load transition on sacroiliac joint during bipedal walking.
Scientific Reports, 10:13683.

[225] Tseng, Z. J. and Binder, W. J. (2010).
Mandibular biomechanics of *Crocuta crocuta*, *Canis lupus*, and the late Miocene *Dinocrocuta gigantea* (Carnivora, Mammalia).
Zoological Journal of the Linnean Society, 158(3):683–696.

[226] Tseng, Z. J., Grohé, C., and Flynn, J. J. (2016).
A unique feeding strategy of the extinct marine mammal kolponomos: Convergence on sabre-tooths and sea otters.
Proceedings of the Royal Society B: Biological Sciences, 283:20160044.

[227] Tseng, Z. J., Mcnitt-Gray, J. L., Flashner, H., Wang, X., and Enciso, R. (2011).
Model sensitivity and use of the comparative finite element method in mammalian jaw mechanics: Mandible performance in the Gray Wolf.
PLoS ONE, 6(4):e19171.

[228] Ungar, P. S. (2015).
Mammalian dental function and wear: A review.
Biosurface and Biotribology, 1:25–41.

[229] Van Valen, L. and Sloan, R. E. (1966).
The extinction of the multituberculates.
Systematic Zoology, 15(4):261–278.

[230] Van Valkenburgh, B. (2007).
Déjà vu: The evolution of feeding morphologies in the Carnivora.
Integrative and Comparative Biology, 47(1):147–163.

[231] Vinyard, C. J., Wall, C. E., Williams, S. H., and Hylander, W. L. (2003).
Comparative functional analysis of skull morphology of tree-gouging primates.
American Journal of Physical Anthropology, 120(2):153–170.

[232] Walker, A., Hoeck, H. N., and Perez, L. (1978).
Microwear of mammalian teeth as an indicator of diet.
Science, 201(4359):908–910.

[233] Weijs, W. A. (1994).
Evolutionary Approach of Masticatory Motor Patterns in Mammals.
In Bels, V., Chardon, M., and Vandewalle, P., editors, *Biomechanics of Feeding in Vertebrates. Advances in Comparative and Environmental Physiology*, pages 281–320. Springer-Verlag Berlin Heidelberg.

[234] Wible, J. R. and Burrows, A. M. (2016).
Does the Jurassic *Agilodocodon* (Mammaliaformes, Docodonta) have any exudativorous dental features?
Palaeontol. Pol., 67:289–299.

[235] Wible, J. R., Rougier, G. W., Novacek, M. J., and Asher, R. J. (2007).
Cretaceous eutherians and Laurasian origin for placental mammals near the K/T boundary.
Nature, 447:1003–1006.

[236] Wible, J. R., Rougier, G. W., Novacek, M. J., and Asher, R. J. (2009).
The Eutherian Mammal *Maelestes gobiensis* from the Late Cretaceous of Mongolia and the Phylogeny of Cretaceous Eutheria.
Bulletin of the American Museum of Natural History, 327:1–123.

[237] Williamson, T. E., Brusatte, S. L., Carr, T. D., Weil, A., and Standhardt, B. R. (2012).
The phylogeny and evolution of Cretaceous-Palaeogene metatherians: Cladistic analysis and description of new early Palaeocene specimens from the Nacimiento Formation, New Mexico.
Journal of Systematic Palaeontology, 10(4):625–651.

[238] Wilson, G. P., Ekdale, E. G., Hoganson, J. W., Calede, J. J., and Vander Linden, A. (2016).
A large carnivorous mammal from the Late Cretaceous and the North American origin of marsupials.
Nature Communications, 7:13734.

[239] Wilson, G. P., Evans, A. R., Corfe, I. J., Smits, P. D., Fortelius, M., and Jernvall, J. (2012).
Adaptive radiation of multituberculate mammals before the extinction of dinosaurs.
Nature, 483:457–460.

[240] Wroe, S. (2008).
Cranial mechanics compared in extinct marsupial and extant African lions using a finite-element approach.
Journal of Zoology, 274(4):332–339.

[241] Wroe, S., Clausen, P., McHenry, C., Moreno, K., and Cunningham, E. (2007).
Computer simulation of feeding behaviour in the thylacine and dingo as a novel test for convergence and niche overlap.
Proceedings of the Royal Society B: Biological Sciences, 274:2819–2828.

[242] Wroe, S., Huber, D. R., Lowry, M., McHenry, C., Moreno, K., Clausen, P., Ferrara, T. L., Cunningham, E., Dean, M. N., and Summers, A. P. (2008).
Three-dimensional computer analysis of white shark jaw mechanics: How hard can a great white bite?
Journal of Zoology, 276(4):336–342.

[243] Young, M. T., Rayfield, E. J., Holliday, C. M., Witmer, L. M., Button, D. J., Upchurch, P., and Barrett, P. M. (2012).
Cranial biomechanics of *Diplodocus* (Dinosauria, Sauropoda): testing hypotheses of feeding behaviour in an extinct megaherbivore.
Naturwissenschaften, 99(8):637–643.

[244] Zhao, L. X. and Zhang, L. Z. (2013).
New fossil evidence and diet analysis of *Gigantopithecus blacki* and its distribution and extinction in South China.
Quaternary International, 286:69–74.

[245] Zheng, M., Zou, Z., silva Bartolo, P. j. D., Peach, C., and Ren, L. (2017).
Finite element models of the human shoulder complex: a review of their clinical implications and modelling techniques.
International Journal for Numerical Methods in Biomedical Engineering, 33(2):e02777.

[246] Zheng, X., Bi, S., Wang, X., and Meng, J. (2013).
A new arboreal haramiyid shows the diversity of crown mammals in the Jurassic period.
Nature, 500:199–202.

[247] Zhou, C. F., Bhullar, B. A. S., Neander, A. I., Martin, T., and Luo, Z. X. (2019a).
New Jurassic mammaliaform sheds light on early evolution of mammal-like hyoid bones.
Science, 365(6450):276–279.

[248] Zhou, Z., Winkler, D. E., Fortuny, J., Kaiser, T. M., and Marcé-Nogué, J. (2019b). Why ruminating ungulates chew sloppily: Biomechanics discern a phylogenetic pattern. *PLoS ONE*, 14(4):e0214510.

[249] Zienkiewicz, O. C. (1971). *The Finite Element Method in Engineering Science*. McGraw-Hill, New York, 1st edition.

[250] Zienkiewicz, O. C. and Taylor, R. L. (2000). *The Finite Element Method. Volume I: The Basis*. Wiley John & Sons, Barcelona, 5th edition.